

Control of T-cell Development and Function in Health and Disease

Institut für Immunologie
Medizinische Fakultät der
Ludwig-Maximilians-Universität München

Schrift zur Erlangung der *venia legendi*
im Fachgebiet „Immunologie“

von

Dr.rer.nat. Natalia Ziętara

München, 2021

Die in dieser Habilitationsschrift beschriebenen Arbeiten wurden von mir an folgenden Institutionen durchgeführt:

2011 bis 2015

Als Research Fellow in der Arbeitsgruppe von Prof. Andreas Krueger am Institut für Immunologie (Leiter: Prof. Reinhold Förster), Medizinische Hochschule Hannover, Hannover

2015 bis 2018

Als Research Fellow in der Arbeitsgruppe von Prof. Christoph Klein am Dr. von Haunerschen Kinderspital, Medizinische Fakultät, Ludwig-Maximilians-Universität München, München

seit 2018

Als Research Fellow und Projektleiterin in der Arbeitsgruppe von Prof. Ludger Klein am Institut für Immunologie (Leiter: Prof. Thomas Brocker), Medizinische Fakultät, Ludwig-Maximilians-Universität München, München

In der vorliegenden kumulativen Habilitationsschrift werden die folgenden fünf Publikationen zusammenfassend beschreiben und im Kontext diskutiert:

[1.] **Ziętara N***, Łyszkiewicz M*, Puchalka J, Witzlau K, Reinhardt A, Förster R, Pabst O, Prinz I, Krueger A. Multicongenic fate mapping quantification of dynamics of thymus colonisation. *J Exp Med*; 212(10), 1589-601 (2015).

**equally contributed first author*

[2.] **Ziętara N***, Łyszkiewicz M*, Witzlau K, Naumann R, Hurwitz R, Langemeier J, Bohne J, Sandrock I, Ballmaier M, Weiss S, Prinz I, Krueger A. Critical role for miR-181a/b-1 in agonist selection of invariant NKT cells. *Proc Natl Acad Sci U S A* 110(18):7407-12 (2013b).

**equally contributed first author*

[3.] Blume J, Zur Lage S, Witzlau K, Georgiev H, Weiss S, Łyszkiewicz M*, **Ziętara N***, Krueger A*. Overexpression of V α 14J α 18 TCR promotes development of iNKT cells in the absence of miR-181a/b-1. *Immunol Cell Biol*; 94(8), 741-6 (2016).

**equally contributed last author*

[4.] Łyszkiewicz M, Winter SJ, Witzlau K, Föhse L, Brownlie R, Puchalka J, Verheyden NA, Kunze-Schumacher H, Imelmann E, Blume J, Raha S, Sekiya T, Yoshimura A, Frueh JT, Ullrich E, Huehn J, Weiss S, Gutierrez MG, Prinz I, Zamoyska R, **Ziętara N***, Krueger A*. miR-181a/b-1 controls thymic selection of Treg cells and tunes their suppressive capacity. *PLoS Biol.* 17(3): e2006716 (2019).

**equally contributed last author*

[5.] Łyszkiewicz M*, **Ziętara N***, Frey L, Pannicke U, Stern M, Liu Y, Fan Y, Puchalka P, Hollizeck S, Somekh I, Rohlf s M, Yilmaz T, Ünal E, Karakukcu M, Patiroğlu T, Kellerer C, Karasu E, Sykora K-W, Lev A, Simon A, Somech R, Roesler J, Hoenig M, Keppler OT, Schwarz K, Klein C. Human FCHO1 deficiency reveals role for clathrin-mediated endocytosis in development and function of T cells. *Nat Commun.* 11(1):1031 (2020 Feb 25).

**equally contributed first author*

Danksagung

Diese Habilitation wäre nicht möglich gewesen ohne die Unterstützung einer Vielzahl von Menschen, denen ich an dieser Stelle danken möchte.

Zunächst möchte ich mich bei all meinen wunderbaren Mentoren bedanken, die mir beigebracht haben, wie man forscht und wie man unabhängig wird. Ich hätte mir keinen besseren Mentor für die Promotion vorstellen können als Dr. Siegfried Weiss. Du hast mir gezeigt, dass Wissenschaft Spaß macht. Deine unabhängige Denkweise, Prinzipien und dein Eifer, eine wissenschaftliche Wahrheit zu finden, auch wenn sie nicht veröffentlicht werden konnte, gaben mir ein sehr starkes Rückgrat und Vertrauen für meine gesamte Forschungskarriere. Es war ein Privileg und eine Ehre, mit Prof. Andreas Krueger zusammenzuarbeiten. Die Zusammenarbeit mit dir war mir immer eine Freude und ich kann kaum in Worte fassen, wie viel ich von dir gelernt habe. Deine Art, wissenschaftliche Probleme anzugehen und zu lösen, deine Offenheit für neue Ideen und Prinzipien sind bis heute mein Kompass. Du hattest immer Zeit für mich, du hast mir immer zugehört und mich wie eine gleichwertige Partnerin behandelt. Ich bin sehr dankbar, dass unsere wissenschaftlichen und nichtwissenschaftlichen Diskussionen immer noch fortgesetzt werden. Ich möchte Prof. Reinhold Förster für seine Unterstützung und Anleitung während meines Aufenthalts an seinem Institut an der Medizinischen Hochschule Hannover und bis heute danken. Die wissenschaftliche und kollegiale Atmosphäre, die du geschaffen hast, wird mich immer inspirieren. Der Eintritt in die Welt der menschlichen Immunologie wäre ohne die Unterstützung und Begeisterung von Prof. Christoph Klein nicht möglich gewesen. Ich möchte mich ganz herzlich bei dir für diese Gelegenheit und für die Möglichkeit bedanken, einen Beitrag zur Betreuung von Kindern mit seltenen Krankheiten zu leisten. Du hattest immer viel Vertrauen in mich und hast mir gezeigt, wie man im akademischen Umfeld überlebt. Ich möchte Prof. Ludger Klein meinen Dank dafür aussprechen, dass er mir die Möglichkeit gegeben hat, in seinem Labor zu arbeiten und meine selbständige Karriere weiterzuentwickeln.

Ich bin sehr dankbar für die Unterstützung und den Rat, den ich von Prof. Thomas Brocker erhalten habe. Ich bin äußerst dankbar für deine Zeit und deine Betreuung während des Habilitationsprozesses und für die Gelegenheit, in deinem Institut zu arbeiten. Ich möchte Marion Dorfmeister und Ursula Jakobeit für ihre Hilfe bei der mitunter unübersichtlichen Verwaltungsarbeit sehr herzlich danken.

Die Gelegenheit, im Labor von Prof. Hiroshi Kawamoto am RIKEN-Institut in Yokohama zu arbeiten, war eine Lehre, aus der ich immer zehren werde. Deine echte Leidenschaft für

Wissenschaft, Begeisterung und Freude an der Diskussion der Experimente sowie deine Liebe zu Musik und Kunst vermisse ich jeden Tag.

Mein besonderer Dank geht an Dr. Maximiliano Gutierrez vom Francis Crick Institute in London, der mir alles beigebracht hat, was ich über konfokale Mikroskopie und Bildanalyse weiß. Deine stets positive und problemlösende Haltung hat mir in schwierigen Zeiten am Mikroskop sehr geholfen. Ich werde niemals deine großzügige und kontinuierliche Unterstützung und aufrichtigen Ratschläge vergessen.

Mein besonderer Dank geht an Dr. Reinhard Obst, ohne den diese Habilitation nicht möglich wäre. Ich bin dankbar für all deine Ratschläge, nicht nur zum Unterrichten und für die Zeit, die du immer für mich hattest. Ich ziehe so viele Lehren aus unseren Diskussionen über Wissenschaft und Jazz.

Es war eine wahre Freude, mit Prof. Vigo Heissmeyer zusammenarbeiten und am Morgen mit dem Fahrrad zum Institut fahren zu können.

Ich hatte das große Glück, mit exzellenten Wissenschaftlern und Wissenschaftlerinnen und wunderbaren Menschen zusammenarbeiten zu können, deren Leistungen und Einstellung mich immer inspirieren werden: Prof. Rose Zamoyska, Prof. David Gray, Dr. Martin Turner, Prof. Georg Holländer, Prof. Klaus Okkenhaug und Prof. Yasser Wali.

Die tägliche Arbeit und die Diskussionen haben dank vieler wunderbarer Kollegen immer Spaß gemacht. Ich möchte besonders erwähnen: Dr. Stefan Lienenklaus, Dr. Nelson Gekara, Dr. Sara Bartels, Prof. Immo Prinz, Dr. Olga und Dr. Stephan Halle, Laura Frey, Yanxin Fan, Dr. Albrecht Matthaei, Tim Jeske, Dr. Christian J. Braun und Dr. Sebastian Hesse, Dr. Lena Wyss, Stefan Ganter, Madlen Steinert, Paulina Ferrada, Andrea Erdle und Franziska Bosch.

Meiner Familie gilt der größte Dank, besonders Marcin, für ihre bedingungslose Unterstützung, Geduld, ihren Glauben an mich und vor allem ihren Sinn für Humor.

Table of contents	6
1. Summary	7
2. Zusammenfassung	8
3. Introduction	9
4. Overview and discussion of research works	17
4.1 Quantification of the dynamics of thymus colonisation	17
4.2 Post-transcriptional control of T-cell development by micro RNAs	20
4.3 Control of T-cell development by changes in the local membrane architecture – implication for human disease	23
5. References	26
6. Appendix	34
6.1 Multicongenic fate mapping quantification of dynamics of thymus colonization	
6.2 Critical role for miR-181a/b-1 in agonist selection of invariant NKT cells	
6.3 Overexpression of V α 14J α 18 TCR promotes development of iNKT cells in the absence of miR-181a/b-1	
6.4 miR-181a/b-1 controls thymic selection of Treg cells and tunes their suppressive capacity	
6.5 Human FCHO1 deficiency reveals role for clathrin-mediated endocytosis in development and function of T cells	

1. Summary

T lymphocytes are at the core of the adaptive immune system. Fitness of T cells defines susceptibility to infections, autoimmune diseases or cancer. Inherited failure in T-cell generation and/or further differentiation might lead to primary immunodeficiencies (PIDs). The generation of healthy T cells is a complex, multistep process that essentially continues throughout the life of an organism. Therefore, its holistic understanding is a prerequisite for the development of therapeutic strategies.

In the works summarised here, T-cell development served as a model to address several fundamental questions in immunology. It starts from the earliest events during the thymus settling and T-cell development. Both depend on minute numbers of precursors that enter this organ from the blood. It was not known precisely how many precursors enter the thymus per day and how this process is regulated. Using fate-mapping experiments and mathematical modelling, we quantified the number of precursors entering the thymus and cellular feedback which regulates this process. This is a very important finding, especially in the context of thymus reconstitution and transplantation. Three further studies demonstrate how fine-tuning of T cell development by single micro RNA (miRNA), miR-181a-1, critically influences the emergence and function of T cells which require strong TCR-signals during their selection, namely invariant NKT (iNKT) cells and regulatory T (T_{reg}) cells. Of note, post-transcriptional changes mediated by miR-181a-1 can imprint long-lasting changes on the protein levels, which has not been yet reported for any other miRNA. Finally, through studying human primary immunodeficiencies, we discovered that gene previously solely associated with the initiation of clathrin-mediated endocytosis (CME) – FCHo1 (F-BAR domain only protein 1) – is essential for human T cell development and activation. This initial genetic discovery followed by experiments on human cellular models and high-resolution confocal microscopy allowed us to show broader principles governing the immune system: endocytosis of T cell receptor (TCR) and in consequence signalling, activation and subsequent lymphocyte selection depend on CME – processes initiated by FCHo1. This opened so far unexplored avenues of research.

2. Zusammenfassung

T-Lymphozyten bilden den Kern des adaptiven Immunsystems. Die Fitness von T-Zellen definiert die Anfälligkeit für Infektionen, Autoimmunerkrankungen oder Krebs. Vererbtes Versagen bei der Erzeugung von T-Zellen und / oder weitere Differenzierungen können zu primären Immundefekten (PIDs) führen. Die Erzeugung gesunder T-Zellen ist ein komplexer, mehrstufiger Prozess, der sich im Wesentlichen während des gesamten Lebens eines Organismus fortsetzt. Daher ist sein ganzheitliches Verständnis eine Voraussetzung für die Entwicklung therapeutischer Strategien.

In den hier zusammengefassten Arbeiten diente die T-Zellen-Entwicklung als Modell zur Beantwortung mehrerer grundlegender Fragen der Immunologie. Es beginnt mit den frühesten Ereignissen während der Thymussiedlung und der T-Zellen-Entwicklung. Beides hängt von der winzigen Anzahl von Vorläuferzellen ab, die aus dem Blut in das Organ gelangen. Es war bislang nicht genau bekannt, wie viele Vorläuferzellen pro Tag in den Thymus gelangen und wie dieser Prozess reguliert wird. Mithilfe von fate-mapping Experimenten und mathematischen Modellen haben wir die Anzahl der Vorläuferzellen quantifiziert, die in den Thymus eintreten und die zelluläre Rückkopplung, die diesen Prozess reguliert. Dies ist ein sehr wichtiger Befund, insbesondere im Zusammenhang mit der Rekonstitution und Transplantation des Thymus.

Drei weitere Studien zeigen, wie die Feinabstimmung der T-Zellen-Entwicklung durch einzelne Mikro-RNA (miRNA), miR-181a-1, die Entstehung und Funktion von T-Zellen, die während ihrer Selektion starke TCR-Signale benötigen, nämlich die invariante NKT (iNKT), Zellen und regulatorische T (Treg) - Zellen entscheidend beeinflusst. Bemerkenswerterweise können durch miR-181a-1 vermittelte post-transkriptionelle Veränderungen langanhaltende Veränderungen des Proteinspiegels erwirken, über die bisher für keine andere miRNA berichtet wurde.

Schließlich entdeckten wir durch Untersuchung der primären Immundefekte beim Menschen, dass das Gen, das zuvor ausschließlich mit der Initiierung der Clathrin-vermittelten Endozytose (CME) assoziiert war - FCHo1 (nur Protein 1 der F-BAR-Domäne) - für die Entwicklung und Aktivierung menschlicher T-Zellen essentiell ist. Diese erste genetische Entdeckung, gefolgt von Experimenten an menschlichen Zellmodellen und hochauflösender konfokaler Mikroskopie, ermöglichte es uns, umfassendere Prinzipien für das Immunsystem aufzuzeigen: Die Endozytose des T-Zellen-Rezeptors (TCR) und folglich die Signalübertragung, Aktivierung und anschließende Selektion der Lymphozyten hängen von CME ab - von FCHo1 initiierten Prozessen. Dies eröffnete bisher unerforschte Forschungswege.

3. Introduction

The basic principle of T-cell biology is shared between mice and humans. Since murine genetic models played a significant role in uncovering the molecular aspects of T-cell development, selection, and function, this introduction will mainly focus on the murine system. Individual species-specific differences will be indicated.

Intrathymic T-cell development

Under physiological conditions, intrathymic T-cell development depends on continual colonisation of the thymus by bone-marrow (BM) derived thymus-seeding progenitors (TSPs) (Serwold et al., 2009). TSPs comprise a heterogeneous mixture of multipotent progenitors (MPPs), common lymphoid progenitors (CLPs), and CLP-like cells as well as already T-lineage committed progenitors. Their phenotypes and physiology have been extensively studied (Bhandoola et al., 2007; Schlenner and Rodewald, 2010). They possess different self-renewal potentials and developmental kinetics, which accounts for the continuous and unperturbed thymic output, despite gated entry to the thymus. The entry of the precursors to the thymus is mediated through the cascade of receptor-ligand interactions (Scimone et al., 2006). The role of particular chemokine receptors such as CCR9, CCR7 and CXCR4, has been extensively studied and indicates the redundant roles of chemokines signals in the embryonic (Calderon and Boehm, 2011; Liu et al., 2006) and adult thymus (Krueger et al., 2010; Zlotoff et al., 2010). Furthermore, the role of various adhesion molecules, including integrins and P-selectin ligand in regulating the periodicity of thymic entry has been demonstrated (Lepique et al., 2003; Rossi et al., 2005; Scimone et al., 2006). TSPs enter the thymus from the blood through the large venules at the cortico-medullary junction (CMJ). This anatomical structure is located at the border of the thymic cortex and medulla. The minimal phenotypic requirement for TSP is the surface expression of CD27 and/or CD135 (Saran et al., 2010; Serwold et al., 2009).

TSPs occupy approximately 160 niches (Kadish and Basch, 1976; Krueger et al., 2017; Scollay et al., 1986; Wallis et al., 1975; Zietara et al., 2015) and give rise to early T-lineage progenitors (ETP), the most immature, detectable thymocyte population. The numbers of ETPs are directly regulated by Notch signalling, and it has been shown that Notch signals directly prevent lineage deviation from T- towards B-cells at this stage of thymocytes development (Feyerabend et al., 2009; Sambandam et al., 2005).

ETPs migrate to the outer cortex, continuously progressing through CD4⁻CD8⁻ double negative (DN) stages of thymocytes development (DN1, DN2, DN3 and DN4). Several critical checkpoints are characteristic for this journey, namely T-lineage commitment at the

DN2 stage, irreversible after expression of transcription factor Bcl11b (Ikawa et al., 2010; Li et al., 2010a; Li et al., 2010b); somatic rearrangements of the TCR initiated at the DN2 stage (*Tcrb*, *Tcrq* and *Tcrd*); β -selection at the DN3 stage. Cells with productive rearrangements of *Tcrb* locus signal through pre-TCR, which leads to allelic exclusion, proliferation and progression to CD4⁺CD8⁺ double-positive (DP) stage (Fehling et al., 1995). DP thymocytes start to rearrange *Tcra* locus (Kishi et al., 1991). This rearrangement leads to generation and surface expression of $\alpha\beta$ TCR (Trop et al., 2000). The fate of DP cells expressing on their surface $\alpha\beta$ TCR is determined during the subsequent selection steps. Positive selection ensures the survival of cells which TCR is capable of recognising peptide:MHC ligands on the surface of antigen-presenting cells (Scott et al., 1989; Teh et al., 1988). Negative selection ensures deletion of cells which TCR has a high affinity for self-ligand:MHC (most likely ubiquitously expressed self-antigens), representing potentially dangerous, autoreactive clones. Positive and negative selection can co-occur in the cortex. Alternatively, after positive selection, developing thymocytes are directed to the medulla where they are probed for recognition of tissue-specific self-antigens, which expression is driven by autoimmune regulator AIRE (Anderson et al., 2002).

Similarly, to negative selection, weak response results in further maturation whereas strong response in elimination. Altogether selection events result in the deletion of 90% of cells which expressed $\alpha\beta$ TCR before positive selection. Whereas minimal TCR signal is required to prevent “death by neglect” during positive selection, TCR affinity plays a more sophisticated role during negative selection in the cortex and medulla. High TCR affinity to self-ligand:MHC results in a clonal deletion, in conversion to regulatory T (T_{reg}) cell lineage or development of invariant natural killer T (iNKT) cells (Klein et al., 2014). Development of such self-reactive mature T cells is also termed agonist selection (Stritesky et al., 2012). Single positive T cells emigrate from the thymus *via* post-capillary venules in the medulla to establish the peripheral naïve T cell pool (**Figure 1**). Whereas in mice thymic output contributes to the majority of naïve T cells generated throughout the life, in adult humans only 10-20% of naïve T cell production is thymus derived with the remaining being generated through homeostatic proliferation in the periphery (den Braber et al., 2012).

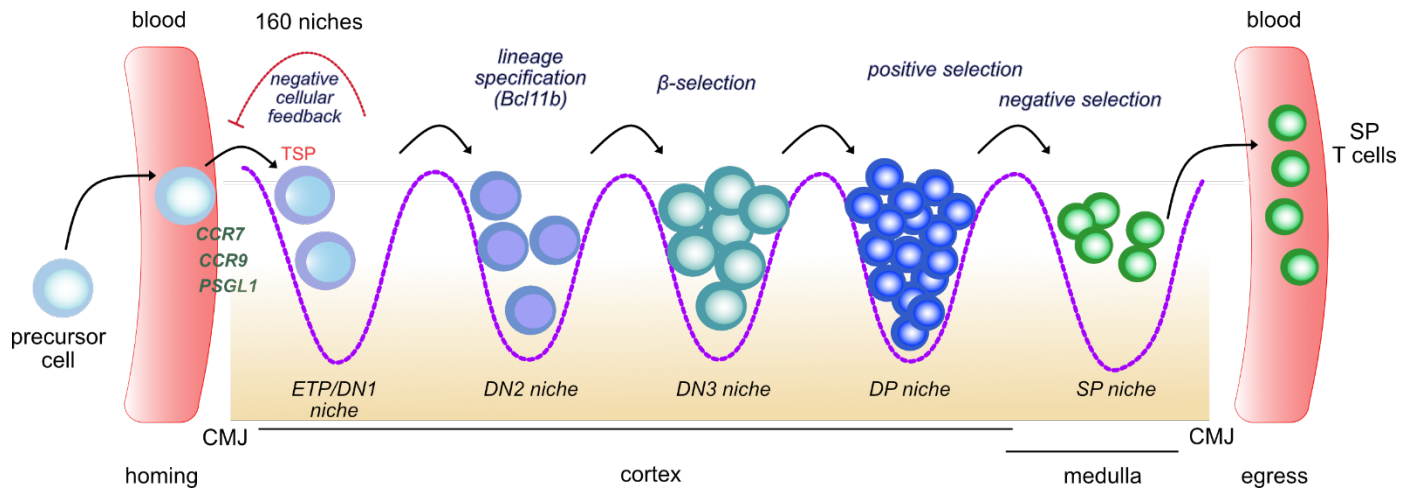


Figure 1. Intrathymic T-cell development. cortico-medullary junction – CMJ; thymus seeding progenitors – TSP; early T-lineage progenitors – ETP; double negative – DN; double-positive – DP; single positive – SP. Modified after T.Boehm and J.B. Swann 2013 (Boehm and Swann, 2013).

Post-transcriptional regulation of T-cell selection by micro RNAs

The lineage fate of developing thymocytes is tightly regulated on several levels, including transcriptional and post-transcriptional regulation (Diaz-Munoz and Turner, 2018; Rothenberg, 2014; Rothenberg et al., 2016b; Seo and Taniuchi, 2016; Winter and Krueger, 2019). The outcome of selection and further T-cell lineage specification critically depend on TCR signal strength (Gascoigne et al., 2016). TCR signalling requires a host of coordinated phosphorylation and dephosphorylation events within a network of intracellular signalling molecules. T cells express over 40 different negative regulators of TCR signalling including multiple phosphatases for each of the essential TCR signalling kinases, such as Lck, Zap70, ERK (Felices and Berg, 2008; Gaud et al., 2018). For a cell to tune its internal activation thresholds, it must simultaneously modulate multiple signalling molecules. The superior ability of non-coding RNAs, like microRNAs (miRNAs) to concurrently regulate hundreds of mRNA transcripts is a major advantage of miR-mediated gene regulation, as the gross effect is significant for entire pathways rather than for individual targets.

Small non-coding RNAs, such as miRNAs, act as a component of post-transcriptional regulation of gene expression. Upon maturation from precursors, individual miRNAs are incorporated into RNA-induced silencing complexes (RISC), through which they bind and destabilise their mRNA target transcripts, blocking translation and promoting mRNA decay (Guo et al., 2010; Huntzinger and Izaurralde, 2011; Roy-Chaudhuri et al., 2014).

Few individual miRNAs have been shown to be involved in early T-cell development (Dooley et al., 2013; Kirigin et al., 2012). Tissue-specific deletion of miRNA processing machinery,

which resulted in the loss of the vast majority of miRNAs, revealed particular importance of this layer of the regulation for the development of agonist-selected T cells, such as iNKT cells and T_{reg} cells, as well as maturation and homeostasis of T-lymphocytes in the periphery (Cobb et al., 2005; Muljo et al., 2005; Zhou et al., 2008).

Among the others, including miR-142 (Mildner et al., 2017), miR-146a (Boldin et al., 2011; Li et al., 2017; Lu et al., 2010), miR-155 (Kohlhaas et al., 2009; Lu et al., 2009; O'Connell et al., 2010), miR-150 (Bezman et al., 2011; Ghisi et al., 2011) and miR17~92 (Regelin et al., 2015) miR-181 family attracted particular attention. It comprises six members, in mice and humans, and can be divided into three mini-clusters, miR-181a/b-1, miR-181a/b-2 and miR-181c/d. Each mini-cluster is encoded on a separate chromosome. Mature miR-181a-1, miR-181a-2, miR-181b-1 and miR-181b-2 have an identical sequence (**Figure 2**).

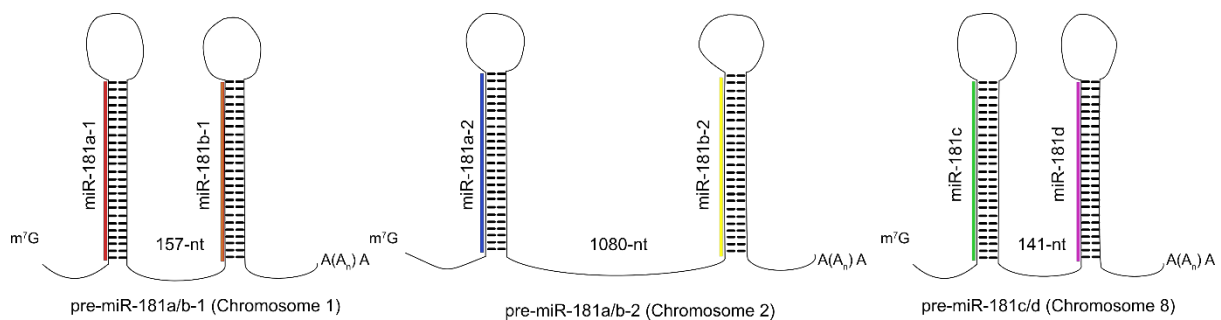


Figure 2. Mouse miR-181 family. Modified after Chen Chan-Zheng (Chen, 2013).

Mini-cluster miR-181a/b-1 is highly expressed in the thymus, which accounts for ~98% of all thymic miRNAs (Neilson et al., 2007; Zietara et al., 2013). Transcripts containing predicted seed matches to miR-181a/b-1 are enriched at the DN3 stage of thymocytes development and underrepresented at DP stage (Ebert et al., 2009; Li et al., 2007; Schaffert et al., 2015; Zietara et al., 2013). This observation together with the unique enrichment of miR-181a/b-1 at the DP stage of thymocytes development led to the hypothesis that miR-181 controls the T-cell selection through regulation of TCR signalling strength. Subsequent experiments helped to establish miR-181 family members as modulators of TCR sensitivity. Recognised targets of miR181a include phosphatases such as SHP-2, PTPN22, DUSP5 and DUSP6, critical during the regulation of TCR signalling (Ebert et al., 2009; Li et al., 2007).

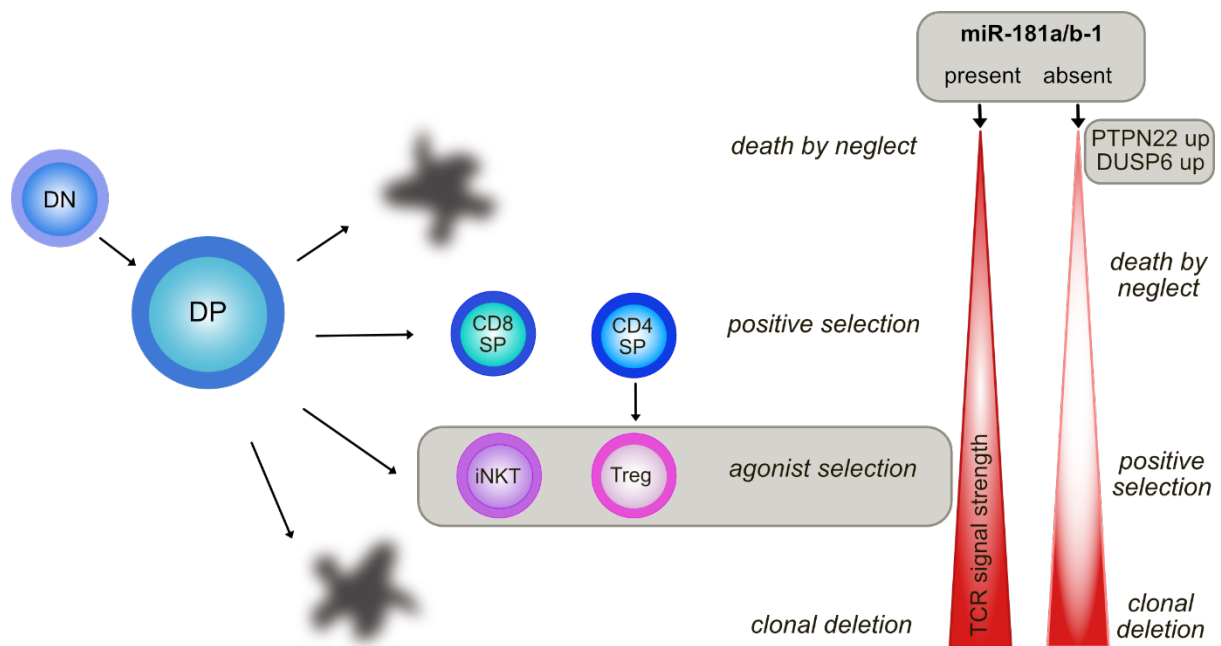


Figure 3. Modulation of TCR-sensitivity by miR-181a/b-1. In the absence of miR-181a/b-1 TCR signal strength is decreased due to elevated levels of several phosphatases (i.e. PTPN22, DUSP6). In consequence, the development of T lineages, which require strong (agonist) TCR signalling is severely compromised. DN-double negative; DP – double positive; SP- single positive; iNKT – invariant NKT cells; Treg – regulatory T cells; TCR – T-cell receptor. Modified after Stritesky G et al. 2012 (Stritesky et al., 2012).

We and others have shown that the members of the miR-181 family are critical for the thymic development of iNKT cells, MAIT cells and T_{reg} cells *in vivo* (Blume et al., 2016; Henao-Mejia et al., 2013; Lyszkiewicz et al., 2019; Winter et al., 2019; Zietara et al., 2013). In particular, the development of iNKT cells and MAIT cells, which express semi-restricted TCR repertoire, has been almost completely abolished in the absence of miR-181a/b-1 (Winter et al., 2019; Zietara et al., 2013), **Figure 3**. The development of T_{reg} cells, which also require strong TCR signalling during selection, is affected to lesser extent by miRNA181a/b-1 than iNKT cells or MAIT cells (Lyszkiewicz et al., 2019). Of note, miR-181a/b-1-deficient T_{reg} cells express elevated levels of CTLA-4, which renders them more suppressive than their wild-type (WT) counterparts. This phenomenon has also been maintained in the periphery, by the mechanism which is not yet completely understood, however, it indicates that post-transcriptional changes imprinted during development can be preserved during the life of a cell.

Control of TCR internalisation and T-cell activation by clathrin adaptor FCHo1

Balanced TCR signalling constitutes an instructive force during T-cell development, as exemplified by studies on particular miRNAs. However, the precise localisation of the TCR

that is continuously internalised and recycled back to the plasma membrane is also of critical importance for the quality of the signal transduced. For instance: (1) activation signals can be amplified *via* the scaffolding on early endosomes, (2) activation signals can be attenuated *via* lysosomal degradation of the TCR, and/or (3) recirculation of the TCR to immune synapses *via* recycling endosomes can modulate TCR-dependent activation signals upon encountering antigen-presenting cells. Moreover, integrating signal strengths relies on spatio-temporal organisation of the TCR and associated signalling molecules (Onnis and Baldari, 2019; Willinger et al., 2015). Abnormalities in TCR and CD4 recycling have been associated with immune system-related diseases, e.g. impaired surface expression of TCR and IL-2 production in T-cells from SLE patients (Fernandez et al., 2009).

The TCR can be internalised *via* clathrin-dependent (Boyer et al., 1991; Dietrich et al., 1994; Ohno et al., 1995; Telerman et al., 1987) or clathrin-independent mechanisms (Compeer et al., 2018; Onnis and Baldari, 2019). The work described here focuses on clathrin-dependent pathway.

Clathrin is a central molecular scaffold protein playing an essential role in the re-organisation of cellular membranes and the transport between compartments. Clathrin-coated vesicles (CCV) formation controls internalisation of membrane-associated proteins and protein transport from the trans-Golgi-network (Robinson, 2015). Clathrin-dependent endocytosis is initiated at the plasma membrane by the recruitment of adaptors including – but not limited to - heterotetrameric AP-2 complex, AP180; and anchor proteins such as FCH domain only 1 and 2, [FCHo1 and 2 in vertebrates] (Cocucci et al., 2012; Henne et al., 2010; Pechstein et al., 2010).

In vitro studies showed that both FCHo1 and FCHo2 proteins play a central role during the formation of clathrin-coated pits (CCP) (Henne et al., 2010). This function does not only involve the facilitation of local membrane nucleation at the very beginning of the process but also a selection and recruitment of specific cargo for endocytosis (McMahon and Boucrot, 2011; Uezu et al., 2011) (**Figure 4 and 6**).

In nematodes, which possess a single *fcho* gene, FCHo deficiency is manifested by severe body malformation and the perturbed formation of CCP (Hollopeter et al., 2014). The function of FCHo has possibly changed during evolution as two FCHo paralogues (FCHo1 and FCHo2) have emerged in vertebrates (Dergai et al., 2016). For example, knockdown of *fcho1* in *Danio rerio* causes severe body malformation at an early developmental stage, whereas silencing of *fcho2* is associated with notochord and somite malformations (Hollopeter et al., 2014).

Thus, FCHo1 could evolve to act as cargo-specific rather than a universally important initiator of clathrin-mediated endocytosis (CME) while FCHo2 preserved its original function (Umasankar et al., 2012). The concept of FCHo1/FCHo2 acting as adaptors specific to certain cargo in higher vertebrates is further corroborated by a series of other studies focusing on central elements essential for CME (Azarnia Tehran et al., 2019). Biochemical analyses of cellular models suggested that FCHo1 can offer an alternative pathway to promote cargo capture. This function could be achieved via AP-2, central adaptor and main protein which recruits cargo from the plasma membrane, or in parallel in the entirely unrelated pathway (Cocucci et al., 2012; Hollopeter et al., 2014; Mulkearns and Cooper, 2012; Umasankar et al., 2012).

Mutations in proteins that are considered to be less pivotal for the CME have been linked to a variety of diseases such as cancer, neuropsychiatric disorders, metabolic syndromes, but not to the defects of the immune system (McMahon and Boucrot, 2011). Furthermore, none of FCHo1/2 direct binding partners has been shown to play a pivotal role in the immune system of human or mice (Henne et al., 2010; Henne et al., 2007; Hollopeter et al., 2014; Iseka et al., 2018; Mulkearns and Cooper, 2012; Reider et al., 2009; Umasankar et al., 2012).

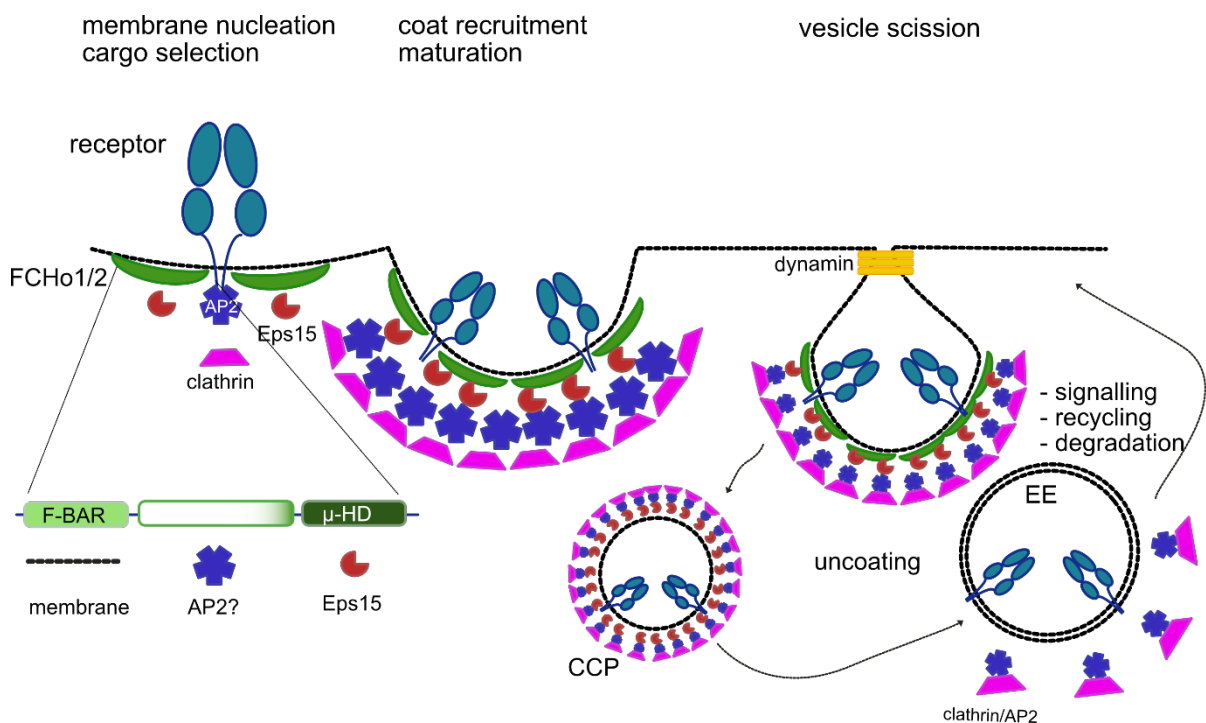


Figure 4. The role of FCHo proteins during initiation of CME. Modified after (Onnis and Baldari, 2019; Reider and Wendland, 2011). CCP – clathrin-coated pit; EE – early endosome.

In this work, three different aspects of the regulation of T-cell development are summarised and discussed. First, the earliest events of intrathymic T cell development, as well as mechanisms which provide cellular feedback to regulate the thymus seeding, have been characterised in detail on a quantitative level. Second, the discovery of miRNA-181a/b-1 as an indispensable post-transcriptional regulator of the TCR-signaling thresholds controlling the generation and emergence of agonist-selected T cells has been explained. The final section addresses the previously unforeseen dependency between the specific adaptor of CME, FCHo1, and the generation and activation of T cells in humans.

The identification and characterisation of cellular and molecular pathways which control T-cell generation and maintenance should provide the basis for new therapeutic approaches that improve the regeneration of the adaptive immune system, especially with functional and competent naïve T cells.

4. Overview and discussion of research works

4.1 Quantification of the dynamics of thymus colonisation

Ziętara N*, Łyszkiewicz M*, Puchałka J, Witzlau K, Reinhardt A, Förster R, Pabst O, Prinz I, Krueger A. Multicongenic fate mapping quantification of dynamics of thymus colonisation. *J Exp Med*; 212(10), 1589-601 (2015)

This section summarises a study which assessed thymus colonisation on the quantitative level. There is a lot of evidence how thymus settling and T cell development are regulated on a qualitative level, by transcription factors-gene regulatory networks, extrinsic signals and specialised tissue microenvironments (Rothenberg et al., 2016a). However, understanding of both qualitative and quantitative aspects of this process is critical for improving the regeneration of the immune system, e.g. after transplantation.

T cell development depends on the continuous colonisation of the thymus by bone-marrow (BM) derived thymus-seeding progenitors (TSPs). They enter the thymus via the bloodstream, and their numbers in the blood are extremely low (Krueger et al., 2017). Process of colonisation cannot be addressed directly as phenotypical characterisation of TSPs within the thymus is not possible using state-of-the-art techniques (too few cells, rapidly differentiating into further stages). Additionally, thymus colonisation is tightly controlled by adhesion molecules, and chemokine receptors, and its receptivity is periodic (Donskoy et al., 2003; Gossens et al., 2009). It was not known how such periodicity is regulated.

To tackle these challenges, we developed a so-called “multicongenic fate mapping” experimental system in combination with mathematical modelling. Additionally, we took advantage of CCR7^{-/-}CCR9^{-/-} (called later DKO) mice, which are particularly receptive to precursor seeding due to the lack of early T-lineage precursors (ETPs) in the thymus (Krueger et al., 2010; Zlotoff et al., 2010). In this study, we demonstrated that the availability of these early intrathymic microenvironmental niches accounts for increased DKO thymus receptivity, with otherwise physiological cellularity and architecture.

We used a defined population of progenitor cells (lin⁻CD117⁺CD135⁺) expressing various congenic markers or fluorescent proteins, yielding up to 13 various protein tags, all traceable using flow cytometry. Such defined progenitors contained all TSPs, yet lack the potential of long-term engraftment of BM, thus the thymus settling was restricted to only one wave of colonisation (Saran et al., 2010; Serwold et al., 2009). We then transplanted non-manipulated wild-type (WT) or DKO mice with defined ratios of such progenitors. After 21

days, we determined the number of missing tags in donor populations. To simulate the colonisation events, we applied a mathematical algorithm based on the Monte Carlo simulation (**Figure 5**).

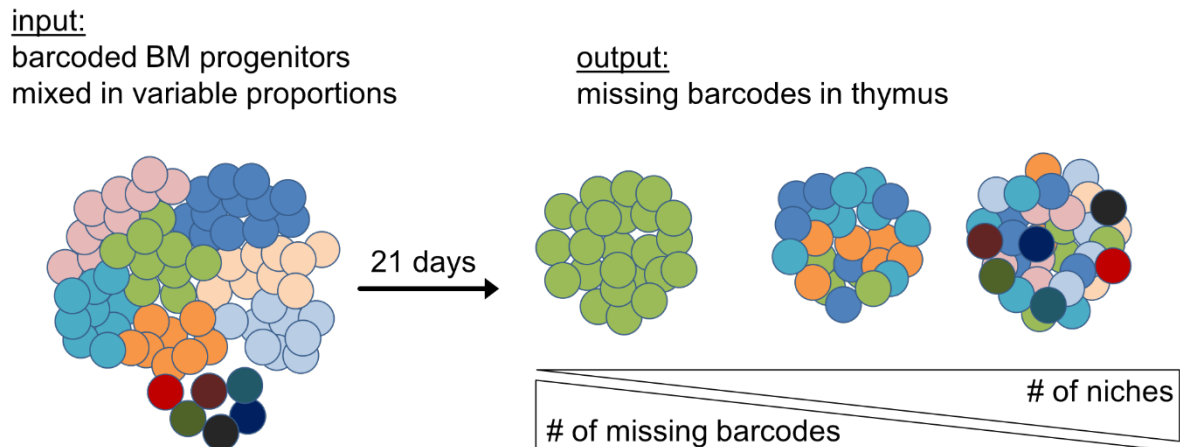


Figure 5. Quantification of the dynamics of thymus colonisation using “multicongenic fate mapping” approach (Krueger et al., 2017). Defined mixtures of tagged BM precursor cells ($\text{lin}^- \text{CD117}^+ \text{CD135}^+$) were injected into non-manipulated recipient mice. Three weeks after transplantation missing tags were counted within the recovered donor population. Using mathematical modelling, it was possible to recapitulate colonisation events and determine the number of intrathymic niches capable of supporting productive T cell development.

Using such an experimental system, our analysis revealed that WT thymus is on average colonised by ten TSPs at given time point. Data recovered from DKO recipients revealed that a maximal number of available niches supporting the earliest thymic progenitors is ~160.

Thymus colonisation has been suggested to be dependent on the periodic opening of a very limited number of progenitor niches about every 3-4 weeks (Foss et al., 2001, 2002; Goldschneider, 2006). To determine how the periodicity of the thymus settling is regulated, we took advantage of our 13-code precursors' library and “empty” status of DKO recipient mice. To this end, we performed a series of transplantation experiments, where individually tagged precursor populations were sequentially injected at three days intervals. Analysis of the composition of mature T cell pool six weeks after last transplantation revealed the periodicity of 9-12 days for thymus colonisation, in both initially empty DKO and WT recipients. This correlates extremely well with the life-time of ETPs (Porritt et al., 2003), hence we concluded that niche occupancy by ETP restricts the access of progenitors to the

adult thymus. In contrast, previous works suggested that double-negative (DN) thymocytes rather than more immature thymocytes provide negative feedback for thymus settling (Prockop and Petrie, 2004).

Quantification of thymus settling using the above described approach and applied mathematical modelling circumvented several problems associated with direct detection and accidental counting of cells, which ultimately did not enter the T-cell lineage. This was possible due to the focus of our counting on the missing tags, hence reducing the readout to the binary present/absent call, instead of taking into account intrathymic differentiation processes.

Periodicity of thymus colonisation with its rather long (9-12 days) refractory periods raises the questions about the regulation of continuous output of mature T cells to the periphery. The fact that multiple physiological progenitors (comprising at least CLP and MPP subsets) with different self-renewal potential can enter the thymus and develop there with different kinetics offers an elegant explanation.

Attempts to quantitate thymus colonisation, mostly of irradiated hosts, have been made over several decades (Scollay et al., 1986; Wallis et al., 1975). These experiments suggested that irradiated thymus is colonised by 10-200 cells per day. However, preconditioning regimens like complete body irradiation are known to induce severe, difficult to control alterations, e.g. damage to the thymic stromal cells on the cellular and genomic levels (Calvo-Asensio et al., 2017) and even lead to the complete dysfunctionality of the thymus in the context of the generation of certain cell populations (Amagai et al., 1987). Therefore, the DKO mice with their superior receptivity for the TSP progenitors and otherwise physiological thymic composition and architecture proved to be an excellent model not only to study the colonisation of the adult thymus but can be successfully used in a variety of transplantation experiments which aim to investigate any stage of intrathymic T-cell development and selection.

Taken together, using fate mapping and mathematical modelling, we faithfully quantified the number of precursors entering the thymus and cellular feedback which regulates this process in non-manipulated mice. Developed here “multicongenic cellular barcoding” approach in combination with a mathematical algorithm constitutes an important tool to study various aspects of thymus settling and reconstitution, especially in the context of transplantation.

4.2 Post-transcriptional control of T-cell development by micro RNAs

Ziętara N*, Łyszkiewicz M*, Witzlau K, Naumann R, Hurwitz R, Langemeier J, Bohne J, Sandrock I, Ballmaier M, Weiss S, Prinz I, Krueger A. Critical role for miR-181a/b-1 in agonist selection of invariant NKT cells. *Proc Natl Acad Sci U S A* 110(18):7407-12 (2013b)

Blume J, Zur Lage S, Witzlau K, Georgiev H, Weiss S, Łyszkiewicz M*, **Ziętara N***, Krueger A*. Overexpression of V α 14Ja18 TCR promotes development of iNKT cells in the absence of miR-181a/b-1. *Immunol Cell Biol*; 94(8), 741-6 (2016)

Łyszkiewicz M, Winter SJ, Witzlau K, Föhse L, Brownlie R, Puchałka J, Verheyden NA, Kunze-Schumacher H, Imelmann E, Blume J, Raha S, Sekiya T, Yoshimura A, Frueh JT, Ullrich E, Huehn J, Weiss S, Gutierrez MG, Prinz I, Zamoyska R, **Ziętara N***, Krueger A*. miR-181a/b-1 controls thymic selection of Treg cells and tunes their suppressive capacity. *PLoS Biol.* 17(3): e2006716 (2019)

MicroRNAs (miRNAs) are non-coding RNAs which act as post-transcriptional regulators of gene expression. Conditional deletion of miRNA processing machinery in developing T cells, which resulted in the loss of the vast majority of the miRNAs, severely compromised the survival of $\alpha\beta$ thymocytes (Cobb et al., 2005).

In this section, three works are summarised, which uncovered the critical *in vivo* role of miRNA mini-cluster, miR-181a/b-1, during T-cell development in the thymus and T-cell function in the periphery. MiR-181a/b-1 is dynamically expressed during T-cell development. It accounts for the largest miRNA enrichment at the DP stage when thymocytes undergo selection (Kirigin et al., 2012; Neilson et al., 2007). Furthermore, members of the miR-181 family have been postulated to act as intrinsic modulators of TCR sensitivity and to set the threshold for the T-cell selection in the thymus through targeting multiple negative regulators of TCR signalling (Ebert et al., 2009; Li et al., 2007). Even though based purely on *in vitro* models, these experiments provided an important framework for the mechanism behind the role of the members of the miR-181 family during T-cell development and selection.

We generated a murine model of miR-181a/b-1-deficiency to study their *in vivo* role during thymopoiesis. Global analysis of these mice revealed normal numbers of thymic and peripheral $\alpha\beta$ T cells with their overall unperturbed development. Of note, TCR signalling of developing thymocytes was drastically impaired in the absence of miR-181a/b-1. In agreement, the mRNA levels of three phosphatases, which are negative regulators of TCR signalling, *Ptpn11*, *Ptpn22* and *Dusp6* were elevated in thymocytes of miR-181a/b-1 knockout mice. Detailed analysis of T cell selection revealed that populations which are selected by agonist ligand, concomitant with the transduction of strong signals through TCR, such as invariant NKT (iNKT) cells and regulatory T (T_{reg}) cells, are particularly sensitive to

the changes induced by the lack of miR-181a/b-1. These data were further substantiated by the discovery of another population of unconventional, agonist-selected T cells, mucosal-associated invariant T (MAIT) cells, being also severely reduced in the absence of miR-181a/b-1 (Winter et al., 2019).

In the absence of miR-181a-1, the development of iNKT cells was almost completely blocked at the very early stage of their selection, which resulted in a dramatic reduction of iNKT cell numbers in the thymus and periphery, as compared to WT mice. This defect further impacted their TCR rearrangement and cytokine production. To test the hypothesis that such profound developmental block is a result of dampened TCR signalling, two independent *in vivo* rescue strategies were employed. First, we applied supraphysiological levels of cognate agonist lipid ligand (α -Galactosylceramide, α -GalCer) and could see that the development of iNKT cells was rescued in the absence of miR-181a/b-1. Second, transgenic overexpression of prearranged TCR V α 14-J α 18, which was concomitant with higher surface expression of TCR and enhanced signal transduction, bypassed the lack of miR-181a/b-1 and provided a complete restoration of impaired iNKT cell development. Both approaches supported our hypothesis that impaired agonist selection in miR-181a/b-1 knockout mice is a major effector of failed iNKT cell generation.

An independent work, where authors characterised conditional miR-181 mice (triple knockout of all miR-181 mini-clusters), proposed that the members of miR-181 family act as a metabolic rheostat of T-cell development through targeting of *Pten* (Heno-Mejia et al., 2013). In agreement, haploinsufficiency of *Pten* was able to partially rescue impaired iNKT cell development. Transgenic overexpression of prearranged V α 14-J α 18 TCR in this study resulted in a two-fold increase of iNKT cell numbers in the absence of miR-181 members, demonstrating TCR-dependent effects, despite the author's divergent conclusions. Of note, in our model rescue of iNKT cell development by overexpression of TCR V α 14-J α 18 did not alter the *Pten* levels.

In sum, scenario emerging accumulated by us and others (Schaffert et al., 2015) points to the primary role of impaired TCR signalling and in consequence agonist selection of iNKT cells and T_{reg} cells in miR-181a/b-1 deficiency with possibly a secondary role of PTEN-mediated metabolic changes.

The second population, which development is in part dependent on miR-181a/b-1 is a population of T_{reg} cells. Using Rag^{GFP} mice as a tool to track newly developing T_{reg} cells in the thymus, we observed their impaired generation in the absence of miR-181a-1. This defect could be completely rescued upon enforced expression of Nur77 (Nr4a1) during T-cell development. Hence, also in this case, impaired TCR signal transduction caused by the lack

of miR-181a/b-1 was directly responsible for the inefficient generation of T_{reg} cells. Since T_{reg} cells can be generated from two different type of precursors, CD25⁺Foxp3⁻ and CD25⁻Foxp3⁺, responsive to stronger and weaker TCR signalling, respectively (Marshall et al., 2014; Moran et al., 2011), the observed defects in their generation were not as dramatic as in the case of iNKT cells or MAIT cells (Winter et al., 2019). The formation of CD25⁺Foxp3⁻ precursors, is virtually not affected in miR-181a/b-1 knockout. Hence, it is plausible that they are replenished by thymocytes otherwise instructed for clonal deletion. Of note, the formation of CD25⁻Foxp3⁺ population is more dependent on miR-181a/b-1, implying that this population constitute a major source of thymic T_{reg} cells, as also suggested by others (Marshall et al., 2014). Both thymic and peripheral miR-181a/b-1-deficient T_{reg} cells expressed elevated levels of CTLA-4 protein, which rendered them more suppressive both *in vitro* and *in vivo*. Principally, peripheral T cells express very low levels of miR-181a-1/b-1. Therefore, it remains incompletely understood what are the mechanisms behind “post-transcriptional legacy” of miR-181a/b-1, which resulted in the maintenance of high CTLA-4 levels in the peripheral T_{reg} cells.

Collectively, we discovered that miR-181a/b-1 control the strength of TCR-receptor signal transduction. As a consequence, T-cells which require strong TCR-signals during selection do not develop in the absence of miR-181a-1/b-1. This is one of the first reports demonstrating that single miRNA can regulate the development of T-cells *in vivo*. Mir-181a/b-1 with its potential to fine-tune TCR-signal strength can be considered as a target to modulate in e.g. CAR T-cell therapy.

4.3 Control of T-cell development by changes in the local membrane architecture – implication for human disease

Łyszkiewicz M*, Ziętara N*, Frey L, Pannicke U, Stern M, Liu Y, Fan Y, Puchałka P, Hollizeck S, Somekh I, Rohlf M, Yilmaz T, Ünal E, Karakukcu M, Patiroğlu T, Kellerer C, Karasu E, Sykora K-W, Lev A, Simon A, Somech R, Roesler J, Hoenig M, Keppler OT, Schwarz K, Klein C. Human FCHO1 deficiency reveals role for clathrin-mediated endocytosis in development and function of T cells. *Nat Commun.* 11(1):1031 (2020 Feb 25)

Primary immunodeficiencies (PIDs) are mostly monogenic. Hence, they provide a unique opportunity to unravel the function of single genes essential for the immune system. In work summarised here, we discovered new PID entity, which allowed us to directly link a specific nucleator of clathrin-mediated endocytosis (CME), FCHO1 (F-BAR domain only protein 1), with T-cell generation and differentiation in humans.

We identified and characterised nine patients, carrying six rare, homozygous mutations in *FCHO1* gene. All of them suffered from severe combined immunodeficiency, in particular, CD4⁺ T-cell lymphopenia. Such conditions predisposed to chronic infections (predominantly fungal (*Candida albicans*) and viral (cytomegalovirus, CMV) and lymphoma formation (diffuse large B-cell lymphoma). Using *in vitro* cellular models, CRISPR/Cas9 genetic editing and high-resolution confocal microscopy, we showed that all mutations resulted in a loss-of-function phenotype. Except for mutants due to an early stop codon, the loss of normal protein function was caused either by the lack of association of mutant FCHO1 to the plasma membrane or lack of interaction with direct binding partners, namely EPS15 or EPS15R. Impaired initiation of CME in the absence of functional FCHO1 led to the inefficient formation of clathrin-coated pits (CCP).

The precise localisation of the TCR that is continuously internalised and recycled back to the plasma membrane is of critical importance for the quality of the signal transduced. Further, the quality of the signal transmitted by pre-T cell receptor (pre-TCR) and TCR is essential for T-cell development, homeostasis as well as effector responses towards invading pathogens. Moreover, integrating signal strengths relies on spatio-temporal organisation of the TCR and associated signalling molecules. The TCR can be internalised *via* clathrin-dependent (Boyer et al., 1991; Dietrich et al., 1994; Ohno et al., 1995; Telerman et al., 1987) or clathrin-independent mechanisms (Compeer et al., 2018). We hypothesised that FCHO1 deficiency could result in impaired TCR internalisation, which would explain the observed T-cell lymphopenia in humans. We could demonstrate that patient T cells were unresponsive to TCR stimulation, resulting in impaired proliferation and production of cytokines. Additionally, we used a human T cell line (Jurkat) to show that in the absence of FCHO1 TCR

internalisation was severely perturbed, yet could be restored upon ectopic expression of WT but not mutant FCHo1. Lastly, we established *in vitro* murine co-culture system, where we used an inhibitor of CME (chlorpromazine) and demonstrated that T-cell development is delayed when CME is reduced.

Given the significance of CME as the conserved and ubiquitous process for internalisation of cargo from the cell surface, we hypothesised that FCHo1 could not act as a global adaptor of CME since the specific consequences of loss-of-function mutations on lymphocytes in human. Endocytosis of the transferrin receptor is a process that solely depends on CME to take place (Mayle et al., 2012). Hence, we tested it on fibroblasts derived from FCHo1-mutant-patient and healthy donors. This process was unaffected in the absence of functional FCHo1. Similarly, the entry of VSV-G pseudotyped HIV into host CD4⁺ T cells is, to a large extent CME dependent (Finkelshtein et al., 2013). Also, here, the internalisation of the virus was unaffected in the absence of FCHo1, pointing towards cargo/cell-specific function of FCHo1 (**Figure 6**).

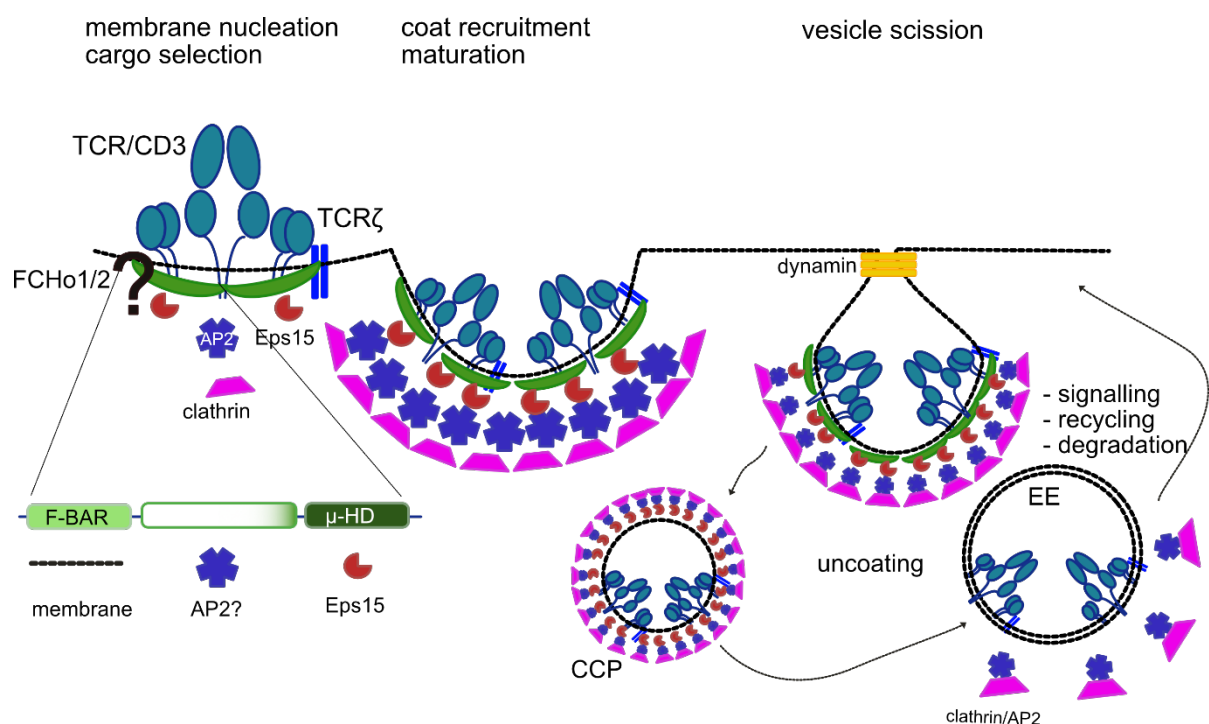


Figure 6. CME adaptor FCHo1 selectively targets TCR to control T-cell development and function in humans. Modified after (Onnis and Baldari, 2019; Reider and Wendland, 2011). CCP – clathrin-coated pit; EE – early endosome. The question mark indicates the point of ongoing investigations, which aim to identify the binding partners of FCHo1 in lymphocytes.

In summary, the discovery of FCHo1 as a specific adaptor of CME targeting lymphocyte receptors, for the first time links the function of the immune system with CME. This exemplifies possibly broader scenario where multiple CME adaptors might be specialised in selecting certain cargo for endocytosis. From the disease perspective, generated knowledge provides a mechanistic explanation for the phenotype behind the life-threatening disease and is of potential therapeutic relevance. From the basic research perspective, it uncovers a completely new layer of control of lymphocyte biology.

Further work will be addressed to answer several open questions of high relevance not only for basic immunology but also for clinical research, namely: *did multiple clathrin adaptors specialised during evolution to act in specific tissues and target specific cargo for endocytosis, the fundamental process maintaining basic functions of the cell? Is such specialisation needed to avoid drastic consequences associated with the ubiquitous role of central proteins, like clathrin or AP2?*

5. References

- Amagai, T., Kina, T., Hirokawa, K., Nishikawa, S., Imanishi, J., and Katsura, Y. (1987). Dysfunction of irradiated thymus for the development of helper T cells. *J Immunol* *139*, 358-364.
- Anderson, M.S., Venanzi, E.S., Klein, L., Chen, Z., Berzins, S.P., Turley, S.J., von Boehmer, H., Bronson, R., Dierich, A., Benoist, C., and Mathis, D. (2002). Projection of an immunological self shadow within the thymus by the aire protein. *Science* *298*, 1395-1401.
- Azarnia Tehran, D., Lopez-Hernandez, T., and Maritzen, T. (2019). Endocytic Adaptor Proteins in Health and Disease: Lessons from Model Organisms and Human Mutations. *Cells* *8*.
- Bezman, N.A., Chakraborty, T., Bender, T., and Lanier, L.L. (2011). miR-150 regulates the development of NK and iNKT cells. *J Exp Med* *208*, 2717-2731.
- Bhandoola, A., von Boehmer, H., Petrie, H.T., and Zuniga-Pflucker, J.C. (2007). Commitment and developmental potential of extrathymic and intrathymic T cell precursors: plenty to choose from. *Immunity* *26*, 678-689.
- Blume, J., Zur Lage, S., Witzlau, K., Georgiev, H., Weiss, S., Lyszkiewicz, M., Zietara, N., and Krueger, A. (2016). Overexpression of Valpha14Jalpha18 TCR promotes development of iNKT cells in the absence of miR-181a/b-1. *Immunol Cell Biol* *94*, 741-746.
- Boehm, T., and Swann, J.B. (2013). Thymus involution and regeneration: two sides of the same coin? *Nat Rev Immunol* *13*, 831-838.
- Boldin, M.P., Taganov, K.D., Rao, D.S., Yang, L., Zhao, J.L., Kalwani, M., Garcia-Flores, Y., Luong, M., Devrekanli, A., Xu, J., *et al.* (2011). miR-146a is a significant brake on autoimmunity, myeloproliferation, and cancer in mice. *J Exp Med* *208*, 1189-1201.
- Boyer, C., Auphan, N., Luton, F., Malburet, J.M., Barad, M., Bizozzero, J.P., Reggio, H., and Schmitt-Verhulst, A.M. (1991). T cell receptor/CD3 complex internalization following activation of a cytolytic T cell clone: evidence for a protein kinase C-independent staurosporine-sensitive step. *Eur J Immunol* *21*, 1623-1634.
- Calderon, L., and Boehm, T. (2011). Three chemokine receptors cooperatively regulate homing of hematopoietic progenitors to the embryonic mouse thymus. *Proc Natl Acad Sci U S A* *108*, 7517-7522.
- Calvo-Asensio, I., Barthlott, T., von Muenchow, L., Lowndes, N.F., and Ceredig, R. (2017). Differential Response of Mouse Thymic Epithelial Cell Types to Ionizing Radiation-Induced DNA Damage. *Front Immunol* *8*, 418.
- Chen, C.Z. (2013). An unsolved mystery: the target-recognizing RNA species of microRNA genes. *Biochimie* *95*, 1663-1676.
- Cobb, B.S., Nesterova, T.B., Thompson, E., Hertweck, A., O'Connor, E., Godwin, J., Wilson, C.B., Brockdorff, N., Fisher, A.G., Smale, S.T., and Merkenschlager, M. (2005). T cell lineage choice and differentiation in the absence of the RNase III enzyme Dicer. *J Exp Med* *201*, 1367-1373.
- Cocucci, E., Aguet, F., Boulant, S., and Kirchhausen, T. (2012). The first five seconds in the life of a clathrin-coated pit. *Cell* *150*, 495-507.

Compeer, E.B., Kraus, F., Ecker, M., Redpath, G., Amiezer, M., Rother, N., Nicovich, P.R., Kapoor-Kaushik, N., Deng, Q., Samson, G.P.B., *et al.* (2018). A mobile endocytic network connects clathrin-independent receptor endocytosis to recycling and promotes T cell activation. *Nat Commun* 9, 1597.

den Braber, I., Mugwagwa, T., Vrisekoop, N., Westera, L., Mogling, R., de Boer, A.B., Willems, N., Schrijver, E.H., Spierenburg, G., Gaiser, K., *et al.* (2012). Maintenance of peripheral naive T cells is sustained by thymus output in mice but not humans. *Immunity* 36, 288-297.

Dergai, M., Iershov, A., Novokhatska, O., Pankivskyi, S., and Rynditch, A. (2016). Evolutionary Changes on the Way to Clathrin-Mediated Endocytosis in Animals. *Genome Biol Evol* 8, 588-606.

Diaz-Munoz, M.D., and Turner, M. (2018). Uncovering the Role of RNA-Binding Proteins in Gene Expression in the Immune System. *Front Immunol* 9, 1094.

Dietrich, J., Hou, X., Wegener, A.M., and Geisler, C. (1994). CD3 gamma contains a phosphoserine-dependent di-leucine motif involved in down-regulation of the T cell receptor. *EMBO J* 13, 2156-2166.

Donskoy, E., Foss, D., and Goldschneider, I. (2003). Gated importation of prothymocytes by adult mouse thymus is coordinated with their periodic mobilization from bone marrow. *J Immunol* 171, 3568-3575.

Dooley, J., Linterman, M.A., and Liston, A. (2013). MicroRNA regulation of T-cell development. *Immunol Rev* 253, 53-64.

Ebert, P.J., Jiang, S., Xie, J., Li, Q.J., and Davis, M.M. (2009). An endogenous positively selecting peptide enhances mature T cell responses and becomes an autoantigen in the absence of microRNA miR-181a. *Nat Immunol* 10, 1162-1169.

Fehling, H.J., Krotkova, A., Saint-Ruf, C., and von Boehmer, H. (1995). Crucial role of the pre-T-cell receptor alpha gene in development of alpha beta but not gamma delta T cells. *Nature* 375, 795-798.

Felices, M., and Berg, L.J. (2008). The Tec kinases Itk and Rlk regulate NKT cell maturation, cytokine production, and survival. *J Immunol* 180, 3007-3018.

Fernandez, D.R., Telarico, T., Bonilla, E., Li, Q., Banerjee, S., Middleton, F.A., Phillips, P.E., Crow, M.K., Oess, S., Muller-Esterl, W., and Perl, A. (2009). Activation of mammalian target of rapamycin controls the loss of TCRzeta in lupus T cells through HRES-1/Rab4-regulated lysosomal degradation. *J Immunol* 182, 2063-2073.

Feyerabend, T.B., Terszowski, G., Tietz, A., Blum, C., Luche, H., Gossler, A., Gale, N.W., Radtke, F., Fehling, H.J., and Rodewald, H.R. (2009). Deletion of Notch1 converts pro-T cells to dendritic cells and promotes thymic B cells by cell-extrinsic and cell-intrinsic mechanisms. *Immunity* 30, 67-79.

Finkelshtein, D., Werman, A., Novick, D., Barak, S., and Rubinstein, M. (2013). LDL receptor and its family members serve as the cellular receptors for vesicular stomatitis virus. *Proc Natl Acad Sci U S A* 110, 7306-7311.

Foss, D.L., Donskoy, E., and Goldschneider, I. (2001). The importation of hematogenous precursors by the thymus is a gated phenomenon in normal adult mice. *J Exp Med* 193, 365-374.

Foss, D.L., Donskoy, E., and Goldschneider, I. (2002). Functional demonstration of intrathymic binding sites and microvascular gates for prothymocytes in irradiated mice. *Int Immunol* 14, 331-338.

Gascoigne, N.R., Rybakin, V., Acuto, O., and Brzostek, J. (2016). TCR Signal Strength and T Cell Development. *Annu Rev Cell Dev Biol* 32, 327-348.

Gaud, G., Lesourme, R., and Love, P.E. (2018). Regulatory mechanisms in T cell receptor signalling. *Nat Rev Immunol* 18, 485-497.

Ghisi, M., Corradin, A., Basso, K., Frasson, C., Serafin, V., Mukherjee, S., Mussolin, L., Ruggero, K., Bonanno, L., Guffanti, A., *et al.* (2011). Modulation of microRNA expression in human T-cell development: targeting of NOTCH3 by miR-150. *Blood* 117, 7053-7062.

Goldschneider, I. (2006). Cyclical mobilization and gated importation of thymocyte progenitors in the adult mouse: evidence for a thymus-bone marrow feedback loop. *Immunol Rev* 209, 58-75.

Gossens, K., Naus, S., Corbel, S.Y., Lin, S., Rossi, F.M., Kast, J., and Ziltener, H.J. (2009). Thymic progenitor homing and lymphocyte homeostasis are linked via S1P-controlled expression of thymic P-selectin/CCL25. *J Exp Med* 206, 761-778.

Guo, H., Ingolia, N.T., Weissman, J.S., and Bartel, D.P. (2010). Mammalian microRNAs predominantly act to decrease target mRNA levels. *Nature* 466, 835-840.

Henao-Mejia, J., Williams, A., Goff, L.A., Staron, M., Licona-Limon, P., Kaech, S.M., Nakayama, M., Rinn, J.L., and Flavell, R.A. (2013). The microRNA miR-181 is a critical cellular metabolic rheostat essential for NKT cell ontogenesis and lymphocyte development and homeostasis. *Immunity* 38, 984-997.

Henne, W.M., Boucrot, E., Meinecke, M., Evergren, E., Vallis, Y., Mittal, R., and McMahon, H.T. (2010). FCHo proteins are nucleators of clathrin-mediated endocytosis. *Science* 328, 1281-1284.

Henne, W.M., Kent, H.M., Ford, M.G., Hegde, B.G., Daumke, O., Butler, P.J., Mittal, R., Langen, R., Evans, P.R., and McMahon, H.T. (2007). Structure and analysis of FCHo2 F-BAR domain: a dimerizing and membrane recruitment module that effects membrane curvature. *Structure* 15, 839-852.

Hollopeter, G., Lange, J.J., Zhang, Y., Vu, T.N., Gu, M., Ailion, M., Lambie, E.J., Slaughter, B.D., Unruh, J.R., Florens, L., and Jorgensen, E.M. (2014). The membrane-associated proteins FCHo and SGIP are allosteric activators of the AP2 clathrin adaptor complex. *Elife* 3.

Huntzinger, E., and Izaurralde, E. (2011). Gene silencing by microRNAs: contributions of translational repression and mRNA decay. *Nat Rev Genet* 12, 99-110.

Ikawa, T., Hirose, S., Masuda, K., Kakugawa, K., Satoh, R., Shibano-Satoh, A., Kominami, R., Katsura, Y., and Kawamoto, H. (2010). An essential developmental checkpoint for production of the T cell lineage. *Science* 329, 93-96.

Iseka, F.M., Goetz, B.T., Mushtaq, I., An, W., Cypher, L.R., Bielecki, T.A., Tom, E.C., Arya, P., Bhattacharyya, S., Storck, M.D., *et al.* (2018). Role of the EHD Family of Endocytic Recycling Regulators for TCR Recycling and T Cell Function. *J Immunol* 200, 483-499.

Kadish, J.L., and Basch, R.S. (1976). Hematopoietic thymocyte precursors. I. Assay and kinetics of the appearance of progeny. *J Exp Med* 143, 1082-1099.

Kirigin, F.F., Lindstedt, K., Sellars, M., Ciofani, M., Low, S.L., Jones, L., Bell, F., Pauli, F., Bonneau, R., Myers, R.M., *et al.* (2012). Dynamic microRNA gene transcription and processing during T cell development. *J Immunol* 188, 3257-3267.

Kishi, H., Borgulya, P., Scott, B., Karjalainen, K., Traunecker, A., Kaufman, J., and von Boehmer, H. (1991). Surface expression of the beta T cell receptor (TCR) chain in the absence of other TCR or CD3 proteins on immature T cells. *EMBO J* 10, 93-100.

Klein, L., Kyewski, B., Allen, P.M., and Hogquist, K.A. (2014). Positive and negative selection of the T cell repertoire: what thymocytes see (and don't see). *Nat Rev Immunol* 14, 377-391.

Kohlhaas, S., Garden, O.A., Scudamore, C., Turner, M., Okkenhaug, K., and Vigorito, E. (2009). Cutting edge: the Foxp3 target miR-155 contributes to the development of regulatory T cells. *J Immunol* 182, 2578-2582.

Krueger, A., Willenzon, S., Lyszkiewicz, M., Kremmer, E., and Forster, R. (2010). CC chemokine receptor 7 and 9 double-deficient hematopoietic progenitors are severely impaired in seeding the adult thymus. *Blood* 115, 1906-1912.

Krueger, A., Zietara, N., and Lyszkiewicz, M. (2017). T Cell Development by the Numbers. *Trends Immunol* 38, 128-139.

Lepique, A.P., Palencia, S., Irjala, H., and Petrie, H.T. (2003). Characterization of vascular adhesion molecules that may facilitate progenitor homing in the post-natal mouse thymus. *Clin Dev Immunol* 10, 27-33.

Li, L., Leid, M., and Rothenberg, E.V. (2010a). An early T cell lineage commitment checkpoint dependent on the transcription factor Bcl11b. *Science* 329, 89-93.

Li, P., Burke, S., Wang, J., Chen, X., Ortiz, M., Lee, S.C., Lu, D., Campos, L., Goulding, D., Ng, B.L., *et al.* (2010b). Reprogramming of T cells to natural killer-like cells upon Bcl11b deletion. *Science* 329, 85-89.

Li, Q.J., Chau, J., Ebert, P.J., Sylvester, G., Min, H., Liu, G., Braich, R., Manoharan, M., Soutschek, J., Skare, P., *et al.* (2007). miR-181a is an intrinsic modulator of T cell sensitivity and selection. *Cell* 129, 147-161.

Li, Z., Zhang, S., Wan, Y., Cai, M., Wang, W., Zhu, Y., Li, Z., Hu, Y., Wang, H., Chen, H., *et al.* (2017). MicroRNA-146a Overexpression Impairs the Positive Selection during T Cell Development. *Front Immunol* 8, 2006.

Liu, C., Saito, F., Liu, Z., Lei, Y., Uehara, S., Love, P., Lipp, M., Kondo, S., Manley, N., and Takahama, Y. (2006). Coordination between CCR7- and CCR9-mediated chemokine signals in prevascular fetal thymus colonization. *Blood* 108, 2531-2539.

Lu, L.F., Boldin, M.P., Chaudhry, A., Lin, L.L., Taganov, K.D., Hanada, T., Yoshimura, A., Baltimore, D., and Rudensky, A.Y. (2010). Function of miR-146a in controlling Treg cell-mediated regulation of Th1 responses. *Cell* 142, 914-929.

Lu, L.F., Thai, T.H., Calado, D.P., Chaudhry, A., Kubo, M., Tanaka, K., Loeb, G.B., Lee, H., Yoshimura, A., Rajewsky, K., and Rudensky, A.Y. (2009). Foxp3-dependent microRNA155 confers competitive fitness to regulatory T cells by targeting SOCS1 protein. *Immunity* 30, 80-91.

Lyszkiewicz, M., Winter, S.J., Witzlau, K., Fohse, L., Brownlie, R., Puchalka, J., Verheyden, N.A., Kunze-Schumacher, H., Imelmann, E., Blume, J., *et al.* (2019). miR-181a/b-1 controls thymic selection of Treg cells and tunes their suppressive capacity. *PLoS Biol* 17, e2006716.

Marshall, D., Sinclair, C., Tung, S., and Seddon, B. (2014). Differential requirement for IL-2 and IL-15 during bifurcated development of thymic regulatory T cells. *J Immunol* 193, 5525-5533.

Mayle, K.M., Le, A.M., and Kamei, D.T. (2012). The intracellular trafficking pathway of transferrin. *Biochim Biophys Acta* 1820, 264-281.

McMahon, H.T., and Boucrot, E. (2011). Molecular mechanism and physiological functions of clathrin-mediated endocytosis. *Nat Rev Mol Cell Biol* 12, 517-533.

Mildner, A., Chapnik, E., Varol, D., Aychek, T., Lampl, N., Rivkin, N., Bringmann, A., Paul, F., Boura-Halfon, S., Hayoun, Y.S., *et al.* (2017). MicroRNA-142 controls thymocyte proliferation. *Eur J Immunol* 47, 1142-1152.

Moran, A.E., Holzapfel, K.L., Xing, Y., Cunningham, N.R., Maltzman, J.S., Punt, J., and Hogquist, K.A. (2011). T cell receptor signal strength in Treg and iNKT cell development demonstrated by a novel fluorescent reporter mouse. *J Exp Med* 208, 1279-1289.

Muljo, S.A., Ansel, K.M., Kanellopoulou, C., Livingston, D.M., Rao, A., and Rajewsky, K. (2005). Aberrant T cell differentiation in the absence of Dicer. *J Exp Med* 202, 261-269.

Mulkearns, E.E., and Cooper, J.A. (2012). FCH domain only-2 organizes clathrin-coated structures and interacts with Disabled-2 for low-density lipoprotein receptor endocytosis. *Mol Biol Cell* 23, 1330-1342.

Neilson, J.R., Zheng, G.X., Burge, C.B., and Sharp, P.A. (2007). Dynamic regulation of miRNA expression in ordered stages of cellular development. *Genes Dev* 21, 578-589.

O'Connell, R.M., Kahn, D., Gibson, W.S., Round, J.L., Scholz, R.L., Chaudhuri, A.A., Kahn, M.E., Rao, D.S., and Baltimore, D. (2010). MicroRNA-155 promotes autoimmune inflammation by enhancing inflammatory T cell development. *Immunity* 33, 607-619.

Ohno, H., Stewart, J., Fournier, M.C., Bosshart, H., Rhee, I., Miyatake, S., Saito, T., Gallusser, A., Kirchhausen, T., and Bonifacino, J.S. (1995). Interaction of tyrosine-based sorting signals with clathrin-associated proteins. *Science* 269, 1872-1875.

Onnis, A., and Baldari, C.T. (2019). Orchestration of Immunological Synapse Assembly by Vesicular Trafficking. *Front Cell Dev Biol* 7, 110.

Pechstein, A., Bacetic, J., Vahedi-Faridi, A., Gromova, K., Sundborger, A., Tomlin, N., Krainer, G., Vorontsova, O., Schafer, J.G., Owe, S.G., *et al.* (2010). Regulation of synaptic

vesicle recycling by complex formation between intersectin 1 and the clathrin adaptor complex AP2. *Proc Natl Acad Sci U S A* 107, 4206-4211.

Porritt, H.E., Gordon, K., and Petrie, H.T. (2003). Kinetics of steady-state differentiation and mapping of intrathymic-signaling environments by stem cell transplantation in nonirradiated mice. *J Exp Med* 198, 957-962.

Prockop, S.E., and Petrie, H.T. (2004). Regulation of thymus size by competition for stromal niches among early T cell progenitors. *J Immunol* 173, 1604-1611.

Regelin, M., Blume, J., Pommerencke, J., Vakilzadeh, R., Witzlau, K., Lyszkiewicz, M., Zietara, N., Saran, N., Schambach, A., and Krueger, A. (2015). Responsiveness of Developing T Cells to IL-7 Signals Is Sustained by miR-17 approximately 92. *J Immunol* 195, 4832-4840.

Reider, A., Barker, S.L., Mishra, S.K., Im, Y.J., Maldonado-Baez, L., Hurley, J.H., Traub, L.M., and Wendland, B. (2009). Syp1 is a conserved endocytic adaptor that contains domains involved in cargo selection and membrane tubulation. *EMBO J* 28, 3103-3116.

Reider, A., and Wendland, B. (2011). Endocytic adaptors--social networking at the plasma membrane. *J Cell Sci* 124, 1613-1622.

Robinson, M.S. (2015). Forty Years of Clathrin-coated Vesicles. *Traffic* 16, 1210-1238.
Rossi, F.M., Corbel, S.Y., Merzaban, J.S., Carlow, D.A., Gossens, K., Duenas, J., So, L., Yi, L., and Ziltener, H.J. (2005). Recruitment of adult thymic progenitors is regulated by P-selectin and its ligand PSGL-1. *Nat Immunol* 6, 626-634.

Rothenberg, E.V. (2014). Transcriptional control of early T and B cell developmental choices. *Annu Rev Immunol* 32, 283-321.

Rothenberg, E.V., Kueh, H.Y., Yui, M.A., and Zhang, J.A. (2016a). Hematopoiesis and T-cell specification as a model developmental system. *Immunol Rev* 271, 72-97.

Rothenberg, E.V., Ungerback, J., and Champhekar, A. (2016b). Forging T-Lymphocyte Identity: Intersecting Networks of Transcriptional Control. *Adv Immunol* 129, 109-174.

Roy-Chaudhuri, B., Valdmanis, P.N., Zhang, Y., Wang, Q., Luo, Q.J., and Kay, M.A. (2014). Regulation of microRNA-mediated gene silencing by microRNA precursors. *Nat Struct Mol Biol* 21, 825-832.

Sambandam, A., Maillard, I., Zediak, V.P., Xu, L., Gerstein, R.M., Aster, J.C., Pear, W.S., and Bhandoola, A. (2005). Notch signaling controls the generation and differentiation of early T lineage progenitors. *Nat Immunol* 6, 663-670.

Saran, N., Lyszkiewicz, M., Pommerencke, J., Witzlau, K., Vakilzadeh, R., Ballmaier, M., von Boehmer, H., and Krueger, A. (2010). Multiple extrathymic precursors contribute to T-cell development with different kinetics. *Blood* 115, 1137-1144.

Schaffert, S.A., Loh, C., Wang, S., Arnold, C.P., Axtell, R.C., Newell, E.W., Nolan, G., Ansel, K.M., Davis, M.M., Steinman, L., and Chen, C.Z. (2015). mir-181a-1/b-1 Modulates Tolerance through Opposing Activities in Selection and Peripheral T Cell Function. *J Immunol* 195, 1470-1479.

Schlenner, S.M., and Rodewald, H.R. (2010). Early T cell development and the pitfalls of potential. *Trends Immunol* 31, 303-310.

- Scimone, M.L., Aifantis, I., Apostolou, I., von Boehmer, H., and von Andrian, U.H. (2006). A multistep adhesion cascade for lymphoid progenitor cell homing to the thymus. *Proc Natl Acad Sci U S A* *103*, 7006-7011.
- Scollay, R., Smith, J., and Stauffer, V. (1986). Dynamics of early T cells: prothymocyte migration and proliferation in the adult mouse thymus. *Immunol Rev* *91*, 129-157.
- Scott, B., Bluthmann, H., Teh, H.S., and von Boehmer, H. (1989). The generation of mature T cells requires interaction of the alpha beta T-cell receptor with major histocompatibility antigens. *Nature* *338*, 591-593.
- Seo, W., and Taniuchi, I. (2016). Transcriptional regulation of early T-cell development in the thymus. *Eur J Immunol* *46*, 531-538.
- Serwold, T., Ehrlich, L.I., and Weissman, I.L. (2009). Reductive isolation from bone marrow and blood implicates common lymphoid progenitors as the major source of thymopoiesis. *Blood* *113*, 807-815.
- Stritesky, G.L., Jameson, S.C., and Hogquist, K.A. (2012). Selection of self-reactive T cells in the thymus. *Annu Rev Immunol* *30*, 95-114.
- Teh, H.S., Kisielow, P., Scott, B., Kishi, H., Uematsu, Y., Bluthmann, H., and von Boehmer, H. (1988). Thymic major histocompatibility complex antigens and the alpha beta T-cell receptor determine the CD4/CD8 phenotype of T cells. *Nature* *335*, 229-233.
- Telerman, A., Amson, R.B., Romasco, F., Wybran, J., Galand, P., and Mosselmans, R. (1987). Internalization of human T lymphocyte receptors. *Eur J Immunol* *17*, 991-997.
- Trop, S., Rhodes, M., Wiest, D.L., Hugo, P., and Zuniga-Pflucker, J.C. (2000). Competitive displacement of pT alpha by TCR-alpha during TCR assembly prevents surface coexpression of pre-TCR and alpha beta TCR. *J Immunol* *165*, 5566-5572.
- Uezu, A., Umeda, K., Tsujita, K., Suetsugu, S., Takenawa, T., and Nakanishi, H. (2011). Characterization of the EFC/F-BAR domain protein, FCHO2. *Genes Cells* *16*, 868-878.
- Umasankar, P.K., Sanker, S., Thieman, J.R., Chakraborty, S., Wendland, B., Tsang, M., and Traub, L.M. (2012). Distinct and separable activities of the endocytic clathrin-coat components Fcho1/2 and AP-2 in developmental patterning. *Nat Cell Biol* *14*, 488-501.
- Wallis, V.J., Leuchars, E., Chwalinski, S., and Davies, A.J. (1975). On the sparse seeding of bone marrow and thymus in radiation chimaeras. *Transplantation* *19*, 2-11.
- Willinger, T., Staron, M., Ferguson, S.M., De Camilli, P., and Flavell, R.A. (2015). Dynamin 2-dependent endocytosis sustains T-cell receptor signaling and drives metabolic reprogramming in T lymphocytes. *Proc Natl Acad Sci U S A* *112*, 4423-4428.
- Winter, S.J., and Krueger, A. (2019). Development of Unconventional T Cells Controlled by MicroRNA. *Front Immunol* *10*, 2520.
- Winter, S.J., Kunze-Schumacher, H., Imelmann, E., Grewers, Z., Osthues, T., and Krueger, A. (2019). MicroRNA miR-181a/b-1 controls MAIT cell development. *Immunol Cell Biol* *97*, 190-202.

Zhou, X., Jeker, L.T., Fife, B.T., Zhu, S., Anderson, M.S., McManus, M.T., and Bluestone, J.A. (2008). Selective miRNA disruption in T reg cells leads to uncontrolled autoimmunity. *J Exp Med* 205, 1983-1991.

Zietara, N., Lyszkiewicz, M., Puchalka, J., Witzlau, K., Reinhardt, A., Forster, R., Pabst, O., Prinz, I., and Krueger, A. (2015). Multicongenic fate mapping quantification of dynamics of thymus colonization. *J Exp Med* 212, 1589-1601.

Zietara, N., Lyszkiewicz, M., Witzlau, K., Naumann, R., Hurwitz, R., Langemeier, J., Bohne, J., Sandrock, I., Ballmaier, M., Weiss, S., *et al.* (2013). Critical role for miR-181a/b-1 in agonist selection of invariant natural killer T cells. *Proc Natl Acad Sci U S A* 110, 7407-7412.

Zlotoff, D.A., Sambandam, A., Logan, T.D., Bell, J.J., Schwarz, B.A., and Bhandoola, A. (2010). CCR7 and CCR9 together recruit hematopoietic progenitors to the adult thymus. *Blood* 115, 1897-1905.

6. Appendix

6.1 Multicongenic fate mapping quantification of dynamics of thymus colonisation

Ziętara N, Łyszkiewicz M, Puchalka J, Witzlau K, Reinhardt A, Förster R, Pabst O, Prinz I, Krueger A.

The Journal of Experimental Medicine 212(10), 1589-601 (2015).

Multicongenic fate mapping quantification of dynamics of thymus colonization

Natalia Ziętara,^{1*} Marcin Łyszkiewicz,^{1*} Jacek Puchałka,² Katrin Witzlau,¹ Annika Reinhardt,¹ Reinhold Förster,¹ Oliver Pabst,^{1,3} Immo Prinz,¹ and Andreas Krueger¹

¹Institute of Immunology, Hannover Medical School, D-30625 Hannover, Germany

²Dr. von Haunersches Kinderspital, University Children's Hospital, Ludwig Maximilian University, D-80337 Munich, Germany

³Institute of Molecular Medicine, RWTH Aachen University, D-52074 Aachen, Germany

Postnatal T cell development depends on continuous colonization of the thymus by BM-derived T lineage progenitors. Both quantitative parameters and the mechanisms of thymus seeding remain poorly understood. Here, we determined the number of dedicated thymus-seeding progenitor niches (TSPNs) capable of supporting productive T cell development, turnover rates of niche occupancy, and feedback mechanisms. To this end, we established multicongenic fate mapping combined with mathematical modeling to quantitate individual events of thymus colonization. We applied this method to study thymus colonization in *CCR7^{-/-}CCR9^{-/-}* (DKO) mice, whose TSPNs are largely unoccupied. We showed that ~160–200 TSPNs are present in the adult thymus and, on average, 10 of these TSPNs were open for recolonization at steady state. Preconditioning of wild-type mice revealed a similar number of TSPNs, indicating that preconditioning can generate space efficiently for transplanted T cell progenitors. To identify potential cellular feedback loops restricting thymus colonization, we performed serial transfer experiments. These experiments indicated that thymus seeding was directly restricted by the duration of niche occupancy rather than long-range effects, thus challenging current paradigms of thymus colonization.

At steady state, T cell development depends on continuous colonization of the thymus by BM-derived T-lineage progenitors. The nature of thymus-seeding progenitors (TSPs) has remained largely elusive. Various candidate populations have been proposed, including multipotent progenitors (MPPs) and lymphoid-restricted progenitors, as well as largely T-lineage-committed cells (Martin et al., 2003; Krueger and von Boehmer, 2007; Bell and Bhandoola, 2008; Wada et al., 2008; Schlenner et al., 2010; Luc et al., 2012). However, none of these BM-derived or circulating progenitors has a clearly detectable, phenotypically equivalent counterpart in adult thymus (Bhandoola et al., 2007). Consequently, it has been suggested that exposure to Notch signals in the thymus results in rapid phenotypic changes of TSPs (Krueger et al., 2006; Schwarz et al., 2007). We and others have shown that multiple progenitor populations, which can be

minimally defined by expression of CD27 and CD135, contribute to T cell development (Serwold et al., 2009; Saran et al., 2010). Phenotypic characterization of TSPs is hampered by the low numbers of cells entering the thymus, whereas, in turn, failure to phenotypically identify TSPs has precluded direct quantification of thymus colonization and its regulation. It has been proposed that the irradiated adult thymus is colonized by as few as 10–200 cells per day (Wallis et al., 1975; Kadish and Basch, 1976; Scollay et al., 1986). Parabiosis experiments have suggested a 2–3% daily turnover of cells within the progenitor niche at steady state (Donskoy and Goldschneider, 1992). Various assay systems have been applied to estimate the quantity of TSPs. Short-term transfers allow direct quantification

CORRESPONDENCE

Andreas Krueger:
Krueger.Andreas@mh-hannover.de
OR

Natalia Ziętara:
Natalia.Zietara@med.uni-muenchen.de

Abbreviations used: CMJ, cortico-medullary junction; DKO, *CCR7^{-/-}CCR9^{-/-}* double knockout mice; DN, double negative; DP, double positive; ETP, early T-lineage progenitor; i.t., intrathymic; lin, lineage; LSFM, light-sheet fluorescence microscopy; MPP, multipotent progenitor; SCZ, subcapsular zone; TEC, thymic epithelial cells; TSP, thymus-seeding progenitor; TSPN, thymus-seeding progenitor niche.

* N. Ziętara and M. Łyszkiewicz contributed equally to this paper.

© 2015 Ziętara et al. This article is distributed under the terms of an Attribution-Noncommercial-Share Alike-No Mirror Sites license for the first six months after the publication date (see <http://www.rupress.org/terms>). After six months it is available under a Creative Commons License (Attribution-Noncommercial-Share Alike 3.0 Unported license, as described at <http://creativecommons.org/licenses/by-nc-sa/3.0/>).

of homing (Scimone et al., 2006; Gossens et al., 2009). However, analysis of early time points precludes distinction between true TSPs that enter the T-lineage developmental pathway and cells that home to the thymus, but fail to differentiate further once inside the thymus. In contrast, long-term transfers selectively permit detection of T-lineage progeny derived from TSPs, but, in this case, intrathymic proliferation and differentiation events preclude straightforward interpretation of data (Wallis et al., 1975; Kadish and Basch, 1976; Scollay et al., 1986). Recently, a combination of short-term transfer followed by analysis of T-lineage potential *in vitro* was applied to estimate TSP numbers (Zhang et al., 2014). However, *in vitro* differentiation assays are highly sensitive and might result in an overestimate of true TSPs (Schlenner and Rodewald, 2010; Richie Ehrlich et al., 2011).

Thymus colonization by BM-derived progenitors is tightly controlled. It depends on various adhesion molecules, including integrins and P-selectin ligand (Lepique et al., 2003; Rossi et al., 2005; Scimone et al., 2006). In addition, chemokine receptors, particularly CCR7 and CCR9, are required for recruitment of BM-derived progenitors to the thymus (Krueger et al., 2010; Zlotoff et al., 2010). Of note, dependency on CCR7 and CCR9 is transiently alleviated after conditioning by irradiation (Zlotoff et al., 2011). To date, the mechanisms limiting progenitor input remain ill characterized. It has been suggested that receptivity of the thymus for progenitors is a periodic event, allowing for colonization approximately every 3.5 wk, possibly dependent on oscillating expression of P-selectin and CCL25 (Donskoy et al., 2003; Gossens et al., 2009). Furthermore, reconstitution experiments in IL-7R- and RAG-deficient mice suggested that thymus colonization is limited by a cellular feedback loop, in which the size of the DN2 and/or DN3 compartment likely restricted progenitor entry. However, the mechanisms underlying this feedback remain unknown.

In this study, we set out to quantitate the overall number of intrathymic microenvironmental niches capable of sustaining productive T cell development and to determine turnover rates of niche occupancy and feedback mechanisms. Extrathymic progenitors from CCR7^{-/-}CCR9^{-/-} (DKO) mice have a severe defect in colonizing a postnatal thymus, resulting in low numbers of early T-lineage progenitors (ETPs) in these mice (Krueger et al., 2010; Zlotoff et al., 2010). This phenotype suggested that DKO mice constituted an excellent model to study colonization of the adult thymus. Indeed, nonmanipulated DKO mice were readily susceptible to thymus seeding. Using these mice in combination with multi-congenic fate mapping of BM-derived progenitors revealed that the adult thymus contains ~160 TSP niches (TSPNs), 6% of which are accessible to recolonization at steady state. Furthermore, consecutive transplantation of congenically tagged progenitors into DKO mice showed that niche occupancy by ETPs is likely to directly control access to these microenvironmental niches. Thus, our study provided a quantitative model of colonization of the postnatal thymus and the underlying mechanisms.

RESULTS

Thymus of CCR7^{-/-}CCR9^{-/-} double knockout mice (DKO) is highly receptive for TSPs

To test the hypothesis that thymi of DKO mice are highly receptive for colonization by WT progenitors, BM-derived lineage-negative (lin⁻) progenitors (CD45.1) were transferred *i.v.* into nonmanipulated DKO and WT recipients (CD45.2). Thymus cellularity was substantially increased in DKO mice after transfer of WT cells, suggesting that recipient thymocytes were not replaced by donor-derived cells (Fig. 1 A). WT mice were largely refractory to thymus seeding by donor-derived cells, displaying a chimerism of ~0.2% at 21 d after transfer (Fig. 1, B and C). In contrast, in DKO recipients, ~50% percent of all thymocytes were of donor origin (Fig. 1, B and C). Developmental progression of donor cells within DKO recipients was normal and comparable to WT recipients 21 d after injection as assessed by CD4 and CD8 surface stainings (Fig. 1 B).

Some lin⁻ progenitors might first colonize BM before thymus seeding and might therefore generate a reservoir for its continuous colonization. Indeed, we detected slightly elevated frequencies (in the range of 1%) of donor cells in DKO spleen and BM compared with WT controls (Fig. 1 D). However, DKO recipients were also much more receptive after transfer of sorted CLPs, which were previously shown to give rise to a single wave of T cell development and do not colonize BM for extended periods of time (Scimone et al., 2006; Krueger and von Boehmer, 2007; Fig. 1, E and F). Of note, overall reconstitution by sorted CLPs was lower in both WT and DKO recipients when compared with lin⁻ BM cells (0.03 vs. 0.23% and 15 vs. 54%, respectively).

The numbers of ETPs and DN2 cells, but not other thymocyte populations, correlate with thymus receptivity

Whereas thymi of DKO mice are almost devoid of ETPs and DN2 cells, they only display a twofold reduction in DN3 cell numbers and mild alterations in numbers of more mature thymocytes (Krueger et al., 2010). This subset distribution suggested that increased thymic receptivity was a result of paucity in ETP/DN2 cells rather than more mature thymocytes. To test this hypothesis, we assessed thymus seeding of CCR7^{-/-} and CCR9^{-/-} single-deficient mice, which display intermediate phenotypes in subset cellularity. CCR7^{-/-} mice were slightly more receptive to seeding by congenic (CD45.1 plus CD45.1/2) WT lin⁻ progenitors displaying 3% donor-derived cells at 21 d after transfer when compared with 1% reconstitution of WT thymi (Fig. 2 A). Deficiency in CCR9 resulted in 11% donor-derived cells at 21 d after transfer, corresponding to an 11-fold increase in thymic receptivity when compared with WT recipients and a fourfold decrease when compared with DKO recipients (Fig. 2 A).

We correlated thymus receptivity to the abundance of various thymocyte subsets, including ETPs, DN2, DN3, and DP cells, in thymi of single mutant and DKO mice. We identified a strong inverse correlation of thymus receptivity with ETP

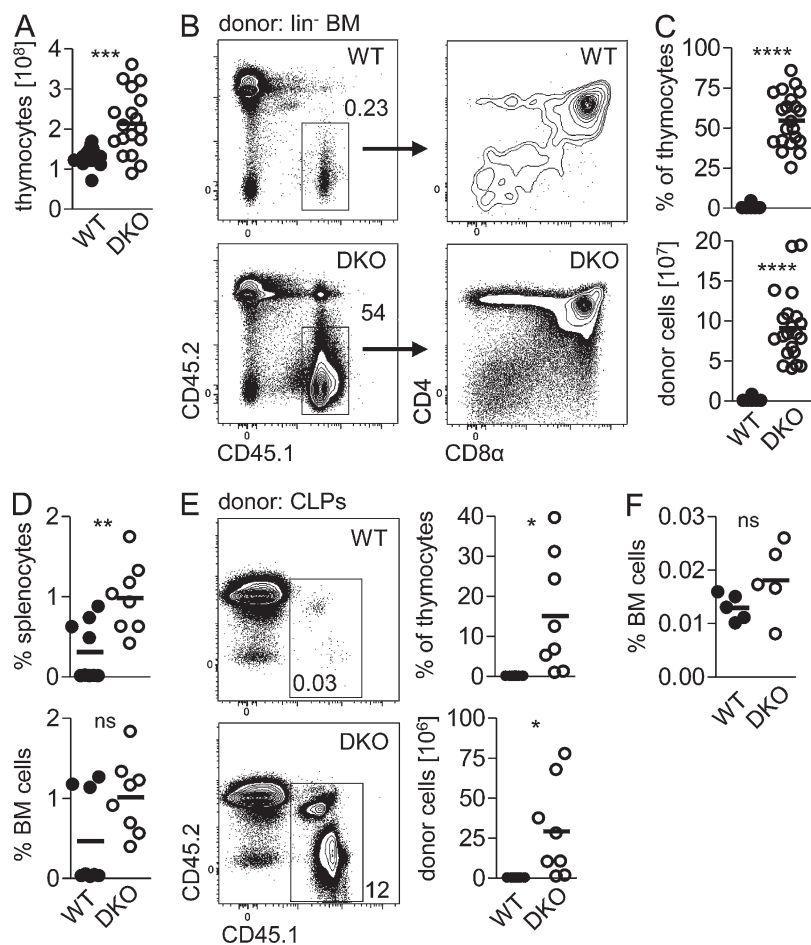


Figure 1. Thymi of $CCR7^{-/-}CCR9^{-/-}$ double deficient mice (DKO) are highly receptive for TSPs. Non-manipulated WT and DKO recipient mice (CD45.2) were injected i.v. with congenic (CD45.1) WT lin^{-} BM-derived precursors. (A) WT and DKO total thymocyte numbers 21 d after injection of WT lin^{-} BM-derived precursors. (B) Analysis of WT and DKO recipient thymi 21 d after injection of WT lin^{-} BM-derived precursors. Representative plots delineating donor and recipient cells (left) and CD8 α versus CD4 profiles of WT donor-derived cells (right). (C) Percentages and absolute numbers of WT donor cells within all thymocytes of WT and DKO recipients. Pooled data from five independent experiments are depicted. (D) Analysis of WT donor cells in spleen (top) and BM (bottom) of WT and DKO recipient mice 21 d after transfer of lin^{-} BM-derived progenitors. Pooled data from four independent experiments are depicted. (E) Analysis of WT and DKO thymi 21 d after injection of WT CLPs (CD45.1 and CD45.1/2). Representative plots of three independent experiments (left). Percentages and absolute numbers of donor cells within all thymocytes (right). (F) Analysis of WT donor cells in BM of WT and DKO recipient mice 21 d after transfer of CLPs. Data from three independent experiments. All recipient mice used in experiments shown in Fig. 1 were 4–6 wk old. Donor mice were 7–10 wk old. Each data point represents an individual mouse. Statistical analysis was performed using unpaired Student's *t* test, where ns, $P > 0.05$; *, $P \leq 0.05$; **, $P \leq 0.01$; ***, $P \leq 0.001$; ****, $P \leq 0.0001$.

and DN2 cell numbers (Fig. 2 B). In contrast, thymus receptivity did not correlate with numbers of DN3 and DP subsets.

Collectively, these data suggest that thymus receptivity depends on the presence of ETPs and DN2 cells, but not on other thymocyte subsets.

Spatial changes in thymic architecture do not accompany enhanced colonization of DKO thymus

TSPs enter the thymus from the bloodstream at the cortico-medullary junction (CMJ; Petrie and Zúñiga-Pflücker, 2007). Therefore, alterations in thymus morphology might account for increased receptivity of DKO thymi. Immunohistological analysis of thymus sections from DKO and WT mice revealed an altered pattern of medullary regions in DKO mice. In sections, medullary areas (Ker5⁺) were smaller in size, but their overall numbers were higher (Fig. 3, A and B). Combining reduced medullary area with increased numbers of medullary regions resulted in an increased ratio of cortical to medullary areas but an equal medullary perimeter per section (Fig. 3 B), suggesting that the overall size of the CMJ is not altered in DKO mice when compared with controls. To validate these conclusions, which were based on analysis in two dimensions, we used light-sheet fluorescence microscopy (LSFM) to assess thymus morphology in complete organs. Medullas

were visualized by staining with UEA-1, followed by quantification of cumulative surface area of UEA-1⁺ structures (Fig. 3 C and Video 1). DKO mice displayed a slightly increased total medullary area when compared with WT mice (Fig. 3 D, left). However, taking into account total thymus size, the relative size of medullary surfaces was comparable between WT and DKO thymi (Fig. 3 D, right). These data further support our conclusion that the size of the CMJ is not increased in thymi of DKO mice. Notably, the observed thymic architecture of DKO mice was highly reminiscent of that of $CCR7^{-/-}$ single-mutant mice (Misslitz et al., 2004; Ueno et al., 2004). Flow cytometric characterization of thymic stromal cells revealed reduced frequencies of medullary, but not cortical, thymic epithelial cells (TECs) or fibroblasts (Fig. 3 E). In addition, we found similar numbers of endothelial cells in DKO and WT thymi, suggesting that thymi of DKO mice do not contain an increased amount of vasculature (Fig. 3 E). Sorted nonhematopoietic cells did not display significant differences in mRNA expression of factors that mediate progenitor recruitment and survival, such as *Ccl19*, *Ccl21a*, *Ccl25*, *Selp* (P-selectin), and *Flt3l* (Fig. 3 F). Furthermore, we analyzed the distribution of cortical CD25^{hi} (DN2/DN3) thymocytes. In contrast to WT mice, which display an enrichment of DN2/DN3 cells at the subcapsular zone (SCZ), DKO mice

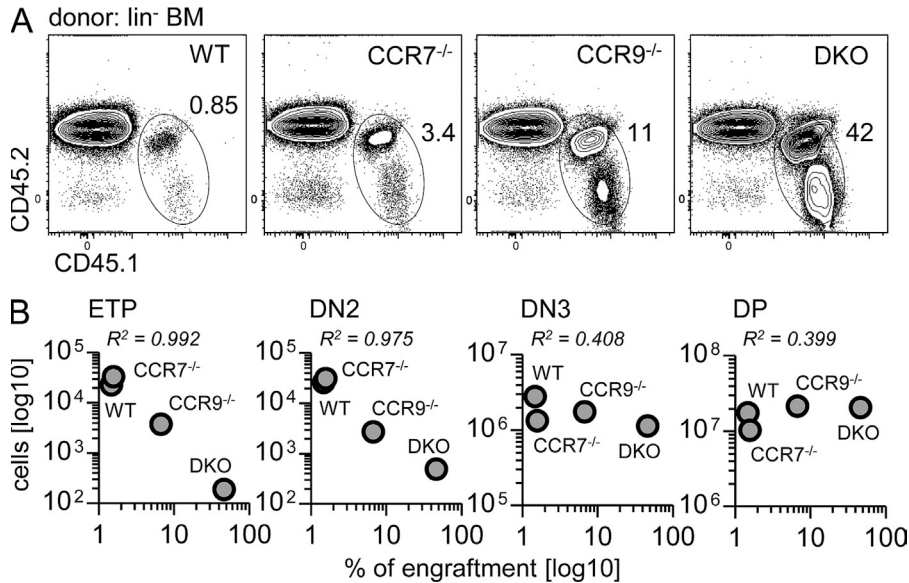


Figure 2. Thymus receptivity correlates with numbers of ETP and DN2 thymocytes. (A) Analysis of WT, CCR7^{-/-}, CCR9^{-/-}, and DKO thymi 21 d after transfer of congenic (CD45.1 and CD45.1/2) WT lin⁻ BM precursors. Representative plots of two independent experiments, $n = 6-8$ for each genotype. (B) Correlation between abundance of recipient thymocyte populations and thymus receptivity, depicted as percentage of engraftment. Recipient mice were 4–11 wk old. Donor mice were 7–8 wk old. Each data point represents an average of six to eight mice/genotype from two independent experiments. R^2 = coefficient of correlation.

showed an equal distribution of these cells, similar to what has been described for CCR9^{-/-} mice (Benz et al., 2004; Fig. 3, A and G). In summary, the thymic architecture of DKO mice combines the key features observed in CCR7^{-/-} and CCR9^{-/-} mice. Thus, we conclude that alterations in thymus morphology are unlikely to account for the massive increase in thymus receptivity of DKO mice when compared with either single mutant or WT mice.

Considering the profound increase in total thymus cellularity of DKO thymi 21 d after transfer of WT BM-derived progenitors, we determined whether the presence of large numbers of WT thymocytes was able to induce morphological changes toward a WT-like thymic architecture. To this end, we injected eGFP-tagged lin⁻ BM-derived progenitors into WT and DKO recipient mice and analyzed thymic sections 21 d later. Donor-derived cells predominantly localized to the medullary regions and to medulla-proximal regions of the cortex, as expected after 21 d of developmental progression (Fig. 3 H). After this period of time, we did not observe any gross changes in thymic architecture of DKO recipients. Therefore, WT-like thymic morphology fails to be induced in adult DKO mice even when up to 50% of thymocytes are CCR7 and CCR9 sufficient.

T-lineage reconstitution in DKO mice is independent of progenitor exit from circulation

Thymus receptivity might be controlled at various nonmutually exclusive levels. It may be regulated via restriction of transit of progenitors from the circulation into the thymic microenvironment, via presence of a defined number of microenvironmental niches and/or via facilitating rapid proliferation of TSPs. To test whether transition from blood stream to the thymic microenvironment contributes to increased receptivity of DKO thymi, we assessed T cell development after direct administration of progenitors into the thymus. Intrathymic transfer of WT congenic lin⁻CD117⁺CD135⁺ BM-derived

progenitors into DKO mice resulted in chimerism of ~40% when compared with 8% of WT mice (Fig. 4, A and B). Thus, in DKO mice, i.t. administration of progenitor cells resulted in equivalent levels of donor-derived T cell development when compared with i.v. administration, whereas in WT recipients i.t. administration resulted in higher levels of reconstitution when compared with the i.v. route. These data indicate that the receptive state in DKO mice is independent of active transition of progenitors from circulation to the thymic microenvironment and suggest that higher degrees of chimerism might be prevented by competition within more mature thymocyte populations. In contrast, in WT mice it is possible that i.t. transfer provides a competitive advantage over endogenous circulating TSPs.

To investigate whether faster proliferation rates of WT progenitors contributed to high donor chimerism within the DKO thymus, we tested incorporation of BrdU after a single 4-h pulse 14 and 21 d after transfer. At 14 d after transfer, donor-derived cells displayed slightly increased BrdU incorporation in DKO recipients when compared with controls, whereas no differences were observed after 21 d (Fig. 4 C). Minute frequencies of donor-derived cells, especially in WT recipients, precluded analysis of proliferation rates at earlier time points.

Thus, we conclude that intrathymic proliferation may in part contribute to enhanced T-lineage reconstitution in DKO mice, whereas active transition from circulation to the thymus appears to play a very limited role. These data suggest that availability of microenvironmental niches may to a large extent account for increased thymic receptivity of DKO mice.

Quantification of the adult thymus progenitor niche using multicongenic fate mapping

Next, we sought to determine the number of available microenvironmental TSPNs in DKO and WT mice. We hypothesized that this number corresponded directly to the number

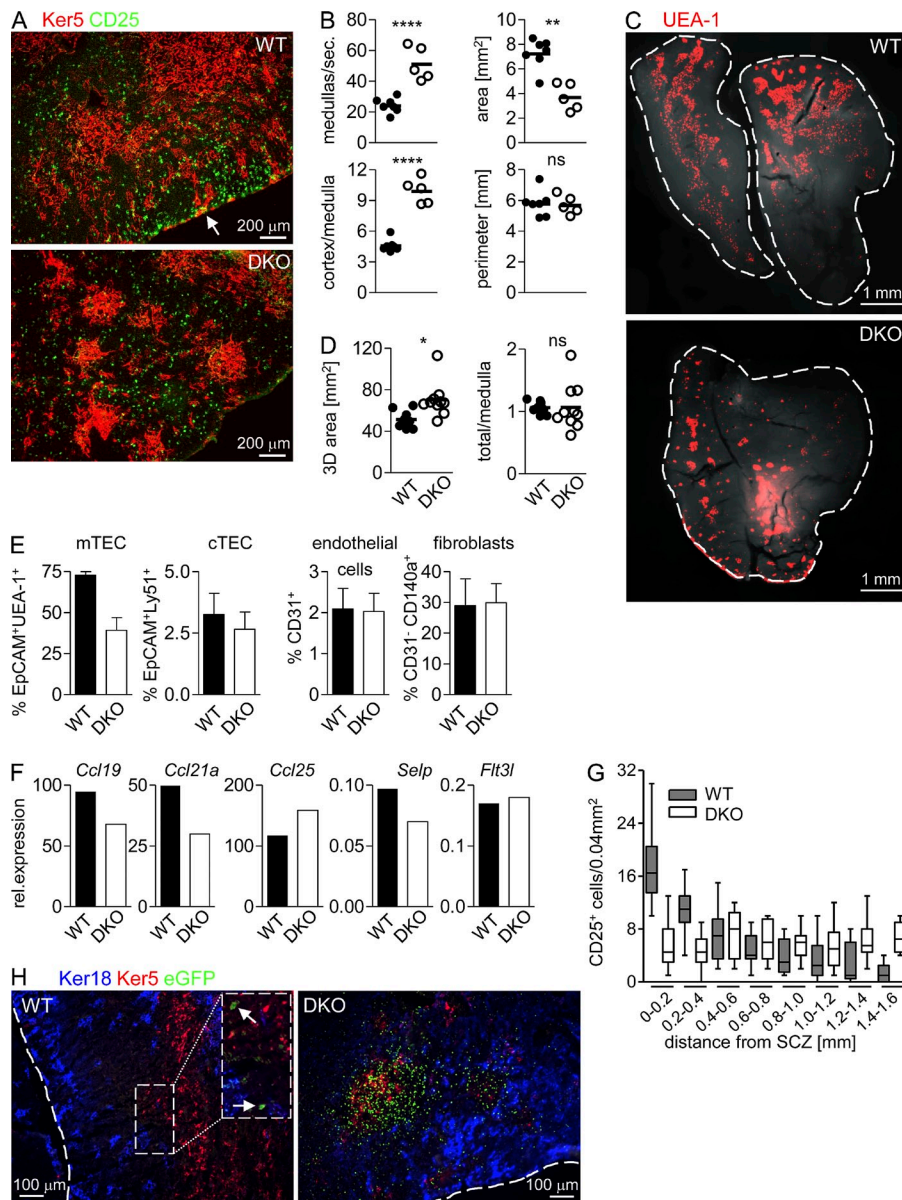


Figure 3. Thymic architecture of DKO recipient mice remains altered after WT progenitor entry. (A–G) Analysis of WT and DKO thymi without prior transfer. (A) Immunofluorescence microscopy of thymus cryosections from WT and DKO mice. Sections were stained with anti-cytokeratin 5 (Ker5, red) and anti-CD25 (green) antibodies. Arrowhead indicates accumulation of CD25^{hi} cells (DN2 and DN3 thymocytes) at the SCZ of WT thymus. Representative sections of three to four thymi/genotype from two independent experiments are shown. (B) Quantification of medullas per section (sec.), their total area, perimeter and cortex to medulla ratios on cryosections of WT and DKO mice. Each dot represents one section of an entire thymus per mouse analyzed in two independent experiments. Statistical analysis was performed using unpaired Student's *t* test, where ns, $P > 0.05$; *, $P \leq 0.05$; **, $P \leq 0.01$; ****, $P \leq 0.0001$. (C) Light-sheet fluorescence microscopy (LSFM) of WT and DKO thymi. Medullas were labeled with UEA-1 (red). Representative images of virtual sections of five mice/genotype analyzed in two independent experiments are depicted. (D) Quantification of 3D areas of medullary regions (left) visualized by LSFM and their contribution within total thymic surface area (right). (E) Frequencies of mTECs (CD45⁺EpCAM⁺UEA-1⁺), cTECs (CD45⁺EpCAM⁺Ly51⁺), endothelial cells (CD45⁺CD31⁺), and fibroblasts (CD45⁺EpCAM⁺CD31⁺CD140a⁺) shown as percentage of nonhematopoietic cells (CD45⁺). Pooled data from three independent experiments are depicted. $n = 3$ –6/genotype. Data are represented as mean + SEM. (F) Gene expression analysis of sorted nonhematopoietic cells of WT and DKO mice by qRT-PCR. mTECs were analyzed for expression of *Ccl19* and *Ccl21a*, cTECs were analyzed for expression of *Ccl25*, thymic endothelial cells were analyzed for expression of P-selectin (*Selp*), and fibroblasts were analyzed for expression of *Flt3l*. Experiments were performed with RNA samples isolated from 5–7 pooled thymi for each genotype. Data from one representative experiment are depicted. (G) Quantification of distance of CD25⁺ cells from SCZ. 200 × 1,600 μm areas were defined on two different regions of section (two random sections for two mice per genotype from two independent experiments as shown in A) using ImageJ software. CD25⁺ cells were counted on 200 × 200 μm squares. Data are represented as mean ± SEM. (H) Immunofluorescence microscopy of thymus cryosections from WT and DKO recipient mice 21 d after transfer of eGFP-tagged BM precursors. Sections were stained with anti-cytokeratin 18 Ab (Ker18, blue) and anti-cytokeratin 5 (Ker5, red) to visualize thymic cortex and medulla. Arrowheads indicate single eGFP-positive cells (green). Representative sections from three mice for each genotype in one experiment are depicted. Mice used for experiments depicted in Fig. 3 were 4–6 wk old. Donor mice in H were 11 wk old.

were analyzed for expression of *Flt3l*. Experiments were performed with RNA samples isolated from 5–7 pooled thymi for each genotype. Data from one representative experiment are depicted. (G) Quantification of distance of CD25⁺ cells from SCZ. 200 × 1,600 μm areas were defined on two different regions of section (two random sections for two mice per genotype from two independent experiments as shown in A) using ImageJ software. CD25⁺ cells were counted on 200 × 200 μm squares. Data are represented as mean ± SEM. (H) Immunofluorescence microscopy of thymus cryosections from WT and DKO recipient mice 21 d after transfer of eGFP-tagged BM precursors. Sections were stained with anti-cytokeratin 18 Ab (Ker18, blue) and anti-cytokeratin 5 (Ker5, red) to visualize thymic cortex and medulla. Arrowheads indicate single eGFP-positive cells (green). Representative sections from three mice for each genotype in one experiment are depicted. Mice used for experiments depicted in Fig. 3 were 4–6 wk old. Donor mice in H were 11 wk old.

of TSPs productively colonizing the thymus, i.e., giving rise to T-lineage progeny, at a given time point. To quantitate productive thymus seeding, we devised an approach of multicongenetic fate mapping. To this end, we generated mouse strains expressing various combinations of congenic markers and/or reporter genes as tags allowing flow cytometric separation of cells of up to 12 distinct origins (Fig. S1 and Table S1; Buchholz et al., 2013). A Monte-Carlo simulation-based algorithm was generated to derive the number of TSPNs from the number

of tags missing from donor-derived progeny (Fig. S2 A). This simulation was adopted from a method for estimating the number of bacteria founding an infection (Lim et al., 2014). It is based on the assumption that each TSP has the same capacity to populate a TSPN, irrespective of its congenic tag. Under this assumption, the probability that a TSP with a given tag populates a TSPN is proportional to the fraction of TSPs carrying this tag in the input population. In this scenario, low numbers of niches and/or the presence of tags with

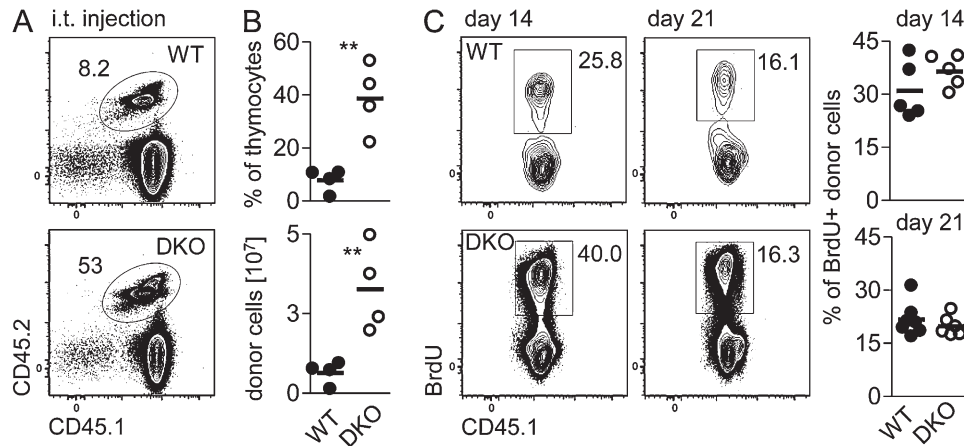


Figure 4. T-lineage reconstitution in DKO mice is independent of progenitor exit from circulation and intrathymic proliferation. (A) Analysis of thymi of WT and DKO recipient mice (CD45.2) 21 d after i.t. transfer of WT BM precursors (CD45.1/2). Representative plots of two independent experiments are depicted, $n = 4$. (B) Percentages and absolute numbers of donor cells within all thymocytes from experiments shown in A. (C) Analysis of BrdU incorporation in donor cells 14 and 21 d after i.v. injection of lin^{-} BM-derived precursors (CD45.1) into WT and DKO recipients (CD45.2). Density plots (left) and percentage of BrdU-positive cells within all donor cells (right). Recipient mice were 5 wk old. Donor mice were 8 wk old. Each data point represents one mouse. Data are representative of two independent experiments. Statistical analysis was performed using unpaired Student's *t* test, where **, $P \leq 0.01$.

low frequencies in the input population should result in failure of some tags to be recovered from donor-derived progeny. Consequently, the mixture of tags had to be composed depending on the suspected number of TSPNs. Counting missing tags then enabled assessment of the number of niches by simulating, several times, colonization events for a given number of TSPNs and then counting cases whenever the result of the simulation was equal to that of the experiment. Performing this procedure for a range of TSPN numbers and averaging the counts permitted identification of a range of most probable TSPN numbers provided that thymus seeding was restricted to a discrete colonization event. Pulse-chase experiments had shown that direct thymus colonization after transfer was essentially complete after 4 h (Spangrude and Weissman, 1988). Thus, circulating cells did not contribute detectably to a potentially extended phase of colonization. Furthermore, defined mixtures of BM-derived progenitors ($lin^{-}CD117^{+}CD135^{+}$), which lack the capacity of long-term engraftment of BM, were used in most fate mapping experiments, thus restricting the generation of a BM-resident source of TSPs. Finally, all donor-derived populations recovered displayed similar developmental progression as assessed by surface staining of CD4 and CD8, with most cells being at the DP and CD4 SP stages and very few DN cells detectable (Fig. S2 B). This finding suggested that all niches were occupied within a similar time frame and that loss of tags below the limit of detection indeed reflected failure to occupy a niche rather than a mere developmental delay. Differential analysis of tags at the DN and DP stages showed that DN and DP cells consistently contained a similar distribution of tags, with no tags being selectively present in DN cells but absent from DP cells. This analysis indicated that most, if not all, donor-derived cells originated from one discrete colonization event defined as within 4 h of transfer. In addition, experiments were designed

in a way that the total number of transferred cells corresponded to saturating levels, which were originally determined to be in the range of 20×10^6 total BM cells (Foss et al., 2002). Accordingly, $4.5\text{--}15 \times 10^4$ $lin^{-}CD117^{+}CD135^{+}$ progenitors, which were previously reported to contain all TSPs and constitute $\sim 0.5\%$ of total BM were transferred (Serwold et al., 2009; Saran et al., 2010). T-lineage potential of CLPs *in vivo* was reported to be in the range of 1 in 20 and it is likely to be in a similar range for lymphoid-primed MPPs, suggesting that sufficient numbers of progenitors were present in the least frequent individually tagged populations (Kondo et al., 1997).

21 d after transfer of defined mixtures of congenically tagged progenitors into WT, DKO, and IL-7R α -deficient recipients, the frequency of all donor-derived populations was determined (Table S1). IL-7R α -deficient mice have been described to be particularly receptive for thymus seeding and were therefore chosen as positive control (Prockop and Petrie, 2004). The sensitivity of the experimental approach was assessed using a Delete-d Jackknife estimation of variance, which showed that the standard deviation of the predicted median did not exceed 20% (Fig. S2 C).

Donor-derived thymocytes in DKO recipients originated from ~ 160 TSPNs (Fig. 5 A). As these mice display high thymic receptivity in conjunction with barely detectable levels of ETPs and DN2 cells, as well as normal levels of key ligands for thymus homing, we suggest that this number is likely to be close to the maximum number of TSPNs available in an empty adult nonconditioned thymus. Interestingly, despite their high degree of responsiveness, IL-7R α -deficient thymi contained only 24 TSPNs. 10 TSPNs were on average colonized by exogenous progenitors in WT mice, suggesting that at steady-state $\sim 6\%$ of TSPNs may be accessible. Furthermore, the distribution of individual progenitor tags in different WT recipients was more heterogeneous than in IL-7R $\alpha^{-/-}$

and DKO recipients (Fig. 5 B). This indicates that entry of BM-derived progenitors into the thymus is a stochastic event.

In conclusion, multicongenic fate mapping provided additional evidence that thymus receptivity directly depended on the availability of unoccupied intrathymic progenitor niches. Furthermore, our data suggested that the total number of microenvironmental progenitor niches in the adult thymus is as low as 160, 6% of which are replenished on average at steady state.

Conditioning of WT and IL-7R $\alpha^{-/-}$ mice through sublethal irradiation liberates TSPNs

Treatment with alkylating agents and/or irradiation is used as conditioning regimen before BM transplantation and affects thymus seeding and T-lineage reconstitution in multiple ways. Multicongenic fate mapping allowed us to directly assess the effect of irradiation on the availability of TSPNs. To this end, sublethally irradiated (4.5 Gy) WT, IL-7R $\alpha^{-/-}$ mice, and non-manipulated DKO mice received a defined mixture of BM-derived progenitors from multicongenic donors. 21 d after transfer, TSPN size was assessed using Monte Carlo simulation as described above. Thymi of sublethally irradiated WT mice contained a similar number of TSPNs as nonmanipulated DKO mice (Fig. 6, A and B). Furthermore, numbers of TSPNs in irradiated IL-7R $\alpha^{-/-}$ mice were increased by fourfold when compared with nonmanipulated IL-7R $\alpha^{-/-}$ mice (Fig. 6, A and B). These data indicate that conditioning through irradiation promotes thymus colonization by liberation of TSPNs and further support the hypothesis that the number of TSPNs identified in DKO mice likely corresponds to the near maximum of TSPNs in the adult thymus.

Occupancy of niches by ETPs regulates thymus seeding

Experiments with CCR7 $^{-/-}$, CCR9 $^{-/-}$, and DKO mice suggested that thymus receptivity was in part controlled by cellular feedback from ETPs and/or DN2 cells (Fig. 2). To investigate cellular feedback restricting progenitor entry at greater details, we again took advantage of the constitutive empty-niche status of DKO mice and multicongenic donor mouse strains. Such progenitors were transferred sequentially at 3-d intervals for 21 d, so that each recipient carried 8 distinct donor cell populations in total (Table S2). Thus, potential periodicity of thymus colonization could be directly assessed within an individual animal. 6 wk after the final transfer, spleens were analyzed for the presence of mature donor-derived T cells. At this time point, the vast majority of progeny of donor cells has dwelled in the periphery for at least 2 wk. Therefore, no bias based on post-thymic proliferation during maturation of recent thymic emigrants should be expected (Boursalian et al., 2004; Föhse et al., 2013). In consequence, frequencies of donor-derived T cells should directly reflect thymic entry of progenitors. Donor cells from transfers at day 0, 12, and 21 contributed the majority of donor-derived T cells with frequencies of $\sim 20\%$ each (Fig. 7 A). In contrast, progenitors transferred at day 3, 6, 15, and 18 gave rise to $\sim 5\%$ each and cells transferred at day 9 generated $\sim 10\%$ of all donor-derived T cells. Thus, the frequency distribution of donor-derived splenic T cells from sequential transfers into DKO hosts reflected a periodicity of 9–12 d for thymus colonization of an initially empty recipient. Data from an analogous experiment using WT recipients showed a similar periodicity, although initial colonization was less efficient, presumably due to competition with endogenous TSPs (Fig. 7 B).

Given that the average life-time of ETPs was determined to be in the range of 10–12 d (Porritt et al., 2003), we conclude

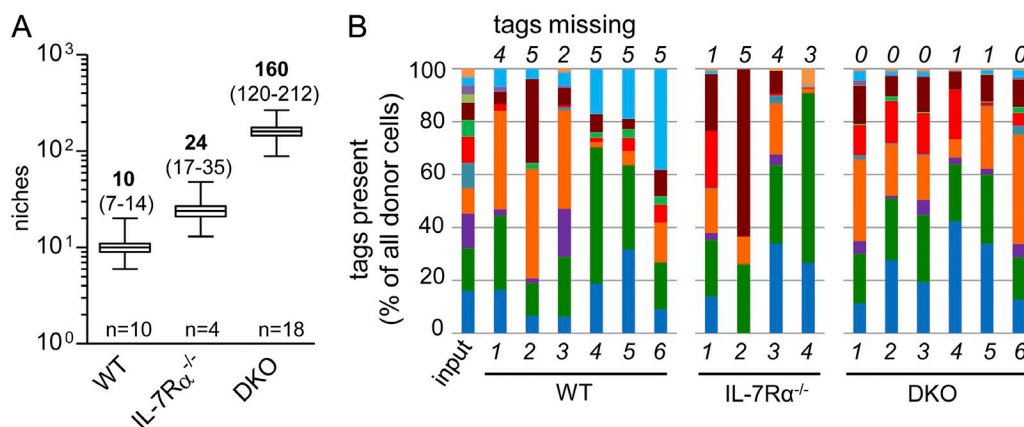


Figure 5. Quantification of early intrathymic niches using multicongenic fate mapping. Up to 12-code library of congenic/fluorescent tagged BM progenitors (multicongenic library) was generated by intercrossing of several mouse strains (Table S1). A mixture (4.8×10^4 to 15×10^4 cells/recipient mouse) consisting of defined ratios of such progenitors (Table S1, input [I], [II], and [III]) was injected into nonmanipulated WT and DKO recipient mice (three independent experiments). Thymi of recipient mice were analyzed 21 d after progenitor injection. (A) Quantification of TSPNs was performed using an algorithm based on Monte Carlo simulation. Bold numbers above each boxplot represent the median number of TSPNs for each genotype. Numbers in brackets indicate 95% confidence intervals. Data from two experiments are depicted, $n = 10$ (WT), $n = 4$ (IL-7R $\alpha^{-/-}$), $n = 18$ (DKO). (B) Distribution of individual tags (each color represents one tag) within donor cells (100%) in different recipient mice 21 d after transfer. Input bar represents distribution of 12 tags within the progenitor mixture, which was injected into individual recipients at day 0. Numbers above each column indicate missing tags in each representative recipient; $n = 6$ (WT), $n = 4$ (IL-7R $\alpha^{-/-}$), $n = 6$ (DKO). Recipient mice were 4 to 7 wk old. Donor mice were 7 to 10 wk old.

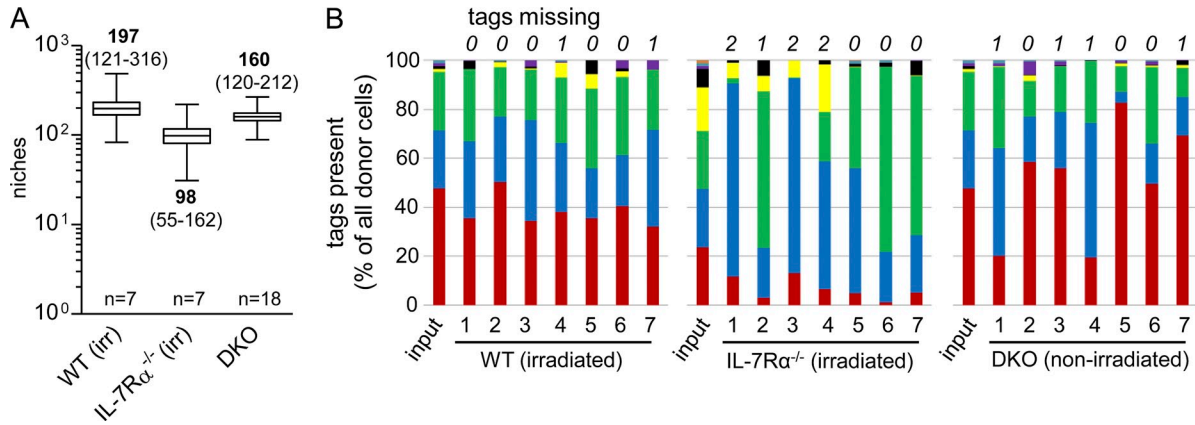


Figure 6. Conditioning of WT mice through irradiation fully liberates progenitor niches. Eight-code library of congenic/fluorescently tagged BM progenitors (multicongenic library) was generated by intercrossing of several mouse strains (Table S1). A mixture (4×10^6 lin⁻ BM cells/recipient mouse) consisting of defined ratios of such progenitors (Table S1, input [IV]) was injected into sublethally irradiated (4.5 Gy) WT and nonmanipulated DKO recipient mice. A mixture (4.5×10^4 [V] and 13×10^4 [VI]) of lin⁻CD117⁺Flt3⁺ sorted BM cells/recipient mouse consisting of defined ratios of such progenitors (Table S1, input [V] and [VI]) was injected into sublethally irradiated (4.5 Gy) IL-7Rα^{-/-} mice. Thymi of recipient mice were analyzed 21 d after progenitor injection. (A) Quantification of TSPNs was performed as described for Fig. 5. Bold numbers above each boxplot represent the median number of TSPNs for each genotype. Numbers in brackets indicate 95% confidence intervals; $n = 7$ (WT irradiated, one experiment), $n = 7$ (IL-7Rα^{-/-} irradiated, 2 experiments), $n = 18$ (DKO, 2 experiments). (B) Distribution of individual tags (each color represents one tag) within donor cells (100%) in different recipient mice 21 d after transfer. Input bar represents distribution of 8 tags within the progenitor mixture, which was injected into individual recipients at day 0. Numbers above each column indicate missing tags in each representative recipient; $n = 7$ (WT irradiated), $n = 7$ (IL-7Rα^{-/-} irradiated), $n = 7$ (DKO). Recipient mice were 4–13 wk old. Donor mice were 7–10 wk old.

from these data that the occupancy of microenvironmental niches by ETPs is likely to constitute the predominant factor restricting access of progenitors to the adult thymus. These data also provide additional evidence that determination of TSPNs by multicongenic fate mapping, indeed, reflected a single colonization event rather than a continuous process.

DISCUSSION

Here, we have established CCR7^{-/-}CCR9^{-/-} (DKO) mice as a model to study quantitative aspects of colonization of adult thymus without prior conditioning and cellular mechanisms restricting import of T lineage progenitors. Our data support a model, in which the average adult murine thymus contains ~160 microenvironmental niches for colonization by BM-derived progenitor cells. At steady state, ~6% of these niches can be replenished at any given time. Comparison of single-mutant and DKO mice indicated that thymus receptivity inversely correlated with numbers of ETPs and DN2

cells. Furthermore, microenvironmental progenitor niches can be refilled with a periodicity of 9–12 d. This number corresponds well to the lifetime of ETPs. Therefore, it is likely that niche occupancy is controlled by self-restriction and niches are liberated by developmental progression of ETPs occupying such niches.

Different strategies and mouse models have been used to study thymus colonization. Irradiation has been used to empty progenitor niches in order to quantify niches or “synchronize” colonization to analyze cellular feedback. However, irradiation causes multiple and difficult to control alterations in thymic architecture and cellular composition; it also alters expression of chemokines and cytokines, resulting in receptivity for progenitors that do not normally settle the adult thymus (Zubkova et al., 2005; Schwarz et al., 2007; Kenins et al., 2008). IL-7Rα-deficient mice also display a high degree of thymic receptivity (Prockop and Petrie, 2004). Although the overall composition of thymocytes by and large corresponds

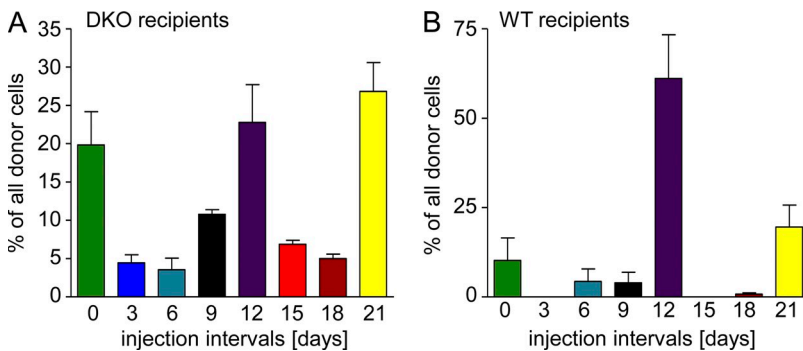


Figure 7. Occupancy of niches by ETPs regulates thymus seeding. Multicongenic BM-derived progenitors were injected into DKO recipient mice, one individual tag (10^6 of lin⁻ BM cells/recipient mouse) every 3 d for 21 d. Analysis of donor-derived splenic T cells was performed 42 d after the final injection. (A) Quantification of donor cells within all splenocytes of DKO recipient mice. (B) Quantification of donor cells within all splenocytes of WT recipient mice. Data are representative of two independent experiments, $n = 7-12$ recipients/genotype. Recipient mice were 5 and 6 wk old. Donor mice were 7–8 wk old.

to that of WT mice in these mice, total thymic cellularity is massively reduced. However, small thymus size did not sufficiently explain our finding that nonmanipulated IL-7R $\alpha^{-/-}$ mice only contained 24 TSPNs, because preconditioning by irradiation was able to liberate additional TSPNs. In contrast to DKO mice, accessibility of TSPNs might not constitute the sole mechanism underlying increased thymic receptivity in IL-7R α -deficient mice. Rather, it is conceivable that in these mice, WT TSPs compete favorably for IL-7 as survival cue. Thus, multiple factors are likely to contribute to the observation of high thymus receptivity, including accessibility of TSPNs, as well as intrathymic competitive advantages for pro-survival and proliferative cues.

Nonmanipulated mice represent the gold standard to assess quantity and regulation of progenitor niches. However, even taking into account periodicity of thymus colonization and use of recipients at an age of optimum receptivity did not result in progenitor entry compared with that of IL-7R $\alpha^{-/-}$ or DKO mice, thus precluding the use of WT mice in quantitative approaches (Gossens et al., 2009). DKO mice display normal thymic cellularity and a gross composition of thymocytes similar to WT mice (Krueger et al., 2010; Zlotoff et al., 2010). However, numbers of ETP and DN2 subsets are massively reduced and numbers of DN3 cells are somewhat reduced, due to a defect of canonical BM-derived progenitors to enter the thymus (Krueger et al., 2010; Zlotoff et al., 2010). Here, we showed that thymi of DKO mice share morphological features of both single mutant mouse strains with smaller but more numerous medullary regions and lack of accumulation of DN2/3 thymocytes at the SCZ. However, similar frequencies of endothelial cells, length and surface area of the CMJ as entry point for progenitors, and expression of homing molecules between DKO and WT mice suggest that altered thymic morphology does not significantly contribute to increased thymic receptivity in DKO mice. Therefore, we concluded that DKO mice represent a valid model for study colonization of the adult thymus.

We combined this model with an approach of combinatorial multicongenetic fate mapping, which allowed us to discriminate up to 12 distinct populations of donor-derived cells. This approach circumvents pitfalls of conventional long- and short-term assays. Short-term homing assays have allowed recovery of comparatively large numbers of donor-derived cells (Mori et al., 2001; Scimone et al., 2006). Although there is no evidence that at steady state, in vivo only a fraction of cells entering the thymus finally ends up in the T-lineage; the majority of cells detectable in the thymus early after transfer is eventually lost (Mori et al., 2001). In contrast, analysis after extended periods of time ensures that only true T-lineage progenitors are taken into account. Moreover, the use of multiple tagged donor populations permitted direct quantification of the original input independent of intrathymic proliferation events. Of note, transfer of mixed populations of donor cells had already been reported four decades ago (Wallis et al., 1975; Ezine et al., 1984). However, limitation to two distinct donor populations permitted only rough estimates of the size of the

TSP pool. Recently, short-term transfers have been combined with subsequent in vitro differentiation thus circumventing detection of false-positive cells that lack T lineage potential (Saran et al., 2010; Zhang et al., 2014). However, although this approach reliably excludes non-T-lineage progenitors, it does not discriminate between homed cells at large and those that indeed entered microenvironments required for productive T cell development.

Combinatorial fate mapping assays using DKO and WT recipients indicated the presence of a total of 160 thymic niches that can be colonized by BM-derived progenitors. 6% of these niches could be replenished, on average, in WT mice. Interestingly, the number obtained for DKO mice, corresponding to the total number of microenvironmental niches lies within the same range as in irradiated animals (Wallis et al., 1975; Kadish and Basch, 1976; Scollay et al., 1986; Spangrude and Scollay, 1990). These studies proposed a range from as few as 10 up to 170 progenitor cells as saturating number of TSPs to fully reconstitute an irradiated thymus. Combinatorial fate mapping analysis in irradiated recipients showed directly that conditioning through irradiation indeed liberated TSPNs, in addition to alterations in thymus size and cellular composition. These findings are in apparent contradiction with a recent study showing that irradiation restricted thymus colonization rather than promoting it as a consequence of loss of intrathymic availability of CCL25 (Zhang et al., 2014). Different doses of irradiation might account for the observed discrepancy, although the effect of lower irradiation doses on expression of intrathymic CCL25 remains to be explored.

Our data indicate that the availability of TSPNs directly depends on the presence of progenitors occupying these niches. These findings are in contrast to a model based on comparison between IL-7R α -deficient and RAG-deficient mice, proposing that more mature, DN3, thymocytes provide direct feedback to restrict thymus colonization (Prockop and Petrie, 2004). However, the extent to which small thymus size and profound alterations in thymic morphology in RAG-deficient animals prevent thymus seeding has not been explored. Elevated levels of expression of *Psel* and *Ccl25* mRNA have been suggested to mediate increased thymus receptivity in IL-7R α -deficient mice (Gossens et al., 2009). Interestingly, neither *Psel* nor *Ccl25* levels were elevated in DKO mice, suggesting that both molecular cues as well as niche occupancy itself may limit thymus colonization in a nonexclusive manner.

Comparison of the contribution of different donor populations showed that CLPs generated a lower degree of chimerism in both WT and DKO recipients when compared with lin^- BM progenitors. This finding might imply that the thymus harbors progenitor-type specific TSPNs. However, it has been shown that CLPs only very transiently contribute to T cell development whereas MPPs, which are also present in lin^- progenitors, sustain T cell development for extended periods of time even after i.t. administration (Saran et al., 2010; Schwarz et al., 2007). Thus, limited reconstitution of the DKO thymus by CLPs as assessed after 21 d is best explained by the transient nature of their progenitor activity.

Sequential transfer experiments in individual DKO mice revealed a periodicity of thymus colonization of 9–12 d. These data are consistent with a previous study showing that thymi of irradiated mice are receptive at 2-wk intervals after i.t. transfer (Foss et al., 2002). As all TSPNs in DKO mice can be considered empty, it is conceivable that this periodicity reflects duration of niche occupation at the individual niche level and is therefore likely to be masked at steady state. Notably, i.v. transfers and parabiosis experiments suggested longer refractory periods of 3–4 wk (Foss et al., 2001, 2002). Analysis of DKO mice at defined ages did not reveal any age-dependent alterations in thymus receptivity. These observations again point toward multiple independent mechanisms controlling thymus seeding and underscore the potential of DKO mice to dissect cellular and molecular mechanisms of colonization of the adult thymus.

Recently, it has been reported that in the absence of cellular competition, intrathymic T cell development becomes autonomous and ultimately results in the formation of T cell leukemia (Peaudecerf et al., 2012; Martins et al., 2012, 2014). These findings highlight the critical role of intercellular communication, directly or via competitive niche occupation. Our findings complement these data by showing that “old” progenitors are not simply pushed away by newcomers, but are rather capable of restricting continual influx from BM. Thus, intercellular communication between early thymocytes at various times after entry into the thymus appears to be pivotal to ensure balanced T cell development. Furthermore, the concept of cellular competition in the thymus predicts that progenitors from DKO mice are less competitive when compared with their WT counterpart. Therefore, it will be interesting to test whether transplantation of WT thymi into DKO mice, and thus competition not only for cytokines but also for location, will result in donor-thymus autonomous T cell development and leukemogenesis.

MATERIALS AND METHODS

Mice. C57BL/6J mice (CD45.2), B6.SJL-*Ptpr^cPep^b/Boy*J mice (termed B6 CD45.1 throughout this manuscript) and IL-7R α -deficient mice (B6.129S7-*Il7rm1Imx/J*) were purchased from Charles River or The Jackson Laboratory or bred at the animal facility of Hannover Medical School. (C57BL/6J x B6 CD45.1) F1 mice (CD45.1/CD45.2 heterozygous) were bred at the animal facility of Hannover Medical School (Hannover, Germany). CCR7^{-/-} (Förster et al., 1999), CCR9^{-/-} (Wurbel et al., 2001), and CCR7^{-/-}CCR9^{-/-} (DKO) mice were backcrossed to the C57BL/6 background for at least eight generations. B6.Cg-Thy1 (B6.Thy1.1), B6.Tg(*Actb-eGFP*) reporter mice (Okabe et al., 1997), and B6.Tg(*Actb-eCFP*) reporter mice (Hadjantonakis et al., 2002) were bred at the animal facility of Hannover Medical School. F1 mice of different fluorescent reporter/congenic intercrosses were bred at the animal facility of Hannover Medical School. Animals were maintained under specific pathogen-free conditions. Mouse care and experimental procedures were performed in accordance with German animal welfare legislation under the approval of the local authorities (Niedersächsisches Landesamt für Verbraucherschutz und Lebensmittelsicherheit, LAVES).

Isolation of lin⁻ BM precursors. Lin⁻ cells were isolated from total BM by labeling of single cell suspensions with a lineage-specific purified rat-anti-mouse-IgG antibody cocktail (anti-CD4, anti-CD8, anti-CD19, anti-CD11b, anti-Gr-1, Ter-119, and anti-NK1.1, all from eBioscience) followed

by incubation with sheep-anti-rat-IgG magnetic beads (Dyna; Invitrogen) and magnetic bead depletion of mature lineages. Lin⁻ BM cells were used directly for injection in some of the experiments or for further cell sorting. Donor mice used for isolation of lin⁻ cells were always 7–10 wk old.

Flow cytometry and cell sorting. Monoclonal antibodies specific for CD4 (RM4-5, GK1.5), CD8 (53-6.7), CD25 (PC61), CD44 (IM7), Gr-1 (RB6-8C5), erythroid cell marker (Ter-119), CD19 (1D3), CD11b (M1/70), pan-NK (DX5), CD45.1 (A20), CD45.2 (104), B220 (RA3-6B2), CD117 (2B8, ACK2), Sca-1 (E13-161.7), CD135 (A2F10), CD127 (A7R.34), BrdU (3D4), were used as biotin, Pacific Blue, fluorescein isothiocyanate (FITC), Alexa Fluor 488, phycoerythrin (PE), peridinin chlorophyll protein-Cy5.5 (PerCP-Cy5.5), PE-Cy7, allophycocyanin (APC), APC-Cy7, or APC-eFluor780 conjugates. Antibodies were purified from hybridoma supernatants using standard procedures or were purchased from eBioscience, BD, or BioLegend. Common lymphoid progenitor (CLP) cells were sorted from lineage-depleted BM as: lin⁻Sca-1⁺CD117^{low/+}CD127⁺CD135⁺. Samples were acquired on an LSR II (BD) and sorted on a FACSAria II (BD). Data were analyzed with FlowJo software, v.9.4.9 (Tree Star). For analysis, dead cells and debris were excluded by gating of forward and side scatter. Sorted cells were of 98% or higher purity, as determined by reanalysis.

Intrathymic transfers. Mice (5 wk) were anesthetized with Ketamin/Rompun (Albrecht GmbH/Bayer; 10 mg/ml/0.04%/mouse in 150 μ l) via i.p. injection and fixed in dorsal recumbency. A small, 4–5 mm transverse incision was made in the skin over the first intercostal space perpendicular to the sternum so that the second rib could be observed clearly. The needle entrance position was in the center of the first intercostal space and the needle angle at \sim 90 degrees relative to the sternum. The injection volume was 20 μ l. The proper injection depth was \sim 3.5–4 mm according to age of the mouse and thymus size and thickness. The skin incision was closed using wound clips. Thymi were analyzed after 21 d for donor-derived cells.

BrdU incorporation. BrdU (Sigma-Aldrich) was injected i.p. (3 mg/mouse) 4 h before analysis. BrdU incorporation was analyzed using the FITC BrdU Flow kit (BD) according to the manufacturer's protocol. Samples were acquired on an LSR II (BD) and analyzed using FlowJo software (Tree Star).

Immunohistology. Thymi were excised from 5–6-wk-old age-matched mice, rinsed in PBS, embedded in Tissue-Tek O.C.T. (Sakura; Finetek), and frozen on dry ice. 8- μ m cryosections were fixed for 10 min in ice-cold acetone and rehydrated in Tris-buffered saline with 0.05% Tween-20, blocked with 10% goat or mouse serum, and stained with the following antibodies at room temperature for 45 min. Rat anti-CD25 Alexa Fluor 488 (PC61 5.3; Invitrogen), polyclonal rabbit anti-cytokeratin 5 (Abcam), washed, and followed by staining with secondary goat anti-rabbit-Cy3 (Jackson ImmunoResearch Laboratories) for 45 min at room temperature. For analysis of thymi after injection of eGFP-tagged BM-derived precursors thymi were first fixed in 2% PFA and 30% sucrose overnight, washed in PBS, and embedded in O.C.T. medium. Sections were stained with monoclonal mouse anti-mouse cytokeratin 18 and biotin conjugated (Abcam), followed by incubation with streptavidin-Cy5 (eBioscience) and with rabbit anti-cytokeratin 5 as described above.

Immunohistological analysis of thymus sections was performed at room temperature using a motorized epifluorescence microscope (BX61; UPlanSApo; objective 10 \times /0.4) equipped with a fluorescence camera (F-View II) and CellSens software (Olympus). Quantification of CD25^{hi} cells was performed with ImageJ software (Schneider et al., 2012). Quantification of medullas and their perimeters and areas was performed using CellSens software (Polygon tool; Olympus).

Isolation and sorting of thymic nonhematopoietic cells. Thymi were excised from 5–6-wk-old age-matched mice, rinsed in PBS, cut into small pieces, collected in plain RPMI-1640, and incubated for 1 h at 4°C with gentle rotations to remove excess thymocytes. Supernatant was removed and

remaining tissue pieces were incubated with Collagenase D (0.2 mg/ml; Roche), Dispase Grade I (0.2 mg/ml; Roche), and DNase-I (0.025 mg/ml; Roche) 2 times for 15 min at 37°C with mixing every 5 min. Cells were collected on ice and incubated with 5 mM EDTA for 10 min. Nonhematopoietic cells were enriched after staining with rat anti-mouse CD45 antibody (30-F11; eBioscience), followed by incubation with sheep anti-rat magnetic beads (Invitrogen) and magnetic depletion. Cells were stained before FACS sorting using the following antibodies: anti-CD45 APC (30-F11; eBioscience), anti-EpCAM eFluor450 (G8.8; eBioscience), anti-Ly51 FITC (6C3; BD), anti-CD31 FITC (390; eBioscience), anti-CD140a PE (APA5; eBioscience), UEA-1 Rhodamine (Vector Laboratories). Cells were sorted on a FACSaria II with 130 μ m nozzle at low speed as follows: cTECs, CD45⁻EpCAM⁺Ly51⁺; mTECs, CD45⁻EpCAM⁺UEA-1⁺; endothelial cells, CD45⁻CD31⁺; fibroblasts, CD45⁻EpCAM⁻CD31⁻CD140a⁺. Sorted cells were of 94–96% purity, as determined by reanalysis.

LSFM. Thymi were excised from 5-wk-old mice and fixed overnight at 4°C in PBS with 2% PFA and 30% sucrose. Further sample preparation was adapted from Renier et al. (2014) and Yokomizo et al. (2012). All steps were performed at room temperature. Samples were washed three times for 1 h in PBS, twice for 1 h in PBS with 0.2% Triton X-100 (Sigma-Aldrich), followed by two additional washing steps for 1 h in PBS with 1% Triton X-100. After overnight permeabilization in PBS with 1% Triton X-100, thymi were blocked in PBS with 0.5% Triton X-100, and 4% BSA for 3 d. After blocking, samples were washed twice for 1 h in PBS with 0.2% Tween-20 (Carl Roth) and stained for 4 d with UEA-1 Rhodamine (Vector Laboratories) in PBS with 0.2% Triton X-100 and 2% BSA. After staining, thymi were sequentially washed in PBS with 0.2% Tween-20 for 10, 30, 60, 120 min for 3 d, and finally in PBS for 15, 30, and 60 min. Sample clearing was performed as previously described (Ertürk et al., 2012) with minor modifications. Thymi were dehydrated in 50% tetrahydrofuran (THF; Sigma-Aldrich) for 2 h, 75% THF, and 100% THF for 3 h each, and finally overnight in 100% THF. Samples were cleared in dibenzylether (Sigma-Aldrich) and directly imaged after clearing was completed. Fluorescence images were acquired using a light-sheet microscope (Ultramicroscope II; LaVision BioTec) equipped with a sCMOS camera (Andor Neo) and a 2 \times /0.5 objective lens. 3D projections were analyzed with Imaris software (version 7.7.2; Bitplane).

qRT-PCR. RNA was prepared from samples with equal cell numbers using the RNeasy Mini kit according to the manufacturer's instructions (QIAGEN). Room temperature reaction was performed using SuperScript II Reverse transcription (Invitrogen) and Oligo(dT)₁₂₋₁₈ primers (Invitrogen) according to the manufacturer's protocol. Quantitative RT-PCR analysis of miRNA expression was performed using the following TaqMan probes (Applied Biosystems): *Cd25*, Mm00436443_m1; *Cd19*, Mm00839967_g1; *Cd21a*, Mm03646971_gH; *Selp*, Mm01295931_m1; *Flt3l*, Mm00442801_m1. Fold differences were calculated using the ΔC_t method normalized to *Hprt* as housekeeping gene (Mm00446968_m1; Applied Biosystems). Reactions were performed using a StepOne Real-Time PCR System (Applied Biosystems).

Quantification of intrathymic niches using Monte Carlo simulation. DKO and WT nonmanipulated recipient mice (experiment I [WT 6 wk old, DKO 6 wk old], II [WT 4 wk old, DKO 4 wk old, IL-7R α ^{-/-} 7 wk old], and III [WT 5 wk old, DKO 5 and 6 wk old]) were i.v. injected with defined mixtures (Table S1, input ratios/percentages) of BM progenitors, sorted as lin⁻CD117^{lo/+}CD135⁺ cells.

In the experiment number IV, V, and VI, empty intrathymic niches were generated by sublethal irradiation (4.5 Gy) of WT and IL-7R α ^{-/-} recipient mice (DKO), and some WT recipients were nonmanipulated (experiment IV [WT 9 wk old, DKO 6 and 9 wk old], experiment V [IL-7R α ^{-/-} 13 wk old], experiment VI [IL-7R α ^{-/-} 4 wk old]). Cell numbers used in individual experiments are indicated in figure legends and Table S1. Proportions of different congenic populations are indicated in Table S1. Donors and recipients mice were sex-matched to prevent deletion caused by XY-chromosome incompatibility.

Thymi of recipient mice were analyzed 21 d after injection by flow cytometry. In total, 2.5×10^6 events were acquired per sample. Each individually tagged population was identified by its surface/fluorescent phenotype (Fig. S1) within total thymocytes of recipients and considered absent upon detection of <40 events (10 events were detected on average in these samples). On average, 4,800 events were detected in the least frequent populations considered present. Quantification of intrathymic niches was performed using an algorithm based on Monte Carlo simulation. This quantification was performed for each group (each experiment and each mouse genotype, non-manipulated DKO, IL-7R α ^{-/-} and WT, as well as irradiated WT in experiment IV, and irradiated IL-7R α ^{-/-} in experiment V and VI), for which the experimental missing set was determined (i.e., the set containing, for each mouse in the group, the number of missing tags).

First, the number of accessible niches was set (niche-count). Subsequently, colonization was simulated by randomly determining which tag occupies every niche. The probability that a certain tag occupies a niche was proportional to its fraction in the tag pool. After the tag for every niche was determined, the number of tags that did not occupy any niche was determined and stored as the results of the simulation. This simulation was repeated, as many times as there were mice in the group, and the results of these were collected together to build one simulated missing set. If this set was equal to the set obtained experimentally for that group, the initially set number of niches was stored, as the result of one simulation of the invasion experiment. The simulation of the invasion experiment was repeated 10,000 times, so that between zero and 10,000 results were stored, constituting the result-set for given niche-count. This whole procedure was run iteratively starting from niche-count equal to 1 and increasing it by 1. The execution was stopped, when for five consecutive niche-counts, the result-set was empty and the niche count was greater than 130 (empirical value). The results-sets were merged together to build the final result-set for the group. If this set contained <10,000 elements, the number of repetitions of simulations of the invasion experiment was increased from 10,000 to a value that assured that the final result-set is of a length of at least 10,000. Finally, for each group 10,000 elements from the final result-set of each group were chosen randomly (with uniform probability), and these sub-sets were used to compute statistics for each group. The algorithm was implemented in R software suite (version 2.15.2; Team, 2012).

Repeated injections of multicongenic BM precursors. 5-wk-old DKO and WT nonmanipulated recipient mice were intravenously injected at 3-d intervals with equal amounts of an individually tagged population of lin⁻ congenic BM progenitors each (10^6 cells/injection day/recipient mouse) for 21 d (Table S2). Spleens of recipient mice were analyzed 6 wk after the final injection. Each individually tagged population was identified by its surface/fluorescent phenotype within total splenocytes of recipient mice.

Statistical analysis. All analysis except for the quantification of intrathymic niches was performed using GraphPad Prism software. Data are represented as mean + SEM or \pm SEM, as indicated. Analysis of significance between 2 groups of mice was performed using unpaired Student's *t* tests, where ns, $P > 0.05$; *, $P \leq 0.05$; **, $P \leq 0.01$; ***, $P \leq 0.001$; ****, $P \leq 0.0001$.

To assess the efficiency of the simulation approach to estimate intrathymic niches, we performed Delete-d Jackknife estimation of variance. In this procedure a set of subsampled results is generated from the original result, by removing a predefined number of single measurements. This yields a set of $\binom{n}{k} = \frac{n!}{(n-k)! \times k!}$ results, where *n* is the group size and *k* the count of elements that were removed. Then the simulation is performed on each set member and the results are collected. As several results are obtained for each original result, the estimation of variance is possible. We performed this procedure for each group, while removing 25% of single experiments (rounded to the nearest integer) and running the simulation for every unique combination of missing clones (as single experiments lead often to the same number of missing clones, there are significantly fewer unique combinations than the total derived by the above formula). The result of such simulation was then weighted according to prevalence of the corresponding combination.

Online supplemental material. Figs. S1 and S2 contain data that support Figs. 1–7. Table S1 contains combinations of alleles used to generate multi-congenic precursors library, their proportions and cell numbers used in individual experiments. Table S2 lists the sequence of injections used to determine cellular feedback which restricts thymus seeding. Video 1 contains LSFM analysis of WT and DKO thymi. Online supplemental material is available at <http://www.jem.org/cgi/content/full/jem.20142143/DC1>.

We thank Harald von Boehmer for critical reading of the manuscript and helpful discussions. We are grateful to Dr. Henrike Fleige and Stefanie Willenzon for help with immunohistology experiments, David Mzinza for help with LSFM, and Mathias Herberg for maintenance of mouse colonies. We would like to acknowledge the assistance of the Cell Sorting Core Facility of the Hannover Medical School supported in part by Braukmann-Wittenberg-Herz-Stiftung and German Research Foundation (DFG).

The work was supported by grants from the German Research Foundation (DFG; Emmy-Noether Program, KR2320/2-1; SFB738-A7; KR2320/3-1, and EXC62, "Rebirth"; to A. Krueger).

The authors declare no competing financial interests.

Author contributions: N. Ziętara, M. Łyszkiewicz, K. Witzlau, and A. Reinhardt performed experiments; N. Ziętara, M. Łyszkiewicz, J. Puchałka, A. Reinhardt, and A. Krueger analyzed data; N. Ziętara, M. Łyszkiewicz, J. Puchałka, A. Reinhardt, I. Prinz, and A. Krueger designed experiments; R. Förster and O. Pabst provided vital tools; N. Ziętara, M. Łyszkiewicz, J. Puchałka, and A. Krueger wrote the manuscript; A. Krueger conceived of the study.

Submitted: 14 November 2014

Accepted: 10 August 2015

REFERENCES

- Bell, J.J., and A. Bhandoola. 2008. The earliest thymic progenitors for T cells possess myeloid lineage potential. *Nature*. 452:764–767. <http://dx.doi.org/10.1038/nature06840>
- Benz, C., K. Heinzl, and C.C. Bleul. 2004. Homing of immature thymocytes to the subcapsular microenvironment within the thymus is not an absolute requirement for T cell development. *Eur. J. Immunol.* 34:3652–3663. <http://dx.doi.org/10.1002/eji.200425248>
- Bhandoola, A., H. von Boehmer, H.T. Petrie, and J.C. Zúñiga-Pflücker. 2007. Commitment and developmental potential of extrathymic and intrathymic T cell precursors: plenty to choose from. *Immunity*. 26:678–689. <http://dx.doi.org/10.1016/j.immuni.2007.05.009>
- Boursalian, T.E., J. Golob, D.M. Soper, C.J. Cooper, and P.J. Fink. 2004. Continued maturation of thymic emigrants in the periphery. *Nat. Immunol.* 5:418–425. <http://dx.doi.org/10.1038/ni1049>
- Buchholz, V.R., M. Flossdorf, I. Hensel, L. Kretschmer, B. Weissbrich, P. Gräf, A. Verschoor, M. Schiemann, T. Höfer, and D.H. Busch. 2013. Disparate individual fates compose robust CD8⁺ T cell immunity. *Science*. 340:630–635. <http://dx.doi.org/10.1126/science.1235454>
- Donskoy, E., and I. Goldschneider. 1992. Thymocytopoiesis is maintained by blood-borne precursors throughout postnatal life. A study in parabiotic mice. *J. Immunol.* 148:1604–1612.
- Donskoy, E., D. Foss, and I. Goldschneider. 2003. Gated importation of prothymocytes by adult mouse thymus is coordinated with their periodic mobilization from bone marrow. *J. Immunol.* 171:3568–3575. <http://dx.doi.org/10.4049/jimmunol.171.7.3568>
- Ertürk, A., K. Becker, N. Jährling, C.P. Mauch, C.D. Hojer, J.G. Egen, F. Hellal, F. Bradke, M. Sheng, and H.U. Dodt. 2012. Three-dimensional imaging of solvent-cleared organs using 3DISCO. *Nat. Protoc.* 7:1983–1995. <http://dx.doi.org/10.1038/nprot.2012.119>
- Ezine, S., I.L. Weissman, and R.V. Rouse. 1984. Bone marrow cells give rise to distinct cell clones within the thymus. *Nature*. 309:629–631. <http://dx.doi.org/10.1038/309629a0>
- Föhse, L., A. Reinhardt, L. Oberdörfer, S. Schmitz, R. Förster, B. Malissen, and I. Prinz. 2013. Differential postselection proliferation dynamics of $\alpha\beta$ T cells, Foxp3⁺ regulatory T cells, and invariant NKT cells monitored by genetic pulse labeling. *J. Immunol.* 191:2384–2392. <http://dx.doi.org/10.4049/jimmunol.1301359>
- Förster, R., A. Schubel, D. Breitfeld, E. Kremmer, I. Renner-Müller, E. Wolf, and M. Lipp. 1999. CCR7 coordinates the primary immune response by establishing functional microenvironments in secondary lymphoid organs. *Cell*. 99:23–33. [http://dx.doi.org/10.1016/S0092-8674\(00\)80059-8](http://dx.doi.org/10.1016/S0092-8674(00)80059-8)
- Foss, D.L., E. Donskoy, and I. Goldschneider. 2001. The importation of hematogenous precursors by the thymus is a gated phenomenon in normal adult mice. *J. Exp. Med.* 193:365–374. <http://dx.doi.org/10.1084/jem.193.3.365>
- Foss, D.L., E. Donskoy, and I. Goldschneider. 2002. Functional demonstration of intrathymic binding sites and microvascular gates for prothymocytes in irradiated mice. *Int. Immunol.* 14:331–338. <http://dx.doi.org/10.1093/intimm/14.3.331>
- Gossens, K., S. Naus, S.Y. Corbel, S. Lin, F.M. Rossi, J. Kast, and H.J. Ziltener. 2009. Thymic progenitor homing and lymphocyte homeostasis are linked via S1P-controlled expression of thymic P-selectin/CCL25. *J. Exp. Med.* 206:761–778. <http://dx.doi.org/10.1084/jem.20082502>
- Hadjantonakis, A.K., S. Macmaster, and A. Nagy. 2002. Embryonic stem cells and mice expressing different GFP variants for multiple non-invasive reporter usage within a single animal. *BMC Biotechnol.* 2:11. <http://dx.doi.org/10.1186/1472-6750-2-11>
- Kadish, J.L., and R.S. Basch. 1976. Hematopoietic thymocyte precursors. I. Assay and kinetics of the appearance of progeny. *J. Exp. Med.* 143:1082–1099. <http://dx.doi.org/10.1084/jem.143.5.1082>
- Kenins, L., J.W. Gill, R.L. Boyd, G.A. Holländer, and A. Wodnar-Filipowicz. 2008. Intrathymic expression of Flt3 ligand enhances thymic recovery after irradiation. *J. Exp. Med.* 205:523–531. <http://dx.doi.org/10.1084/jem.20072065>
- Kondo, M., I.L. Weissman, and K. Akashi. 1997. Identification of clonogenic common lymphoid progenitors in mouse bone marrow. *Cell*. 91:661–672. [http://dx.doi.org/10.1016/S0092-8674\(00\)80453-5](http://dx.doi.org/10.1016/S0092-8674(00)80453-5)
- Krueger, A., and H. von Boehmer. 2007. Identification of a T lineage-committed progenitor in adult blood. *Immunity*. 26:105–116. <http://dx.doi.org/10.1016/j.immuni.2006.12.004>
- Krueger, A., A.I. Garbe, and H. von Boehmer. 2006. Phenotypic plasticity of T cell progenitors upon exposure to Notch ligands. *J. Exp. Med.* 203:1977–1984. <http://dx.doi.org/10.1084/jem.20060731>
- Krueger, A., S. Willenzon, M. Łyszkiewicz, E. Kremmer, and R. Förster. 2010. CC chemokine receptor 7 and 9 double-deficient hematopoietic progenitors are severely impaired in seeding the adult thymus. *Blood*. 115:1906–1912. <http://dx.doi.org/10.1182/blood-2009-07-235721>
- Lepique, A.P., S. Palencia, H. Irjala, and H.T. Petrie. 2003. Characterization of vascular adhesion molecules that may facilitate progenitor homing in the post-natal mouse thymus. *Clin. Dev. Immunol.* 10:27–33. <http://dx.doi.org/10.1080/10446670310001598492>
- Lim, C.H., S. Voedisch, B. Wahl, S.F. Rouf, R. Geffers, M. Rhen, and O. Pabst. 2014. Independent bottlenecks characterize colonization of systemic compartments and gut lymphoid tissue by salmonella. *PLoS Pathog.* 10:e1004270. <http://dx.doi.org/10.1371/journal.ppat.1004270>
- Luc, S., T.C. Luis, H. Boukarabila, I.C. Macaulay, N. Buza-Vidas, T. Bouriez-Jones, M. Lutteropp, P.S. Woll, S.J. Loughran, A.J. Mead, et al. 2012. The earliest thymic T cell progenitors sustain B cell and myeloid lineage potential. *Nat. Immunol.* 13:412–419. <http://dx.doi.org/10.1038/ni.2255>
- Martin, C.H., I. Aifantis, M.L. Scimone, U.H. von Andrian, B. Reizis, H. von Boehmer, and F. Gounari. 2003. Efficient thymic immigration of B220⁺ lymphoid-restricted bone marrow cells with T precursor potential. *Nat. Immunol.* 4:866–873. <http://dx.doi.org/10.1038/ni965>
- Martins, V.C., E. Ruggiero, S.M. Schlenner, V. Madan, M. Schmidt, P.J. Fink, C. von Kalle, and H.R. Rodewald. 2012. Thymus-autonomous T cell development in the absence of progenitor import. *J. Exp. Med.* 209:1409–1417. <http://dx.doi.org/10.1084/jem.20120846>
- Martins, V.C., K. Busch, D. Juraeva, C. Blum, C. Ludwig, V. Rasche, F. Lasitschka, S.E. Mastitsky, B. Brors, T. Hielscher, et al. 2014. Cell competition is a tumour suppressor mechanism in the thymus. *Nature*. 509:465–470. <http://dx.doi.org/10.1038/nature13317>
- Misslitz, A., O. Pabst, G. Hintzen, L. Ohl, E. Kremmer, H.T. Petrie, and R. Förster. 2004. Thymic T cell development and progenitor localization depend on CCR7. *J. Exp. Med.* 200:481–491. <http://dx.doi.org/10.1084/jem.20040383>

- Mori, S., K. Shortman, and L. Wu. 2001. Characterization of thymus-seeding precursor cells from mouse bone marrow. *Blood*. 98:696–704. <http://dx.doi.org/10.1182/blood.V98.3.696>
- Okabe, M., M. Ikawa, K. Kominami, T. Nakanishi, and Y. Nishimune. 1997. 'Green mice' as a source of ubiquitous green cells. *FEBS Lett.* 407:313–319. [http://dx.doi.org/10.1016/S0014-5793\(97\)00313-X](http://dx.doi.org/10.1016/S0014-5793(97)00313-X)
- Peaudecerf, L., S. Lemos, A. Galgano, G. Krenn, F. Vasseur, J.P. Di Santo, S. Ezine, and B. Rocha. 2012. Thymocytes may persist and differentiate without any input from bone marrow progenitors. *J. Exp. Med.* 209:1401–1408. <http://dx.doi.org/10.1084/jem.20120845>
- Petrie, H.T., and J.C. Zúñiga-Pflücker. 2007. Zoned out: functional mapping of stromal signaling microenvironments in the thymus. *Annu. Rev. Immunol.* 25:649–679. <http://dx.doi.org/10.1146/annurev.immunol.23.021704.115715>
- Porritt, H.E., K. Gordon, and H.T. Petrie. 2003. Kinetics of steady-state differentiation and mapping of intrathymic-signaling environments by stem cell transplantation in nonirradiated mice. *J. Exp. Med.* 198:957–962. <http://dx.doi.org/10.1084/jem.20030837>
- Prockop, S.E., and H.T. Petrie. 2004. Regulation of thymus size by competition for stromal niches among early T cell progenitors. *J. Immunol.* 173:1604–1611. <http://dx.doi.org/10.4049/jimmunol.173.3.1604>
- Renier, N., Z. Wu, D.J. Simon, J. Yang, P. Ariel, and M. Tessier-Lavigne. 2014. iDISCO: a simple, rapid method to immunolabel large tissue samples for volume imaging. *Cell*. 159:896–910. <http://dx.doi.org/10.1016/j.cell.2014.10.010>
- Richie Ehrlich, L.I., T. Serwold, and I.L. Weissman. 2011. In vitro assays misrepresent in vivo lineage potentials of murine lymphoid progenitors. *Blood*. 117:2618–2624. <http://dx.doi.org/10.1182/blood-2010-05-287102>
- Rossi, F.M., S.Y. Corbel, J.S. Merzaban, D.A. Carlow, K. Gossens, J. Duenas, L. So, L. Yi, and H.J. Ziltener. 2005. Recruitment of adult thymic progenitors is regulated by P-selectin and its ligand PSGL-1. *Nat. Immunol.* 6:626–634. <http://dx.doi.org/10.1038/ni1203>
- Saran, N., M. Łyszkiewicz, J. Pommerencke, K. Witzlau, R. Vakilzadeh, M. Ballmaier, H. von Boehmer, and A. Krueger. 2010. Multiple extrathymic precursors contribute to T-cell development with different kinetics. *Blood*. 115:1137–1144. <http://dx.doi.org/10.1182/blood-2009-07-230821>
- Schlenner, S.M., and H.R. Rodewald. 2010. Early T cell development and the pitfalls of potential. *Trends Immunol.* 31:303–310. <http://dx.doi.org/10.1016/j.it.2010.06.002>
- Schlenner, S.M., V. Madan, K. Busch, A. Tietz, C. Läufler, C. Costa, C. Blum, H.J. Fehling, and H.R. Rodewald. 2010. Fate mapping reveals separate origins of T cells and myeloid lineages in the thymus. *Immunity*. 32:426–436. <http://dx.doi.org/10.1016/j.immuni.2010.03.005>
- Schneider, C.A., W.S. Rasband, and K.W. Eliceiri. 2012. NIH Image to ImageJ: 25 years of image analysis. *Nat. Methods*. 9:671–675. <http://dx.doi.org/10.1038/nmeth.2089>
- Schwarz, B.A., A. Sambandam, I. Maillard, B.C. Harman, P.E. Love, and A. Bhandoola. 2007. Selective thymus settling regulated by cytokine and chemokine receptors. *J. Immunol.* 178:2008–2017. <http://dx.doi.org/10.4049/jimmunol.178.4.2008>
- Scimone, M.L., I. Aifantis, I. Apostolou, H. von Boehmer, and U.H. von Andrian. 2006. A multistep adhesion cascade for lymphoid progenitor cell homing to the thymus. *Proc. Natl. Acad. Sci. USA*. 103:7006–7011. <http://dx.doi.org/10.1073/pnas.0602024103>
- Scollay, R., J. Smith, and V. Stauffer. 1986. Dynamics of early T cells: prothymocyte migration and proliferation in the adult mouse thymus. *Immunol. Rev.* 91:129–157. <http://dx.doi.org/10.1111/j.1600-065X.1986.tb01487.x>
- Serwold, T., L.I. Ehrlich, and I.L. Weissman. 2009. Reductive isolation from bone marrow and blood implicates common lymphoid progenitors as the major source of thymopoiesis. *Blood*. 113:807–815. <http://dx.doi.org/10.1182/blood-2008-08-173682>
- Spangrude, G.J., and R. Scollay. 1990. Differentiation of hematopoietic stem cells in irradiated mouse thymic lobes. Kinetics and phenotype of progeny. *J. Immunol.* 145:3661–3668.
- Spangrude, G.J., and I.L. Weissman. 1988. Mature T cells generated from single thymic clones are phenotypically and functionally heterogeneous. *J. Immunol.* 141:1877–1890.
- Team, R.C. 2012. R: A language and environment for statistical computing. R Foundation for Statistical Computing, Version 2.15.2.
- Ueno, T., F. Saito, D.H. Gray, S. Kuse, K. Hieshima, H. Nakano, T. Kakiuchi, M. Lipp, R.L. Boyd, and Y. Takahama. 2004. CCR7 signals are essential for cortex-medulla migration of developing thymocytes. *J. Exp. Med.* 200:493–505. <http://dx.doi.org/10.1084/jem.20040643>
- Wada, H., K. Masuda, R. Satoh, K. Kakugawa, T. Ikawa, Y. Katsura, and H. Kawamoto. 2008. Adult T-cell progenitors retain myeloid potential. *Nature*. 452:768–772. <http://dx.doi.org/10.1038/nature06839>
- Wallis, V.J., E. Leuchars, S. Chwalinski, and A.J. Davies. 1975. On the sparse seeding of bone marrow and thymus in radiation chimaeras. *Transplantation*. 19:2–11. <http://dx.doi.org/10.1097/00007890-197501000-00002>
- Wurbel, M.A., M. Malissen, D. Guy-Grand, E. Meffre, M.C. Nussenzweig, M. Richelme, A. Carrier, and B. Malissen. 2001. Mice lacking the CCR9 CC-chemokine receptor show a mild impairment of early T- and B-cell development and a reduction in T-cell receptor gamma delta(+) gut intraepithelial lymphocytes. *Blood*. 98:2626–2632. <http://dx.doi.org/10.1182/blood.V98.9.2626>
- Yokomizo, T., T. Yamada-Inagawa, A.D. Yzaguirre, M.J. Chen, N.A. Speck, and E. Dzierzak. 2012. Whole-mount three-dimensional imaging of internally localized immunostained cells within mouse embryos. *Nat. Protoc.* 7:421–431. <http://dx.doi.org/10.1038/nprot.2011.441>
- Zhang, S.L., X. Wang, S. Manna, D.A. Zlotoff, J.L. Bryson, B.R. Blazar, and A. Bhandoola. 2014. Chemokine treatment rescues profound T-lineage progenitor homing defect after bone marrow transplant conditioning in mice. *Blood*. 124:296–304. <http://dx.doi.org/10.1182/blood-2014-01-552794>
- Zlotoff, D.A., A. Sambandam, T.D. Logan, J.J. Bell, B.A. Schwarz, and A. Bhandoola. 2010. CCR7 and CCR9 together recruit hematopoietic progenitors to the adult thymus. *Blood*. 115:1897–1905. <http://dx.doi.org/10.1182/blood-2009-08-237784>
- Zlotoff, D.A., S.L. Zhang, M.E. De Obaldia, P.R. Hess, S.P. Todd, T.D. Logan, and A. Bhandoola. 2011. Delivery of progenitors to the thymus limits T-lineage reconstitution after bone marrow transplantation. *Blood*. 118:1962–1970. <http://dx.doi.org/10.1182/blood-2010-12-324954>
- Zubkova, I., H. Mostowski, and M. Zaitseva. 2005. Up-regulation of IL-7, stromal-derived factor-1 alpha, thymus-expressed chemokine, and secondary lymphoid tissue chemokine gene expression in the stromal cells in response to thymocyte depletion: implication for thymus reconstitution. *J. Immunol.* 175:2321–2330. <http://dx.doi.org/10.4049/jimmunol.175.4.2321>

SUPPLEMENTAL MATERIAL

Ziętara et al., <http://www.jem.org/cgi/content/full/jem.20142143/DC1>

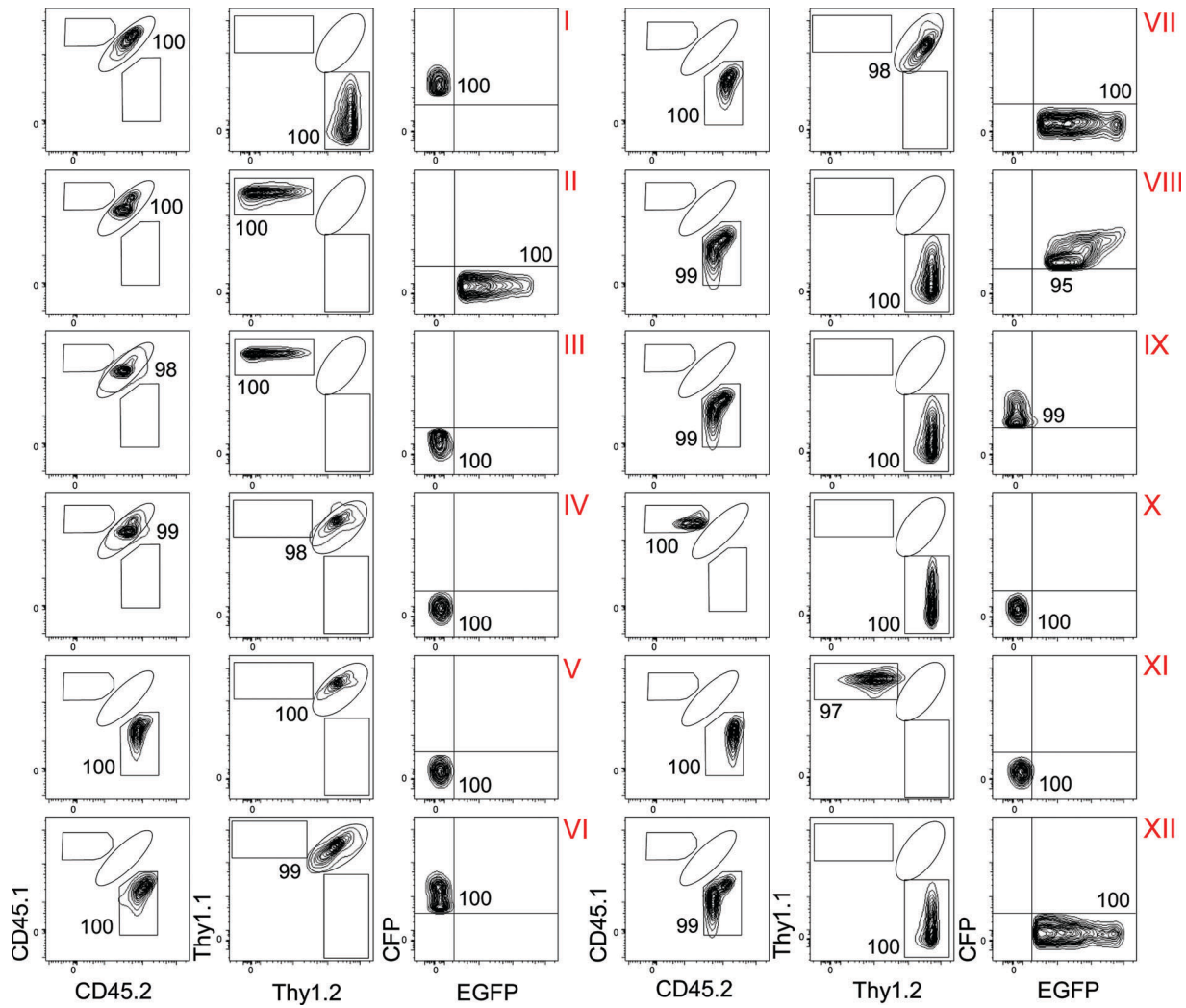


Figure S1. Phenotype of multicongenic progenitors in the thymus. Thymus of DKO recipient mice 21 d after injection and representative plots of individual tags from multicongenic progenitor library. Age of recipient mice used in individual experiments is indicated in the Materials and methods section. Donor mice were 7–10 wk old. The experiment was performed 4 times, with $n = 30$ (DKO).

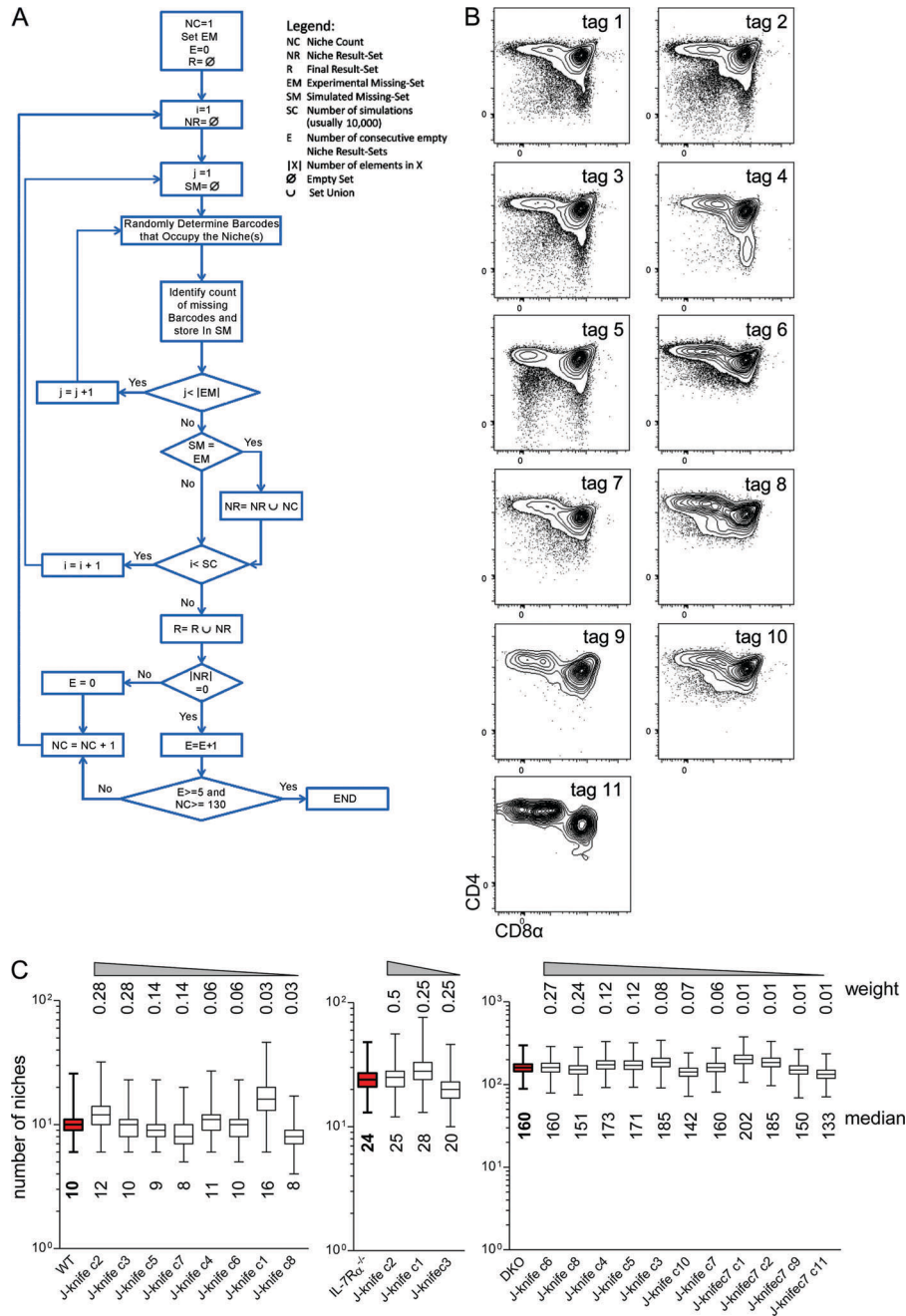
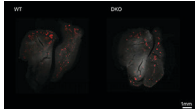


Figure S2. Quantification of thymus colonization using Monte-Carlo simulation. (A) Block diagram scheme for the algorithm used to quantify TSPNs. (B) Representative plots of individual tags of multicongenic progenitors injected i.v. into DKO recipients and their i.t. development measured by surface expression of CD4 and CD8α (data from experiment I, Table S1). (C) Delete-d Jackknife estimation of variance performed to estimate the sensitivity of Monte Carlo simulation to experimental errors. A set of subsampled results was generated from the original result by removing a predefined number of single measurements. This yields a set of $\binom{n}{k} = \frac{n!}{(n-k)! \times k!}$ results, where n is the group size and k the count of elements that were removed.

Then the simulation was performed on each set member and the results were collected. As several results are obtained for each original result the estimation of variance is possible. This procedure was performed for each group while removing 25% of single experiments (rounded to the nearest integer) and running the simulation for every unique combination of missing clones (as single experiments lead often to the same number of missing clones, there are significantly fewer unique combinations than the total derived by the above formula). The result of such simulation was then weighted according to the prevalence of the corresponding combination.



Video 1. LSFM analysis of WT (left) and DKO (right) thymi. Optical cross sections through whole thymi are shown. Medulla staining (UEA-1, red) and background autofluorescence (white) are depicted. z-step: 10 μm . Number of optical sections: 300 (WT) and 350 (DKO). Representative movie of five mice/genotype from two independent experiments.

Table S1, available as an Excel file, shows a combination of alleles used to generate multicongenic library of BM precursors. Multicongenic library of BM-derived progenitors was generated by intercrossing of indicated mouse strains. F1 animals with appropriate combination of surface/fluorescent phenotype, as determined by flow cytometry, were used for experiments; Exp (I) $n = 5$ (WT) and 6 (DKO); Exp (II) $n = 6$ (WT) 6 (DKO) and 4 (IL-7R $\alpha^{-/-}$); Exp (III) $n = 10$ (WT) and 11 (DKO); Exp (IV) $n = 7$ (WT_{int}) and 7 (DKO); Exp (V) $n = 3$ (IL-7R $\alpha^{-/-}$ _{int}); Exp (VI) $n = 4$ (IL-7R $\alpha^{-/-}$ _{int}).

Table S2, available as an Excel file, shows a phenotype and sequence of injections used to determine cellular feedback which allows for entry of new progenitors from BM. Multicongenic F1 mice were generated as indicated in Table S1 and their surface/fluorescent phenotype was determined by flow cytometry before injection. BM-derived progenitors (10^6 lin⁻ BM cells/recipient mouse per single injection) from these animals were injected, at 3 d intervals for 21 d; Exp (I) $n = 7$ (WT) and 7 (DKO); Exp (II) $n = 12$ (WT) and 12 (DKO).

6.2 Critical role for miR-181a/b-1 in agonist selection of invariant NKT cells

Ziętara N, Łyszkiewicz M, Witzlau K, Naumann R, Hurwitz R, Langemeier J, Bohne J, Sandrock I, Ballmaier M, Weiss S, Prinz I, Krueger A

Proceedings of the National Academy of Sciences of the United States of America

110(18): 7407-12 (2013)

Critical role for miR-181a/b-1 in agonist selection of invariant natural killer T cells

Natalia Ziętara^{a,1}, Marcin Łyszczewicz^{a,1}, Katrin Witzlau^a, Ronald Naumann^b, Robert Hurwitz^c, Jörg Langemeier^d, Jens Bohne^d, Inga Sandrock^a, Matthias Ballmaier^e, Siegfried Weiss^f, Immo Prinz^{a,2}, and Andreas Krueger^{a,2,3}

^aInstitute for Immunology, ^dInstitute for Virology, and ^eDepartment of Pediatric Hematology and Oncology, Hannover Medical School, 30625 Hannover, Germany; ^bTransgenic Core, Max-Planck-Institute of Molecular Cell Biology and Genetics, 01307 Dresden, Germany; ^cCore Facility of Protein Chemistry, Max-Planck-Institute for Infection Biology, 10117 Berlin, Germany; and ^fDepartment of Molecular Immunology, Helmholtz Centre for Infection Research, 38124 Braunschweig, Germany

Edited* by Klaus Rajewsky, Max-Delbrück-Center for Molecular Medicine, Berlin, Germany, and approved March 28, 2013 (received for review December 17, 2012)

T-cell receptor (TCR) signal strength determines selection and lineage fate at the CD4⁺CD8⁺ double-positive stage of intrathymic T-cell development. Members of the miR-181 family constitute the most abundantly expressed microRNA at this stage of T-cell development. Here we show that deletion of miR-181a/b-1 reduced the responsiveness of double-positive thymocytes to TCR signals and virtually abrogated early invariant natural killer T (iNKT) cell development, resulting in a dramatic reduction in iNKT cell numbers in thymus as well as in the periphery. Increased concentrations of agonist ligand rescued iNKT cell development in miR-181a/b-1^{-/-} mice. Our results define a critical role of miR-181a/b-1 in early iNKT cell development and show that miR-181a/b-1 sets a TCR signaling threshold for agonist selection.

Natural killer T (NKT) lymphocytes share features characteristic for NK cells as well as T cells, including the T-cell receptor (TCR). Upon TCR triggering they are able to rapidly release cytokines, such as IL-4 and IFN- γ , without prior priming. Thus, NKT cells are able to shape T helper cell differentiation and may, consequently, promote or suppress immune responses (1). NKT cells constitute various populations, the most extensively characterized of which comprises the invariant (i)NKT cells. These cells share a semiinvariant TCR that recognizes lipid antigen bound to the nonclassical MHC I molecule CD1d (2). It is composed of a V α 14J α 18 TCR α chain in mouse (V α 24J α 18 in human) and a limited pool of TCR β chains, with a bias toward V β 8, V β 7, and V β 2 (3). During intrathymic T-cell development the iNKT cell lineage diverges from conventional $\alpha\beta$ T cells at the CD4⁺CD8⁺ double-positive (DP) thymocyte stage and can be identified by its reactivity to CD1d-tetramers loaded with lipid antigen, such as α -galactosyl-ceramide (α GalCer) (4). Differentiation of iNKT cells proceeds through four phenotypically distinct precursor stages: CD24⁺DP^{dim} (stage 0), CD44⁺NK1.1⁻ (stage 1), CD44⁺NK1.1⁻ (stage 2), and CD44⁺NK1.1⁺ (stage 3) (5–7). Stage 3 likely comprises a mixture of freshly generated as well as recirculating iNKT cells.

iNKT cells, as well as other nonconventional T cells, have been shown to be autoreactive to a certain degree (2). Consequently, iNKT cells have been proposed to be selected through strong TCR signals in a process termed “agonist selection.” They undergo massive intrathymic proliferation, and mature cells are CD44⁺, indicating an antigen-experienced phenotype. Furthermore, they express high levels of Nur77, which can be considered as a surrogate marker for TCR signal strength, immediately after positive selection (8). A further increase of TCR signal strength by addition of supraphysiological amounts of ligand or transgenic expression of CD1d provided some evidence for negative selection of iNKT cells (9, 10). Of note, the nature of positively selecting ligands remains largely elusive and is controversially discussed (1). In addition to strong TCR signals, development of iNKT cells depends on costimulatory signals. These are mediated through homotypic interactions of signaling lymphocytic-activation molecule (SLAM) family members (11). Consequently, mice deficient in the SLAM-associated protein (SAP) and its downstream kinase Fyn have

severe defects in iNKT cell development at the stage 0 to stage 1 transition (11–15).

microRNAs (miRNAs) are short noncoding RNAs that modulate a large number of biological processes, mostly by down-regulating expression of target genes via mRNA degradation, mRNA destabilization, or interference with translation. miR-181 comprises a family of six miRNAs, which are organized in three clusters (miR-181a/b-1, miR-181a/b-2, miR-181c/d). miR-181a constitutes the most prominently expressed miRNA species in DP thymocytes (16, 17) and has been associated with modulating TCR signal strength via targeting serine/threonine as well as tyrosine phosphatases (18). Consequently, elevated expression of miR-181a results in reduced phosphatase activity and increased TCR signal strength. Recently it has been shown that miR-181a expression prevents the generation of $\alpha\beta$ T cells that are strongly reactive toward positively selecting peptides (19).

To date, the effect of aberrant expression of miR-181a on TCR signaling has only been analyzed using short-term assays and in vitro organ cultures. Here we studied the consequences of deletion of miR-181a/b-1 on T-cell development in vivo in the steady state. We found that miR-181a/b-1-deficient mice displayed an almost complete block in early iNKT cell development, resulting in dramatically reduced numbers of iNKT cells in thymus as well as in the periphery. DP thymocytes from miR-181a/b-1-deficient mice displayed diminished signaling upon TCR triggering, leading to an altered TCR β repertoire in iNKT cells and reduced cytokine production in the periphery. In turn, increasing the availability of agonist ligand overcame the early block in iNKT cell development in these mice.

Taken together, we identified miR-181a/b-1 as a regulator of iNKT cell development and provided evidence for the critical importance of fine-tuned TCR signal strength for agonist-selected T cells.

Results and Discussion

Development of $\alpha\beta$ T Cells in Mice Lacking miR-181a/b-1. Among all miRNAs, miR-181a/b is most prominently expressed in DP thymocytes, in which it constitutes up to 40% of all miRNAs (16, 17). We generated mice carrying a targeted deletion in miR-

Author contributions: N.Z., M.L., I.P., and A.K. designed research; N.Z., M.L., K.W., R.N., J.L., J.B., I.S., M.B., I.P., and A.K. performed research; R.H. and S.W. contributed new reagents/analytic tools; N.Z., M.L., J.B., I.P., and A.K. analyzed data; and N.Z., M.L., and A.K. wrote the paper.

The authors declare no conflict of interest.

*This Direct Submission article had a prearranged editor.

¹N.Z. and M.L. contributed equally to this work.

²I.P. and A.K. contributed equally to this work.

³To whom correspondence should be addressed. E-mail: krueger.andreas@mh-hannover.de.

This article contains supporting information online at www.pnas.org/lookup/suppl/doi:10.1073/pnas.1221984110/-DCSupplemental.

181a/b-1 (miR-181a/b-1^{-/-} mice) (Fig. S1). Deletion of miR-181a/b-1 was verified by Northern blot (Fig. 1A). Quantitative RT-PCR with primers recognizing both miR-181a-1 and miR-181a-2 showed that deletion of miR-181a/b-1 resulted in a reduction of all miR-181a species by 98%. This confirmed that miR-181a/b-1 but not miR-181a/b-2 is predominantly expressed in thymus (Fig. 1B). Thymus cellularity of miR-181a/b-1^{-/-} mice was indistinguishable from WT and heterozygous littermate controls both at 2 wk and 8 wk of age, and gross composition as assessed by staining for CD4 or CD8 was essentially normal (Fig. 1C–E). In addition, we did not detect major alterations in early thymocyte subsets (Fig. 1F). Despite reduced expression of miR-181a-1 and miR-181b-1 in heterozygous miR-181a/b-1^{+/-} mice, T-cell development in these mice was comparable to that in WT littermates. Therefore, miR-181a/b-1^{+/-} mice were used as controls throughout this study. We detected a mild effect of homozygous deletion of miR-181a/b-1 in development of conventional $\alpha\beta$ T cells, reflected by slight alterations in early T lineage progenitor numbers compared with controls, an ~4% decrease in the frequency of DP thymocytes, and a concomitant increase in the frequency of CD4 single positive (SP) thymocytes. These findings are consistent with minor alterations in thymocyte subsets in a different mouse model of deletion of miR-181a/b-1 (20). Taken together, these data indicate that deletion of miR-181a/b-1 does not result in substantial defects in early T-cell development.

Development of iNKT Cells Depends on miR-181a/b-1. Next we analyzed whether deletion of miR-181a/b-1 resulted in altered generation of iNKT cells. Thymi from miR-181a/b-1^{-/-} mice showed a 15-fold reduced frequency of iNKT cells, as assessed by surface staining for TCR β ⁺, NK1.1⁺ in conjunction with α GalCer CD1d tetramers (CD1d-tet), compared with controls (Fig. 2A and B). Absolute numbers of iNKT cells were reduced to a similar extent (Fig. 2B). CD1d-tet⁻TCR β ⁺NK1.1⁺ variant (v)NKT cell frequencies and numbers, which are present at much lower frequencies in WT mice than iNKT cells, were also reduced in miR-181a/b-1^{-/-} mice, albeit less dramatically, compared with iNKT cells (Fig. 2C). To test whether the paucity of thymic iNKT cells penetrated into the periphery, we assessed frequencies and numbers of splenic and liver iNKT cells. In both organs we found ninefold and 11-fold reduced numbers, respectively, of iNKT cells in miR-181a/b-1^{-/-} mice compared with controls (Fig. 2B). Analysis of vNKT cells in spleen and liver yielded comparable results as analysis of thymus, although the observed differences might be underestimated because low frequencies of vNKT cells and lack of specific staining reagents rendered analysis of this subset difficult (Fig. 2C). Thus, we conclude that deletion of miR-181a/b-1 results in impaired generation of iNKT cells, which cannot be compensated for in the periphery. Mice lacking miR-150 display a defect in the development of iNKT cells, resulting in a modest reduction of iNKT cell numbers in the thymus, which does not penetrate into the periphery (21, 22). Nevertheless, our data imply that the previously reported massive defect in iNKT cell development in mice with conditional deletion of the RNA-processing enzyme Dicer, which is essential for the generation of miRNAs, in hematopoietic cells or DP thymocytes, can be attributed to a large extent to a lack of miR-181a/b-1 (23–25). Of note, other unconventional T-cell populations that have been suggested to depend on agonist selection, such as some $\gamma\delta$ T cells and intestinal intraepithelial lymphocytes (iIELs), remained essentially unaffected by deletion of miR-181a/b-1 (Fig. S2). $\gamma\delta$ T cells do not pass the DP stage during development, and it is a matter of debate whether iIELs are derived from DP thymocytes (26, 27). Relative expression of miR-181a/b-1 is highest in DP cells, whereas it is expressed at lower levels in double-negative (DN) cells (17). Therefore, it is conceivable that miR-181a/b-1 selectively controls unconventional T-cell subsets that originate from DP thymocytes, such as iNKT cells.

Deletion of miR-181a/b-1 might prevent the generation of iNKT cells because of failure of extrinsic signals. To directly assess whether deficiency in miR-181a/b-1 inhibited generation of iNKT cells in a cell-intrinsic manner we generated mixed bone marrow (BM) chimeras. To this end, BM cells from congenic competitors (CD45.1/CD45.2) were mixed at a 1:1 ratio with BM cells from miR-181a/b-1^{-/-} mice or heterozygous controls (CD45.2) and transferred into lethally irradiated hosts (CD45.1). Analysis of mixed chimeras after 12 wk revealed that only few iNKT cells derived from miR-181a/b-1-deficient donor cells were found in thymus and spleen, indicating that lack of miR-181a/b-1 results in a cell-intrinsic defect to generate iNKT cells (Fig. 2D–F). Of note, heterozygous controls were not significantly outcompeted by WT competitors, further arguing for the absence of a gene dosage effect of miR-181a/b-1 in iNKT cell development (Fig. 2D–F). Although we noted a slight competitive disadvantage of miR-181a/b-1^{-/-} DP thymocytes compared with their DN precursors, loss of cells derived from miR-181a/b-1^{-/-} donors was much more prominent in the iNKT cell fraction compared with DP thymocytes (Fig. 2E). This suggests that miR-181a/b-1 acts at or after the DP stage of development.

miR-181a/b-1 Controls Development of iNKT Cells at the Transition from Stage 0 to Stage 1. Development of iNKT cells originates from DP thymocytes and then proceeds through CD1d-tet⁺ stages distinguishable by differential expression of CD24, CD44, and NK1.1. To define the developmental stage at which miR-181a/b-1 is required for generation of iNKT cells, we first assessed the

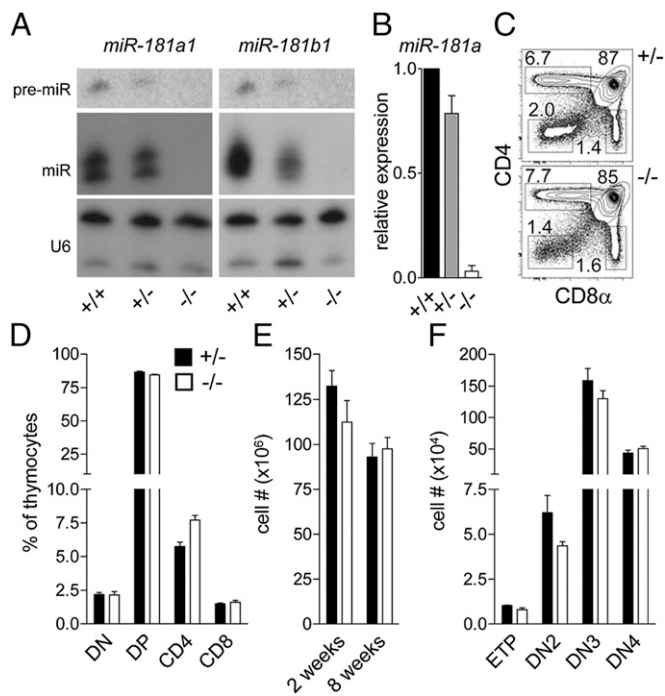


Fig. 1. Development of $\alpha\beta$ T cells in mice lacking miR-181a/b-1. (A) Northern blot analysis of miR-181a-1 and miR-181b-1 expression in total thymocytes of miR-181a/b-1^{-/-}, miR-181a/b-1^{+/-}, and miR-181a/b-1^{+/+} mice. U6 snRNA expression was assessed as loading control. (B) Quantitative RT-PCR for mature miR-181a expression in total thymocytes of miR-181a/b-1^{+/-}, miR-181a/b-1^{+/-}, and miR-181a/b-1^{-/-} mice. $n = 3$ for each genotype. (C) FACS analysis of DN, DP, and SP thymocytes from miR-181a/b-1^{-/-} and miR-181a/b-1^{+/-} mice. Representative plots of multiple experiments are depicted. Quantitative plot for DN, DP, and SP thymocytes, $n = 5$. Percentage within of total thymocytes is shown. (D) Frequency of major thymic subsets and (E) thymus cellularity in miR-181a/b-1^{+/-} and miR-181a/b-1^{-/-} mice at various ages (mean \pm SEM, $n = 5$ –7). (F) FACS analysis of DN thymocyte subsets; ETP, early T lineage progenitor (lineage⁻CD44⁺CD117⁺CD25⁻); DN2 (lineage⁻CD44⁺CD117⁺CD25⁺); DN3 (lineage⁻CD44^{lo}CD117⁺CD25⁺); DN4 (lineage⁻CD44^{lo}CD117⁺CD25⁻). Mean \pm SEM, $n = 3$ –4.

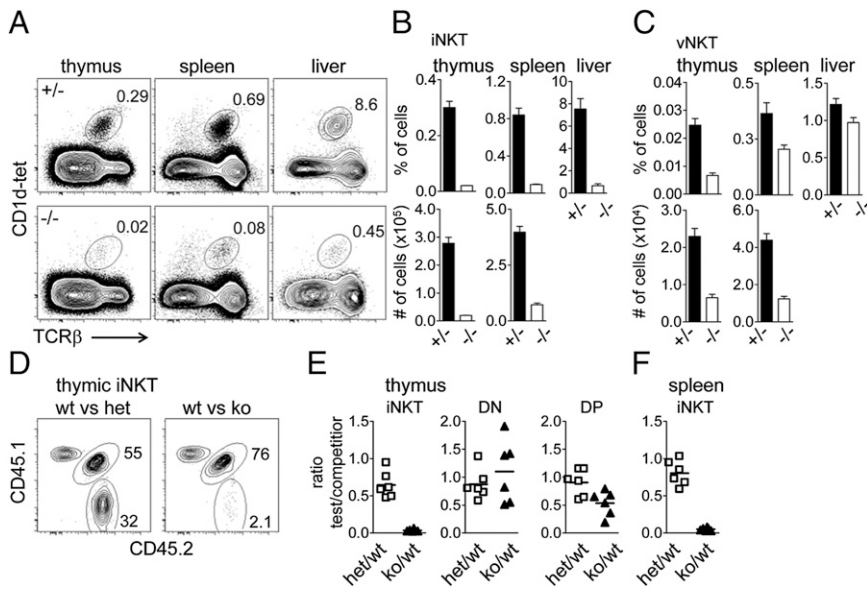


Fig. 2. Development of iNKT cells depends on miR-181a/b-1. (A) FACS analysis of CD1d-tet⁺ iNKT cells from thymus, spleen, and liver. Plots are representative from two to four individual experiments with three to five mice each. (B) Percentage and absolute numbers of iNKT cells (CD1d-tet⁺TCRβ⁺) in thymus and spleen. Percentage of iNKT cells (CD1d-tet⁺TCRβ⁺) in liver. Mean + SEM, *n* = 3–10 for each genotype. (C) Percentage and absolute numbers of vNKT cells (CD1d-tet⁺NK1.1⁺TCRβ⁺) in thymus and spleen. Percentage of vNKT cells (CD1d-tet⁺NK1.1⁺TCRβ⁺) in liver. Mean + SEM, *n* = 3–10 for each genotype. (D) iNKT cell reconstitution in thymi of competitive BM chimeras. Recipients were CD45.1, competitor donor BM was CD45.1/2, and miR-181a/b-1^{-/-} or miR-181a/b-1^{+/-} test BM was CD45.2. Competitor and test BM were administered at a 1:1 ratio. Twelve weeks after BM transplantation, cells were analyzed by FACS. Plots are representative for six mice from two individual experiments. (E) Analysis of indicated thymocyte subsets from competitive BM chimeras. DN, double negative thymocytes. *x* axis labels denote genotypes of test populations. Each dot represents an individual mouse. (F) iNKT cell reconstitution in spleens of competitive BM chimeras as described in D. Each dot represents an individual mouse.

frequency of preselection (CD5⁺TCRβ^{lo}) DP thymocytes carrying Vα14Jα18 TCRα rearrangements. Vα14Jα18 rearrangements occur late during the life of a DP thymocyte and, thus, impaired thymocyte survival might affect development of iNKT cells as has been previously reported for mice deficient in the transcription factor *c-Myb* (28). Semiquantitative RT-PCR analysis revealed that preselection DP thymocytes displayed a similar frequency of Vα14Jα18 rearrangements compared with heterozygous controls, indicating that miR-181a/b-1 is not required to control iNKT cell precursor frequency before selection (Fig. 3A).

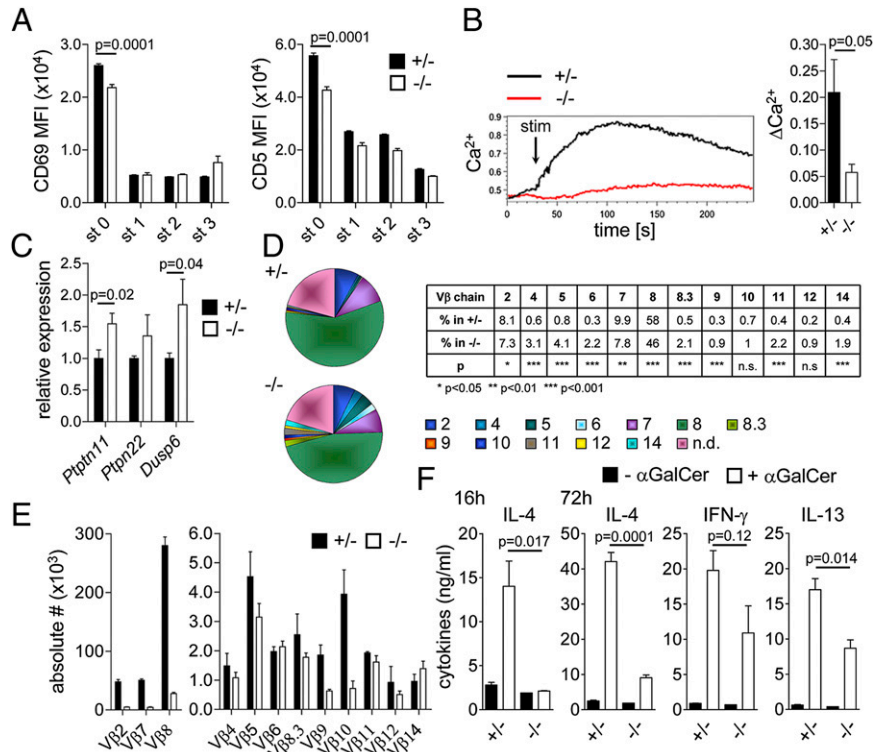
To faithfully quantify rare progenitor populations, we enriched CD1d-tet⁺ cells from young mice using magnetic beads (Fig. 3B). Frequencies of stage 2 and stage 3 iNKT cells were similar in thymi of miR-181a/b-1^{-/-} and miR-181a/b-1^{+/-} mice (Fig. 3B–D). However, whereas most CD44⁺NK1.1⁺ precursors in miR-181a/b-1^{+/-} mice were at stage 1 (CD24⁺), the vast majority of CD44⁺NK1.1⁺ precursors had retained CD24 expression, indicating that miR-181a/b-1 is required to promote the transition from stage 0 to stage 1 (Fig. 3B and C). Analysis of absolute numbers of iNKT cell precursors revealed a minor reduction of stage 0 precursors in thymi of miR-181a/b-1^{-/-} mice compared with heterozygous controls (Fig. 3D). However, in contrast to controls even fewer stage 1 than stage 0 precursors were detectable in thymi of miR-181a/b-1^{-/-} mice, substantiating the conclusion that the stage 0 to stage 1 transition of iNKT cell development is dependent on miR-181a/b-1. Absolute numbers of stage 2 and stage 3 iNKT cells were also reduced, indicating that these cells do not undergo sufficient compensatory proliferation. To directly test whether the observed developmental block is due to a failure of proliferation, we administered a 2-h BrdU pulse to 13-d-old miR-181a/b-1^{-/-} mice and heterozygous controls before isolation of iNKT cell precursors. Consistent with our previous observations, a massively reduced number of stage 0 miR-181a/b-1-deficient iNKT cell precursors had incorporated BrdU, whereas all other subsets showed similar levels of BrdU incorporation (Fig. 3E). Taken together, we conclude that miR-181a/b-1 is critical for proliferative expansion of stage 0 iNKT cell precursors. Similarly, failure to undergo proliferative expansion toward developmental stage 1 has been demonstrated in *c-Myc*-deficient as well as in *Pdk1*-deficient mice (29, 30). However, this developmental block may also reflect a direct consequence of aberrant TCR signaling during selection as shown for mice deficient in the transcription factors *Egr1* and *Egr2* (31). Both factors are rapidly induced upon TCR triggering. Analysis of expression of the transcriptional regulators of iNKT

cell development promyelocytic leukemia zinc finger (PLZF), *Egr1*, *Egr2*, and *c-Myc* at stage 0 and 1 revealed no clear differences between cells from miR-181a/b-1^{+/-} and miR-181a/b-1^{-/-} mice (Fig. S3). These data suggest that either miR-181a/b-1 acts independently of these transcription factors or, alternatively, that miR-181a/b-1-deficient stage 1 iNKT cells represent cells that have escaped developmental arrest. The latter explanation is supported by normal rates of BrdU incorporation at developmental stages 1–3.

Impaired Agonist Selection of iNKT Cells in the Absence of miR-181a/b-1. To assess whether impaired development of iNKT cells in miR-181a/b-1^{-/-} mice is a consequence of altered TCR signal strength, we first analyzed expression levels of CD69 and CD5 as indicators of TCR signal strength. Stage 0 cells from miR-181a/b-1^{-/-} mice displayed a consistent, albeit mild, reduction of expression levels of CD69 and CD5 compared with heterozygous controls (Fig. 4A). Lower levels of CD69 were not apparent in preselection DP cells or at later stages of development, whereas CD5 expression remained lower until stage 3. Next we assessed whether miR-181a/b-1 directly modulated the TCR response of DP thymocytes. To this end, thymocytes from miR-181a/b-1^{-/-} mice and controls were stimulated with anti-CD3 antibody and assessed for Ca²⁺-flux. In contrast to controls, miR-181a/b-1-deficient DP thymocytes generated only little Ca²⁺ signal upon TCR triggering, directly demonstrating that TCR signaling is impaired in the absence of miR-181a/b-1 (Fig. 4B). Targets of miR-181a comprise several phosphatases capable of negatively regulating TCR signaling (18). Thus, we assessed whether these targets displayed altered expression levels in DP thymocytes from miR-181a/b-1^{-/-} mice. We found that levels of mRNA coding for *Ptpn22*, *Shp-2* (encoded by *Ptpn11*), and *Dusp6* were increased between 1.3- and 1.8-fold (Fig. 4C). This differential expression was comparable to alterations of phosphatase expression induced by targeting of miR-181a in vitro (18). Thus, permanent ablation of miR-181a/b-1 does not result in compensatory restoration of phosphatase levels. These data are consistent with a previous report implicating miR-181a as a positive regulator of TCR signaling (18) and support the hypothesis that increased expression of miR-181a/b-1-dependent negative regulators results in impaired TCR signaling in thymocytes from miR-181a/b-1^{-/-} mice.

It has been reported that the restricted Vβ chain use in WT iNKT cells is a consequence of antigen recognition and that changes in

Fig. 4. Impaired agonist selection of iNKT cells in the absence of miR-181a/b-1. (A) Surface expression of CD5 and CD69 on iNKT cells at different developmental stages of iNKT cells at 13 d of age. Data are shown as mean fluorescence intensity (mean \pm SEM). (B) Total thymocytes were stimulated with anti-CD3, and Ca^{2+} -flux was recorded flow cytometrically over time. Plots for electronically gated DP thymocytes are representative for five mice from two individual experiments. "stim" indicates time point of stimulation. Bar graph shows analysis of peak Ca^{2+} -flux over background from five mice per group from two independent experiments. (C) Analysis of expression of *Ptpn22*, *Ptpn11* (encoding Shp-2), and *Dusp6* in DP thymocytes by quantitative RT-PCR. Expression levels were normalized to *Actb*. Data are shown as mean relative expression \pm SEM from four mice per group out of two individual experiments. (D) TCR V β repertoire of splenic CD1d-tet⁺ TCR β ⁺ iNKT cells was analyzed by flow cytometry. Pie charts represent frequencies of individual V β chains within these iNKT cells. Cumulative data from 13 to 14 mice per genotype from four independent experiments. Table represents quantification of data presented in pie charts. Statistical analysis was performed using unpaired Student *t* test. (E) Absolute numbers of splenic CD1d-tet⁺ TCR β ⁺ iNKT cells expressing different V β chains. (F) Cytokine production by splenic iNKT cells from miR-181a/b-1^{+/-} or miR-181a/b-1^{-/-} mice after stimulation with α GalCer-loaded splenocytes for the indicated periods of time. IFN γ , IL-4, and IL-13 concentrations were determined using cytometric bead assays. Data are shown as mean \pm SEM from five mice in two independent experiments. Statistical analysis was performed using unpaired Student *t* test.



Taken together, our data indicate that deficiency in miR-181a/b-1 results in reduced TCR signaling and, consequently, in an altered TCR repertoire and peripheral responsiveness of iNKT cells. Conversely, rescue by supraphysiological concentrations of agonist ligand supports the hypothesis that miR-181a/b-1 controls iNKT cell development by modulating agonist selection. Modest alterations of target gene expression, such as increased expression of *Ptpn22*, *Shp-2*, and *Dusp6* in miR-181a/b-1^{-/-} mice, seem to be the rule rather than an exception for gene regulation by miRNA. Consequently, it has been suggested that, rather than controlling major biological switches, miRNAs contribute to managing noise and/or setting regulatory thresholds (34). Thus, virtually complete control of development of a cell lineage by a single miRNA as described in this study is to our knowledge unparalleled in the immune system. miRNAs have been suggested to frequently target multiple genes within a particular pathway, thus generating synergistic effects (35). Here, deletion of miR-181a/b-1 resulted in increased expression of

multiple negative regulators of TCR signaling, and it has been proposed that their coordinated, but not individual, regulation by miR-181a modulates TCR signaling thresholds (18). iNKT cells seem to be particularly sensitive to alterations in TCR signal strength. For example, reduction of TCR signal strength by reduction of immunoreceptor tyrosine-based activation motif motifs in the CD3 ζ chain resulted in a preferential defect in iNKT cell development (36). In addition, generation of iNKT cells is dependent on costimulation via SLAM-SAP-Fyn signaling (11). Fyn activity is also negatively regulated by target phosphatases of miR-181a/b-1, suggesting that its deletion results in defective integration of TCR stimulation and costimulation, thus providing an additional explanation why iNKT cell development is selectively controlled by miR-181a/b-1. In conclusion, we have identified a single miRNA species, miR-181a/b-1, that controls differentiation of iNKT cells by setting a threshold for agonist selection.

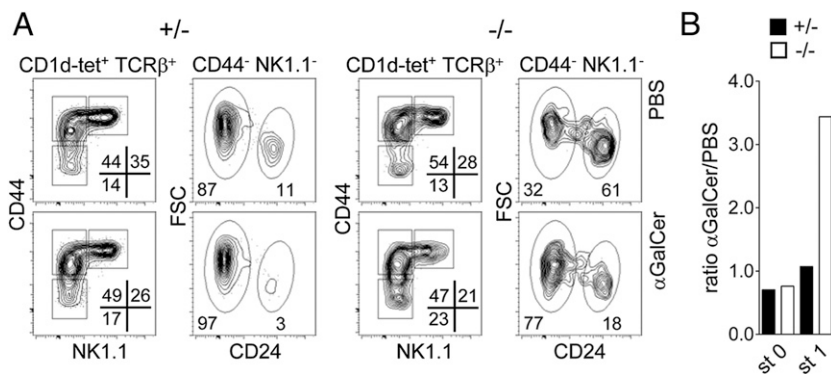


Fig. 5. Exogenous ligand rescues iNKT cell development beyond stage 0 in miR-181a/b-1^{-/-} mice. (A) Flow cytometric analysis of thymic iNKT cells from 13-d-old mice 16 h after i.p. injection of α GalCer or vehicle control. Plots are representative for 10–13 mice from each genotype from two individual experiments. (B) Numbers of stage 0 and stage 1 iNKT cell precursors after i.p. injection of α GalCer relative to vehicle control. *n* = 10–13 for each genotype.

Materials and Methods

Mice. C57BL/6J mice (CD45.2) were purchased from Charles River. B6.SJL-*Ptprc^aPepc^b/BoyJ* mice (termed "B6 CD45.1" throughout this article) and (C57BL/6J × B6 CD45.1) F1 mice (CD45.1/CD45.2 heterozygous) were bred at the animal facility of Hannover Medical School. Animals were maintained under specific-pathogen-free conditions. All animal experiments were conducted in accordance with local and institutional guidelines (Permit: 33.9-42502-04-12/0869, 07/1393, 08/1480). Generation of miR-181a/b-1 knockout mice is described in detail in *SI Materials and Methods*.

Flow Cytometry and Cell Sorting. Phycoerythrin (PE)- and allophycocyanin (APC)-conjugated CD1d/αGalCer tetramer was provided by R. Hurwitz (Max Planck Institute for Infection Biology, Berlin, Germany), PE conjugated CD1d/αGalCer tetramer was purchased from Prolimmune. APC-conjugated CD1d/PBS-57 (αGalCer analog) loaded and unloaded tetramer were provided by the National Institutes of Health Tetramer Facility at Emory University (Atlanta, GA). Monoclonal antibodies used in this study are described in *SI Materials and Methods*.

Enrichment and Analysis of iNKT Development. For analysis of iNKT cells, thymocyte single-cell suspensions obtained from 13-d-old mice were stained for 15 min at room temperature with APC-labeled CD1d/PBS-57 tetramers. CD1d-tet⁺ cells were then enriched with anti-APC magnetic microbeads by using a magnetic-activated cell sorting cell separator (Miltenyi Biotec) and subjected to further staining by flow cytometry.

Application of αGalCer. Thirteen-day-old miR-181a/b-1^{+/-} or miR-181a/b-1^{-/-} mice were injected i.p. with αGalCer (Alexis Biochemicals) at 1 μg per mouse per 50 μl of PBS, or PBS/DMSO. Sixteen hours later, mice were killed, and intrathymic development of iNKT cells was analyzed as described above.

Additional Methods. Northern Blot analysis, PCR, procedures for enrichment of DN thymocytes, generation of competitive BM chimeras, analysis of TCR Vβ chain repertoire, measurement of intracellular Ca²⁺-flux in DP thymocytes, and BrdU incorporation are described in *SI Materials and Methods*.

Statistical Analysis. All analysis was performed using GraphPad Prism software. Data are represented as mean + SEM. Analysis of significance between two groups of mice was performed using unpaired Student *t* tests.

ACKNOWLEDGMENTS. We thank Reinhold Förster and Oliver Pabst for critical reading of the manuscript; Susanne zur Lage, Jasmin Boelter, and Annkatrin Arlt for technical assistance; and Michaela Scherr, Hannover Medical School, for help with quantitative PCR. Assistance was provided by the Cell Sorting Core Facility of the Hannover Medical School, supported in part by Braukmann-Wittenberg-Herz-Stiftung and German Research Foundation (DFG). The allophycocyanin-conjugated CD1d tetramer loaded with PBS-57, an analog of αGalCer, as well as unloaded CD1d tetramer were kindly provided by the National Institutes of Health Tetramer Facility at Emory University. The work was supported by grants from the DFG (Emmy-Noether Program, KR2320/2-1; SFB738-A7; and EXC62, "Rebirth") (to A.K.).

- Bendelac A, Savage PB, Teyton L (2007) The biology of NKT cells. *Annu Rev Immunol* 25:297–336.
- Bendelac A, et al. (1995) CD1 recognition by mouse NK1+ T lymphocytes. *Science* 268(5212):863–865.
- Wei DG, Curran SA, Savage PB, Teyton L, Bendelac A (2006) Mechanisms imposing the Vβ bias of Valpha14 natural killer T cells and consequences for microbial glycolipid recognition. *J Exp Med* 203(5):1197–1207.
- Gapin L, Matsuda JL, Surh CD, Kronenberg M (2001) NKT cells derive from double-positive thymocytes that are positively selected by CD1d. *Nat Immunol* 2(10):971–978.
- Benlagha K, Kyin T, Beavis A, Teyton L, Bendelac A (2002) A thymic precursor to the NK T cell lineage. *Science* 296(5567):553–555.
- Benlagha K, Wei DG, Veiga J, Teyton L, Bendelac A (2005) Characterization of the early stages of thymic NKT cell development. *J Exp Med* 202(4):485–492.
- Pellicci DG, et al. (2002) A natural killer T (NKT) cell developmental pathway involving a thymus-dependent NK1.1(-)CD4(+) CD1d-dependent precursor stage. *J Exp Med* 195(7):835–844.
- Moran AE, et al. (2011) T cell receptor signal strength in Treg and iNKT cell development demonstrated by a novel fluorescent reporter mouse. *J Exp Med* 208(6):1279–1289.
- Chun T, et al. (2003) CD1d-expressing dendritic cells but not thymic epithelial cells can mediate negative selection of NKT cells. *J Exp Med* 197(7):907–918.
- Pellicci DG, et al. (2003) Intrathymic NKT cell development is blocked by the presence of alpha-galactosylceramide. *Eur J Immunol* 33(7):1816–1823.
- Griewank K, et al. (2007) Homotypic interactions mediated by Slamf1 and Slamf6 receptors control NKT cell lineage development. *Immunity* 27(5):751–762.
- Gadue P, Morton N, Stein PL (1999) The Src family tyrosine kinase Fyn regulates natural killer T cell development. *J Exp Med* 190(8):1189–1196.
- Eberl G, Lowin-Kropf B, MacDonald HR (1999) Cutting edge: NKT cell development is selectively impaired in Fyn- deficient mice. *J Immunol* 163(8):4091–4094.
- Pasquier B, et al. (2005) Defective NKT cell development in mice and humans lacking the adapter SAP, the X-linked lymphoproliferative syndrome gene product. *J Exp Med* 201(5):695–701.
- Nichols KE, et al. (2005) Regulation of NKT cell development by SAP, the protein defective in XLP. *Nat Med* 11(3):340–345.
- Neilson JR, Zheng GXY, Burge CB, Sharp PA (2007) Dynamic regulation of miRNA expression in ordered stages of cellular development. *Genes Dev* 21(5):578–589.
- Kirigin FF, et al. (2012) Dynamic microRNA gene transcription and processing during T cell development. *J Immunol* 188(7):3257–3267.
- Li Q-J, et al. (2007) miR-181a is an intrinsic modulator of T cell sensitivity and selection. *Cell* 129(1):147–161.
- Ebert PJR, Jiang S, Xie J, Li Q-J, Davis MM (2009) An endogenous positively selecting peptide enhances mature T cell responses and becomes an autoantigen in the absence of microRNA miR-181a. *Nat Immunol* 10(11):1162–1169.
- Fragoso R, et al. (2012) Modulating the strength and threshold of NOTCH oncogenic signals by miR-181a-1/b-1. *PLoS Genet* 8(8):e1002855.
- Zheng Q, Zhou L, Mi Q-S (2012) MicroRNA miR-150 is involved in Vα14 invariant NKT cell development and function. *J Immunol* 188(5):2118–2126.
- Bezman NA, Chakraborty T, Bender T, Lanier LL (2011) miR-150 regulates the development of NK and iNKT cells. *J Exp Med* 208(13):2717–2731.
- Fedeli M, et al. (2009) Dicer-dependent microRNA pathway controls invariant NKT cell development. *J Immunol* 183(4):2506–2512.
- Zhou L, et al. (2009) Tie2^{cre}-induced inactivation of the miRNA-processing enzyme Dicer disrupts invariant NKT cell development. *Proc Natl Acad Sci USA* 106(25):10266–10271.
- Seo KH, et al. (2010) Loss of microRNAs in thymus perturbs invariant NKT cell development and function. *Cell Mol Immunol* 7(6):447–453.
- Yamagata T, Mathis D, Benoist C (2004) Self-reactivity in thymic double-positive cells commits cells to a CD8 alpha alpha lineage with characteristics of innate immune cells. *Nat Immunol* 5(6):597–605.
- Lambolez F, et al. (2006) The thymus exports long-lived fully committed T cell precursors that can colonize primary lymphoid organs. *Nat Immunol* 7(1):76–82.
- Hu T, Simmons A, Yuan J, Bender TP, Alberola-Ila J (2010) The transcription factor c-Myb primes CD4+CD8+ immature thymocytes for selection into the iNKT lineage. *Nat Immunol* 11(5):435–441.
- Dose M, et al. (2009) Intrathymic proliferation wave essential for Valpha14+ natural killer T cell development depends on c-Myc. *Proc Natl Acad Sci USA* 106(21):8641–8646.
- Finlay DK, et al. (2010) Temporal differences in the dependency on phosphoinositide-dependent kinase 1 distinguish the development of invariant Valpha14 NKT cells and conventional T cells. *J Immunol* 185(10):5973–5982.
- Seiler MP, et al. (2012) Elevated and sustained expression of the transcription factors Egr1 and Egr2 controls NKT lineage differentiation in response to TCR signaling. *Nat Immunol* 13(3):264–271.
- Schümann J, Mycko MP, Dellabona P, Casorati G, MacDonald HR (2006) Cutting edge: Influence of the TCR Vβ domain on the selection of semi-invariant NKT cells by endogenous ligands. *J Immunol* 176(4):2064–2068.
- Schümann J, Voyle RB, Wei B-Y, MacDonald HR (2003) Cutting edge: Influence of the TCR V beta domain on the avidity of CD1d:alpha-galactosylceramide binding by invariant V alpha 14 NKT cells. *J Immunol* 170(12):5815–5819.
- Herranz H, Cohen SM (2010) MicroRNAs and gene regulatory networks: Managing the impact of noise in biological systems. *Genes Dev* 24(13):1339–1344.
- Tsang JS, Ebert MS, van Oudenaarden A (2010) Genome-wide dissection of microRNA functions and cotargeting networks using gene set signatures. *Mol Cell* 38(1):140–153.
- Becker AM, et al. (2010) Invariant NKT cell development requires a full complement of functional CD3 zeta immunoreceptor tyrosine-based activation motifs. *J Immunol* 184(12):6822–6832.

6.3 Overexpression of V α 14J α 18 TCR promotes development of iNKT cells in the absence of miR-181a/b-1

Blume J, Zur Lage S, Witzlau K, Georgiev H, Weiss S, Łyszkiewicz M, **Ziętara N**, Krueger A

Immunology and Cell Biology; 94(8), 741-6 (2016)

ORIGINAL ARTICLE

Overexpression of V α 14J α 18 TCR promotes development of iNKT cells in the absence of miR-181a/b-1

Jonas Blume¹, Susanne zur Lage², Katrin Witzlau¹, Hristo Georgiev¹, Siegfried Weiss^{1,2}, Marcin Łyszkiewicz^{1,3,4}, Natalia Zięta^{1,3,4} and Andreas Krueger^{1,4,5}

Expression of microRNA miR-181a/b-1 is critical for intrathymic development of invariant natural killer T (iNKT) cells. However, the underlying mechanism has remained a matter of debate. On the one hand, growing evidence suggested that miR-181a/b-1 is instrumental in setting T-cell receptor (TCR) signaling threshold and thus permits agonist selection of iNKT cells through high-affinity TCR ligands. On the other hand, alterations in metabolic fitness mediated by miR-181a/b-1-dependent dysregulation of phosphatase and tensin homolog (Pten) have been proposed to cause the iNKT-cell defect in miR-181a/b-1-deficient mice. To re-assess the hypothesis that modulation of TCR signal strength is the key mechanism by which miR-181a/b-1 controls the development of iNKT cells, we generated miR-181a/b-1-deficient mice expressing elevated levels of a V α 14J α 18 TCR α chain. In these mice, development of iNKT cells was fully restored. Furthermore, both subset distribution of iNKT cells as well as TCR V β repertoire were independent of the presence of miR-181a/b-1 once a V α 14J α 18 TCR α chain was overexpressed. Finally, levels of Pten protein were similar in V α 14J α 18 transgenic mice irrespective of their miR-181a/b-1 status. Collectively, our data support a model in which miR-181 promotes development of iNKT cells primarily by generating a permissive state for agonist selection with alterations in metabolic fitness possibly constituting a secondary effect.

Immunology and Cell Biology (2016) **94**, 741–746; doi:10.1038/icb.2016.40

Developing T cells undergo selection processes in the thymus depending on the affinity of their T-cell receptors (TCRs) for major histocompatibility complex (MHC):antigen complexes. Most developing thymocytes recombine a non-functional TCR that fails to recognize MHC:antigen complexes and thus dies by neglect. Those thymocytes carrying a functional TCR are positively selected by low-affinity TCR-MHC:antigen interactions and are induced to undergo apoptosis upon high-affinity contact with MHC:antigen. However, development of certain T-cell lineages, including regulatory T cells, some $\gamma\delta$ T cells and the so-called invariant natural killer T (iNKT) cells, is dependent on high-affinity TCR-MHC:ligand interactions in a process termed agonist selection.¹ iNKT cells express a semi-invariant TCR comprising a V α 14J α 18 TCR α chain in mouse (V α 24J α 18 in humans) and a restricted repertoire of V β chains mostly comprising V β 8, V β 7 and V β 2.² These TCRs preferentially recognize lipid antigens in the context of the non-classical MHC molecule CD1d and are selectively enriched during selection.^{3,4}

iNKT cells represent an innate-like lymphocyte lineage and are therefore prewired to express cytokines directly upon stimulation.

Recently, iNKT cells have been classified into three distinct lineages, NKT1, NKT2 and NKT17, based on the expression of signature transcription factors and their propensity to release distinct cytokines.⁵

MicroRNAs are essential for the development of iNKT cells. We and others have shown that, in particular, miR-181a/b-1 is critical in this process.^{6–9} We showed that miR-181a/b-1-deficient mice had substantially reduced numbers of iNKT cells in both the thymus and peripheral organs owing to a developmental block at the stage of their selection.⁹ Earlier studies had indicated that miR-181a/b-1 targets comprised negative regulators of TCR signaling, including serine/threonine as well as tyrosine phosphatases. In consequence, miR-181a/b-1 acted as a modulator of TCR signal strength and positive selection.^{10,11} Consistently, we found that miR-181a/b-1-deficient thymocytes displayed a poor Ca²⁺-response to TCR stimuli and this was recently confirmed by Schaffert *et al.*¹² Furthermore, residual NKT cells in miR-181-deficient mice displayed an aberrant TCR β repertoire with predominant depletion of canonical V β chains and a reduced propensity to produce cytokines, especially interleukin (IL)-4, upon stimulation. Finally, iNKT-cell development in these mice was

¹Institute of Immunology, Hannover Medical School, Hannover, Germany and ²Molecular Immunology, Helmholtz Centre for Infection Research, Braunschweig, Germany

³Current address: Dr von Haunersches Kinderspital, University Children's Hospital, Munich, Germany.

⁴These authors contributed equally to this work

⁵Current address: Institute for Molecular Medicine, Goethe University Frankfurt, Frankfurt am Main, Germany.

Correspondence: Dr N Zięta, Dr von Haunersches Kinderspital, University Children's Hospital, Lindwurmstr. 4, München 80337, Germany.

E-mail: natalia.zietara@med.uni-muenchen.de

or Professor A Krueger, Institute for Molecular Medicine, Goethe University Frankfurt, Theodor-Stern-Kai 7, Frankfurt am Main D-60590, Germany.

E-mail: andreas.krueger@kgu.de

Received 22 February 2016; revised 1 April 2016; accepted 2 April 2016; accepted article preview online 19 April 2016; advance online publication, 10 May 2016

rescued by administration of agonist ligand. Taken together, these studies strongly support the hypothesis that miR-181a/b-1 is a critical modulator of agonist selection of iNKT cells.^{9–12} However, based on an analysis of an independently generated miR-181a/b-1-deficient mouse, Heno-Mejia *et al.*⁷ concluded that a defect in metabolic fitness rather than impaired agonist selection was the primary cause of iNKT-cell deficiency in these mice. This defect in metabolic fitness was attributed to the elevated expression of phosphatase Pten (phosphatase and tensin homolog) in the absence of miR-181a/b-1. Most notably, in this study the expression of a transgenic TCR as a means to increase TCR signal strength was not able to fully restore the development of iNKT cells.

In order to reconcile these apparently conflicting experimental data, we re-assessed iNKT-cell development in miR-181a/b-1-deficient mice expressing a transgenic V α 14J α 18 TCR α chain.¹³ We hypothesized that introduction of this transgene would result in increased availability of surface TCR capable of signal transduction and would therefore compensate for a miR-181a/b-1-mediated reduction in TCR signal strength. We demonstrate that in these mice numbers of iNKT cells were fully restored to levels of miR-181a/b-1-sufficient mice. Furthermore, V β chain usage was independent of miR-181a/b-1 in V α 14 transgenic mice and the proportion of iNKT-cell subsets was

restored. Finally, we show that the expression of Pten protein was independent of miR-181a/b-1, suggesting that metabolic alterations are downstream rather than upstream of TCR signaling in miR-181a/b-1-deficient mice. Collectively, the present re-analysis of iNKT-cell development supports our earlier interpretation that impaired agonist selection is a major effector of failed iNKT-cell generation in miR-181a/b-1-deficient mice.

RESULTS

Expression of a prearranged V α 14J α 18 TCR α chain restores iNKT-cell development in miR-181a/b-1^{-/-} mice

In order to re-assess the hypothesis that miR-181a/b-1 promotes the development of iNKT cells by controlling TCR signal thresholds, we generated miR-181a/b-1^{-/-} mice with developing T cells expressing a prearranged V α 14J α 18 TCR α chain (V α 14-Tg).¹³ Transgenic expression of a prearranged TCR α chain resulted in markedly increased TCR β surface expression on thymic iNKT cells in both miR-181a/b-1-deficient and -sufficient mice when compared with non-transgenic (non-Tg) mice (Figure 1a). Of note, neither non-Tg nor V α 14-Tg miR-181a/b-1^{-/-} mice displayed reduced levels of surface TCR expression when compared with their miR-181a/b-1-sufficient counterparts, suggesting that miR-181a/b-1 acts downstream rather than upstream of the TCR (Figure 1a and Zietara *et al.*⁹).

As previously reported, miR-181a/b-1-sufficient V α 14-Tg mice displayed a massive relative and absolute increase in thymic iNKT-cell numbers when compared with non-Tg controls (Figures 1b–d). Thymi of V α 14-Tg/miR-181a/b-1^{-/-} mice displayed highly comparable frequencies and numbers of iNKT cells as their V α 14-Tg miR-181a/b-1-sufficient counterparts. Similar to the observations in the thymus, V α 14-Tg mice showed elevated frequencies of iNKT cells in the spleen and liver independent of the expression of miR-181a/b-1 (Figure 1d). Thus introduction of a transgenic V α 14J α 18 TCR α chain and concomitantly elevated TCR levels efficiently restored iNKT-cell development in miR-181a/b-1^{-/-} mice.

miR-181a/b-1-deficient iNKT population is skewed toward NKT2 and NKT17 subsets

iNKT cells can be subdivided into three distinct subsets based on the expression profile of T-bet and PLZF or use of surface markers CD122 and CD4 (Figure 2a). These subsets predominantly secrete the cytokines interferon- γ (NKT1, CD4^{+/+}-CD122⁺), IL-4 (NKT2, CD4⁺-CD122⁻) or IL-17 (NKT17, CD4⁻-CD122⁻).¹⁴ Recently, C-X-C motif chemokine receptor 3 (CXCR3) was reported to be expressed exclusively on NKT1 cells and can therefore be used interchangeably with CD122 in the periphery.¹⁵ In the thymi of miR-181a/b-1^{-/-} mice, we detected an increased proportion of NKT2 and NKT17 cells at the expense of NKT1 cells (Figure 2b).

Similar to the subdivision of iNKT-cell subsets in the thymus, we segregated splenic iNKT cells by surface expression of CXCR3 and CD4.¹⁵ In accordance with the results from the thymus, splenic iNKT cells of miR-181a/b-1^{-/-} mice showed an increase in the frequency of NKT2 and NKT17 cells compared with miR-181a/b-1-sufficient NKT cells (Figure 2c). Analysis of liver-resident iNKT cells revealed an almost complete absence of NKT2 cells in miR-181a/b-1^{-/-} mice (Supplementary Figure S1a). Analysis of NKT-cell subsets based on the expression of signature transcription factors PLZF and T-bet yielded highly similar results as segregation via surface markers CXCR3 and CD4 (Figure 2d). Interestingly, PLZF and T-bet expression levels were lower in miR-181a/b-1^{-/-} mice (Figure 2e). These data suggest that, in the absence of miR-181a/b-1, differentiation into distinct NKT subsets might not be complete.

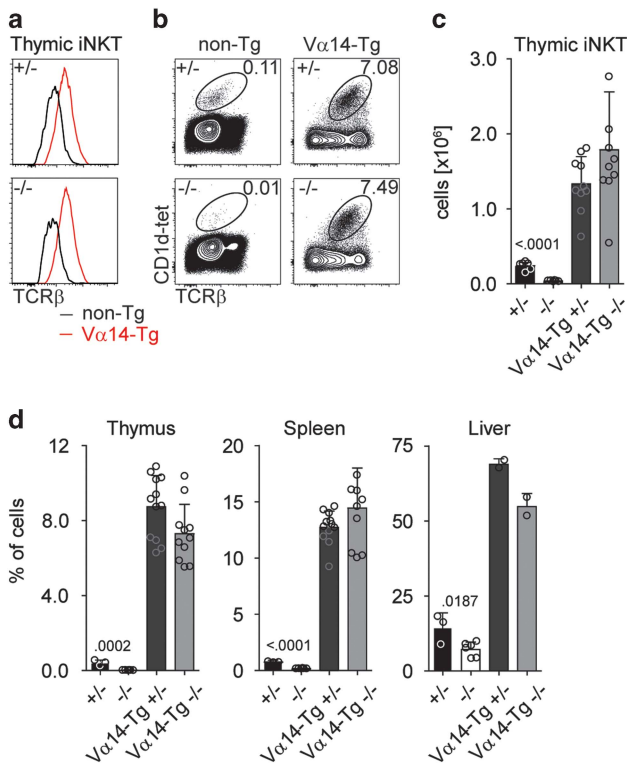


Figure 1 Expression of a prearranged V α 14J α 18 TCR α chain restores iNKT-cell development in miR-181a/b-1^{-/-} mice. (a) Representative histogram of TCR β expression in iNKT cells of the indicated genotype. (b) Representative contour plots of thymocytes from non-Tg and V α 14-Tg miR-181a/b-1 sufficient (+/-) and deficient (-/-) mice. Values in plots indicate relative amount of iNKT cells identified by binding of α GalCer-loaded tetramer. (c) Absolute counts of thymic iNKT cells in non-Tg and V α 14-Tg mice sufficient (black and dark gray bars) and deficient (white and light gray bars) for miR-181a/b-1 and (d) relative proportion of thymic, splenic and liver resident iNKT cells in the indicated genotypes. (b–d) Pooled data of 5–6 mice from two independent experiments. Error bars indicate s.d. Numbers in bar graphs indicate *P*-value of unpaired *t*-test.

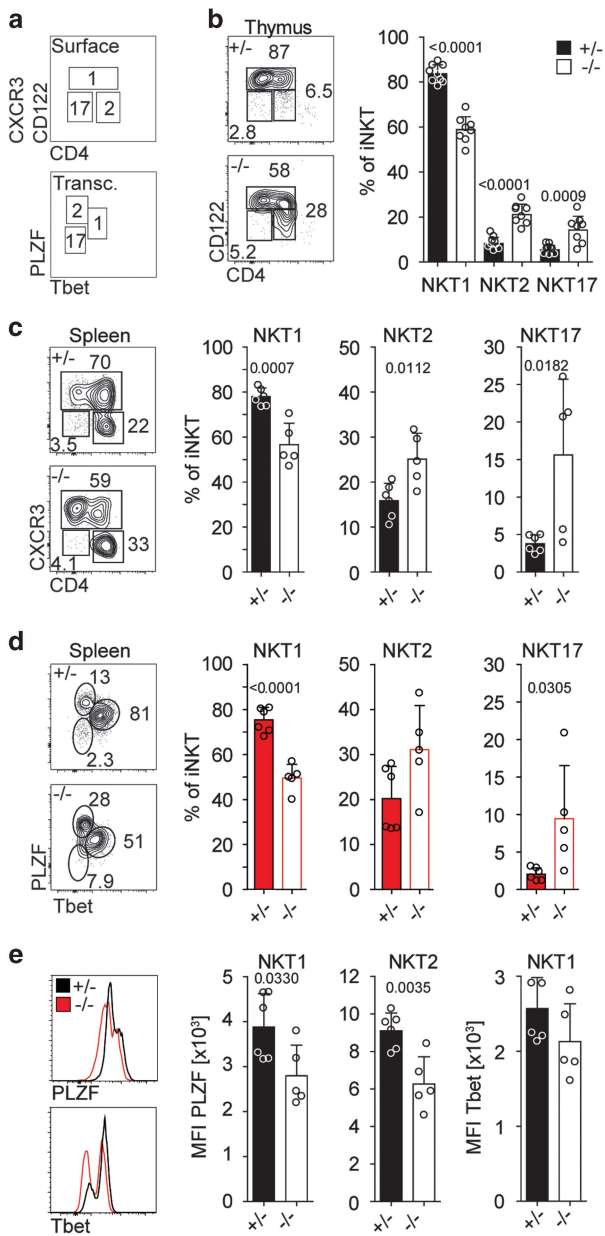


Figure 2 miR-181a/b-1-deficient iNKT population is skewed toward NKT2 and NKT17 subsets. (a) Schematic gating for NKT1, NKT2 and NKT17 subsets based on surface expression of CD122 (thymus) or CXCR3 (periphery) and CD4 or by expression of PLZF and Tbet. (b, c) Representative contour plots and quantification of thymic (b) and splenic (c) iNKT cells from non-Tg mice sufficient (+/-, black bars) and deficient (-/-, white bars) for miR-181a/b-1. (d) Representative contour plots and quantification of splenic NKT1, NKT2 and NKT17 subsets of the indicated genotypes derived from surface and transcriptional classification. (e) Overlay of histograms for transcription factor expression in the indicated genotypes and quantification of PLZF and Tbet as mean fluorescence intensity of the indicated populations and genotypes. (b-e) Pooled data of 5-6 mice from two independent experiments. Error bars indicate s.d. Numbers in bar graphs indicate *P*-value of unpaired *t*-test.

P rearranged TCR α chain restores iNKT-cell development and polarization

Next we analyzed iNKT subsets in V α 14-Tg mice. In the thymus of V α 14-Tg mice, we detected a marked increase in the frequency of NKT17 subset, identified by the lack of CD4 and CD122 expression.

Of note, no differences in subset distribution that were dependent on the presence of miR-181a/b-1 could be identified in V α 14-Tg mice (Figure 3a). Analysis of iNKT subsets in the periphery recapitulated observations obtained from the thymus. Loss of miR-181a/b-1 did not result in detectable differences regarding iNKT subsets in V α 14-Tg mice when compared with miR-181a/b-1-sufficient controls (Figure 3b and Supplementary Figure S1a). Interestingly, in V α 14-Tg mice, there was a miR-181a/b-1-independent ~10-fold increase of the CD4⁻CXCR3⁻ NKT17 subset compared with that in non-Tg mice (Figure 3b and Supplementary Figure S1a). This change towards NKT17 cells appeared to be mostly due to the low expression levels of CD4 (Figures 3c and d). Indeed, analysis of iNKT-cell subsets based on transcription factor signatures showed a much smaller, but still clearly detectable, difference to non-Tg mice (Figure 3e). These data are consistent with overall lower levels of CD4 on the thymocytes of these mice and suggest that the expression of CD4 cannot be employed to faithfully define iNKT-cell subsets in V α 14-Tg mice.¹³

Importantly, we observed no detectable differences in subset distribution dependent on the presence of miR-181a/b-1. Notably, the previously observed reduced expression of PLZF and Tbet in miR-181a/b-1^{-/-} mice was not detectable in the presence of the V α 14 transgene (Figure 3e). This is in line with recent findings placing PLZF induction downstream of TCR signaling during iNKT differentiation.¹⁶

Analysis of V β chain usage by iNKT cells in V α 14-Tg/miR-181a/b-1^{-/-} and V α 14-Tg/miR-181a/b-1^{+/-} mice revealed that transgenic V α 14 TCR expression fully restored the loss of V β bias observed previously in miR-181a/b-1^{-/-} mice (Figure 3f).⁹ Taken together, these data suggest that the expression of a transgenic V α 14 TCR is able to rescue all developmental defects and alterations in polarization of NKT cells in miR-181a/b-1^{-/-} mice.

Levels of Pten protein are not affected by a V α 14 TCR transgene

Dysregulation of Pten was implicated in causing alterations in the metabolic fitness of developing thymocytes, in turn resulting in loss of iNKT cells in miR-181a/b-1^{-/-} mice.⁷ Therefore, we tested whether introduction of a prearranged V α 14 TCR α chain would have an effect on its expression at the protein level. Western blottings on total thymocyte lysates showed a modest, statistically non-significant, 1.2-fold increase in Pten expression in thymocytes from miR-181a/b-1^{-/-} mice when compared with miR-181a/b-1-sufficient cells and an even smaller miR-181a/b-1-dependent difference in V α 14-Tg mice (Figure 4). Thus, whereas a V α 14 TCR α transgene can fully restore iNKT-cell development and polarization in miR-181a/b-1^{-/-} mice, it has little effect at best on the protein levels of Pten. In conclusion, our data suggest that modulation of Pten by miR-181a/b-1 only exerts a minor or secondary effect on iNKT-cell development.

DISCUSSION

In this study, we have re-assessed the molecular mechanisms resulting in impaired development of iNKT cells in miR-181a/b-1^{-/-} mice. MiR-181a/b-1^{-/-} mice carrying a V α 14 α 18 transgenic TCR were phenotypically virtually indistinguishable from their miR-181-sufficient counterparts. Thus these data provide additional evidence that miR-181 primarily controls TCR signaling to support the development of agonist-selected iNKT cells.

Similar TCR surface levels in miR-181a/b-1-deficient and -sufficient mice suggest that miR-181a/b-1 acts downstream rather than upstream of TCR. Thus, in contrast to our observations, deletion of miR-181a/b-1 should also affect iNKT cells expressing high levels of the V α 14 α 18 transgenic TCR. However, our data indicate that high

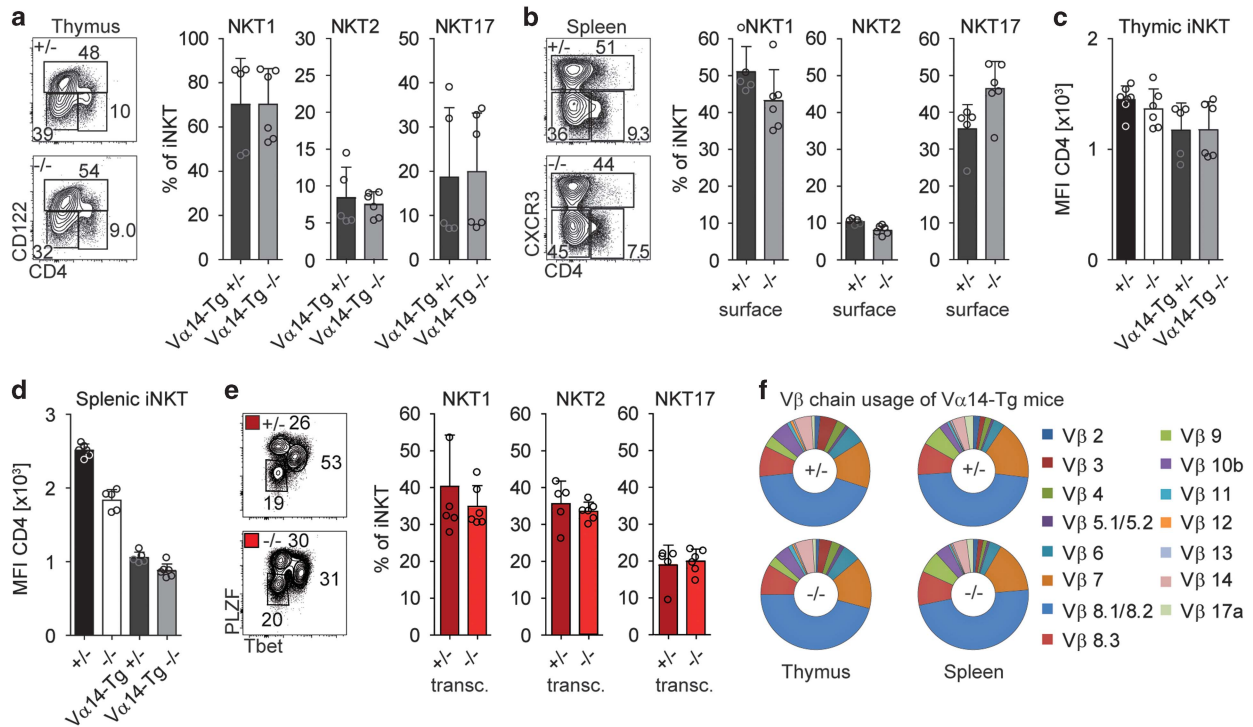


Figure 3 Prearranged TCR α chain restores iNKT-cell development and polarization. (a) Representative contour plots and quantification of thymic NKT1, NKT2 and NKT17 subsets via CD122 and CD4 surface expression for the indicated genotypes, pregated on iNKT cells from V α 14-Tg miR-181a/b-1 sufficient (+/-) and deficient (-/-) mice. (b) Representative contour plots of splenic NKT1, NKT2 and NKT17 subsets via CXCR3 and CD4 surface expression for the indicated genotypes, pregated on iNKT cells. (c, d) Quantification of CD4 expression as mean fluorescence intensity of total iNKT cells of the indicated genotypes from thymus (c) and spleen (d). (e) Representative contour plots and quantification of splenic NKT1, NKT2 and NKT17 subsets of V α 14-Tg miR-181a/b-1 sufficient (+/-) and deficient (-/-) mice based on transcriptional classification. (f) Doughnut graph of V β chain usage of iNKT cells in the thymus and spleen of two V α 14-Tg miR-181a/b-1 sufficient (+/-) and deficient (-/-) mice. (a-d) Pooled data of 5-6 mice from two independent experiments. Error bars indicated s.d. Numbers in bar graphs indicate *P*-value of unpaired *t*-test.

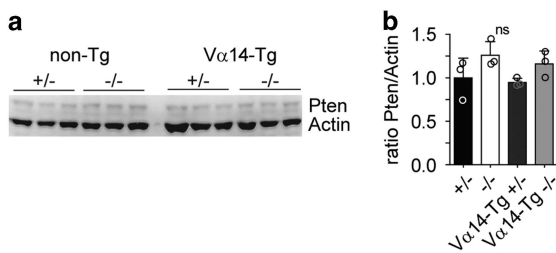


Figure 4 Levels of Pten protein are not affected by a V α 14 TCR transgene. (a) Relative protein levels of Pten determined by western blotting of 1×10^6 thymocytes from the indicated genotypes. (b) Quantification of western blotting data. Expression was normalized to Actin and set to 1 for miR-181a/b-1^{-/-} thymocytes. Pooled data of three mice. Error bars indicate s.d.

levels of the V α 14 α 18 transgenic TCR are sufficient to transmit signals strong enough to overcome the threshold for agonist selection irrespective of a dampening effect caused by the absence of miR-181a/b-1.

Our data remain at odds with another study suggesting that control of anabolic metabolism by the phosphatase Pten is impaired in miR-181-deficient mice, thus limiting iNKT-cell development.⁷ Henaio-Mejia *et al.*⁷ observed a miR-181-dependent reduction of iNKT-cell numbers in the thymus by 20-fold on a non-TCR-transgenic background, which is in good agreement with our own observations. Expression of a transgenic V α 14 α 18 TCR resulted in a reduction of the miR-181-dependent difference in NKT-cell formation

to approximately twofold, showing, in fact, a high degree of TCR-dependent rescue despite the authors' divergent conclusion.

The small discrepancy between both rescue approaches might be explained by the use of different V α 14 α 18 TCR transgenic lines with different levels or timing of transgene expression. In this study, we employed mice expressing the V α 14 α 18 TCR α chain under control of a V α 11 promoter, resulting in high levels of expression.¹³ Although in these mice a non-CD1d-restricted TCR α transgenic population might arise, presumably owing to premature expression of the transgene, these cells are unlikely to account for the higher degree of rescue in our study, because the artificial emergence of such cells would have been reflected in an altered V β repertoire.² However, in our experiments V β usage in V α 14 α 18 transgenic mice was independent of miR-181a expression.

Consistent with the study of Henaio-Mejia *et al.*,⁷ we detected a trend toward increased Pten protein levels in the thymocytes of miR-181-deficient mice, which was retained in the thymocytes from V α 14 α 18 transgenic mice. However, low detection levels of Pten protein at present preclude this point from being definitely addressed. Taken together, these data suggest that elevated expression of Pten in miR-181-deficient thymocytes is of little consequence for iNKT-cell development or can at least be overridden by elevated TCR expression. MicroRNAs have been reported to frequently target multiple components of a given signaling pathway or cellular process.¹⁷ Accordingly, we do not presume that miR-181 exclusively controls the development of iNKT cells by modulating agonist selection via setting TCR signaling thresholds. Rather, metabolic changes by direct or indirect regulation of the expression of Pten might also contribute to the observed phenotype.

Nevertheless, the scenario emerging from all the evidence accumulated by us and others points to a primary role of impaired agonist selection and possibly a secondary role of Pten-mediated metabolic changes.

Limited and dysbalanced cytokine secretion was observed in peripheral iNKT cells from miR-181-deficient mice,⁹ prompting us to analyze whether this finding was reflected by alteration in frequencies of different NKT-cell lineages. Somewhat surprisingly, we found a small increase in frequency of NKT2 cells despite our earlier finding that IL-4 production was more severely affected in miR-181-deficient NKT cells when compared with other cytokines. However, it has been shown that NKT1 cells are also capable of secreting IL-4 upon stimulation. Given their higher frequency in B6 mice, under normal circumstances they might substantially contribute to the amount of IL-4 secreted.⁵ Furthermore, in the absence of miR-181, the expression of both PLZF and T-bet had a wider distribution with a large frequency of cells emerging that expressed intermediate levels of T-bet and PLZF. Thus a clear distinction into NKT1, NKT2 and NKT17 subsets might prove difficult in miR-181-deficient mice. This finding is consistent with a profound deficiency in NKT cells expressing the canonical V β chains in these mice.⁹ Unfortunately, exceedingly low cell numbers preclude further molecular analysis of NKT cells in miR-181-deficient mice.

In summary, our study has provided additional evidence to support the hypothesis that miR-181 expression helps to establish TCR signaling threshold, thus permitting agonist selection of iNKT cells.

METHODS

Mice

B6.Mirc14^{tm1Ankr} mice (termed miR-181a/b-1^{-/-} mice throughout this study)⁹ and V α 14 α 18 TCR α transgenic mice were bred at the animal facility of the Helmholtz Centre for Infection Research in Braunschweig and Hannover Medical School. Animals were maintained under specific-pathogen-free conditions. C57BL/6 V α 14 α 18 transgenic mice¹³ were kindly provided by Dr Albert Bendelac (Department of Pathology, The University of Chicago, Chicago, IL, USA) and Dr Florian Winau (Department of Microbiology and Immunobiology and the Department of Pediatrics, Harvard Medical School, Boston, MA, USA).

Flow cytometry

APC-conjugated CD1d/PBS-57 (α GalCer analog) loaded tetramer was provided by the NIH Tetramer Facility at Emory University (Atlanta, GA, USA). Monoclonal antibodies specific for CD4 (RM4-5, GK1.5), TCR β (H57-597), CXCR3 (CD183; CXCR3-173), CD122 (TM-b1), PLZF (Mags.21F7) and T-bet (4B10) were used as various fluorescent or biotin conjugates. Antibodies were purified from hybridoma supernatants or were purchased from eBioscience (Frankfurt, Germany), BD Biosciences (Heidelberg, Germany), Biogegend (Fell, Germany) or Santa Cruz (Heidelberg, Germany). TCR V β repertoire was analyzed using the Mouse V β TCR Screening Panel (BD) according to the manufacturer's instructions. Transcription factors were stained using the Foxp3/Transcription Factor Staining Buffer Set (eBioscience), and cytokines were stained with Intracellular Fixation and Permeabilization Buffer Set (eBioscience), both according to the manufacturer's instructions. Flow cytometry was conducted on an LSRII (Becton Dickinson, Heidelberg, Germany) and analyzed in FlowJo (10.0, TreeStar, Ashland, OR, USA).

Liver-resident lymphocytes were extracted using an established protocol.¹⁸ Whole organs were passed through 100- μ m cell strainers (BD) into precooled isolation buffer (phosphate-buffered saline+3% fetal calf serum+2 mM EDTA). Lymphoid cells were enriched by a 70%/40% Percoll (GE Healthcare, Darmstadt, Germany) gradient centrifugation (20 min, 300 g) and used for further analysis.

Western blotting

For western blotting analysis, 2 \times 10⁶ lysed total thymocytes were lysed (Cell Lysis Buffer, Cell Signaling, Leiden, The Netherlands), denaturated (NuPAGE

LDS sample buffer, Thermo Fisher, Darmstadt, Germany) and loaded onto NuPAGE Novex 4–12% Bis-Tris protein gels and transferred to Hybond ECL nitrocellulose membranes (Amersham, GE Healthcare, Darmstadt, Germany). Pten (A2B1, Santa Cruz) and Actin (C4, Millipore, Darmstadt, Germany) were detected by ECL reaction with secondary horseradish peroxidase goat anti-mouse antibody (Southern Biotech, Birmingham, AL, USA) using a Fusion FX7 (Vilber Lourmat, Eberhardzell, Germany). Quantification of band intensities was performed with Fusion CaptAdvanced (Vilber Lourmat), utilizing the built-in quantification module (rolling ball method).

Statistics

All analysis was performed using the GraphPad Prism Software (La Jolla, CA, USA). Data are represented as mean+s.d. Statistical significance of differences between two groups was analyzed using non-paired *t*-tests. Samples were not randomized or blinded. Sample size estimates were performed qualitatively based on preliminary data and the data published in Zietara *et al.*⁹

Study approval

All animal experiments were conducted in accordance with local and institutional regulations.

CONFLICT OF INTEREST

The authors declare no conflict of interest.

ACKNOWLEDGEMENTS

V α 14 α 18 TCR transgenic mice were kindly provided by Florian Winau. The allophycocyanin-conjugated CD1d tetramer loaded with PBS-57, an analog of α GalCer, as well as unloaded CD1d tetramer, were kindly provided by the NIH Tetramer Facility at Emory University (Atlanta, GA, USA). The work was supported by grants from the German Research Foundation (DFG, SFB738-A7; KR2320/3-1, KR2320/5-1 and EXC62, 'Rebirth') (to AK).

Author contributions: M \ddot{L} , NZ, JB, SW and AK designed research; JB, NZ, M \ddot{L} , HG, SL and KW performed research; JB, NZ, M \ddot{L} and AK analyzed data; JB and AK wrote the manuscript.

- 1 Sritesky GL, Jameson SC, Hogquist KA. Selection of self-reactive T cells in the thymus. *Annu Rev Immunol* 2012; **30**: 95–114.
- 2 Wei DG, Curran SA, Savage PB, Teyton L, Bendelac A. Mechanisms imposing the Vbeta bias of Valpha14 natural killer T cells and consequences for microbial glycolipid recognition. *J Exp Med* 2006; **203**: 1197–1207.
- 3 Schumann J, Mycko MP, Dellabona P, Casorati G, MacDonald HR. Cutting edge: influence of the TCR Vbeta domain on the selection of semi-invariant NKT cells by endogenous ligands. *J Immunol* 2006; **176**: 2064–2068.
- 4 Schumann J, Voyle RB, Wei BY, MacDonald HR. Cutting edge: influence of the TCR V beta domain on the avidity of CD1d:alpha-galactosylceramide binding by invariant V alpha 14 NKT cells. *J Immunol* 2003; **170**: 5815–5819.
- 5 Lee YJ, Holzapfel KL, Zhu J, Jameson SC, Hogquist KA. Steady-state production of IL-4 modulates immunity in mouse strains and is determined by lineage diversity of iNKT cells. *Nat Immunol* 2013; **14**: 1146–1154.
- 6 Fedeli M, Napolitano A, Wong MP, Marçais A, de Lalla C, Colucci F *et al*. Dicer-dependent microRNA pathway controls invariant NKT cell development. *J Immunol* 2009; **183**: 2506–2512.
- 7 Henao-Mejia J, Williams A, Goff LA, Staron M, Licona-Limon P, Kaech SM *et al*. The microRNA miR-181 is a critical cellular metabolic rheostat essential for NKT cell ontogenesis and lymphocyte development and homeostasis. *Immunity* 2013; **38**: 984–997.
- 8 Zhou L, Seo KH, He HZ, Pacholczyk R, Meng DM, Li CG *et al*. Tie2cre-induced inactivation of the miRNA-processing enzyme Dicer disrupts invariant NKT cell development. *Proc Natl Acad Sci USA* 2009; **106**: 10266–10271.
- 9 Zietara N, Lyszkiewicz M, Witzlau K, Naumann R, Hurwitz R, Langemeier J *et al*. Critical role for miR-181a/b-1 in agonist selection of invariant natural killer T cells. *Proc Natl Acad Sci USA* 2013; **110**: 7407–7412.
- 10 Ebert PJ, Jiang S, Xie J, Li QJ, Davis MM. An endogenous positively selecting peptide enhances mature T cell responses and becomes an autoantigen in the absence of microRNA miR-181a. *Nat Immunol* 2009; **10**: 1162–1169.
- 11 Li QJ, Chau J, Ebert PJ, Sylvester G, Min H, Liu G *et al*. miR-181a is an intrinsic modulator of T cell sensitivity and selection. *Cell* 2007; **129**: 147–161.
- 12 Schaffert SA, Loh C, Wang S, Arnold CP, Axtell RC, Newell EW *et al*. mir-181a-1/b-1 modulates tolerance through opposing activities in selection and peripheral T cell function. *J Immunol* 2015; **195**: 1470–1479.

- 13 Bendelac A, Hunziker RD, Lantz O. Increased interleukin 4 and immunoglobulin E production in transgenic mice overexpressing NK1 T cells. *J Exp Med* 1996; **184**: 1285–1293.
- 14 Georgiev H, Ravens I, Shibuya A, Förster R, Bernhardt G. CD155/CD226-interaction impacts on the generation of innate CD8+ thymocytes by regulating iNKT-cell differentiation. *Eur J Immunol* 2015; **46**: 993–1003.
- 15 Lee YJ, Wang H, Starrett GJ, Phuong V, Jameson SC, Hogquist KA. Tissue-specific distribution of iNKT cells impacts their cytokine response. *Immunity* 2015; **43**: 566–578.
- 16 Seiler MP, Mathew R, Liszewski MK, Spooner CJ, Barr K, Meng F *et al*. Elevated and sustained expression of the transcription factors Egr1 and Egr2 controls NKT lineage differentiation in response to TCR signaling. *Nat Immunol* 2012; **13**: 264–271.
- 17 Tsang JS, Ebert MS, van Oudenaarden A. Genome-wide dissection of microRNA functions and cotargeting networks using gene set signatures. *Mol Cell* 2010; **38**: 140–153.
- 18 Sandrock I, Zietara N, Lyszkiewicz M, Oberdorfer L, Witzlau K, Krueger A *et al*. MicroRNA-181a/b-1 is not required for innate gammadelta NKT effector cell development. *PLoS One* 2015; **10**: e0145010.

The Supplementary Information that accompanies this paper is available on the Immunology and Cell Biology website (<http://www.nature.com/icb>)

6.4 miR-181a/b-1 controls thymic selection of Treg cells and tunes their suppressive capacity

Łyszkiewicz M, Winter SJ, Witzlau K, Föhse L, Brownlie R, Puchałka J, Verheyden NA, Kunze-Schumacher H, Imelmann E, Blume J, Raha S, Sekiya T, Yoshimura A, Frueh JT, Ullrich E, Huehn J, Weiss S, Gutierrez MG, Prinz I, Zamoyska R, **Ziętara N**, Krueger A

PLoS Biology 17(3): e2006716 (2019)

RESEARCH ARTICLE

miR-181a/b-1 controls thymic selection of Treg cells and tunes their suppressive capacity

Marcin Łyszkiewicz^{1,2}, Samantha J. Winter³, Katrin Witzlau¹, Lisa Föhse¹, Rebecca Brownlie⁴, Jacek Puchałka⁵, Nikita A. Verheyden³, Heike Kunze-Schumacher³, Esther Imelmann³, Jonas Blume¹, Solaiman Raha¹, Takashi Sekiya⁶, Akihiko Yoshimura⁶, Jochen T. Frueh^{7,8}, Evelyn Ullrich^{7,8}, Jochen Huehn⁹, Siegfried Weiss¹, Maximiliano G. Gutierrez¹⁰, Immo Prinz¹, Rose Zamoyska⁴, Natalia Ziętara^{1,2}, Andreas Krueger^{1,3}*



1 Institute of Immunology, Hannover Medical School, Hannover, Germany, **2** Institute for Immunology, Ludwig-Maximilians University, Planegg-Martensried, Germany, **3** Institute for Molecular Medicine, Goethe University Frankfurt am Main, Frankfurt, Germany, **4** Institute for Immunology and Infection Research, The University of Edinburgh, Edinburgh, United Kingdom, **5** Department of Pediatrics, Dr. von Hauner Kinderspital, Ludwig-Maximilians University, Munich, Germany, **6** Department of Microbiology and Immunology, Keio University School of Medicine, Tokyo, Japan, **7** Experimental Immunology, Department for Children and Adolescents Medicine, Hospital of the Goethe University Frankfurt, Frankfurt, Germany, **8** LOEWE Center for Cell and Gene Therapy, Goethe University, Frankfurt, Germany, **9** Department of Experimental Immunology, Helmholtz Centre for Infection Research, Braunschweig, Germany, **10** The Francis Crick Institute, London, England, United Kingdom

OPEN ACCESS

Citation: Łyszkiewicz M, Winter SJ, Witzlau K, Föhse L, Brownlie R, Puchałka J, et al. (2019) miR-181a/b-1 controls thymic selection of Treg cells and tunes their suppressive capacity. *PLoS Biol* 17(3): e2006716. <https://doi.org/10.1371/journal.pbio.2006716>

Academic Editor: Avinash Bhandoola, National Cancer Institute, United States of America

Received: May 18, 2018

Accepted: February 27, 2019

Published: March 11, 2019

Copyright: © 2019 Łyszkiewicz et al. This is an open access article distributed under the terms of the [Creative Commons Attribution License](https://creativecommons.org/licenses/by/4.0/), which permits unrestricted use, distribution, and reproduction in any medium, provided the original author and source are credited.

Data Availability Statement: Gene expression data are available at GEO (<https://www.ncbi.nlm.nih.gov/geo/>), accession numbers GSE115391 and GSE124594). T-cell receptor repertoire data are available at SRA (<https://www.ncbi.nlm.nih.gov/sra>), accession number SRP148988).

Funding: German Research Foundation (DFG) (grant number KR2320/5-1), to AK. The funder had no role in study design, data collection and analysis, decision to publish, or preparation of the manuscript. German Research Foundation (DFG)

* These authors contributed equally to this work.
 ✉ Current address: The Peter Doherty Institute for Infection and Immunity, The University of Melbourne, Australia
 * andreas.krueger@kgu.de (AK); natalia.zietara@med.uni-muenchen.de (NZ)

Abstract

The interdependence of selective cues during development of regulatory T cells (Treg cells) in the thymus and their suppressive function remains incompletely understood. Here, we analyzed this interdependence by taking advantage of highly dynamic changes in expression of microRNA 181 family members miR-181a-1 and miR-181b-1 (miR-181a/b-1) during late T-cell development with very high levels of expression during thymocyte selection, followed by massive down-regulation in the periphery. Loss of miR-181a/b-1 resulted in inefficient de novo generation of Treg cells in the thymus but simultaneously permitted homeostatic expansion in the periphery in the absence of competition. Modulation of T-cell receptor (TCR) signal strength in vivo indicated that miR-181a/b-1 controlled Treg-cell formation via establishing adequate signaling thresholds. Unexpectedly, miR-181a/b-1-deficient Treg cells displayed elevated suppressive capacity in vivo, in line with elevated levels of cytotoxic T-lymphocyte-associated 4 (CTLA-4) protein, but not mRNA, in thymic and peripheral Treg cells. Therefore, we propose that intrathymic miR-181a/b-1 controls development of Treg cells and imposes a developmental legacy on their peripheral function.

(grant number SFB738-A7). to AK. The funder had no role in study design, data collection and analysis, decision to publish, or preparation of the manuscript. German Research Foundation (DFG) (grant number SFB902-B15). to AK. The funder had no role in study design, data collection and analysis, decision to publish, or preparation of the manuscript. German Research Foundation (DFG) (grant number EXC62 "REBIRTH"). to AK. The funder had no role in study design, data collection and analysis, decision to publish, or preparation of the manuscript. Boehringer Ingelheim Fonds Travel Grant. to NZ. The funder had no role in study design, data collection and analysis, decision to publish, or preparation of the manuscript. Cancer Research UK (grant number FC001092). to MGG. The funder had no role in study design, data collection and analysis, decision to publish, or preparation of the manuscript. UK Medical Research Council (grant number MC_UP_1202/11, FC001092). to MGG. The funder had no role in study design, data collection and analysis, decision to publish, or preparation of the manuscript. Wellcome Trust (grant number FC001092). to MGG. The funder had no role in study design, data collection and analysis, decision to publish, or preparation of the manuscript.

Competing interests: The authors have declared that no competing interests exist.

Abbreviations: APC, allophycocyanin; BM, bone marrow; CD4, cluster of differentiation 4; CHX, cycloheximide; Cre, Cre recombinase; CTLA-4, cytotoxic T-lymphocyte-associated protein 4; DLR, Dual-Luciferase Reporter; DP, CD4⁺CD8⁺ double positive; DPSS, diode-pumped solid state; *Dusp6*, dual specificity phosphatase 6; EEA1, early endosome antigen 1; ERT2, tamoxifen-inducible estrogen receptor 2; FACS, fluorescence-activated cell scan; FITC, fluorescein isothiocyanate; Foxp3, forkhead box protein P3; GFP, green fluorescent protein; GITR, glucocorticoid-induced tumor necrosis factor receptor-related protein; GM130, *cis*-Golgi matrix protein 130; hCD2, human cluster of differentiation 2; IL, interleukin; *Il7r*, interleukin-7 receptor α gene; *InduRag1*, inducible recombination-activating gene 1; *INKT*, invariant natural killer T; ITAM, immunoreceptor tyrosine-based activation motif; iTreg, induced Treg; KO, knockout; LAMP2, lysosome-associated membrane protein 2; LAVES, Niedersächsisches Landesamt für Verbraucherschutz und Lebensmittelsicherheit; LBD, ligand-binding domain; *let-7g*, *lethal-7g*; *lin*, lineage; LSK, lineage-negative, stem cell antigen-1-positive, Kit-positive; MAIT, Mucosal-Associated Invariant T; MFI, mean fluorescence intensity; MHC, major

Author summary

T cells are pivotal in orchestrating an adaptive immune response. They are produced in the thymus and undergo selection processes resulting in elimination of nonfunctional and self-reactive cells in order to prevent autoimmune disease. One type of T cells, called regulatory T cells (Treg cells), is generated either in the thymus or in the periphery through a process termed agonist selection. Peripheral Treg cells are crucial for the suppression of unwanted immune responses. However, too much suppressive function of Treg cells can also impair immune responses directed against tumors. Here, we have analyzed the mechanisms that regulate this process and show that a microRNA, miR-181a/b-1, controls de novo generation of Treg cells by modulating agonist selection. We show that thymic and peripheral Treg cells deficient in miR-181a/b-1 contain higher levels of the key effector molecule CTLA-4, and as a consequence, such Treg cells display increased suppressive capacity. We observe that the expression of miR-181a/b-1 in peripheral Treg cells is much lower when compared to thymocytes; thus, our study implies that peripheral Treg-cell effector function is imprinted during intrathymic differentiation.

Introduction

Regulatory T cells (Treg cells) expressing the lineage-defining transcription factor forkhead box protein P3 (Foxp3) form an integral part of the adaptive immune system and function to prevent unwanted immune responses [1,2]. Treg cells are generated during T-cell development in the thymus (thymic [t]Treg cells) as well as via peripheral induction of naive T cells (induced [i]Treg cells). Development of tTreg cells depends on strong T-cell receptor (TCR) signals [3]. Accordingly, tTreg cells are generated when a TCR of a developing T cell recognizes a self-antigen with high affinity, as has been demonstrated in mouse models transgenic for both a TCR and its cognate antigen [4,5] and by analysis of polyclonal superantigen-reactive T cells [6,7]. tTreg cells can develop through two distinct precursor (prec) stages. Some Treg-cell precursors are found within a cluster of differentiation (CD) 4 single-positive (SP) Foxp3⁺, glucocorticoid-induced tumor necrosis factor receptor-related protein high (GITR^{hi}), CD25⁺ population [8]. These cells are the first precursors generated in double transgenic TCR/cognate-antigen mouse models [9,10]. More recently, an additional CD4SP Foxp3⁺CD25⁻ Treg-cell precursor has been described [11]. These cells are phenotypically less mature than tTreg cells, are generated with similar kinetics as tTreg cells upon induction of T-cell development in vivo, and efficiently become tTreg cells in vitro and in vivo [10,11]. Generation of both precursors is dependent on strong TCR signals, although on average, Foxp3⁺CD25⁻ Treg-cell precursors have received somewhat weaker signals than their Foxp3⁻GITR^{hi}CD25⁺ counterparts [10]. Further differentiation into mature Foxp3⁺CD25⁺ tTreg cells is then dependent on γ c cytokines [8,10–12]. The level of TCR signal strength required for tTreg cell generation in comparison to TCR signals resulting in clonal deletion have not been fully established. Data from a TCR signaling reporter as well as repertoire studies suggest that signal strength required for tTreg-cell development overlaps with that inducing clonal deletion in other autoreactive thymocytes [3,13–15]. However, reduction of major histocompatibility complex (MHC) ligand levels on medullary thymic epithelial cells rescued autoreactive T cells from clonal deletion but resulted in a concomitant increase in Treg-cell development, suggesting that at least some tTreg cells are generated through weaker TCR signals than those inducing clonal deletion [16].

Treg cells suppress T-cell immune responses using multiple molecular mechanisms, including consumption of interleukin-2 (IL-2) and production of suppressive cytokines, as well as

histocompatibility complex; MID, multiplex identifier; miR-181a/b-1, microRNA family members 181a-1 and 181b-1; miRNA, microRNA; mLN, mesenteric lymph node; *Nr4a1*, Nuclear receptor subfamily 4 group A member 1; Nur77, Nuclear hormone receptor NUR77 encoded by *Nr4a1*; OT-II, ovalbumin-specific MHC class II-restricted alpha beta TCR; OVA, chicken ovalbumin; PE, phycoerythrin; PerCP-Cy5.5, peridinin chlorophyll protein-Cy5.5; pLN, peripheral lymph node; PMA, phorbol 12-myristate 13-acetate; prec, precursor; *Ptpn*, protein tyrosine phosphatase, nonreceptor type; qRT-PCR, quantitative reverse-transcription PCR; Rab11, Ras-related in brain protein 11; *Rag1*, recombination activating gene 1; RIPmOVA, rat insulin promoter-driven membrane-bound chicken ovalbumin; RNAseq, RNA sequencing; RTE, recent thymic emigrant; sCLN, subcutaneous lymph node; snoR412, small nucleolar RNA 412; SP, single positive; Tconv, conventional T cell; TCR, T-cell receptor; TNF, tumor necrosis factor; Treg cell, regulatory T cell; tTreg, thymic Treg; WT, wild type; Zap-70, Zeta-chain-associated tyrosine protein kinase of 70 kD.

expression of the coinhibitory receptor cytotoxic T-lymphocyte-associated protein 4 (CTLA-4) [17,18]. Mice specifically lacking the inhibitory receptor CTLA-4 in Treg cells succumb to fatal autoimmune disease, indicating that CTLA-4 plays a major role in suppressive function [19]. It has been proposed that CTLA-4 on Treg cell surfaces acts through capture of the costimulatory ligands CD80 and CD86 on antigen-presenting cells, thereby curtailing full activation of conventional T cells [20].

MicroRNAs (miRNAs) play a critical role in immune homeostasis and tolerance. Global loss of miRNAs results in defective development of tTreg cells [21]. However, no individual miRNA has been demonstrated to control intrathymic generation of Treg cells. miRNA miR-181a is the most prominently expressed miRNA in double-positive (DP) thymocytes, and it has been shown in vitro that miR-181a serves as a rheostat for TCR signals in T cells and thymocytes through targeting a combination of tyrosine and dual-specificity phosphatases, including protein tyrosine phosphatase, nonreceptor type (*Ptpn* 11, *Ptpn*22, and dual specificity phosphatase 6 (*Dusp*6) [22–24]. Deletion of miR-181a/b-1 in mice resulted in an almost complete failure in development of invariant natural killer T (iNKT) cells and Mucosal-Associated Invariant T (MAIT) cells [25–27] due to a defect in thymic agonist selection [26,28]. Furthermore, loss of miR-181a/b-1 caused altered selection of conventional T cells in a TCR transgenic model with a shift towards positive selection [29]. However, counterintuitively, miR-181a/b-1^{-/-} mice display increased resistance to experimental autoimmunity, which has not been fully explained [29].

Here, we tested the hypothesis that miR-181a/b-1 controlled intrathymic development of Treg cells. De novo production of miR-181a/b-1^{-/-} tTreg cells was impaired because of altered sensitivity to TCR signals during selection. Generation of Treg cells in the absence of miR-181a/b-1 resulted in elevated expression of CTLA-4, which penetrated into the periphery despite the fact that peripheral WT Treg cells express very low amounts of miR-181a. As a consequence, miR-181a/b-1^{-/-} Treg cells had an increased suppressive capacity.

Results

miR-181a/b-1 controls intrathymic Treg-cell development

First, we tested the hypothesis that miR-181a/b-1 might play a role during Treg-cell development. Using a recombination activating gene 1–green fluorescent protein (*Rag1*^{GFP}) knock-in allele to discriminate between nascent and mature thymus-resident or recirculating Treg cells, we found that frequencies and absolute numbers of de novo generated *Rag1*^{GFP}-positive Treg cells were reduced by 2- to 3-fold in miR-181a/b-1^{-/-} mice when compared to control (ctrl), indicating that expression of miR-181a/b-1 is required for normal Treg-cell development in the thymus (Fig 1A). Competitive bone marrow (BM) chimeras with 1:1 mixtures of donor cells from wild-type (WT) and miR-181a/b-1^{-/-} mice revealed a disadvantage in Treg-cell generation, but not more immature double-negative and DP as well as CD4SP populations, from thymocytes of miR-181a/b-1^{-/-} origin, indicating that miR-181a/b-1 controls Treg-cell formation in a cell-intrinsic manner (Fig 1B and S1A Fig). In order to test how miR-181a/b-1 influenced developmental progression towards Foxp3⁺CD25⁺ Treg cells, we analyzed inducible *Rag1* (Indu*Rag1*) miR-181a/b-1^{-/-} mice, in which a wave of T-cell development can be induced by transient initiation of *Rag1* gene expression through a tamoxifen-inducible Cre recombinase (Cre) [30]. At day 7 after *Rag1* induction, only a few CD4SP thymocytes were generated, precluding robust analysis of Treg cell development (S1B and S1C Fig). However, we noted reduced frequencies of postselection DP thymocytes as well as postselection CD4SP thymocytes at this time point in miR-181a/b-1^{-/-} mice when compared to ctrls (S1D Fig). These data support the notion that selection processes are altered in the absence of miR-181a/

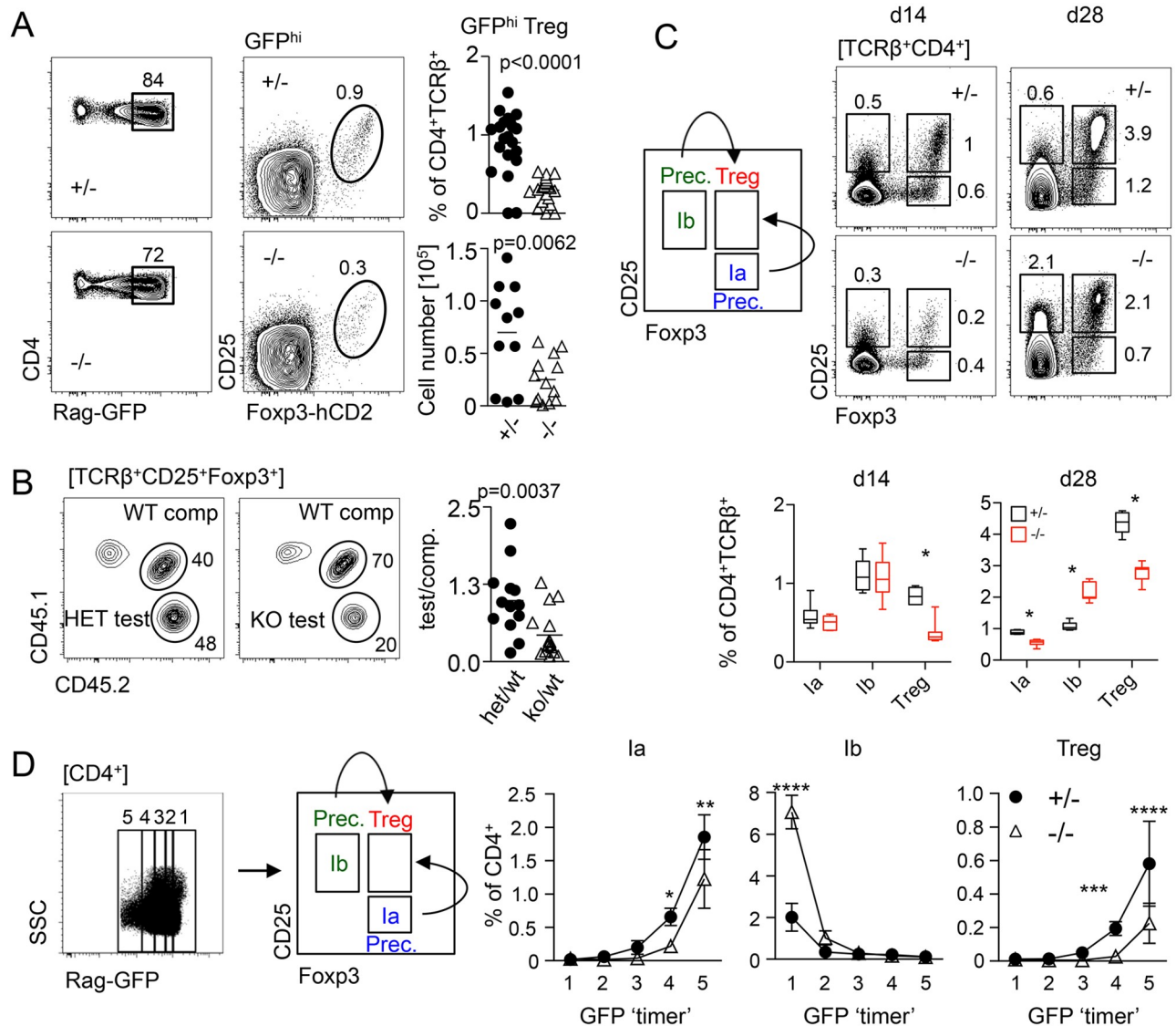


Fig 1. miR-181a/b-1 control intrathymic development of Treg cells. (A) Representative plots, frequencies, and absolute numbers of TCRβ⁺CD4⁺RagGFP^{hi} Treg cells in miR-181-sufficient and deficient mice. Data from 5 independent experiments; each data point represents one mouse. (B) Competitive BM chimeras. BM cells from miR-181a/b-1^{-/-} (het) or miR-181a/b-1^{-/-} (KO) mice (both CD45.2) were mixed in a 1:1 ratio with competitor WT BM cells (CD45.1/2) and injected into lethally irradiated WT recipients (CD45.1). Chimeras were analyzed 12 weeks later for the generation of TCRβ⁺CD4⁺Fxp3⁺ cells in the thymus. Plots are representative of 2 independent experiments with *n* = 8 for each genotype. Graph shows ratio of TCRβ⁺CD4⁺Fxp3⁺ cells within test versus competitor populations. Each data point represents an individual mouse. (C) Frequencies of tTreg cells (TCRβ⁺CD4⁺CD25⁺Fxp3⁺) and their precursors TCRβ⁺CD4⁺CD25⁺Fxp3⁻ (Ia) and TCRβ⁺CD4⁺CD25⁺Fxp3⁻ (Ib) on d 14 and 28 after initial induction of Rag1 expression in InduRag1 mice sufficient and deficient for miR-181a/b-1. Depicted data are from 2 independent experiments, with *n* = 1–4 for each genotype and time point analyzed. Below, quantification of the experiment presented in (C). (D) Molecular age of miR-181a/b-1 Treg cells and their precursors assessed using Rag1^{GFP} reporter mice. Representative plot and gating strategy (left) and quantification (right). Data from 2 independent experiments, *n* = 3–4 for each genotype. Statistical analysis was performed using unpaired Student's *t* test (A, B), multiple *t* test (C), and two-way ANOVA (D, *p*-values for effect of genotype, ***p* = 0.0021, ****p* = 0.0002 and *****p* < 0.001). Numerical values are available in S1 Data. BM, bone marrow; CD, cluster of differentiation; d, day; Fxp3, forkhead box protein P3; GFP, green fluorescent protein; hCD2, human CD 2; InduRag1, inducible recombination-activating gene 1; KO, knockout; miR-181, microRNA-181; prec, precursor; Rag1, recombination-activating gene 1; TCR, T-cell receptor; Treg cell, regulatory T cell; tTreg cell, thymic Treg cell; WT, wild type.

<https://doi.org/10.1371/journal.pbio.2006716.g001>

b-1. At day 14 and day 28, frequencies of Treg cells within CD4SP thymocytes were lower in miR-181a/b-1^{-/-} mice when compared to ctrls (Fig 1C). Consistent with findings at steady state, these data indicate that Treg-cell formation is less efficient in the absence of miR-181a/b-1. Next, we analyzed miR-181a/b-1-dependent formation of Fxp3⁻CD25⁺ (prec lb) or

Foxp3⁺CD25⁻ (prec 1a) Treg-cell precursors in the InduRag1 model. At day 14 after induction, both intermediates were present at somewhat similar frequencies in miR-181a/b-1^{-/-} mice when compared to ctrl, whereas at day 28, we observed reduced frequencies of Foxp3⁺CD25⁻ precursors and an accumulation of Foxp3⁻CD25⁺ precursors, suggesting that precursor generation is not restricted by a developmental block (Fig 1C). Taken together, these data indicate that in the absence of miR-181a/b-1, Treg cells are formed with slower kinetics rather than being subject to a defined developmental block. Treg-cell development in the thymus follows a somewhat different course in the absence of a full CD4SP compartment [10]. To account for such differences, we complemented the analysis of InduRag1 mice by taking advantage of the *Rag1*^{GFP} knock-in allele described above to temporally separate Treg-cell development at steady state. Green fluorescent protein (GFP⁺) cells were arbitrarily gated into 5 populations based on different GFP levels, with loss of GFP expression indicating increasing amounts of time since cessation of Rag gene expression, which occurs in DP thymocytes. Frequencies of precursor 1b were elevated in GFP^{hi} cells from miR-181a/b-1^{-/-} mice when compared to ctrls. In contrast, generation of precursor 1a as well as Treg cells was delayed in miR-181a/b-1^{-/-} mice when compared to ctrls (Fig 1D), which is consistent with data obtained in the InduRag1 model. We conclude that loss of miR-181a/b-1 results in an overall delay of Treg-cell formation, which is likely to be initiated prior to the emergence of defined Treg-cell precursors and cannot be compensated for by increased frequencies of Foxp3⁻CD25⁺ precursors.

TCR signal strength determines miR-181a/b-1-dependent Treg-cell development

In order to test whether TCR signal strength differed in thymocytes from miR-181a/b-1^{-/-} mice, we assessed expression of Nuclear hormone receptor NUR/77 (Nur77) as a surrogate marker. Of note, miR-181a/b-1^{-/-} DP cells expressed lower levels of Nur77 prior to stimulation when compared to ctrls (Fig 2A). Furthermore, ex vivo stimulation of miR-181a/b-1^{-/-} DP cells failed to induce WT levels of Nur77, together suggesting that miR-181a/b-1^{-/-} DP cells received weaker TCR signals and failed to respond to TCR triggering with the same sensitivity as their WT counterparts (Fig 2A). In order to test whether TCR signaling was impaired prior to Treg-cell generation, we assessed surface expression of CD5, which correlates with TCR signal strength, on thymocyte subsets [31]. At steady state, total DP thymocytes, the majority of which have not undergone selection, displayed similar levels of surface CD5 in the presence and absence of miR-181a/b-1 (Fig 2B). However, CD4SP thymocytes from miR-181a/b-1^{-/-} mice displayed lower surface levels when compared to ctrls. tTreg cells from either genotype expressed similar levels of Nur77 transcripts (Fig 2C), together indicating that miR-181a/b-1 limits TCR signal strength prior to the emergence of Treg cells.

Next, we took advantage of a system mimicking increased TCR signal strength during Treg-cell development via inducible nuclear translocation of the Nur77 family member Nr4a2 [32]. BM chimeric mice were generated to carry miR-181a/b-1-deficient or miR-181a/b-1-sufficient ovalbumin-specific MHC class II-restricted alpha beta (OT-II) TCR transgenic cells expressing inducible Nr4a2. Transduction with ctrl virus resulted in generation of low frequencies of Treg cells from miR-181a/b-1-sufficient mice, and even fewer Treg cells emerged from miR-181a/b-1^{-/-} donor BM cells (Fig 2D). Upon activation of Nr4a2, frequencies of Treg cells generated from miR-181a^{+/-} donors were slightly, albeit not significantly, reduced, suggesting that activation of Nr4a2 promotes a shift towards clonal deletion. In contrast, in the absence of miR-181a/b-1, Treg-cell development was rescued upon activation of Nr4a2, supporting the hypothesis that limited TCR signal strength accounts for defective Treg-cell differentiation in miR-181a/b-1^{-/-} mice. To corroborate these data, we analyzed chimeric mice

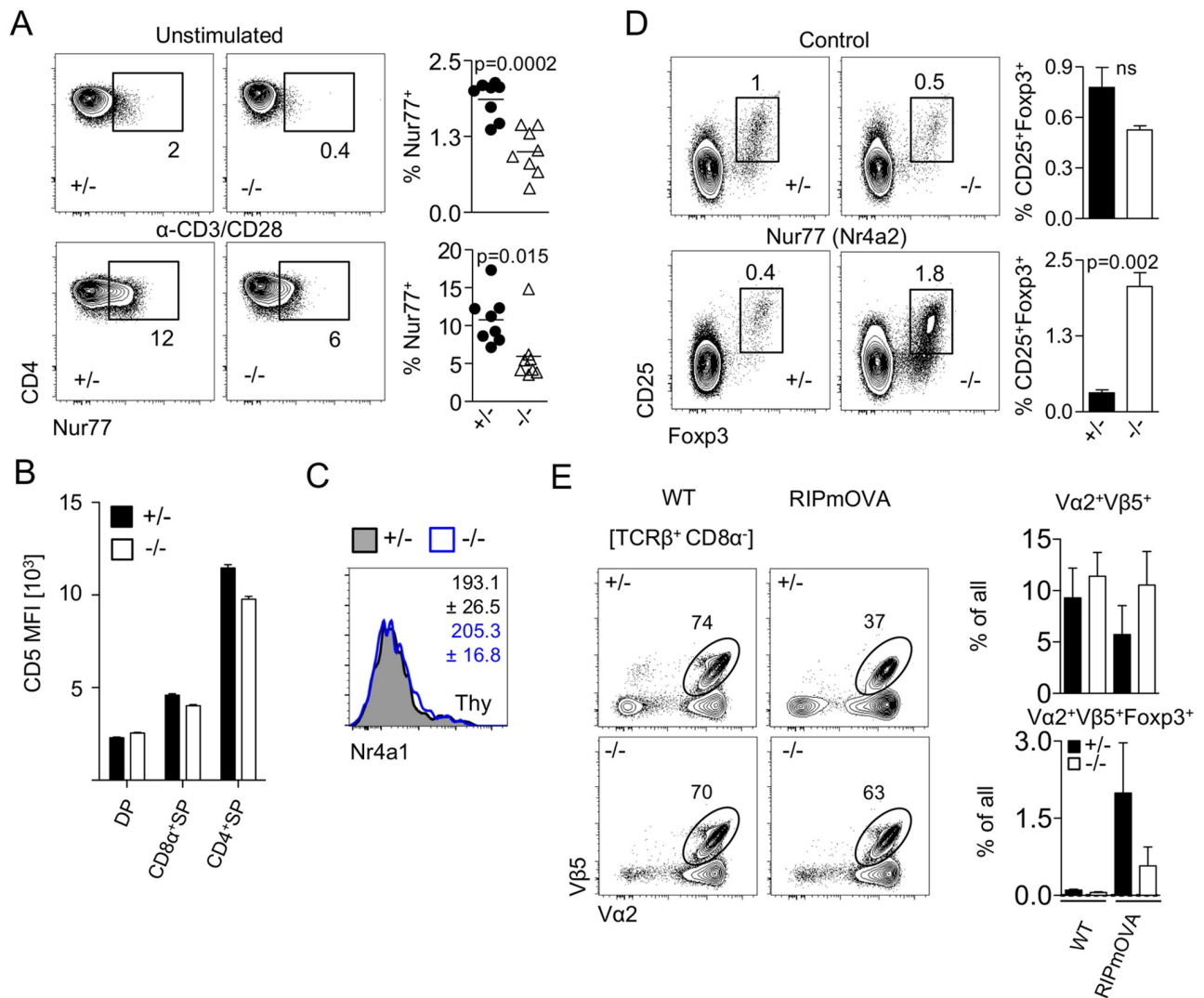


Fig 2. TCR signal strength determines miR-181a/b-1-dependent Treg-cell development. (A) Expression of Nur77 in DP thymocytes in the absence of miR-181a/b-1. Unstimulated or stimulated (3 h, 37 °C, α CD3/CD28 2.5 μ g/ml) thymocytes from miR-181a/b-1 het and KO mice were stained for intracellular Nur77. Plots are representative of 2 independent experiments with $n = 3-4$ for each genotype. Graphs show frequencies of Nur77-positive cells for indicated conditions in CD4⁺CD8 α ⁺ DP thymocytes. (B) Reduced CD5 expression in the absence of miR-181a/b-1 mirrors impaired TCR signaling. Data from 2 independent experiments with $n = 8-9$ per group. (C) RNA flow-cytometry analysis of the expression of *Nr4a1* (encoding Nur77) by TCR β ⁺CD4⁺Foxp3⁺ tTreg cells. Numbers indicate average MFI \pm SD. Data from 2 independent experiments with $n = 2-3$ per experiment. (D) Overexpression of Nr4a2 (Nur77 family) rescues development of Treg cells deficient for miR-181a/b-1. LSK cells from OT-II \times miR-181a/b-1^{+/-} or OT-II \times miR-181a/b-1^{-/-} mice were sorted and transduced with a retrovirus expressing a chimeric Nr4a2 molecule in which the Nr4a2 LBD is replaced by that of a mutant human estrogen receptor- α (Nr4a2- Δ LBD-ERT2) or ctrl retrovirus. Cells were injected into lethally irradiated WT recipients, and 7 weeks later, expression of Nr4a2 was induced via tamox administration for 5 consecutive days before analysis. Plots depict frequencies of Treg cells generated from precursor cells transduced with ctrl vector (upper panels) and from precursors transduced with vector carrying inducible Nr4a2 (lower panels). Graphs show summary of the results from 2 independent experiments, with $n = 3$ for each genotype and condition. (E) Less efficient clonal deletion and Treg-cell formation in the absence of miR-181a/b-1. OT-II \times RIPmOVA chimeras were generated after lethal irradiation of RIPmOVA recipient mice (ctrl: WT/WT; transgenic: tg/WT) and injection of OT-II \times miR-181a/b-1^{+/-} or OT-II \times miR-181a/b-1^{-/-} BM cells. Mice were analyzed after 8 weeks. Plots depict frequencies of V α 2⁺V β 5⁺ OVA-specific donor cells in ctrl and tg recipients, which express OVA during negative selection. Graphs show summary of this analysis (upper panel) and absolute numbers as well as frequencies of V α 2⁺V β 5⁺Foxp3⁺ Treg cells generated in the presence or absence of miR-181a/b-1 (lower panels). Data are representative of 2 independent experiments with $n = 6-9$ for each recipient/donor combination. Statistical analysis was performed using unpaired Student's *t* test (A, C, D). Numerical values are available in S1 Data. BM, bone marrow; CD, cluster of differentiation; ctrl, control; DP, double positive; ERT2, tamoxifen-inducible estrogen receptor 2; Foxp3, forkhead box protein P3; LBD, ligand-binding domain; LSK, lineage-negative, stem cell antigen-1-positive, Kit-positive; MFI, mean fluorescence intensity; miR-181, microRNA-181; *Nr4a1*, Nuclear receptor subfamily 4 group A member 1; Nur77, Nuclear hormone receptor NUR/77 encoded by *Nr4a1*; OT-II, ovalbumin-specific MHC class II-restricted alpha beta TCR; OVA, chicken ovalbumin; prec, precursor; RIPmOVA, rat insulin-promoter-driven membrane-bound chicken ovalbumin; SP, single positive; tamox, Tamoxifen; TCR, T-cell receptor; tg, transgenic; Treg cell, regulatory T cell; WT, wild type.

<https://doi.org/10.1371/journal.pbio.2006716.g002>

generated using OT-II TCR transgenic miR-181a/b-1-sufficient (OT-II-ctrl) or deficient (OT-II-knockout [KO]) donor cells transferred into RIPmOVA recipients. RIPmOVA mice express the cognate antigen for the OT-II TCR in the thymus, resulting in clonal deletion of OT-II TCR transgenic cells as well as generation of low numbers of Treg cells. OT-II-KO>RIPmOVA chimeras showed lower levels of clonal deletion and generated considerably lower numbers of Treg cells when compared to OT-II-ctrl>RIPmOVA chimeras (Fig 2E). OT-II-ctrl>WT as well as OT-II-KO>WT chimeras failed to generate sizeable numbers of OT-II Treg cells and showed no signs of clonal deletion of OT-II thymocytes. We conclude that impaired generation of Treg cells in miR-181a/b-1-deficient mice is due to restricted TCR signal strength during thymic selection.

Homeostatic expansion generates normal Treg-cell numbers in the periphery of miR-181a/b-1^{-/-} mice

To address potential consequences of impaired tTreg-cell development in the absence of miR-181a/b-1, we next determined frequencies of Treg cells in the periphery. We did not observe any differences in frequencies and absolute numbers of peripheral Treg cells in spleens from miR-181a/b-1^{-/-} mice compared to ctrls (Fig 3A). Consistently, frequencies of recirculating or thymus-resident (*Rag1*^{GFP}-negative) Treg cells in the thymus were largely unaffected in the absence of miR-181a/b-1, but we observed reduced frequencies of *Rag1*^{GFP}-positive recent thymic emigrants (RTEs) among peripheral Treg cells (S2A and S2B Fig). Equilibration of Treg-cell numbers in the periphery can occur through homeostatic expansion of tTreg cells or preferential peripheral induction from naive T cells. Spleens of miR-181a/b-1-sufficient and deficient mice contained comparable frequencies of RTEs (TCRβ⁺Rag1-GFP⁺) cells, which are enriched in peripheral Treg cell precursors (S2B Fig) [33]. Furthermore, CD4⁺CD25⁻ RTEs from miR-181a/b-1^{-/-} mice did not produce more iTreg cells upon transfer into lymphopenic interleukin-7 receptor α gene (*Il7r*)^{-/-} hosts when compared to ctrls, suggesting that Treg-cell induction is not the primary mechanism to equilibrate peripheral Treg-cell numbers in miR-181a/b-1^{-/-} mice (S2C Fig). Chimeric mice generated with 1:1 mixtures of miR-181a/b-1^{-/-} and WT BM showed that miR-181a/b-1^{-/-} Treg cells had a competitive disadvantage in the periphery when WT Treg cells were present, indicating that niche availability permits homeostatic expansion of tTreg cells in miR-181a/b-1^{-/-} mice (Fig 3B). This conclusion was supported by Helios staining and TCR repertoire analysis. Elevated Helios expression has been associated with Treg-cell activation and proliferation [34]. Comparison of tTreg cells from miR-181a/b-1-sufficient and deficient mice showed low and similar expression of Helios between genotypes (Fig 3C). Staining in peripheral lymphoid organs (spleen, subcutaneous lymph node [scLN], and mesenteric lymph node [mLN]) revealed elevated numbers of Helios⁺ Treg cells in miR-181a/b-1^{-/-} mice, indicating that in these mice, more Treg cells are in an activated/proliferative state (Fig 3C).

We predicted that limited de novo generation and increased peripheral expansion resulted in reduced TCR diversity in peripheral Treg cells in the absence of miR-181a/b-1. Comparison of numbers of unique CDR3 sequences as well as calculation of effective number of species as a measure for repertoire diversity showed that TCR diversity in peripheral Treg cells from miR-181a/b-1^{-/-} mice was significantly reduced (Fig 3D and S3A Fig). In contrast, in the thymus, Treg cells from miR-181a/b-1^{-/-} mice displayed comparable TCR diversity as their ctrl counterparts (Fig 3E and S3A Fig). Thus, these data indicate that, as a consequence of less efficient generation, fewer clones egress from the thymus to be available for peripheral expansion.

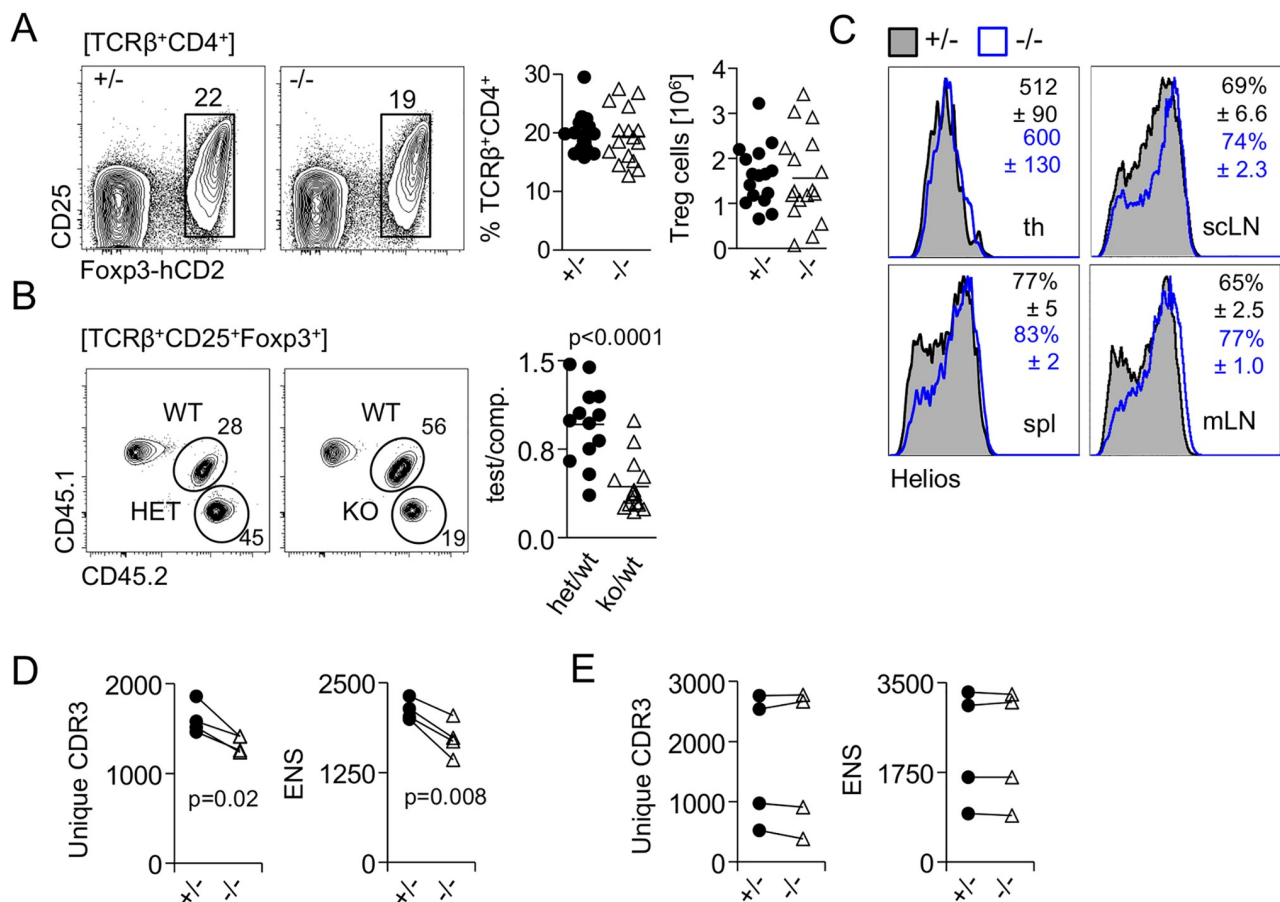


Fig 3. Homeostatic expansion generates normal Treg-cell numbers in the periphery of miR-181a/b-1^{-/-} mice. (A) Frequencies and absolute numbers of splenic Treg cells in Foxp3^{hCD2} reporter mice crossed to miR-181a/b-1 KO mice. Plots are representative of 6 independent experiments. Graph shows summary of all experiments, in which each data point represents one mouse. (B) Competitive BM chimeras. BM cells isolated from miR-181a/b-1^{+/-} (het) or miR-181a/b-1^{-/-} (KO) mice (both CD45.2) were mixed in 1:1 ratio with competitor BM cells, WT (CD45.1/2), and injected into lethally irradiated WT recipients (CD45.1). Chimeras were analyzed 12 weeks after injection for the generation of TCRβ⁺CD4⁺Foxp3⁺ cells in the spl. Plots are representative of 2 independent experiments with *n* = 8 for each genotype. Graph shows ratio of TCRβ⁺CD4⁺Foxp3⁺ cells within tested to competitive populations. Each data point represents an individual mouse. (C) Higher frequencies of Helios-positive cells in peripheral lymphoid organs of miR-181a/b-1^{-/-} mice. Representative histograms and plots from 2 independent experiments (*n* = 6–9 for each genotype) are depicted. Numbers indicated average MFI or frequencies of positive cells, ±SD. Statistical analysis was performed using unpaired Student's *t* test. (D,E) High-throughput sequencing of TCRα (CDR3 fragment of Vα8–Cα chain) in splenic Treg (D) and tTreg (E) cells sorted from miR-181a/b-1^{+/-} or miR-181a/b-1^{-/-} mice. Left graph shows number of all unique CDR3 sequences (CDR3). Right graphs show ENS calculated for each sample. Depicted are 4 independent sequencing experiments; samples from the same experiment are paired. Statistical analysis was performed using paired Student's *t* test. Numerical values are available in S1 Data. BM, bone marrow; CD, cluster of differentiation; comp., competitor; ENS, effective number of species; Foxp3, forkhead box protein P3; hCD2, human CD2; KO, knockout; MFI, mean fluorescence intensity; miR-181, microRNA-181; mLN, mesenteric lymph node; scLN, subcutaneous lymph node; spl, spleen; TCR, T-cell receptor; th, thymus; Treg cell, regulatory T cell; tTreg cell, thymic Treg cell; WT, wild type.

<https://doi.org/10.1371/journal.pbio.2006716.g003>

Inefficient intrathymic generation of Treg cells results in a post-transcriptional increase in CTLA-4 expression

Next, we assessed whether impaired generation in the thymus altered the phenotype of Treg cells in the absence of miR-181a/b-1. Expression of miR-181a progressively decreases after thymocytes exit the DP stage, with CD4⁺SP thymocytes and thymic Treg cells expressing 2-fold and 15-fold lower levels, respectively (Fig 4A). In the periphery, expression of miR-181a was further reduced to 30-fold and 75-fold lower levels for CD4⁺ conventional T cells (Tconv) and Treg cells, respectively, when compared to DP thymocytes. Peripheral miR-181a/b-1^{-/-} Treg cells showed a virtually identical global gene expression profile to their ctrl counterparts.

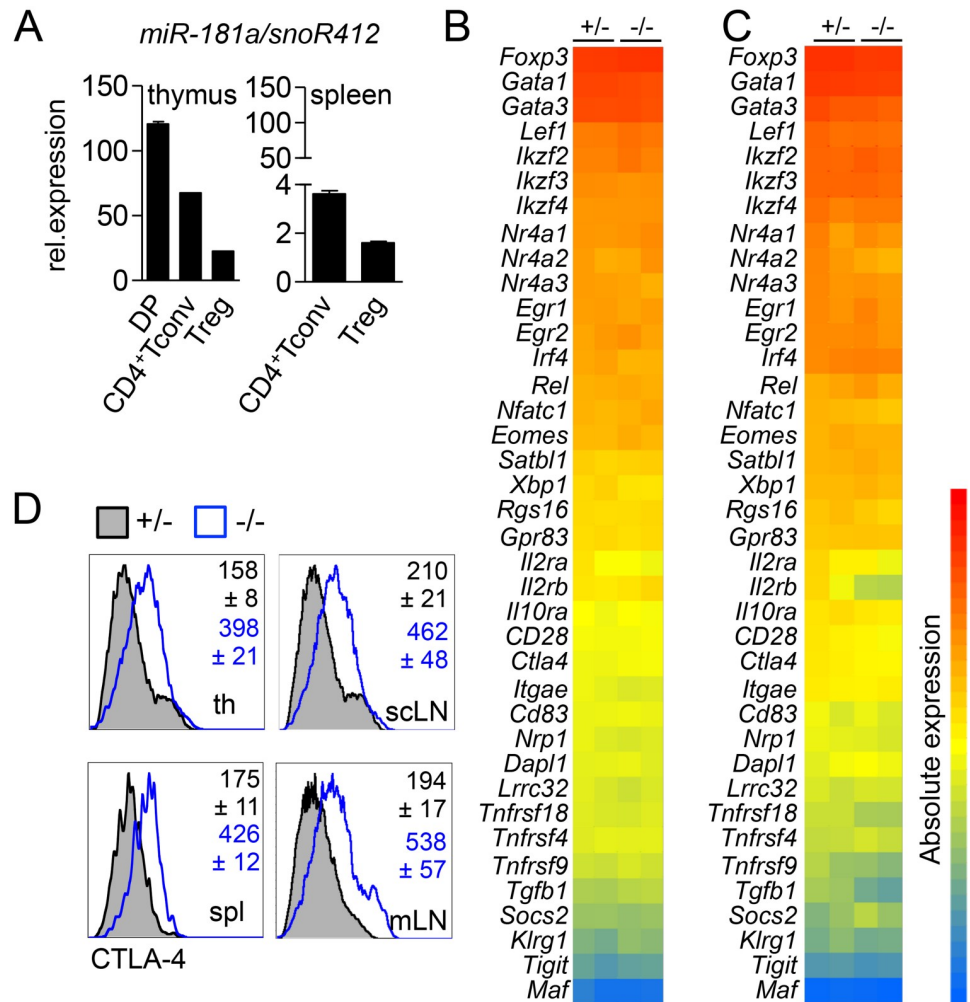


Fig 4. Inefficient intrathymic generation of Treg cells results in post-transcriptional increase in CTLA-4 expression. (A) qRT-PCR analysis of miR-181a expression in sorted thymic populations (left graph) and splenic populations (right graph). Data from 2 independent experiments, with $n = 6-7$ (pool) for each genotype and one experiment for tTreg cells and CD4⁺ Tconv cells, $n = 7$ (pool). Expression of miR-181a was normalized to the expression of housekeeping small RNA, snoR412. Linearized ΔC_T values are displayed on the graph. Transcriptional analysis of splenic Treg (B) and tTreg (C) cells. Heat map of signature genes (absolute expression) in miR-181a/b-1^{+/-} or miR-181a/b-1^{-/-} Treg cells. Columns on the heat map represent 2 individual samples from pooled thymi of 5-7 animals for each genotype. (D) Flow-cytometry analysis of CTLA-4 expression in tTreg and peripheral Treg cells. Representative histograms of 2 independent experiments ($n = 6-9$ for each genotype) are depicted. Numbers indicate average MFI \pm SD. Numerical values are available in S1 Data. CD, cluster of differentiation; CTLA-4, cytotoxic T-lymphocyte-associated protein 4; *Dapl1*, death-associated protein-like 1; DP, double positive; *Egr*, early growth response gene; *Eomes*, eomesodermin; *Foxp3*, forkhead box protein P3; *Gata*, GATA-binding factor; *Gpr83*, G-protein-coupled receptor 83; *Il2ra*, interleukin-2 receptor alpha; *Il2rb*, interleukin-2 receptor beta; *Il10ra*, interleukin-10 receptor alpha; *Ikzf*, Ikaros zinc finger; *Irf4*, interferon regulatory factor 4; *Itgae*, integrin alpha E; *Klrg1*, killer cell lectin-like receptor subfamily G member 1; *Lef1*, lymphoid enhancer-binding factor 1; *Lrrc32*, leucine-rich repeat containing 32; *Maf*, musculoaponeurotic fibrosarcoma oncogene homolog; MFI, mean fluorescence intensity; miR-181, microRNA-181; mLN, mesenteric lymph node; *Nfatc1*, nuclear factor of activated T cells c1; *Nrp1*, neuropilin 1; *Nr4a*, Nuclear receptor subfamily 4 group A; qRT-PCR, quantitative reverse-transcription PCR; *Rel*, homolog to the oncogen protein of the reticuloendotheliosis virus strain; *Rgs16*, regulator of G protein signaling 16; *Satb1*, special AT-rich sequence-binding protein-1; scLN, supraclavicular lymph node; snoR412, small nucleolar RNA 412; *Socs2*, suppressor of cytokine signaling 2; spl, spleen; Tconv, conventional T; *Tgfb1*, transforming growth factor beta 1; th, thymus; *Tigit*, T-cell immunoreceptor with Ig and ITIM domains; *Tnfrsf4*, tumor necrosis factor receptor superfamily member 4; Treg cell, T regulatory cell; tTreg cell, thymic Treg cell; *Xbp1*, X-box binding protein 1.

<https://doi.org/10.1371/journal.pbio.2006716.g004>

Notably, this was also the case for key Treg-cell signature genes (Fig 4B). Comparison of transcriptomes of thymic miR-181a/b-1^{-/-} Treg cells with their WT counterparts also revealed no significant differences both globally as well as with regard to Treg-cell signature genes (Fig 4C). Given that miRNAs may also act on a post-transcriptional level, we next assessed expression levels of Treg-cell signature receptors and transcription factors. Peripheral and tTreg cells from miR-181a/b-1^{-/-} mice showed similar expression levels of most surface receptors and transcription factors analyzed as WT ctrls (S4A, S4B and S4C Fig). Notably, we detected strongly increased levels of total CTLA-4 protein in both peripheral and tTreg cells from miR-181a/b-1^{-/-} mice when compared to ctrls (Fig 4D). Although the coding sequence of *Ctla4* mRNA contains putative miR-181 binding sites, direct modulation of CTLA-4 expression by miR-181 could not be observed in luciferase assays (S5A and S5B Fig).

We conclude from these data that thymic generation in the absence of miR-181a/b-1 results in post-transcriptionally controlled up-regulation of CTLA-4 protein in Treg cells while other Treg-cell signature genes remain unaffected. Loss of miR-181a expression in WT peripheral Treg cells suggests that elevated expression of CTLA-4 in these cells is imprinted during development.

Elevated levels of CTLA-4 in the absence of miR-181a/b-1 are maintained via increased rates of translation

In order to understand the underlying mechanisms of how elevated levels of CTLA-4 protein are maintained in peripheral miR-181a/b-1^{-/-} Treg cells, we analyzed its intracellular distribution using confocal microscopy. We confirmed elevated expression of CTLA-4 protein in the absence of miR-181a/b-1 (Fig 5A). Next, we determined intracellular localization of CTLA-4 by costaining for Ras-related in brain protein 11 (Rab11, marking recycling endosomes), lysosome-associated membrane protein 2 (LAMP2, late endosomes), early endosome antigen 1 (EEA1, early endosomes), and *cis*-Golgi matrix protein 130 (GM130, Golgi). We detected no differences in the extent of colocalization of CTLA-4 with early endosomes and the Golgi apparatus in Treg cells from miR-181a/b-1^{-/-} mice compared to ctrls (Fig 5B). However, we noted reduced colocalization of CTLA-4 with recycling endosomes but a marked increase in colocalization with late endosomes in miR-181a/b-1^{-/-} Treg cells when compared to ctrls (Fig 5C).

In order to assess whether aberrant localization of CTLA-4 in miR-181a/b-1^{-/-} Treg cells affected protein degradation, we stimulated Treg cells in the absence or presence of the translation inhibitor cycloheximide. Inhibition of translation for 2 h reduced CTLA-4 protein to similar levels in miR-181a/b-1^{-/-} Treg cells and ctrls (Fig 5D). Given the higher protein levels when translation is active, these data imply that degradation rates of CTLA-4 are higher in the absence of miR-181a/b-1, which is consistent with its preferential localization in late endosomes rather than recycling endosomes. Furthermore, these data predict that if protein degradation is intact, elevated levels of CTLA-4 protein arise as a result of increased rates of protein translation. To test this prediction, we assessed accumulation of CTLA-4 protein in Treg cells in the presence of bafilomycin, an inhibitor of lysosomal protein degradation, *in vitro*. Over the course of 3 hours, miR-181a/b-1^{-/-} Treg cells accumulated significantly more CTLA-4 protein when compared to their WT counterparts (Fig 5E). Together, these data indicate that elevated levels of CTLA-4 in peripheral Treg cells in the absence of miR-181a/b-1 are due to increased rates of translation. Increased protein translation in the absence of altered mRNA levels may be induced by loss of miRNAs other than miR-181a/b-1. To test this possibility, we performed small RNA sequencing (small RNAseq) of miR-181a/b-1-sufficient and deficient peripheral Treg cells. Consistent with the overall small changes in the transcriptome, we identified 4 miRNAs (miR-15b, miR-150, miR-342, and lethal (*let*)-7g) that were moderately

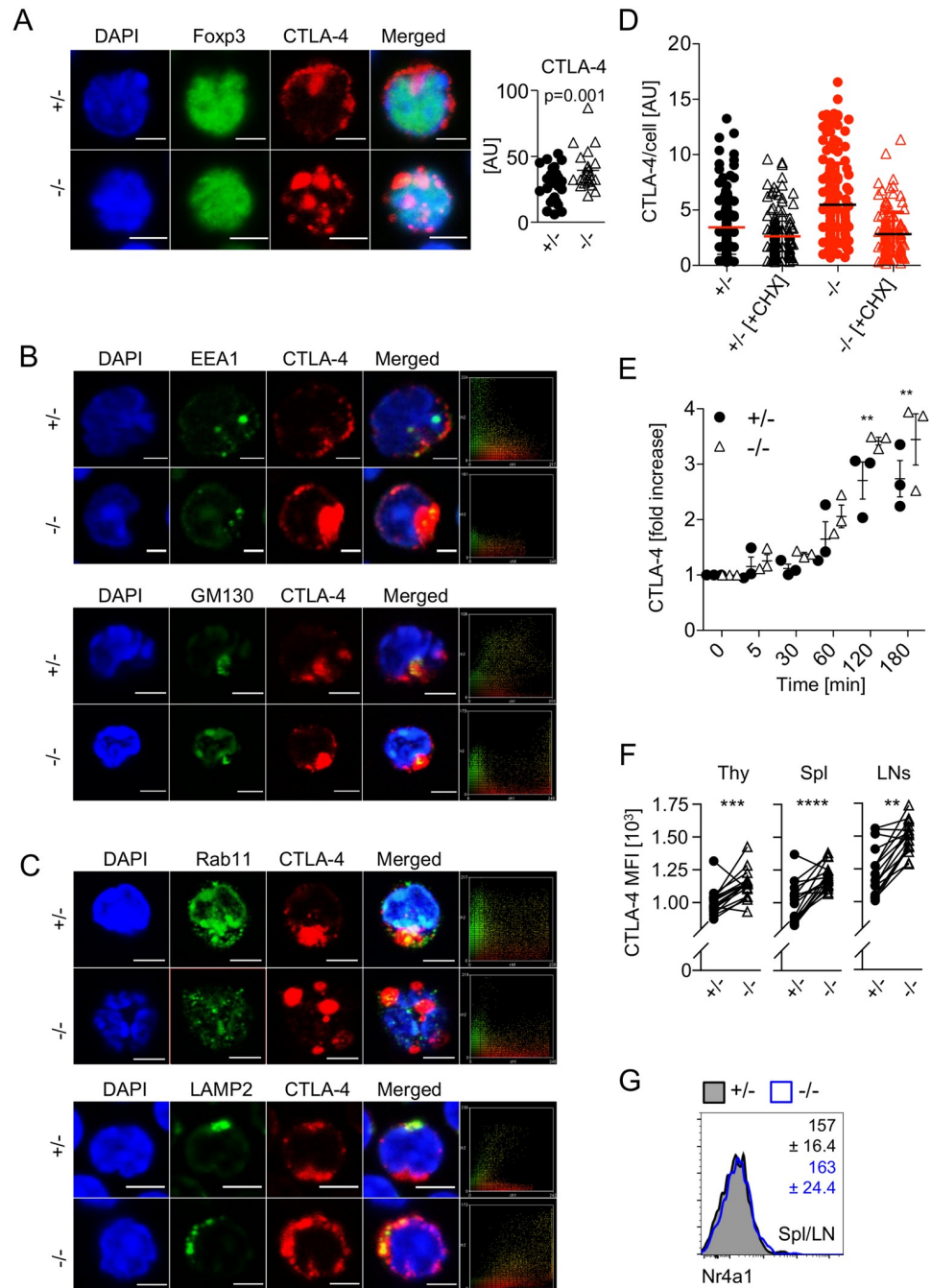


Fig 5. Elevated levels of CTLA-4 in the absence of miR-181a/b-1 are cell-intrinsically maintained via increased rates of translation. (A) Immunofluorescence staining of Treg cells from miR-181a/b-1^{+/-} or miR-181a/b-1^{-/-} mice with antibodies against Foxp3 and CTLA-4. Right panel, quantification of integrated density for CTLA-4 fluorescence normalized to the area of each individual cell. Data are representative of 3 independent experiments with *n* = 3 for each genotype (pooled). Data were analyzed using ImageJ software. DAPI, nuclear staining. Scale bar, 2 μ m. (B) Immunofluorescence staining of CD4⁺ T cells from miR-181a/b-1^{+/-} or miR-181a/b-1^{-/-} mice with antibodies against murine CTLA-4, EEA1 (upper panel) and GM130 (lower panel). Data are representative of 3 independent experiments with *n* = 3 (pool). Right panels show colocalization scatter plots. (C) Immunofluorescence staining of CD4⁺ T cells from miR-181a/b-1^{+/-} or miR-181a/b-1^{-/-} mice with antibodies against murine CTLA-4, Rab11 (upper panel) and LAMP2 (lower panel). Data are representative of 3 independent experiments with *n* = 3 (pool). Right panels show colocalization scatter plots. Data were analyzed using ImageJ software. DAPI, nuclear staining. Scale bar, 2 μ m. (D) Enhanced degradation of CTLA-4 in the absence of miR-181a/b-1. CD4⁺ T cells isolated from spls and subcutaneous LNs of miR-181a/b-1^{+/-} or miR-181a/b-1^{-/-} mice were stimulated for 2 h with α CD3/ α CD28 antibodies. In order to

monitor protein degradation, CHX was added and incubated with cells for an additional 3 h. Each dot represents an individual cell from 10–12 randomly chosen fields of view. Quantification of integrated density for CTLA-4 fluorescence per cell was quantified using ImageJ software. (E) CD4⁺CD25⁺-enriched T cells were incubated in the presence of an inhibitor of lysosomal degradation, bafilomycin, for indicated time points. Accumulation of CTLA-4 was detected using FACS, and fold increase of MFI was calculated using time point 0 as reference. Data from 3 independent experiments, $n = 3$. (F) Cell-intrinsic up-regulation of CTLA-4 in the absence of miR-181a/b-1. Mixed BM chimeras were generated by mixing BM cells from miR-181a/b-1^{+/-} (CD45.1) and miR-181a/b-1^{-/-} (CD45.2) mice in a 1:1 ratio and injecting them into lethally irradiated WT recipients (CD45.1/2). Chimeras were analyzed 8 weeks after reconstitution for CTLA-4 expression in TCRβ⁺CD4⁺Foxp3⁺ cells from the Thy, spl, and LNs. Plots are representative of 2 independent data points with $n = 9$ per experiment. Each set of paired data points represents an individual mouse. (G) RNA flow-cytometry analysis of the expression of *Nr4a1* by TCRβ⁺CD4⁺Foxp3⁺ Treg cells from pooled spl and LNs. Numbers indicate average MFI ± SD. Data from 2 independent experiments with $n = 2-3$ per experiment. Statistical analysis was performed using unpaired Student's *t* test (A), two-way ANOVA (E, *p*-values for effect of genotype, ** $p = 0.0021$) and paired Student's *t* test (F, *p*-values for effect of each genotype, ** $p = 0.0021$, *** $p = 0.0002$, and **** $p < 0.0001$). Numerical values are available in [S1 Data](#). AU, arbitrary unit; BM, bone marrow; CD, cluster of differentiation; CHX, cycloheximide; CTLA-4, cytotoxic T-lymphocyte-associated protein 4; EEA1, early endosome antigen 1; FACS, fluorescence-activated cell scan; Foxp3, forkhead box protein P3; GM130, *cis*-Golgi matrix protein 130; LAMP2, lysosome-associated membrane protein 2; LN, lymph node; MFI, mean fluorescence intensity; miR-181, microRNA-181; *Nr4a*, Nuclear receptor subfamily 4 group A; Rab11, Ras-related in brain protein 11; spl, spleen; TCR, T-cell receptor; Thy, thymus; Treg cell, regulatory T cell; WT, wild type.

<https://doi.org/10.1371/journal.pbio.2006716.g005>

down-regulated in Treg cells from miR-181a/b-1^{-/-} mice (S5C and S5D Fig). However, in silico analysis of *Ctla4* mRNA using Targetscan7 and RNA22 provided no evidence for the existence of either canonical or noncanonical binding sites for any of these miRNAs, suggesting that elevated protein levels of CTLA-4 are not caused by reduced miRNA expression. Next, we assessed whether peripheral expansion contributed to sustained expression of CTLA-4 in peripheral Treg cells. To this end, we generated mixed BM chimeras and analyzed CTLA-4 levels on miR-181a/b-1^{-/-} and WT Treg cells isolated from the same mice. CTLA-4 levels were consistently higher in miR-181a/b-1-deficient Treg cells despite competition by their WT counterparts, indicating that CTLA-4 levels are regulated cell-intrinsically and do not depend on peripheral expansion (Fig 5F). Finally, we tested whether alterations in tonic TCR signaling might result in elevated expression of CTLA-4. Freshly isolated peripheral Treg cells from miR-181a/b-1^{-/-} and WT mice expressed comparable levels of *Nr4a1* mRNA, suggesting that tonic signaling through the TCR is similar (Fig 5G). Taken together, these findings further support the hypothesis that miR-181a/b-1-dependent ctrl of CTLA-4 expression is elicited in the thymus and subsequently sustained in the periphery.

Treg cells from miR-181a/b-1^{-/-} mice display increased suppressive capacity

In order to test the functional consequences of elevated levels of CTLA-4 in miR-181a/b-1^{-/-} Treg cells, we assessed their suppressive capacity. First, loss of miR-181a/b-1 resulted in reduced levels of tumor necrosis factor (TNF)α, IL-4, and IL-2 by conventional CD4⁺ T cells (Fig 6A). In contrast, expression of IL-17 and IL-10 remained unaffected. Whereas levels of TNFα were also reduced in miR-181a/b-1^{-/-} Treg cells, we did not observe additional significant miR-181a/b-1-dependent alterations in cytokine production by Treg cells or CD8⁺ T cells (Fig 6A and S6A Fig). Such alterations in cytokine profiles might be due to cell-intrinsic effects or due to modulation of Treg-cell suppressive capacity. Therefore, we next assessed in vivo suppressive capacity of Treg cells by transfer of congenically marked 1:1 mixtures of miR-181a/b-1-sufficient or miR-181a/b-1-deficient Treg cells (CD45.2) and conventional T cells (CD45.1) into *Rag1*^{-/-} recipients. Suppression of lymphopenia-driven expansion of Tconv cells is dependent on CTLA-4 [35]. At 14 days after transfer, homeostatic expansion of Tconv cells was assessed. We observed lower frequencies of Tconv cells (CD45.1) in spleens of mice

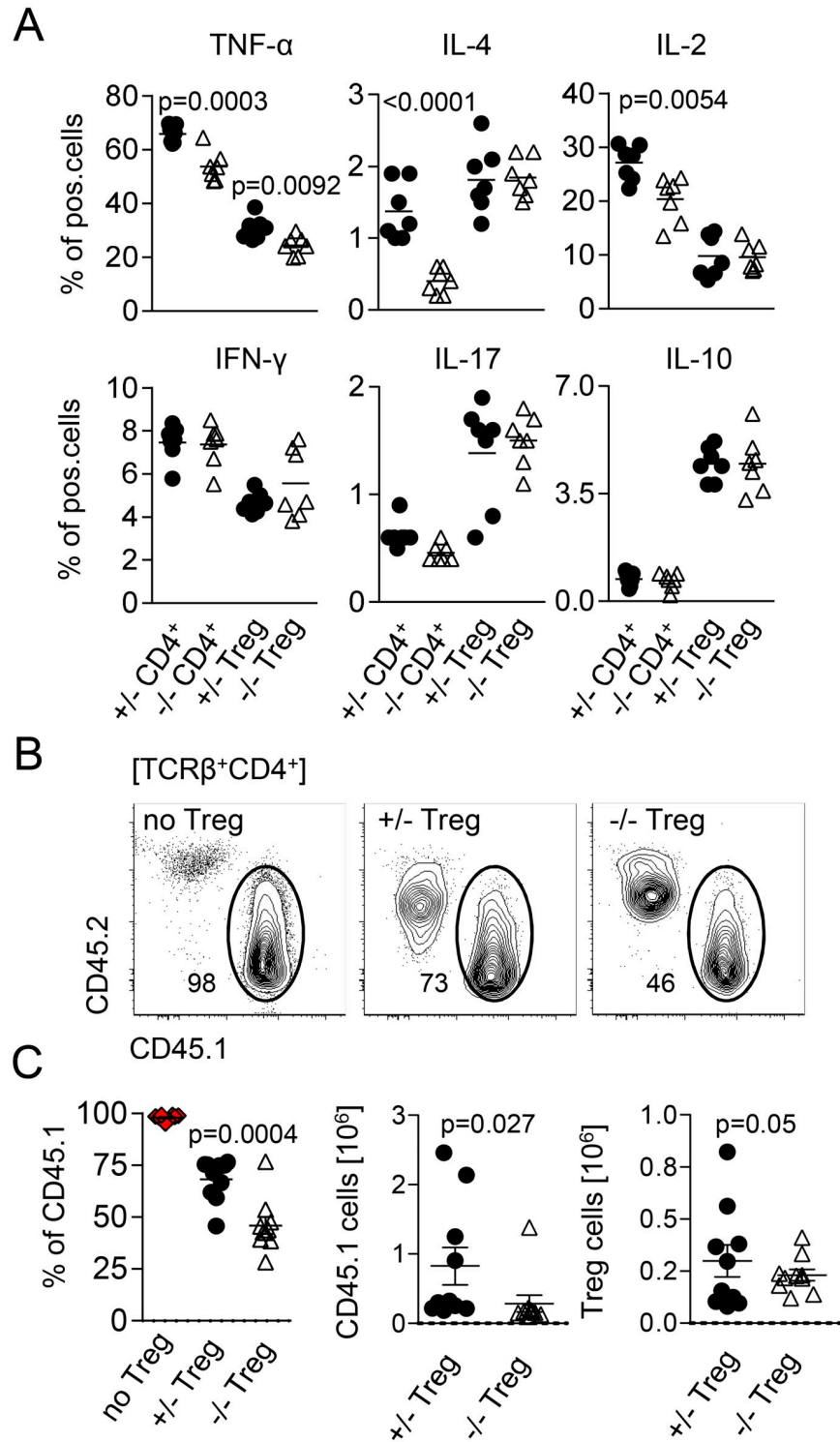


Fig 6. Treg cells from miR-181a/b-1^{-/-} mice display increased suppressive capacity. (A) Production of cytokines by splenic CD4⁺ T cells and Treg cells after stimulation with PMA/ionomycin. Graphs represent quantification of the data from 3 independent experiments, $n = 4-5$ for each genotype. (B) In vivo suppression of homeostatic proliferation in lymphopenic Rag^{-/-} mice by miR-181a/b^{+/-} and miR-181a/b^{-/-} Treg cells. Depicted is expansion of Tconv in the absence (no Treg cells) and presence of miR-181a/b-1^{+/-} or miR-181a/b-1^{-/-} Treg cells 14 days after coinjection of T cells. (C) Quantification and absolute numbers of recovered Tconv cells and Treg cells. Data are representative of 2 independent experiments, with $n = 7-8$ (recipient mice). Statistical analysis was performed using unpaired Student's t

test. Numerical values are available in [S1 Data](#). CD, cluster of differentiation; IFN- γ , interferon gamma; IL, interleukin; miR-181, microRNA-181; PMA, phorbol 12-myristate 13-acetate; pos., positive; Tconv, conventional T; TCR, T-cell receptor; TNF, tumor necrosis factor; Treg cell, regulatory T cell.

<https://doi.org/10.1371/journal.pbio.2006716.g006>

co-transferred with miR-181a/b-1^{-/-} Treg cells when compared to those co-transferred with miR-181-a/b-1-sufficient Treg cells (Fig 6B). This reduction in frequency was reflected by lower absolute numbers of Tconv cells recovered in the presence of miR-181a/b-1^{-/-} Treg cells, whereas absolute numbers of Treg cells recovered were similar in both conditions (Fig 6C). Together, these data indicate that in the absence of miR-181a/b-1, Treg cells have a stronger capacity to suppress lymphopenia-driven expansion of Tconv cells in vivo. Of note, we did not observe significant alterations in suppressive capacity of miR-181a/b-1^{-/-} Treg cells in vitro (S6B Fig). Taken together, our data indicate that miR-181a/b-1 controls intrathymic Treg cell development in a TCR-dependent manner. Impaired Treg-cell development in the absence of miR-181a/b-1 is associated with post-transcriptional up-regulation of CTLA-4, which penetrates into the periphery and results in increased suppressive capacity. Low levels of miR-181a in peripheral WT Treg cells suggest that the effects of loss of miR-181a/b-1 are imprinted during intrathymic development.

Discussion

Here, we demonstrated that intrathymic generation of Treg cells depends on miR-181a/b-1 via establishing signaling thresholds to adequately respond to strong TCR signals. In the absence of miR-181a/b-1, de novo generation of Treg cells was attenuated and resulted in Treg cells expressing elevated levels of CTLA-4. Homeostatic expansion resulted in a completely filled peripheral Treg-cell compartment while CTLA-4 levels remained elevated via a post-transcriptional mechanism, resulting in Treg cells with increased suppressive capacity.

Treg cells develop from CD4SP thymocytes through two possible intermediates, Foxp3⁻CD25⁺ and Foxp3⁺CD25⁻ [8,11]. It has been suggested that generation of these precursors occurs through a TCR-dependent step, whereas further maturation into mature Foxp3⁺CD25⁺ Treg cells is dependent on the cytokines IL-2 and IL-15 [8,10,11]. Analysis of InduRag1 mice as well as a *Rag1*^{GFP} virtual timer indicated that miR-181a/b-1 predominantly affects formation of Foxp3⁺CD25⁻ precursors, whereas Foxp3⁻CD25⁺ are more frequent in miR-181a/b-1-deficient mice. Nevertheless, these precursors cannot compensate for the partial loss of Foxp3⁺CD25⁻ precursors, suggesting that the major route of Treg-cell development is through the latter. Indeed, it has been shown that in WT mice, only approximately 20% of CD4⁺Foxp3⁻CD25⁺ cells ultimately give rise to Treg cells [8,10]. Treg-cell development via Foxp3⁻CD25⁺ intermediates predominantly occurs in double transgenic mouse lines expressing a transgenic TCR plus its cognate antigen [9]. Furthermore, these cells express higher levels of a Nur77^{GFP} reporter than either Foxp3⁺CD25⁻ precursors or mature Treg cells [10]. Thus, it has been suggested that Foxp3⁻CD25⁺ intermediates arise at the extreme end of the TCR affinity spectrum and might increase in frequency by an influx of cells otherwise targeted for clonal deletion. Accordingly, reduction in MHCII levels on thymic epithelial cells in a monoclonal system diverted thymocytes from clonal deletion into the Treg cell lineage [16]. TCR repertoire analyses and autoreactivity suggest that TCR signal strength required for tTreg-cell generation overlaps both with that of positively selected thymocytes as well as that of cells normally undergoing clonal deletion [3,13,14]. Rescue experiments performed in this study agree with both non-mutually exclusive models. Fewer donor-derived miR-181a/b-1^{-/-} OT-II Treg cells developed in RIPmOVA antigen transgenic mice compared to WT OT-II Treg cells. Concomitantly, clonal deletion of miR-181a/b-1^{-/-} OT-II cells was also impaired in RIPmOVA mice,

suggesting that in this particular paired TCR–antigen model, TCR signal strength is reduced through loss of miR-181a/b-1 to limit both Treg-cell formation and clonal deletion. Conversely, induced expression of Nr4a2 promoted Treg-cell production in the absence of miR-181a/b-1 but resulted in somewhat limited production of Treg cells in the presence of miR-181a/b-1, suggesting that in the latter case, clonal deletion might be favored over Treg-cell development.

Intrathymic development of Treg cells depends on CD28-mediated costimulatory signals [36]. Thus, it might be possible that elevated expression of CTLA-4 by Treg cells in the thymus contributes to impaired development. Costimulation via CD28 is required for efficient generation of Foxp3⁺CD25⁺ Treg-cell precursors but less so during later Treg-cell development, suggesting that CD28 signaling protects thymocytes from clonal deletion [36–39]. Loss of CD28 signaling does not result in export of autoreactive cells into the periphery, indicating that it does not simply act as an amplifier of TCR signal strength [39]. Consistently, loss of CD28-mediated costimulation and loss of miR-181a/b-1 generate phenotypically distinct developmental defects, also supporting the notion that elevated levels of CTLA-4 in miR-181a/b-1^{-/-} Treg cells are a consequence rather than cause of inefficient generation of Treg cells in these mice.

Consequences of altered TCR signal strength in the thymus have been previously analyzed in mice carrying hypomorphic mutations of key signal mediators, such as zeta-chain-associated kinase of 70 kD (Zap-70), or reduced numbers of immunoreceptor tyrosine-based activation motifs (ITAMs) within CD3 ζ molecules [40–42]. Collectively, these studies showed that alterations in TCR signal affected positive and negative selection as well as Treg-cell formation, albeit in a manner that is not easily predictable. Thus, these data indicate that the quantitative relationship between proximal TCR signaling and efficient thymic selection needs to be tightly balanced. Furthermore, mutations characterized in these studies equally affect T-cell activation and tonic signaling in the periphery, precluding analysis of developmental consequences of altered TCR signaling exclusively occurring in the thymus.

In contrast, expression levels of miR-181a/b-1 in peripheral Treg cells are very low and should therefore allow WT-like levels of tonic TCR signaling. Notably, peripheral TCR signaling controls Treg-cell homeostasis and helps to maintain functional Treg cells [43,44]. For instance, in the absence of peripheral TCR expression, levels of CTLA-4 protein are reduced, and suppressive capacity is compromised [44].

Our data suggest that alterations in thymic selection caused by the absence of miR-181a/b-1 have long-term impact and are translated to increased suppressive activity of peripheral Treg cells. We therefore propose that the developmental legacy of TCR signal strength during agonist selection determines Treg-cell function in the periphery. Thus, altered TCR thresholds during selection might affect a Treg cell's responsiveness to tonic signaling. Similar observations have previously been reported for both CD4 and CD8 Tconv cells [45,46]. The avidity of positively selecting self-peptides and thus strength of the TCR signal during selection determines the outcome of a T-cell immune response even of T cells recognizing the same foreign antigen with an identical avidity [45]. In contrast to Treg cells, differential reactivity to self-peptide by CD8 Tconv cells was accompanied by clear differences in gene expression profiles [46]. Although in Tconv cells, the capacity for tonic signaling in the periphery contributes to distinct responsiveness to pathogens, thymically predetermined levels of the feedback regulator of TCR signaling CD5 are likely to help control tonic signals [45]. Thus, the quality of protective T-cell responses as well as Treg-cell mediated suppression appear to be preset during thymic selection.

How TCR signal strength during thymic agonist selection confers long-term changes in CTLA-4 protein expression remains unclear. Our study supports a model in which expression of CTLA-4 is cell-intrinsically sustained in the periphery through a post-transcriptional

mechanism controlling its translation rate. Translational control can be exerted at multiple different levels, including changes in mRNA composition through alternative splicing and miRNAs as well as RNA binding proteins. Given the lack of unambiguous evidence for one of these mechanisms being predominant, our data suggest that multiple factors may act in concert to control CTLA-4 protein. Tight control of CTLA-4 expression is likely to be paramount for tuning suppressive capacity of Treg cells.

Our study establishes miR-181a/b-1 as a central regulator of agonist-selected $\alpha\beta$ T cells. Earlier studies showed that miR-181a/b-1 is critical for the development of innate-like T cells expressing semi-invariant TCRs, such as iNKT cells and MAIT cells (but not their $\gamma\delta$ TCR-expressing counterparts) [25,26,47]. Here, we demonstrated that the role of miR-181a/b-1 can be extended to highly diverse polyclonal T-cell populations. This finding was not anticipated because it might be expected that a shift in integrated signal strength might be compensated for by a shift in the repertoire. Such compensation might partly explain why the effect of miR-181a/b-1 deletion on Treg cells is somewhat milder when compared to other agonist selected T cells. Finally, based on the dramatic down-regulation of miR-181a after the DP stage, our study implies that the lineage fate decision to become a Treg cell manifests itself early during selection.

Materials and methods

Ethics statement

All experiments were performed in accordance with German law on care and use of laboratory animals or with the institutional and ethical guidelines of the University of Edinburgh and have been approved by the Niedersächsisches Landesamt für Verbraucherschutz und Lebensmittelsicherheit (LAVES) (33.12-42502-04-08-1480; 11/0533; 12/0869; 13/1224; 15/1846), the Regierungspräsidium Darmstadt (V54–19c20/15–FU/1119; FU/1155; FU/1159; FU/1178) or under a project license granted by the UK Home Office (PPL60_4510 procedure 19b 5), respectively. Animals were killed by CO₂ inhalation, in some cases followed by cervical dislocation.

Mice

MiR-181a/b-1^{-/-} and miR-181a/b-1^{+/-} mice (B6.Mirc14^{tm1.1Ankr}) were generated as described in [26] and bred at the Hannover Medical School and Goethe University, Frankfurt, Germany. OT-II mice (B6.Cg-Tg(TcraTcrb)^{425Cbn/J}) were purchased from The Jackson Laboratory, crossed with miR-181a/b-1^{-/-} and miR-181a/b-1^{+/-} mice, and bred at the Hannover Medical School. RIPmOVA mice (C57BL/6-Tg(Ins2-TFRC/OVA)^{296W^{ehi}/W^{ehi}}) were purchased from The Jackson Laboratory and crossed with B6 CD45.1. F1 mice (RIPmOVA CD45.1/2) were bred at the Hannover Medical School. C57BL/6J mice (CD45.2), B6.SJL-*Ptprc^a Pepc^b*/BoyJ mice (termed “B6 CD45.1” throughout this manuscript), and IL-7R α -deficient mice (B6.129S7-Il7r^{tm1Imx/J}) were purchased from Charles River or The Jackson Laboratory or bred at the animal facility of Hannover Medical School. (C57BL/6J \times B6 CD45.1) F1 mice (CD45.1/CD45.2 heterozygous) and IL-7R α ^{-/-} CD45.1 mice were bred at the animal facility of Hannover Medical School. InduRag1^{fl/fl} \times Rosa26-CreERT2 mice (termed InduRag1 here) were obtained by crossing InduRag1^{fl/fl} mice with Rosa26-CreERT2 mice (kindly provided by Prof. Anton Berns, The Netherlands Cancer Institute, Amsterdam, The Netherlands) and bred at the Helmholtz Centre for Infection Research [30]. These mice were crossed to miR-181a/b-1^{-/-} (InduRag1 \times miR-181a/b-1^{-/-}) and miR-181a/b-1^{+/-} (InduRag1 \times miR-181a/b-1^{+/-}) mice bred and maintained at the Helmholtz Centre for Infection Research in Braunschweig. Foxp3^{hCD2} \times Rag1^{GFP} mice were obtained by crossing Foxp3^{hCD2} mice [48] with Rag1^{GFP}

mice [49] (kindly provided by Nobuo Sakaguchi, Kumamoto, Japan). These mice were crossed to miR-181a/b-1^{-/-} and miR-181a/b-1^{+/-} mice and bred at the Helmholtz Centre for Infection Research in Braunschweig. *Rag1*^{-/-} mice and B6 CD45.1 mice used in the in vivo suppression assay were bred and maintained at the University of Edinburgh. All mice were used between 7–12 weeks of age and were maintained under specific-pathogen-free conditions.

In vivo induction of Treg-cell development

Treg-cell development was induced in 6- to 8-week-old InduRag1 × miR-181a/b-1^{-/-} and InduRag1 × miR-181a/b-1^{+/-} mice by oral administration of tamoxifen (Ratiopharm, Ulm, Germany) in corn oil (Sigma Aldrich, St. Louis, MO, USA), 0.6 mg/400 μl/mouse every 4 days. To ensure proper tamoxifen solubility, in the first step, it was dissolved in 100% ethanol prewarmed to 55 °C and later in prewarmed corn oil. Before each oral administration, the mixture was always prewarmed to 37 °C.

Competitive BM chimeras

B6 CD45.1⁺ recipient mice were lethally irradiated (9 Gy). Donor BM from both WT (CD45.1/2⁺) and miR-181a/b-1^{+/-} or miR-181a/b-1^{-/-} (CD45.2⁺) mice mixed at a 1:1 ratio was injected into the lateral tail vein within 24 h postirradiation (a total of 4 × 10⁶ cells/mouse). Mice were provided with antibiotic-containing water and were housed in sterile microisolator cages. Analysis of BM chimeras was performed 8–12 weeks after transplantation.

Overexpression of Nr4a2 in BM chimeras

BM cells were isolated from the tibia and femur of age-matched (7–10 weeks) OT-II × miR-181a^{-/-} and OT-II × miR-181a^{+/-} mice. First, lineage-negative (lin⁻) cells were enriched by incubation with the cocktail of purified rat-anti-mouse antibodies (CD19 [1D3], CD11b [M1/70], Gr-1 [RB6-8C5], NK1.1 [PK136], Ter-119, CD4 [RM4.4], and CD8α [53–6.7]; all from eBioscience, Thermo Fisher Scientific, Waltham, MA, USA) followed by incubation with sheep-anti-rat dynabeads (Dyna; Invitrogen, Carlsbad, CA, USA) and magnetic separation. Cells were stained with a phycoerythrin (PE)-Cy7-conjugated cocktail of lin antibodies (CD19 [6D5], CD11b [M1/70], Gr-1 [RB6-8C5], NK1.1 [PK136], Ter-119, CD4 [GK1.5], and CD8α [53–6.7]; all from eBioscience) and Sca-1 (E13–161.7) PacificBlue, c-kit (CD117) allophycocyanin (APC), and sorted as lin⁻Sca-1⁺c-kit⁺ to 98% purity. Cells were cultured overnight at a density of 5 × 10⁴ cells/100 μl (on 96-well plate) with mouse IL-6 (20 ng/ml), mouse IL-7 (25 ng/ml), mouse Flt-3L (25 ng/ml), and mouse SCF (50 ng/ml; all obtained from PeproTech, Rocky Hill, NJ, USA), in DMEM containing 10% FBS. Next day, cells were infected by centrifugation at 700 g for 45 min at 32 °C on retronectin-coated plates (50 μg/ml, 4 °C overnight) loaded (3 × 100 μl/well, 2,000 g, 20 min at 32 °C) with Nr4a2-ΔLBD-ERT2-expressing retrovirus or ctrl retrovirus (both carrying Thy1.1 tag detectable by flow cytometry) in the presence of polybrene (8 μg/ml) and the abovementioned cytokines. Fresh medium was supplemented after 24 h. After 48 h, cells were collected, and transduction efficacy (frequency of Thy1.1⁺ cells) was determined. Routinely, it was approximately 60%, and thus cells were later sorted to 100% of Thy1.1⁺. B6 CD45.2⁺Thy1.2⁺ recipient mice were lethally irradiated (9 Gy). Sorted cells were intravenously injected (1 × 10⁵/recipient). Mice were provided with antibiotic-containing water and were housed in sterile microisolator cages.

Six weeks after injection, mice were orally administered 0.6 mg/400 μl of tamoxifen (Ratiopharm) dissolved in corn oil (Sigma Aldrich) per recipient mouse for 5 consecutive days. Tamoxifen preparation was performed as for induction of Treg-cell development in InduRag1 mice. Twelve hours after the final administration, mice were analyzed.

Intracellular staining of Nur77 in thymocytes

Thymocytes isolated from miR-181a^{+/-} and miR-181a^{-/-} mice were left untreated or were stimulated for 3 h at 37 °C in the presence of plate-bound α CD3 (17A2, 2.5 μ g/ml) and soluble α CD28 (37.51, 2.5 μ g/ml). Next, cells were stained for surface CD4 and CD8 α and intracellular Nur77 with intracellular staining buffer set (eBioscience).

RIPmOVA \times OT-II BM chimeras

BM cells were isolated from the tibia and femur of age-matched (7–10 weeks) OT-II \times miR-181a/b-1^{-/-} and OT-II \times miR-181a/b-1^{+/-} mice. Red blood cells were lysed, and cells were counted and injected (5×10^6 /recipient) into the lateral tail vein of lethally (2×4.5 Gy) irradiated RIPmOVA (CD45.1/2⁺) recipient mice. Mice were provided with antibiotic-containing water and were housed in sterile microisolator cages. Analysis of BM chimeras was performed 8–12 weeks after transplantation.

Flow cytometry and cell sorting

Monoclonal antibodies specific for CD4 (RM4.4, GK1.5), CD8 α (53–6.7), CD25 (PC61.5, eBio7D4 for sort), CD24 (M1/69), CD27 (LG.3A10), CD28 (37.51), CD103 (M290), CD122 (TM- β 1), CD127 (A7R34), Gr-1 (RB6-8C5), erythroid cell marker (Ter-119), CD19 (1D3, 6D5), CD11b (M1/70), CD45.1 (A20), CD45.2 (104), CD117 (c-kit) (2B8, ACK2), Sca-1 (E13–161.7), NK1.1 (PK136), CD11c (N418), TCR β (H57-597), Foxp3 (MF23, FJK-16s), human CD2 (RPA-2.10), Qa2 (1-1-2), Nur77 (12.14), V β 5.1/5.2 TCR (MR9-4), V α 2 TCR (B20.1), CTLA-4 (UC10-4B9, UC10-4F10-11), Helios (22F6), TGF- β R (RI/ALK-5), GITR (DTA-1), PLZF (Mags.21F7), Gata3 (TWAJ), Egr2 (erongr2), Irf4 (3E4), c-Rel (1RELAH5), and KLRG1 (2F1) were used as biotin, PacificBlue, fluorescein isothiocyanate (FITC), Alexa Fluor 488, PE, peridinin chlorophyll protein-Cy5.5 (PerCP-Cy5.5), PE-Cy7, APC, APC-Cy7, APC-eFluor780, Brilliant Violet 421, eFluor450, and Alexa Fluor 647 conjugates. Antibodies were purified from hybridoma supernatants using standard procedures or were purchased from eBioscience, BD Biosciences (San Jose, CA, USA), BioLegend (San Diego, CA, USA), or R&D Systems (Minneapolis, MN, USA). For intracellular stainings, an intracellular staining buffer set and a Foxp3/transcription factor staining buffer set (both eBioscience) were used according to the manufacturer's protocol. RNA flow cytometry was performed using the PrimeFlow system (Thermo Fisher Scientific). Cells were stained with Nr4a1-AF647. Samples were acquired on LSRII (BD Biosciences) cytometers and sorted on a FACS Aria II (BD Biosciences). Data were analyzed with FlowJo software, v.9.4.9 (Tree Star, Ashland, OR, USA). For analysis, dead cells and debris were excluded by gating of forward and side scatter. Sorted cells were of 98% or higher purity, as determined by reanalysis.

In vivo Treg-cell induction assay

RTEs depleted of Treg cells were sorted as Rag1^{GFP+}CD4⁺CD8 α ⁻CD25⁻ from the spleens of Foxp3^{hCD2} \times Rag1^{GFP} \times miR-181a/b-1^{-/-} and Foxp3^{hCD2} \times Rag1^{GFP} \times miR-181a/b-1^{+/-} mice. 5×10^5 cells were injected into the lateral tail vein of lymphopenic IL-7R α ^{-/-} (CD45.1) recipients. Spleens, peripheral lymph nodes (pLNs: inguinal, brachial, axillary, and cervical), and mLN were analyzed for the induction of Foxp3 within donor population (CD45.2) 28 days later.

In vitro suppression assay

Splenic antigen-presenting cells (CD45.1⁺) were purified using sheep-anti-rat magnetic beads and depletion of CD19, CD3, NK1.1, and Gr-1-positive cells as described above. Cells were

plated on a U-bottom-shaped 96-well plate coated with α CD3 antibody (17A2, 10 μ g/ml) at 4 °C, overnight, at the density 1×10^4 cells/100 μ l/well. Next, they were loaded with OVA_{323–339} peptide (2 μ g/ml; AnaSpec, Fremont, CA, USA) for 45 min at 37 °C and washed 3 times to remove unbound peptide. Naïve, CD4⁺ OT-II cells (CD45.1/2⁺) were purified using a CD4⁺T cell negative depletion kit (Invitrogen). Cells were further labeled with 1 μ M CFSE (Molecular Probes, Eugene, OR, USA) for 10 min at 37 °C and washed twice. They were added to peptide-loaded antigen-presenting cells at a density of 1×10^5 cells/well (antigen-presenting cell/OT-II ratio 1:10). Treg cells (CD45.2⁺) were sorted as CD4⁺CD25⁺ cells from spleens of miR-181a/b-1^{+/-} and miR-181a/b-1^{-/-} mice (purity always >98%), and their graded concentrations were added to antigen-presenting cell/OT-II cocultures in the presence of murine IL-2 (100 U/ml, PeproTech). Assay was analyzed after 48–60 h by flow cytometry.

In vivo suppression assay

To analyze the function of Treg cells in vivo, sorted populations of naïve CD45.1⁺ (1×10^5 to 4×10^5 cells) together with CD45.2⁺ miR-181a/b-1^{+/-} or miR-181a/b-1^{-/-} Treg cells were injected intravenously into *Rag1*^{-/-} recipients and analyzed after 14 days.

TCR sequencing

Total RNA was isolated using the RNeasy Mini Kit (Qiagen, Hilden, Germany) from 1×10^5 sorted thymic CD3⁺CD4⁺CD25⁺ miR-181a/b-1^{+/-} or miR-181a/b-1^{-/-} Treg cells and 4×10^5 sorted splenic CD3⁺CD4⁺CD25⁺ miR-181a/b-1^{+/-} or miR-181a/b-1^{-/-} Treg cells. Purity was above 98% as determined by reanalysis. Four independent sorts were performed (pooled 4–5 mice/genotype), and so were 2 independent sequencing experiments. cDNA templates were synthesized using SuperScript II reverse transcriptase (Invitrogen) according to the manufacturer's recommendation. To generate template libraries of rearranged TCR CDR3 regions from Treg-cell cDNA for the Genome Sequencer FLX system (454 sequencing; Roche, Basel, Switzerland), we used primers spanning the variable region between constant C α and V elements of the V α 8 family (comprising TRAV12-1*01, TRAV12-1*03, TRAV12-1*04, TRAV12-1*05, TRAV12D-2*01, TRAV12D-2*02, TRAV12D-2*03, TRAV12D-2*04, TRAV12D-2*05, TRAV12D-3*01, TRAV12D-3*02, and TRAV12D-3*03) [50]. Forward and reverse primers contained at their 5' ends the universal adapter sequences and a multiplex identifier (MID), respectively. Amplicons were purified by agarose gel electrophoresis and QIAquick Gel Extraction Kit (Qiagen) and quantified by Quant-iT dsDNA HS Assay Kit (Invitrogen). Single PCR amplicon molecules were immobilized onto DNA capture beads within an oil-water emulsion to enable clonal amplification in a second PCR process with universal primers. The emulsion was then disrupted, and isolated beads were loaded onto PicoTiterPlates. Sequencing reactions were performed by ultradeep 454 pyrosequencing on the Genome Sequencer FLX system (Roche). Productive rearrangements and CDR3 α regions were defined by comparing nucleotide sequences to the reference sequences from IMGT, the international ImMunoGeneTics information system (<http://www.imgt.org>) [51]. Rearrangements were analyzed and CDR3 α regions were defined using IMGT/HighV-QUEST [52].

Confocal microscopy

CD4⁺ T cells were purified from spleens and pLN of miR-181a/b-1^{+/-} and miR-181a/b-1^{-/-} mice using CD4⁺ T-cell negative isolation kit (Dyna, Invitrogen). Next, cells were plated on glass coverslips (Assistant, 0.13–0.16 mm, Thermo Fisher Scientific) coated with poly-L-lysine (Sigma Aldrich) or Histogrip (Invitrogen) for 2 h at 37 °C. In some experiments, glass coverslips were additionally coated with α CD3 antibody (10 μ g/ml, 17A2) and α CD28 antibody

(10 $\mu\text{g/ml}$, 37.51). After 2 h, cells were fixed in 3% (v/v) electron-microscopy-grade PFA (Electron Microscopy Sciences). CTLA-4, Foxp3, LAMP2, EEA1, GM130, and Rab11 were stained using indirect immunofluorescence. The following primary antibodies were used: purified α -mouse CTLA-4 (UC10-4F10-11, BD Biosciences) labeled with DyLight650 antibody labeling kit (Pierce, Thermo Fisher Scientific) according to the manufacturer's protocol, Alexa-Fluor488-labeled rat- α -mouse Foxp3 (MF23, BD Biosciences), purified rat- α -mouse LAMP2 (Hybridoma Bank), α -mouse EEA-1 (14/EEA1, BD Biosciences), α -mouse GM130 (35/GM130, BD Biosciences), and α -mouse Rab11 (D4F5, Cell Signaling, Danvers, MA). The following secondary antibodies were used, all conjugated to AlexaFluor488 (all Molecular Probes): mouse- α -rat, rat- α -mouse, and goat- α -rabbit. Nuclear staining was performed using DAPI (Molecular Probes). Coverslips were mounted on glass slides using aqueous mounting medium (DakoCytomation, Glostrup, Denmark). Samples were analyzed by confocal fluorescent microscopy using a Leica SP5 inverted microscope (Leica Microsystems, Wetzlar, Germany). During imaging, a single focal plane was monitored in x-y-z scanning mode using 63 \times /1.4–0.6 NA oil HCX PL APO lambda blue DIC oil objective, UV laser (405 nm), argon laser (488 nm), diode-pumped solid-state (DPSS) laser (561 nm), and helium–neon (HeNe) laser (633 nm) at a scanner frequency of 400 Hz, line averaging 4. In order to avoid fluorescence overlap, sequential scans were performed. Images were analyzed using LAS AF Lite (Leica Microsystems) and ImageJ software. Quantification of fluorescence intensity and image analysis was performed using ImageJ software.

Inhibition of lysosomal degradation in Treg cells

CD4⁺CD25⁺ Treg cells were enriched from spleens and LNs of miR-181a/b-1^{+/-} or miR-181a/b-1^{-/-} mice using a MACS isolation kit (Miltenyi Biotec, Bergisch Gladbach, Germany). Cells were incubated in the absence or presence of 50 nM bafilomycin (InvivoGen, San Diego, CA, USA) and collected after 30, 60, 120, and 180 min. Samples were stained with α CD4, α CD25, and α hCD2 (Foxp3) antibodies and intracellularly for CTLA-4. For intracellular stainings, the Foxp3/transcription factor staining buffer set (eBioscience) was used according to the manufacturer's protocol. Samples were acquired on LSRII (BD Biosciences). Data were analyzed with FlowJo software, v.9.4.9 (Tree Star). For analysis, dead cells and debris were excluded via staining with Zombie Aqua reagent (BioLegend) prior to fixation and permabilization of cells.

Microarrays

RNA isolation, cDNA preparation, and DNA microarray analysis of gene expression were performed at the Microarray Genechip Facility of the University of Tübingen (MFT Services). Fluorescent images of hybridized microarrays (MOE-430 version 2.0; Affymetrix, Santa Clara, CA, USA) were obtained using an Affymetrix Genechip Scanner. Microarray data were analyzed using BioConductor Suite 2.1 software. All samples were repeated two times with individually sorted cells and averaged.

Small RNAseq

Treg cells (1×10^5) sorted from 3 pooled WT and miR-181a/b-1^{-/-} thymi were stored in RNA-protect Cell Reagent (Qiagen). Small RNAseq was performed by Admera Health (South Plainfield, NJ, USA) using the SMARTer smRNA-Seq Kit (Takara, Kusatsu, Japan). Adapters were trimmed with Flexbar 3.4, and rRNA was removed using Bowtie 2. The remaining reads were aligned using STAR aligner and counted using HTSeq. Differential expression analysis was performed in R using the DESeq2 package. Three biological replicates per genotype were analyzed.

Luciferase assay

Part of the CTLA-4 coding sequence (CTLA-4^{WT}, 294 bp) and a version devoid of the putative miR-181a binding site (CTLA-4^{del}, 271 bp) were synthesized by GeneArt (Regensburg, Germany) and cloned into PsiCheck2.0 Vector (Promega, Madison, WI, USA). 3T3 cells overexpressing murine miR-181a or ctrl cells were established by retroviral transduction and sorted to 100% purity (GFP reporter). Viral particles were produced in HEK293T cells by co-transfection with pCLEco (coexpressing MLV gag, pol, and env) and the plasmids MDH1-PGK-GFP_2.0 (Addgene plasmid #11375) or MDH1-miR-181a-1-PGK-GFP (Addgene plasmid #11376), which were gifts from Chang-Zheng Chen [53]. 3T3 cells were cultured in complete DMEM (Life Technologies, Carlsbad, CA, USA) (10% FCS, 100 U PenStrep, 1 mM Na-pyruvate, 25 µg/mL Geneticin [Life Technologies]). 250,000 cells were electroporated with 0.1 µg of PsiCheck2.0 (250 V, 950 µF, Biorad Gene Pulser II) and cultured for 24 h on 6-well plates. Dual-Luciferase Reporter (DLR) assays (Promega) were conducted according to the manufacturer's instructions. Luciferase activity was measured using Lumat LB 9507 machine (Berthold).

qRT-PCR

RNA was prepared using the miRNeasy Kit according to the manufacturer's instructions (Qiagen). RT reaction was performed using TaqMan MicroRNA Reverse Transcription Kit (Applied Biosystems, Thermo Fisher Scientific, Waltham, MA, USA) and miRNA-specific primers according to the manufacturer's protocol. Quantitative RT-PCR analysis of miRNA expression was carried out using the following Taqman probes: hsa-miR-181a, TM: 000480; mmu-miR-15b, TM: 000390; mmu-miR-150-5p, TM: 000473; mmu-miR-342, TM: 002260; mmu-let-7g-5p, TM: 002282 (Applied Biosystems). Fold differences were calculated using the ΔC_t method normalized to snoRNA412 as housekeeping miRNA gene (Applied Biosystems, TM: 001243).

Statistical analyses

All analyses were performed using GraphPad Prism software. Data are represented as mean \pm SD. Statistical analyses of significance were performed using unpaired or paired Student's *t* test, multiple *t* test, or two-way ANOVA with Bonferroni post *t* test or Sidak's multiple comparison test.

Supporting information

S1 Fig. Early development of Treg cells in the absence of miR-181a/b-1. (A) Competitive BM chimeras. BM cells from miR-181a/b-1^{+/-} (het) or miR-181a/b-1^{-/-} (KO) (both CD45.2) were mixed in a 1:1 ratio with competitor WT BM cells (CD45.1/2) and injected into lethally irradiated WT recipients (CD45.1). Chimeras were analyzed 12 weeks later for the generation of CD4⁻CD8 α ⁻ (DN), CD4⁺CD8 α ⁺ (DP), and CD4⁺CD8 α ⁻ (CD4⁺SP) cells in the thymus. Plots are representative of 2 independent experiments with *n* = 8 for each genotype. Graph shows ratio of cells within test versus competitor populations. Each data point represents an individual mouse. (B) FACS analysis of thymi from InduRag1 mice sufficient and deficient for miR-181a/b-1, 7 days after induction of Rag1 expression. (C) Frequencies of tTreg cells (TCR β ⁺CD4⁺CD25⁺Foxp3⁺), their precursors TCR β ⁺CD4⁺CD25⁻Foxp3⁺ (Ia), and TCR β ⁺CD4⁺CD25⁺Foxp3⁻ (Ib) on day 7 after initial induction of Rag1 expression in InduRag1 mice sufficient and deficient for miR-181a/b-1. (D) FACS analysis of CD4 T-cell selection, 7 days after Rag1 induction in InduRag1 mice. Depicted data are from 2

independent experiments, with $n = 1-4$ for each genotype and time point analyzed. Numerical values are available in [S1 Data](#). BM, bone marrow; CD, cluster of differentiation; DN, double negative; DP, double positive; FACS, fluorescence-activated cell scan; Foxp3, forkhead box protein P3; InduRag1, inducible recombination-activating gene 1; KO, knockout; miR-181, microRNA-181; prec, precursor; *Rag1*, recombination-activating gene 1; SP, single positive; Treg cell, regulatory T cell; tTreg cell, thymic Treg cell; WT, wild type. (JPG)

S2 Fig. miR-181a/b-1 deficiency impairs generation of Treg cells in the thymus and does not influence their peripheral induction from naïve T cells. (A) Plots show gating strategy to discriminate newly generated tTreg cells (Foxp3^{hCD2+} cells positive for *Rag1*^{GFP}) and the population consisting of peripheral immigrants and thymus-residing mature Treg cells (Foxp3^{hCD2+}GFP⁻ Treg cells). Representative plots of 5 independent experiments are shown. Right panel, quantification; each data point represents one mouse. (B) Frequencies of RTEs (*Rag1*^{GFP+}CD4⁺CD25⁻) in spleens of miR-181a/b-1^{+/-} and miR-181a/b-1^{-/-} mice, left panel. Frequencies of Treg-cell RTEs (*Rag1*^{GFP+}CD4⁺Foxp3^{hCD2+}) in spleens of miR-181a/b-1^{+/-} and miR-181a/b-1^{-/-} mice, right panel. (C) De novo induction of Treg cells is not enhanced in the absence of miR-181a/b-1. RTEs (*Rag1*^{GFP+}CD4⁺CD25⁻) were sorted from spleens of *Rag1*^{GFP/WT} × miR-181a/b-1-sufficient and deficient mice (CD45.1⁺/CD45.2⁺ or CD45.2⁺) and injected into lymphopenic *Il7ra*^{-/-} recipients (CD45.1). Generation of Treg cells within donor cells was analyzed after 28 days. Plots are representative of 2 independent experiments, $n = 3-4$. Graphs show frequencies of CD25⁺Foxp3⁺ cells generated within donor TCRβ⁺CD4⁺ cells in spleen, pLNs, and mLNs. Statistical analysis was performed using unpaired Student's *t* test. Numerical values are available in [S1 Data](#). CD, cluster of differentiation; Foxp3, forkhead box protein P3; GFP, green fluorescent protein; hCD2, human CD2; *Il7r*, interleukin-7 receptor alpha; miR-181, microRNA-181; mLN, mesenteric lymph node; pLN, peripheral lymph node; *Rag1*, recombination activating gene 1; RTE, recent thymic emigrant; TCR, T-cell receptor; Treg cell, regulatory T cell; tTreg cell, thymic Treg cell. (JPG)

S3 Fig. Peripheral expansion of miR-181a/b-1-deficient Treg cells compensates for their impaired development. (A) TCR repertoire of miR-181a/b-1-deficient tTreg (upper graph) and splenic Treg (lower graph) cells. Vα8-Cα amplicons were amplified from cDNA of Treg cells before high-throughput sequencing. Frequencies of individual Vα-Cα sequences detected in miR-181a/b-1^{+/-} (black) and miR-181a/b-1^{-/-} (red) Treg cells. The copy number of Vα-Cα sequences is displayed against the number of individual nucleotide sequences. Data are derived from 2 independent experiments with samples sorted from $n = 4-6$ mice (pool). Numerical values are available in [S1 Data](#). cDNA, complementary DNA; miR-181, microRNA-181; TCR, T-cell receptor; Treg cell, regulatory T cell; tTreg cell, thymic Treg cell. (JPG)

S4 Fig. Flow-cytometry analysis of miR-181a/b-1-deficient Treg cells. Selected surface and intracellular proteins expressed by tTreg (A), splenic Treg (B), and LN-resident Treg (C) cells. Representative histograms and plots from 2 independent experiments ($n = 6-9$ for each genotype) are depicted. Numbers indicate average MFI or frequencies of positive cells, ±SD. Numerical values are available in [S1 Data](#). LN, lymph node; MFI, mean fluorescence intensity; miR-181, microRNA-181; Treg cell, regulatory T cell; tTreg cell, thymic Treg cell. (JPG)

S5 Fig. No evidence for post-transcriptional regulation of CTLA-4 by miR-181a/b-1 or miRNAs down-regulated in miR-181a/b-1-deficient Treg cells. (A) Predicted base-pairing

of miR-181a with the target sequence in the cds of CTLA-4. The seed sequence in the miRNA and the complementary sequence in the cds are displayed in bold letters. Number indicates the position within the CTLA-4 cds. (B) Relative luciferase intensities of CTLA-4 coding sequence (CTLA-4^{WT}) and cds lacking 23 bp of the predicted miR-181a binding site (CTLA-4^{del}) normalized to empty luciferase vector ctrl in 3T3 cells overexpressing miR-181a (miR-181a) or respective ctrls. Bars represent mean of >20 experiments and SD. (C) Small RNAseq volcano plot of differentially regulated miRNAs in miR-181a/b-1^{-/-} compared to WT tTreg cells. (D) qRT-PCR analysis of differentially regulated miRNAs identified in small RNAseq analysis in sorted tTreg cell (left column) and splenic Treg cell populations (right column). Data from 3 independent experiments, with $n = 2-7$ (pool) for each genotype. Expression of each miRNA was normalized to the expression of housekeeping small RNA, snoR412. $\Delta\Delta C_T$ values are displayed on the graph. Numerical values are available in [S1 Data](#). cds, coding sequence; CTLA-4, cytotoxic T-lymphocyte-associated protein 4; ctrl, control; miRNA, microRNA; miR-181, microRNA-181; qRT-PCR, quantitative reverse-transcription PCR; RNAseq, RNA sequencing; snoR412, small nucleolar RNA 412; Treg cell, regulatory T cell; tTreg cell, thymic Treg cell; WT, wild type.

(JPG)

S6 Fig. miR-181a/b-1-deficient Treg cells are more suppressive in vitro. (A) Production of cytokines by splenic CD8⁺ T cells after stimulation with PMA/ionomycin. Graphs represent quantification of the data from 2 independent experiments, $n = 4-5$ for each genotype. (B) In vitro suppression assay. Splenic antigen-presenting cells were loaded with OVA₃₂₃₋₃₃₉ peptide and cocultured with OT-II cells in the presence of graded numbers of sorted Treg cells from spleens of miR-181a/b-1^{+/-} and miR-181a/b-1^{-/-} mice. Graph shows percent of suppression calculated as follows: The number of CFSE^{low} OT-II cells (dividing) in the absence of Treg cells (ctrl sample) was set as 100%. Further, numbers of CFSE^{low} OT-II cells that survived in the presence of Treg cells were transformed to frequencies according to ctrl sample, and this number was subtracted from 100%, which gave the percent of suppression exhibited by a given number of Treg cells. Data are representative of 4 independent experiments, with $n = 7-8$ for Treg cell donor mice. Numerical values are available in [S1 Data](#). CFSE, carboxy-fluorescein succinimidyl ester; ctrl, control; miR-181, microRNA-181; OT-II, ovalbumin-specific MHC class II-restricted alpha beta TCR; OVA, chicken ovalbumin; PMA, phorbol 12-myristate 13-acetate; Treg cell, regulatory T cell.

(JPG)

S1 Data. Numerical values for graphical representations of data shown in all figures.

(XLSX)

Acknowledgments

We thank Dr. Ludger Klein for critically reading the manuscript. We are grateful to Prof. Hans H. Kreipe from the Institute for Pathology of Hannover Medical School for pathological analyses of miR-181a/b-1-deficient mice. The authors thank Dr. Tadashi Yokosuka from the Laboratory for Cell Signaling at the RIKEN Research Center for Allergy and Immunology in Yokohama for advice on confocal microscopy of CTLA-4. The authors would like to thank Regina Lesch, Suzanne zur Lage, Dr. Rene Teich, and Dr. Maria Szente-Pasztoi from the Helmholtz Centre for Infection Research in Braunschweig and Dr. Stephan Halle from Hannover Medical School for help with mouse colonies. We would like to acknowledge the assistance of the Cell Sorting Core Facility of the Hannover Medical School.

Author Contributions

Conceptualization: Marcin Łyszkiewicz, Samantha J. Winter, Immo Prinz, Natalia Zięta, Andreas Krueger.

Data curation: Marcin Łyszkiewicz, Samantha J. Winter, Lisa Föhse, Jacek Puchałka, Nikita A. Verheyden, Heike Kunze-Schumacher, Solaiman Raha, Siegfried Weiss, Maximiliano G. Gutierrez, Immo Prinz, Natalia Zięta, Andreas Krueger.

Formal analysis: Marcin Łyszkiewicz, Samantha J. Winter, Lisa Föhse, Rebecca Brownlie, Jacek Puchałka, Nikita A. Verheyden, Jonas Blume, Solaiman Raha, Jochen Huehn, Siegfried Weiss, Maximiliano G. Gutierrez, Immo Prinz, Rose Zamoyska, Natalia Zięta, Andreas Krueger.

Funding acquisition: Maximiliano G. Gutierrez, Natalia Zięta, Andreas Krueger.

Investigation: Marcin Łyszkiewicz, Samantha J. Winter, Katrin Witzlau, Lisa Föhse, Rebecca Brownlie, Heike Kunze-Schumacher, Esther Imelmann, Jonas Blume, Jochen T. Frueh, Immo Prinz, Rose Zamoyska, Natalia Zięta, Andreas Krueger.

Methodology: Marcin Łyszkiewicz, Samantha J. Winter, Katrin Witzlau, Lisa Föhse, Rebecca Brownlie, Jacek Puchałka, Esther Imelmann, Jonas Blume, Takashi Sekiya, Akihiko Yoshimura, Jochen T. Frueh, Evelyn Ullrich, Maximiliano G. Gutierrez, Immo Prinz, Rose Zamoyska, Natalia Zięta, Andreas Krueger.

Project administration: Natalia Zięta, Andreas Krueger.

Resources: Takashi Sekiya, Akihiko Yoshimura, Jochen T. Frueh, Evelyn Ullrich, Jochen Huehn, Siegfried Weiss, Andreas Krueger.

Software: Lisa Föhse, Jacek Puchałka, Solaiman Raha.

Supervision: Maximiliano G. Gutierrez, Immo Prinz, Rose Zamoyska, Natalia Zięta, Andreas Krueger.

Validation: Marcin Łyszkiewicz, Samantha J. Winter, Lisa Föhse, Heike Kunze-Schumacher, Solaiman Raha, Maximiliano G. Gutierrez, Immo Prinz, Natalia Zięta, Andreas Krueger.

Visualization: Marcin Łyszkiewicz, Samantha J. Winter, Lisa Föhse, Nikita A. Verheyden, Jonas Blume, Immo Prinz, Natalia Zięta, Andreas Krueger.

Writing – original draft: Natalia Zięta, Andreas Krueger.

Writing – review & editing: Marcin Łyszkiewicz, Samantha J. Winter, Nikita A. Verheyden, Maximiliano G. Gutierrez, Immo Prinz, Natalia Zięta, Andreas Krueger.

References

1. Fontenot JD, Gavin MA, Rudensky AY. Foxp3 programs the development and function of CD4+CD25+ regulatory T cells. *Nat Immunol.* 2003; 4(4):330–6. <https://doi.org/10.1038/ni904> PMID: 12612578.
2. Khattri R, Cox T, Yasayko SA, Ramsdell F. An essential role for Scurfin in CD4+CD25+ T regulatory cells. *Nat Immunol.* 2003; 4(4):337–42. <https://doi.org/10.1038/ni909> PMID: 12612581.
3. Moran AE, Holzapfel KL, Xing Y, Cunningham NR, Maltzman JS, Punt J, et al. T cell receptor signal strength in Treg and iNKT cell development demonstrated by a novel fluorescent reporter mouse. *J Exp Med.* 2011; 208(6):1279–89. <https://doi.org/10.1084/jem.20110308> PMID: 21606508
4. Jordan MS, Boesteanu A, Reed AJ, Petrone AL, Hohenbeck AE, Lerman MA, et al. Thymic selection of CD4+CD25+ regulatory T cells induced by an agonist self-peptide. *Nat Immunol.* 2001; 2(4):301–6. <https://doi.org/10.1038/86302> PMID: 11276200.
5. Apostolou I, Sarukhan A, Klein L, von Boehmer H. Origin of regulatory T cells with known specificity for antigen. *Nat Immunol.* 2002; 3(8):756–63. <https://doi.org/10.1038/ni816> PMID: 12089509.

6. Romagnoli P, Hudrisier D, van Meerwijk JP. Preferential recognition of self antigens despite normal thymic deletion of CD4(+)CD25(+) regulatory T cells. *J Immunol.* 2002; 168(4):1644–8. PMID: [11823492](#).
7. Ribot J, Enault G, Pilipenko S, Huchenq A, Calise M, Hudrisier D, et al. Shaping of the autoreactive regulatory T cell repertoire by thymic cortical positive selection. *J Immunol.* 2007; 179(10):6741–8. PMID: [17982064](#)
8. Lio CW, Hsieh CS. A two-step process for thymic regulatory T cell development. *Immunity.* 2008; 28(1):100–11. <https://doi.org/10.1016/j.immuni.2007.11.021> PMID: [18199417](#)
9. Wirnsberger G, Mair F, Klein L. Regulatory T cell differentiation of thymocytes does not require a dedicated antigen-presenting cell but is under T cell-intrinsic developmental control. *Proc Natl Acad Sci U S A.* 2009; 106(25):10278–83. <https://doi.org/10.1073/pnas.0901877106> PMID: [19515822](#)
10. Marshall D, Sinclair C, Tung S, Seddon B. Differential requirement for IL-2 and IL-15 during bifurcated development of thymic regulatory T cells. *J Immunol.* 2014; 193(11):5525–33. <https://doi.org/10.4049/jimmunol.1402144> PMID: [25348623](#)
11. Tai X, Erman B, Alag A, Mu J, Kimura M, Katz G, et al. Foxp3 transcription factor is proapoptotic and lethal to developing regulatory T cells unless counterbalanced by cytokine survival signals. *Immunity.* 2013; 38(6):1116–28. <https://doi.org/10.1016/j.immuni.2013.02.022> PMID: [23746651](#)
12. Burchill MA, Yang J, Vang KB, Moon JJ, Chu HH, Lio CW, et al. Linked T cell receptor and cytokine signaling govern the development of the regulatory T cell repertoire. *Immunity.* 2008; 28(1):112–21. <https://doi.org/10.1016/j.immuni.2007.11.022> PMID: [18199418](#)
13. Hsieh CS, Zheng Y, Liang Y, Fontenot JD, Rudensky AY. An intersection between the self-reactive regulatory and nonregulatory T cell receptor repertoires. *Nat Immunol.* 2006; 7(4):401–10. <https://doi.org/10.1038/ni1318> PMID: [16532000](#).
14. Hsieh CS, Liang Y, Tzgnik AJ, Self SG, Liggitt D, Rudensky AY. Recognition of the peripheral self by naturally arising CD25+ CD4+ T cell receptors. *Immunity.* 2004; 21(2):267–77. <https://doi.org/10.1016/j.immuni.2004.07.009> PMID: [15308106](#).
15. Simons DM, Picca CC, Oh S, Perng OA, Aitken M, Erikson J, et al. How specificity for self-peptides shapes the development and function of regulatory T cells. *J Leukoc Biol.* 2010; 88(6):1099–107. <https://doi.org/10.1189/jlb.0310183> PMID: [20495071](#)
16. Hinterberger M, Aichinger M, Prazeres da Costa O, Voehringer D, Hoffmann R, Klein L. Autonomous role of medullary thymic epithelial cells in central CD4(+) T cell tolerance. *Nat Immunol.* 2010; 11(6):512–9. <https://doi.org/10.1038/ni.1874> PMID: [20431619](#).
17. Wing JB, Sakaguchi S. Multiple treg suppressive modules and their adaptability. *Front Immunol.* 2012; 3:178. <https://doi.org/10.3389/fimmu.2012.00178> PMID: [22754556](#)
18. Yamaguchi T, Wing JB, Sakaguchi S. Two modes of immune suppression by Foxp3(+) regulatory T cells under inflammatory or non-inflammatory conditions. *Semin Immunol.* 2011; 23(6):424–30. <https://doi.org/10.1016/j.smim.2011.10.002> PMID: [22055883](#).
19. Wing K, Onishi Y, Prieto-Martin P, Yamaguchi T, Miyara M, Fehervari Z, et al. CTLA-4 control over Foxp3+ regulatory T cell function. *Science.* 2008; 322(5899):271–5. <https://doi.org/10.1126/science.1160062> PMID: [18845758](#).
20. Qureshi OS, Zheng Y, Nakamura K, Attridge K, Manzotti C, Schmidt EM, et al. Trans-endocytosis of CD80 and CD86: a molecular basis for the cell-extrinsic function of CTLA-4. *Science.* 2011; 332(6029):600–3. <https://doi.org/10.1126/science.1202947> PMID: [21474713](#)
21. Cobb BS, Hertweck A, Smith J, O'Connor E, Graf D, Cook T, et al. A role for Dicer in immune regulation. *J Exp Med.* 2006; 203(11):2519–27. <https://doi.org/10.1084/jem.20061692> PMID: [17060477](#)
22. Kirigin FF, Lindstedt K, Sellars M, Ciofani M, Low SL, Jones L, et al. Dynamic microRNA gene transcription and processing during T cell development. *J Immunol.* 2012; 188(7):3257–67. <https://doi.org/10.4049/jimmunol.1103175> PMID: [22379031](#)
23. Li QJ, Chau J, Ebert PJ, Sylvester G, Min H, Liu G, et al. miR-181a is an intrinsic modulator of T cell sensitivity and selection. *Cell.* 2007; 129(1):147–61. <https://doi.org/10.1016/j.cell.2007.03.008> PMID: [17382377](#).
24. Ebert PJ, Jiang S, Xie J, Li QJ, Davis MM. An endogenous positively selecting peptide enhances mature T cell responses and becomes an autoantigen in the absence of microRNA miR-181a. *Nat Immunol.* 2009; 10(11):1162–9. <https://doi.org/10.1038/ni.1797> PMID: [19801983](#)
25. Winter SJ, Kunze-Schumacher H, Imelmann E, Grewers Z, Osthues T, Krueger A. MicroRNA miR-181a/b-1 controls MAIT cell development. *Immunol Cell Biol.* 2019 Feb; 97(2):190–202. Epub 2018 Nov 12. <https://doi.org/10.1111/imcb.12211> PMID: [30291723](#).
26. Zietara N, Lyszkiewicz M, Witzlau K, Naumann R, Hurwitz R, Langemeier J, et al. Critical role for miR-181a/b-1 in agonist selection of invariant natural killer T cells. *Proc Natl Acad Sci U S A.* 2013; 110(18):7407–12. <https://doi.org/10.1073/pnas.1221984110> PMID: [23589855](#)

27. Henao-Mejia J, Williams A, Goff LA, Staron M, Licona-Limon P, Kaech SM, et al. The microRNA miR-181 is a critical cellular metabolic rheostat essential for NKT cell ontogenesis and lymphocyte development and homeostasis. *Immunity*. 2013; 38(5):984–97. <https://doi.org/10.1016/j.immuni.2013.02.021> PMID: 23623381
28. Blume J, Zur Lage S, Witzlau K, Georgiev H, Weiss S, Lyszkiewicz M, et al. Overexpression of Valpha14Jalpha18 TCR promotes development of iNKT cells in the absence of miR-181a/b-1. *Immunol Cell Biol*. 2016; 94(8):741–6. <https://doi.org/10.1038/icb.2016.40> PMID: 27089939.
29. Schaffert SA, Loh C, Wang S, Arnold CP, Axtell RC, Newell EW, et al. mir-181a-1/b-1 Modulates Tolerance through Opposing Activities in Selection and Peripheral T Cell Function. *J Immunol*. 2015; 195(4):1470–9. <https://doi.org/10.4049/jimmunol.1401587> PMID: 26163591
30. Duber S, Hafner M, Krey M, Lienenklaus S, Roy B, Hobeika E, et al. Induction of B-cell development in adult mice reveals the ability of bone marrow to produce B-1a cells. *Blood*. 2009; 114(24):4960–7. <https://doi.org/10.1182/blood-2009-04-218156> PMID: 19812384.
31. Azzam HS, Grinberg A, Lui K, Shen H, Shores EW, Love PE. CD5 expression is developmentally regulated by T cell receptor (TCR) signals and TCR avidity. *J Exp Med*. 1998; 188(12):2301–11. PMID: 9858516
32. Sekiya T, Kashiwagi I, Yoshida R, Fukaya T, Morita R, Kimura A, et al. Nr4a receptors are essential for thymic regulatory T cell development and immune homeostasis. *Nat Immunol*. 2013; 14(3):230–7. <https://doi.org/10.1038/ni.2520> PMID: 23334790.
33. Paiva RS, Lino AC, Bergman ML, Caramalho I, Sousa AE, Zelenay S, et al. Recent thymic emigrants are the preferential precursors of regulatory T cells differentiated in the periphery. *Proc Natl Acad Sci U S A*. 2013; 110(16):6494–9. <https://doi.org/10.1073/pnas.1221955110> PMID: 23576744
34. Akimova T, Beier UH, Wang L, Levine MH, Hancock WW. Helios expression is a marker of T cell activation and proliferation. *PLoS ONE*. 2011; 6(8):e24226. <https://doi.org/10.1371/journal.pone.0024226> PMID: 21918685
35. Sojka DK, Hughson A, Fowell DJ. CTLA-4 is required by CD4+CD25+ Treg to control CD4+ T-cell lymphopenia-induced proliferation. *Eur J Immunol*. 2009; 39(6):1544–51. <https://doi.org/10.1002/eji.200838603> PMID: 19462377
36. Tai X, Cowan M, Feigenbaum L, Singer A. CD28 costimulation of developing thymocytes induces Foxp3 expression and regulatory T cell differentiation independently of interleukin 2. *Nat Immunol*. 2005; 6(2):152–62. <https://doi.org/10.1038/ni1160> PMID: 15640801.
37. Lio CW, Dodson LF, Deppong CM, Hsieh CS, Green JM. CD28 facilitates the generation of Foxp3(-) cytokine responsive regulatory T cell precursors. *J Immunol*. 2010; 184(11):6007–13. <https://doi.org/10.4049/jimmunol.1000019> PMID: 20421644
38. Vang KB, Yang J, Pagan AJ, Li LX, Wang J, Green JM, et al. Cutting edge: CD28 and c-Rel-dependent pathways initiate regulatory T cell development. *J Immunol*. 2010; 184(8):4074–7. <https://doi.org/10.4049/jimmunol.0903933> PMID: 20228198
39. Hinterberger M, Wirsberger G, Klein L. B7/CD28 in central tolerance: costimulation promotes maturation of regulatory T cell precursors and prevents their clonal deletion. *Front Immunol*. 2011; 2:30. <https://doi.org/10.3389/fimmu.2011.00030> PMID: 22566820
40. Siggs OM, Miosge LA, Yates AL, Kucharska EM, Sheahan D, Brdicka T, et al. Opposing functions of the T cell receptor kinase ZAP-70 in immunity and tolerance differentially titrate in response to nucleotide substitutions. *Immunity*. 2007; 27(6):912–26. <https://doi.org/10.1016/j.immuni.2007.11.013> PMID: 18093540
41. Sakaguchi N, Takahashi T, Hata H, Nomura T, Tagami T, Yamazaki S, et al. Altered thymic T-cell selection due to a mutation of the ZAP-70 gene causes autoimmune arthritis in mice. *Nature*. 2003; 426(6965):454–60. <https://doi.org/10.1038/nature02119> PMID: 14647385.
42. Hwang S, Song KD, Lesourne R, Lee J, Pinkhasov J, Li L, et al. Reduced TCR signaling potential impairs negative selection but does not result in autoimmune disease. *J Exp Med*. 2012; 209(10):1781–95. <https://doi.org/10.1084/jem.20120058> PMID: 22945921
43. Levine AG, Arvey A, Jin W, Rudensky AY. Continuous requirement for the TCR in regulatory T cell function. *Nat Immunol*. 2014; 15(11):1070–8. Epub 2014/09/30. <https://doi.org/10.1038/ni.3004> PMID: 25263123
44. Vahl JC, Drees C, Heger K, Heink S, Fischer JC, Nedjic J, et al. Continuous T cell receptor signals maintain a functional regulatory T cell pool. *Immunity*. 2014; 41(5):722–36. Epub 2014/12/04. <https://doi.org/10.1016/j.immuni.2014.10.012> PMID: 25464853.
45. Persaud SP, Parker CR, Lo WL, Weber KS, Allen PM. Intrinsic CD4+ T cell sensitivity and response to a pathogen are set and sustained by avidity for thymic and peripheral complexes of self peptide and MHC. *Nat Immunol*. 2014; 15(3):266–74. <https://doi.org/10.1038/ni.2822> PMID: 24487322

46. Fulton RB, Hamilton SE, Xing Y, Best JA, Goldrath AW, Hogquist KA, et al. The TCR's sensitivity to self peptide-MHC dictates the ability of naive CD8(+) T cells to respond to foreign antigens. *Nat Immunol*. 2015; 16(1):107–17. <https://doi.org/10.1038/ni.3043> PMID: 25419629
47. Sandrock I, Zięta N, Łyszkiewicz M, Oberdörfer L, Witzlau K, Krueger A, Prinz I. MicroRNA-181a/b-1 Is Not Required for Innate $\gamma\Delta$ NKT Effector Cell Development. *PLoS ONE*. 2015 Dec 16; 10(12): e0145010. <https://doi.org/10.1371/journal.pone.0145010> PMID: 26673421
48. Komatsu N, Mariotti-Ferrandiz ME, Wang Y, Malissen B, Waldmann H, Hori S. Heterogeneity of natural Foxp3+ T cells: a committed regulatory T-cell lineage and an uncommitted minor population retaining plasticity. *Proc Natl Acad Sci U S A*. 2009; 106(6):1903–8. <https://doi.org/10.1073/pnas.0811556106> PMID: 19174509
49. Kuwata N, Igarashi H, Ohmura T, Aizawa S, Sakaguchi N. Cutting edge: absence of expression of RAG1 in peritoneal B-1 cells detected by knocking into RAG1 locus with green fluorescent protein gene. *J Immunol*. 1999; 163(12):6355–9. PMID: 10586023.
50. Fohse L, Suffner J, Suhre K, Wahl B, Lindner C, Lee CW, et al. High TCR diversity ensures optimal function and homeostasis of Foxp3+ regulatory T cells. *Eur J Immunol*. 2011; 41(11):3101–13. <https://doi.org/10.1002/eji.201141986> PMID: 21932448.
51. Lefranc MP, Giudicelli V, Ginestoux C, Jabado-Michaloud J, Folch G, Bellahcene F, et al. IMGT, the international ImMunoGeneTics information system. *Nucleic Acids Res*. 2009; 37(Database issue): D1006–12. <https://doi.org/10.1093/nar/gkn838> PMID: 18978023
52. Brochet X, Lefranc MP, Giudicelli V. IMGT/V-QUEST: the highly customized and integrated system for IG and TR standardized V-J and V-D-J sequence analysis. *Nucleic Acids Res*. 2008; 36(Web Server issue):W503–8. <https://doi.org/10.1093/nar/gkn316> PMID: 18503082
53. Chen CZ, Li L, Lodish HF, Bartel DP. MicroRNAs modulate hematopoietic lineage differentiation. *Science*. 2004; 303(5654):83–6. <https://doi.org/10.1126/science.1091903> PMID: 14657504.

6.5 Human FCHO1 deficiency reveals role for clathrin-mediated endocytosis in development
and function of T cells

Łyszkiewicz M, **Ziętara N**, Frey L, Pannicke U, Stern M, Liu Y, Fan Y, Puchałka P, Hollizeck S, Somekh I, Rohlf s M, Yilmaz T, Ünal E, Karakukcu M, Patiroğlu T, Kellerer C, Karasu E, Sykora K-W, Lev A, Simon A, Somech R, Roesler J, Hoenig M, Keppler OT, Schwarz K, Klein C

Nature Communications 11(1):1031 (2020 Feb 25).

Human FCHO1 deficiency reveals role for clathrin-mediated endocytosis in development and function of T cells

Marcin Łyszkiewicz^{1,12,13}, Natalia Zięta^{1,12,13}, Laura Frey¹, Ulrich Pannicke², Marcel Stern³, Yanshan Liu¹, Yanxin Fan¹, Jacek Puchałka^{1,14}, Sebastian Hollizeck¹, Ido Somekh¹, Meino Rohlf¹, Tuğba Yilmaz⁴, Ekrem Ünal⁴, Musa Karakucukcu⁴, Türkan Patiroğlu^{4,5}, Christina Kellerer², Ebru Karasu², Karl-Walter Sykora⁶, Atar Lev⁷, Amos Simon⁷, Raz Somech⁷, Joachim Roesler⁸, Manfred Hoening⁹, Oliver T. Keppler^{3,10}, Klaus Schwarz^{2,11} & Christoph Klein¹

Clathrin-mediated endocytosis (CME) is critical for internalisation of molecules across cell membranes. The FCH domain only 1 (FCHO1) protein is key molecule involved in the early stages of CME formation. The consequences of mutations in *FCHO1* in humans were unknown. We identify ten unrelated patients with variable T and B cell lymphopenia, who are homozygous for six distinct mutations in *FCHO1*. We demonstrate that these mutations either lead to mislocalisation of the protein or prevent its interaction with binding partners. Live-cell imaging of cells expressing mutant variants of FCHO1 provide evidence of impaired formation of clathrin coated pits (CCP). Patient T cells are unresponsive to T cell receptor (TCR) triggering. Internalisation of the TCR receptor is severely perturbed in FCHO1-deficient Jurkat T cells but can be rescued by expression of wild-type FCHO1. Thus, we discovered a previously unrecognised critical role of FCHO1 and CME during T-cell development and function in humans.

¹Department of Pediatrics, Dr. von Hauner Children's Hospital, University Hospital, LMU, Munich, Germany. ²Institute for Transfusion Medicine, University of Ulm, Ulm, Germany. ³Max von Pettenkofer Institute, Virology, National Reference Center for Retroviruses, Faculty of Medicine, LMU München, Munich, Germany. ⁴Department of Pediatrics, Division of Pediatric Hematology & Oncology, Erciyes University, Kayseri, Turkey. ⁵Department of Pediatrics, Division of Pediatric Immunology, Erciyes University, Kayseri, Turkey. ⁶Department of Pediatric Hematology/Oncology, Hannover Medical School, Hannover, Germany. ⁷Pediatric Department A and the Immunology Service, Jeffrey Modell Foundation Center, Edmond and Lily Safra Children's Hospital, Sheba Medical Center, Tel Hashomer and Sackler Faculty of Medicine Tel Aviv University, Tel Aviv, Israel. ⁸Department of Pediatrics, Carl Gustav Carus Technical University Dresden, Dresden, Germany. ⁹Department of Pediatrics, University Medical Centre Ulm, Ulm, Germany. ¹⁰German Center for Infection Research (DZIF), Partner Site Munich, Munich, Germany. ¹¹Institute for Clinical Transfusion Medicine and Immunogenetics Ulm, German Red Cross Blood Service Baden-Wuerttemberg, Hessen, Germany. ¹²Present address: Institute for Immunology, Biomedical Center Munich, Ludwig-Maximilians-Universität München, Planegg-Martinsried, 82152 Munich, Germany. ¹³These authors contributed equally: Marcin Łyszkiewicz, Natalia Zięta. ¹⁴Deceased: Jacek Puchałka. ✉email: Marcin.Lyszkiewicz@med.uni-muenchen.de; Christoph.Klein@med.uni-muenchen.de

Eukaryotic cells are characterised by a structural and functional compartmentalisation. Biological membrane systems are critically involved in the establishment and maintenance of the cellular compartments. The highly dynamic modulation of membranes is a key feature for their role in a variety of biological processes, such as endocytosis, secretion, signal transduction or migration. Clathrin, a central molecular scaffold, plays an essential role in the re-organisation of cellular membranes and the transport between compartments. Clathrin-coated vesicles (CCV), first described as “clathrin-coated pits” (CCP) in mosquito oocytes¹ and later purified from pig brain², control internalisation of membrane-associated proteins and protein transport from the trans-Golgi-network³.

Clathrin-dependent endocytosis (CME) is initiated at the plasma membrane by the recruitment of adaptors (heterotrimeric AP-2 complex, AP180; clathrin assembly lymphoid myeloid leukaemia, CALM; and anchor proteins (FCH domain only 1 and 2, [FCHO1 and 2]; epidermal growth factor receptor substrate 15, [EPS15]; and intersectin)^{4–6}. These factors are enriched within PIP2 (phosphatidylinositol 4,5-bisphosphate)-rich regions of the membrane and trigger the assembly of the clathrin proteins into clusters⁷. During maturation, the clathrin-enriched membrane patches undergo a local curvature and an invaginated spheric clathrin-coated pit is generated. The connection of this pit to the plasma membrane is detached by dynamin⁸.

The molecular details of the formation of a new vesicle are still not fully understood. In vitro, the presence of clathrin, an adaptor protein (i.e., AP-1, AP-2) and dynamin are sufficient to form a vesicle⁹. However, in vivo, the mechanism is much more complex. It has been shown by live-cell total internal reflection fluorescence (TIRF) imaging with single-molecule EGFP sensitivity and high-temporal resolution that the formation of a vesicle can originate from two AP-2 molecules with a clathrin tri-skeleton⁴. In contrast, another report suggested that FCHO1 and FCHO2 need to be associated with the membrane prior to AP-2 recruitment to initiate the process⁵. FCHO1/2 interact and show similar kinetics at the membrane as the scaffold proteins EPS15 and intersectin, two factors that are important for clathrin-dependent endocytosis^{6,10}. Upon downregulation of EPS15 expression by small-interfering RNA, FCHO1/2 show a diffuse pattern of distribution at the cell membrane. This observation suggests that EPS15 is critical for the specific agglomeration of FCHO1/2 on the site of the formation of clathrin-coated vesicles⁵.

Since the early clinical discoveries of monogenic immune disorders by Rolf Kostmann¹¹ and Ogden Bruton¹², >400 primary immunodeficiency diseases have been delineated¹³, many of which have opened unprecedented insights into molecular mechanisms orchestrating differentiation and function of the human immune system.

Here, we describe ten human patients with T-cell deficiency and loss-of-function mutations in *FCHO1*. Our experiments demonstrate that the absence of functional FCHO1 results in perturbed clathrin-mediated endocytosis in several tissues, as well as dysfunctional internalisation of the TCR. Pharmacological inhibition of CME during in vitro T-cell development results in marked delay of T-cell differentiation. In summary, we identify an essential and non-redundant role for the clathrin adaptor FCHO1 in T-cell differentiation and function, linking CME to the function of the human immune system.

Results

Clinical phenotype and molecular genetics. We collected seven pedigrees with ten patients presenting with features of T-cell immunodeficiency (Fig. 1a and Supplementary Fig. 1). All

patients suffered from severe bacterial, viral or fungal infections indicative of a primary immunodeficiency disorder. Three patients (B1, C1, D1) developed B-cell lymphoma prior to allogeneic hematopoietic stem cell transplantation, and three patients (A1, D1, E1) had neurological disease (Table 1). Immunological parameters were ranging from a moderate decrease in peripheral CD4⁺ T cells (F2 and G1) to severe combined immunodeficiency with virtually absent B- and T-cells (A1, B1, E1). With the exception of G1, all patients had hypogammaglobulinemia (Supplementary Table 1). Thus, the common immunophenotypic denominator for all these patients was CD4⁺ T-cell deficiency.

In order to identify the underlying genetic defect, we performed whole-exome sequencing (WES) followed by Sanger sequencing of candidate genes on patients and family members (see Online Methods). We have identified six distinct, novel and segregating homozygous mutations in *FCHO1* in seven pedigrees (Fig. 1b and Supplementary Figs. 2 and 3; Table 1 and Supplementary Table 2). At the DNA level, the mutation in kindred A results in a nucleotide substitution at the position c.2036 G > C, in kindred B in a nucleotide substitution at the position c.100 G > C, whereas the mutations of the pedigrees C and D (not known to be connected by kinship) are insertions c.2023insG resulting in a frameshift and premature termination of the protein (Fig. 1b, c). The mutations of kindred E (changing the first nucleotide of intron 8 c.489 + 1 G > A) and kindred F (contained in the intron 6 splice acceptor site; c.195-2 A > C) affect splicing of pre-mRNA (Fig. 1c and Supplementary Fig. 2). Effects on FCHO1 transcripts in fibroblasts, peripheral blood mononuclear cell (PBMC) and EBV-LCL are shown in Supplementary Figs. 2 and 3. No bands corresponding to wild-type FCHO1 were detected in these analyses. In kindred G, a single-nucleotide substitution at position c.1948C > T results in a predicted premature stop codon at amino acid position 650. All identified patient-associated mutations are summarised in Supplementary Table 2.

FCHO1 consists of three main segments organised into two major domains (Fig. 1c). The N-terminal F-BAR domain (also known as extended FCH), which is responsible for membrane binding, is followed by a structurally less organised and evolutionary poorly conserved segment that binds the adaptor protein AP-2. The C-terminal part (~270 amino acids) forms a μ homology domain (μ HD), which directly binds to epidermal growth factor receptor pathway substrate 15 (EPS15) and EPS15-like 1 (EPS15L1) also known as EPS15R⁵.

The mutation in kindred A results in an Arg to Pro substitution at the position 679 in the μ HD domain. The crystal structure of the *Danio rerio* μ HD domain of Fcho1 has been resolved together with a fragment of EPS15 allowing for direct modelling the effect of the amino acid substitution on this structure (Fig. 1d)¹⁴. Although the patient-associated mutations are not directly located at the protein-binding trough, replacing the charged side chain of Arg with a nonpolar and rigid ring of Pro may result in steric alterations in the μ HD subdomain A and thus affect interaction with its binding partners (Fig. 1d).

The point mutation in kindred B results in an amino acid substitution in the alpha-helix structure of the F-BAR domain (p. Ala34Pro). The F-BAR domain of FCHO1 has not been crystallised. However, the structure of its functional and structural paralogue FCHO2 has been resolved, which allows for modelling of the patient-associated mutation¹⁴. The substitution of Ala with Pro at position 34 is likely to result in a disruption of the alpha-helix structure, which in turn may lead to alterations in the membrane-binding properties of the entire domain (Fig. 1e).

In addition to mutations resulting in amino acid substitutions, we identified three distinct variants resulting in a premature stop

Table 1 Summary of clinical features of patients carrying mutations in FCHO1.

Patient	Origin	Genetic variant ^a	Consequences of mutation	Immunological findings	Infections	Other clinical findings	Therapy and outcome
A1	Germany	FCHO1 c.2036 G > C	aa substitution in μHD domain (p.R679P)	<ul style="list-style-type: none"> T- and B-cell lymphopenia hypogammaglobulinemia 	<ul style="list-style-type: none"> Recurrent pneumonia and viral gastroenteritis Relapsing oro-genital mycoses Broncholitis obliterans Postpneumonic pulmonary fibrosis Otitis media Recurrent pneumonia Recurrent fungal infections CMV infection Recurrent pulmonary infections Recurrent fungal infections Otitis media 	<ul style="list-style-type: none"> Moya-Moya syndrome Transient left hemiparesis upon cerebral ischaemia Failure to thrive Microcephaly 	Reduced cardiopulmonary performance, stable Moya-Moya 9 years after HLA-matched HSCT
B1	Turkey	FCHO1 c.100 G > C	aa substitution in F-BAR domain (p.A34P)	<ul style="list-style-type: none"> T- and B-cell lymphopenia hypogammaglobulinemia 	<ul style="list-style-type: none"> Recurrent pneumonia Recurrent fungal infections CMV infection Recurrent pulmonary infections Recurrent fungal infections Otitis media 	<ul style="list-style-type: none"> DLBCL Renal metastases 	Deceased as consequence of DLBCL, age 16 years
C1	Turkey	FCHO1 c.2023msG	Truncated (p.Stop687)	<ul style="list-style-type: none"> CD4+ T-cell lymphopenia hypogammaglobulinemia 	<ul style="list-style-type: none"> Recurrent pneumonia HSV infection 	<ul style="list-style-type: none"> EBV+ Hodgkin lymphoma Failure to thrive hepatosplenomegaly Renal masses Xantho-granulomatous pyelonephritis DLBCL stage IV Liver lesions Spleen lesions Lung lesions Aphthous stomatitis Gingivitis Encephalitis Mild brain atrophy 	IVIG replacement and antibiotics; awaiting allo-HSCT
D1	Turkey	FCHO1 c.2023msG	Truncated (p.Stop687)	<ul style="list-style-type: none"> CD4+ T-cell lymphopenia hypogammaglobulinemia 	<ul style="list-style-type: none"> Recurrent pneumonia HSV infection 	<ul style="list-style-type: none"> Deceased, age 10 years 	
E1	Palestine	FCHO1 c.489 + 1G > A	Alternative splicing IVS8 splice donor	<ul style="list-style-type: none"> CD4+ T-cell and B-lymphopenia hypogammaglobulinemia not available 	<ul style="list-style-type: none"> Recurrent pneumonia Chronic diarrhoea CMV infection Fungal infection Recurrent pneumonia Chronic diarrhoea Recurrent pneumonia Chronic diarrhoea EBV infection 	<ul style="list-style-type: none"> IVIG replacement and antibiotics; awaiting allo-HSCT 	
E2	Palestine	FCHO1 c.489 + 1G > A	Alternative splicing IVS8 splice donor	<ul style="list-style-type: none"> CD4+ T-cell lymphopenia hypogammaglobulinemia 	<ul style="list-style-type: none"> Recurrent pneumonia Chronic diarrhoea EBV infection 	<ul style="list-style-type: none"> Deceased after cardiac arrest, age 2 years 	
E3	Palestine	FCHO1 c.489 + 1G > A	Alternative splicing IVS8 splice donor	<ul style="list-style-type: none"> CD4+ T-cell lymphopenia hypogammaglobulinemia 	<ul style="list-style-type: none"> Recurrent pneumonia Chronic diarrhoea EBV infection 	<ul style="list-style-type: none"> IVIG replacement and antibiotics; awaiting allo-HSCT 	
F1	Saudi Arabia	FCHO1 c.195-2 A > C	Alternative splicing IVS6 splice acceptor	<ul style="list-style-type: none"> CD4+ T-cell lymphopenia hypogammaglobulinemia 	<ul style="list-style-type: none"> Recurrent pneumonia Chronic diarrhoea Cryptosporidiosis Recurrent stomatitis (HSV) 	<ul style="list-style-type: none"> Failure to thrive 	<ul style="list-style-type: none"> HSCT at age 5 yrs (no conditioning), MFD (mother), a + cGvHD, complete donor chimerism, normal immune function, off IVIG, 10 yrs follow up HSCT at age 1.5 yrs, (no conditioning), MSD, no GvHD, post-transplant intracranial EBV-PTLD and atypical mycobacterium-associated mastoiditis; mixed chimerism (T-cells 100% donor, non-T-MNCs 5-10% donor, red cells recipient), normal immune function, off IVIG, 12.5 yrs follow up HSCT (MFD) at age 5 years, doing well
F2	Saudi Arabia	FCHO1 c.195-2 A > C	Alternative splicing IVS6 splice acceptor	<ul style="list-style-type: none"> CD4 + T-cell lymphopenia 	<ul style="list-style-type: none"> Recurrent pneumonia Chronic diarrhoea Cryptosporidiosis Multiple viruses (adenovirus, RSV, enterovirus) 		
G1	Algeria	FCHO1 c.1948C > T	Truncated p.R650X p.Stop650	<ul style="list-style-type: none"> CD4 + T-cell lymphopenia Weak response to vaccination 	<ul style="list-style-type: none"> Recurrent broncho-pulmonary infections Candidiasis CMV infection 	<ul style="list-style-type: none"> Failure to thrive 	

EBV Epstein-Barr virus, DLBCL diffuse large B-cell lymphoma, PTLD post-transplant lymphoproliferative disorder, HLA human leucocyte antigen, HSCT haematopoietic stem cell transplantation, MFD matched family donor, IVIG intravenous immunoglobulin, a + cGvHD acute and chronic graft versus host disease.

^asequence of coding DNA is given from the first nucleotide of the translation start codon.

^bsequence of protein is given from the first amino acid.

of these amino acids, it is likely that, in case a protein is stably expressed, it disrupts the alpha-helix structure of the F-BAR domain. Finally, the kindred F-associated mutation in the splice acceptor region gives rise to three possible splice variants, each of them resulting in a premature stop codon shortly downstream of exon 6. It prevents correct splicing and by prediction presumably leads to expression of a very short (~7.1 kDa), non-functional form of FCHO1 (Supplementary Fig. 3b–e).

Effects of patient-associated mutations on FCHO1 function.

Based on CADD and PolyPhen-2 scores, all patient-associated mutations are deleterious for the FCHO1 protein function (Supplementary Table 2). To test this, we first established a heterologous system, where HEK239T cells were transiently transfected with vectors carrying wild-type (wt) or mutated versions of the *FCHO1* complementary DNA (cDNA). None of the herein tested mutations altered protein stability, albeit p.Stop687 resulted in the expression of a shorter protein (Fig. 2a and Supplementary Fig. 4). The encoded proteins were tested for co-immunoprecipitation with their direct interacting partners EPS15 and its homologue EPS15R. Recovery of the EPS15 and EPS15R was strongly reduced in both mutants affecting the μ HD domain (c.R679P and p.Stop687). In contrast, the FCHO1 mutant affecting the F-BAR domain (p.A34P) did not alter the interaction with EPS15 and EPS15R (Fig. 2a).

The function of FCHO1 critically depends not only on its biochemical interaction with partner proteins but also on the spatiotemporal organisation of its interactome. Nucleation of FCHO1-mediated clathrin-coated vesicles (CCV) occurs only at the plasma membrane⁵. We, therefore, set out to test whether the identified *FCHO1* mutations altered the subcellular location of the corresponding protein. We employed SK-MEL-2 cells expressing a RFP-tagged clathrin light chain from one allele of its endogenous locus¹⁵. In order to circumvent confounding effects of the endogenously encoded FCHO1 protein, the *FCHO1* gene was deleted using CRISPR/Cas9-mediated gene editing. Transient expression of wt FCHO1-GFP fusion protein in knockout (ko) cells showed scattered bright puncta associated with the plasma membrane as previously reported^{5,14} (Fig. 2b–d and Supplementary Figs. 5–7). In contrast, expression of the F-BAR mutated (p.A34P) FCHO1 form resulted in the formation of large plasma membrane-dissociated agglomerations (Fig. 2b–d and Supplementary Figs. 5–7).

Further, both p.R679P and p.Stop687 μ HD mutants failed to form any punctated structures. These mutants appeared as a diffuse network, mostly dissociated from the plasma membrane (Fig. 2b–d and Supplementary Fig. 5). In accordance with the co-immunoprecipitation results, only wt and p.A34P FCHO1 colocalized with their partners EPS15 and adaptin (Fig. 2b–c, and for quantification Fig. 2e). Importantly, all mutants failed to colocalize with endogenous clathrin (Fig. 2d–e). We chose a model system with physiological expression levels of FCHO1. While this is advantageous in many respects⁵, it is limited with respect to poor signal-to-noise ratio. To improve signal intensities, we additionally transduced SK-MEL-2 cells to stably over-express RFP-tagged clathrin light chains. As shown in Supplementary Fig. 7, these data confirm that only wild-type FCHO1, but none of the mutants, colocalize with clathrin.

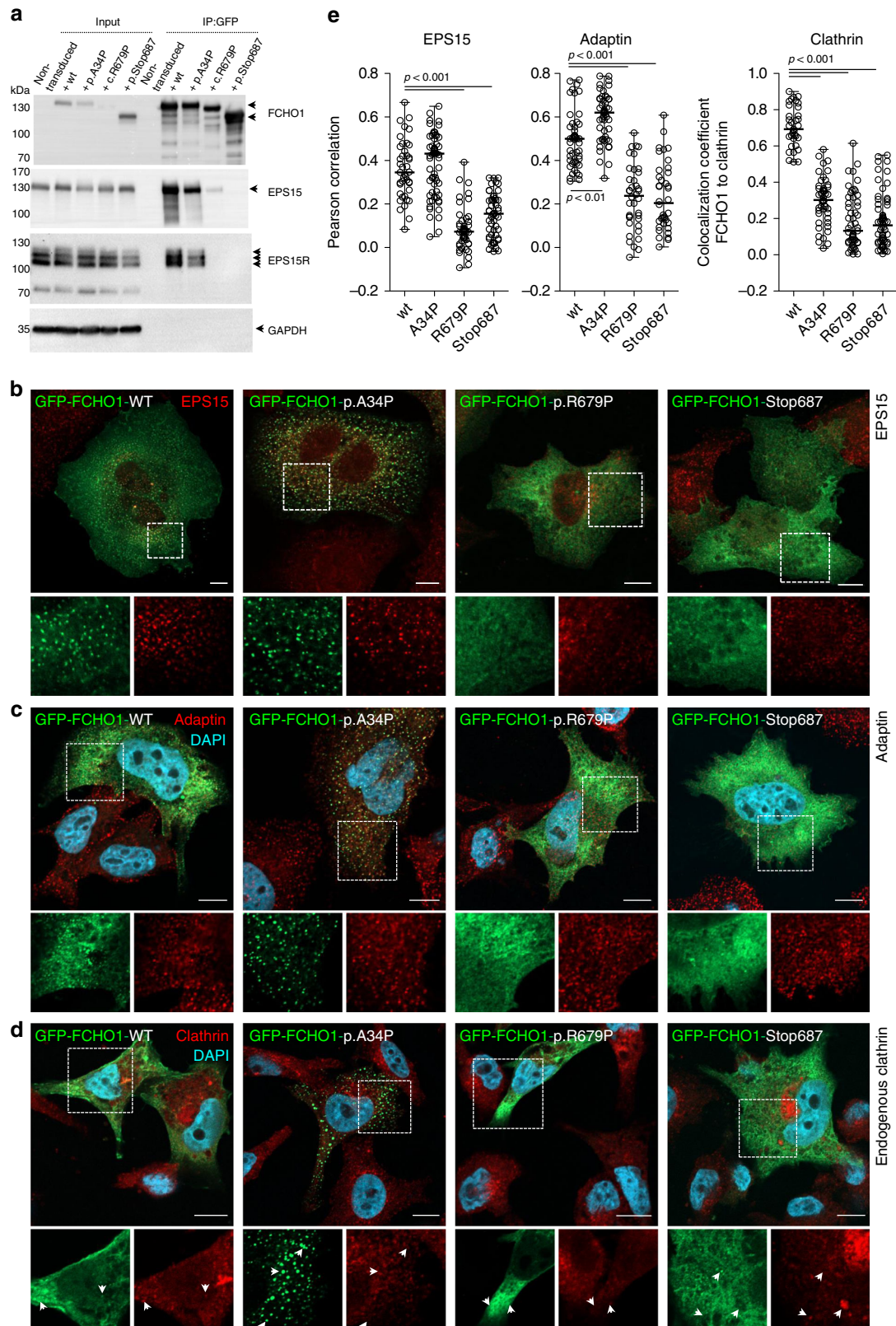
Nucleation of CCV is a highly dynamic process. To measure the dynamics of protein–protein interaction between FCHO1 and clathrin, we established live-cell imaging models. Here, we followed wt FCHO1 and both point mutants (p.R679P and p.A34P). As anticipated, wt GFP-FCHO1 initiated the formation of clathrin-coated pits, whereas both mutants failed to do so (Fig. 3a–c and Supplementary Movies 1–3). FCHO1 carrying the

μ HD-associated p.R679P mutation prevented the formation of productive pits and thus failed to facilitate the formation of CCV. Since the sensitivity of the confocal microscope does not allow to discriminate single molecules, we cannot exclude that small, abortive pits may have been formed. However, we failed to detect any aggregation of FCHO1 carrying this mutation. In striking contrast, the F-BAR-associated mutation p.A34P resulted in the formation of fast moving, large aggregates of GFP-FCHO1 fusion proteins. Moreover, such membrane-dissociated aggregates tended to merge, leading to the formation of cytoplasmic protein intrusions (Supplementary Fig. 5). These pits appeared to be abortive, since they failed to interact with clathrin (Fig. 3a–c).

These results illustrate that the identified mutations in *FCHO1* constitute loss-of-function alleles: whereas the mutation in the μ HD domain results in loss-of-interaction with its main interacting partners and partial dissociation from the plasma membrane, the mutation in the F-BAR domain alters the subcellular localisation of the FCHO1 protein. Irrespective of their nature, all mutations ultimately result in inefficient nucleation of CCV.

FCHO1 regulates endocytosis of the T-cell receptor. The *FCHO1* mutations identified in our patients predominantly result in a severe T-cell defect while other cells of the immune system appear largely unaffected. The key designate of T-cell fate during ontogeny is the quality and strength of the T-cell receptor (TCR) signal^{16–18}. The TCR has no intrinsic catalytic activity. TCR-dependent signal propagation requires a multi-protein complex comprises TCR α - and β -chains non-covalently coupled to immunoreceptor tyrosine-based activation motif (ITAM)-rich CD3 ϵ , γ , δ and ζ molecules. Internalisation of the CD3:TCR complex depends on the formation of CCP^{19–24}. We hypothesised that FCHO1 may be involved in TCR internalisation during T-cell activation. To test this, we took advantage of the CD4-positive human Jurkat T-cell lymphoma line in which we deleted the endogenous *FCHO1* gene using CRISPR/Cas9 gene editing. FCHO1-deficient Jurkat clones were reconstituted with either wt or mutated FCHO1 using retroviral vectors encoding a bicistronic FCHO1 and GFP cDNA separated by an internal ribosomal entry site (IRES). In order to understand the effect of FCHO1 on TCR internalisation and clustering, we analysed TCR distribution upon stimulation using confocal microscopy. After 60 min of TCR triggering by an α -CD3 monoclonal Ab, large intracellular CD3-positive puncta were formed in wt cells, whereas in FCHO1 ko clones CD3 molecules remained in diffuse form (Fig. 4a and Supplementary Fig. 8). Knockout clones reconstituted with wt FCHO1 formed large CD3-positive puncta, essentially indistinguishable from those in wt cells. In contrast, none of the FCHO1 mutants were able to rescue the phenotype and thus nearly all CD3 molecules remained diffused upon TCR-activation (Fig. 4a). We also noted plasma membrane invagination and nucleus segmentation in FCHO1-deficient Jurkat cells. This effect was not observed in SK-MEL-2 cells (Figs. 2b–d and 4a, and Supplementary Fig. 5). It is therefore possible, that FCHO1 deficiency has a more general effect on plasma membrane structure in T cells.

To assess TCR internalisation in a quantitative manner, we next measured the intracellular accumulation of CD3:TCR complexes upon anti-CD3-mediated TCR triggering over time using flow cytometry. Consistent with our confocal microscopy studies, we noted that FCHO1 ko cells accumulated approximately two-fold less CD3:TCR complexes when compared to wt cells (Fig. 4b). Finally, as the TCR cross-linking and its subsequent internalisation are essential for quality and strength of the triggered signal, we assessed whether FCHO1 directly



modulated TCR responsiveness. To this end, Jurkat cells sufficient or deficient for FCHO1 were stimulated with an α -CD3 antibody and assessed for release of intracellular Ca^{2+} . When compared to controls, FCHO1-deficient cells released less Ca^{2+} upon CD3: TCR triggering (Fig. 4c). Furthermore, only reconstitution with

wt but not mutated forms of FCHO1 restored normal levels of Ca^{2+} , directly demonstrating that physiological TCR signalling depends on FCHO1.

During CME adaptor proteins recognise cargoes at the cell surface and direct them to the clathrin pits. FCHO1 binds its

Fig. 2 Patient-associated mutations alter either binding properties or subcellular localisation of the FCHO1 protein. **a** Whole-cell lysates from HEK293T cells overexpressing either wt or indicated mutant GFP-FCHO1 fusion proteins were used for immunoprecipitation. Specific bands are indicated with arrows. Anti-FCHO1 or anti-GFP antibodies were used independently to detect FCHO1-specific bands. Representative data of three independent experiments are shown. Uncropped blots are shown in Supplementary Fig. 4. **b–d** FCHO1-deficient SK-MEL-2 cells expressing RFP-tagged clathrin light chain from endogenous locus ($CLTA^{RFP/wt}$) were transiently transfected with either wt or mutated GFP-FCHO1 and fixed 24 to 36 h post transfection. Representative confocal microscopy pictures show that the F-BAR-domain-associated mutation p.A34P alters the subcellular localisation of FCHO1 and leads to the formation of large aggregates dissociated from the plasma membrane. The μ HD domain-associated mutations (p.R679P and p.Stop687) abolish the interaction of FCHO1 with its interacting partners EPS15, and adaptin. All mutations obliterate interaction with endogenous clathrin. Enlarged and colour-separated regions corresponding to boxed areas are shown below each main picture. In **d** arrows indicate presumptive interaction of clathrin with wild-type FCHO1 and lack of such interaction for all tested mutants. Scale bar represents 5 μ m for main pictures and 10 μ m for enlarged regions. Colour code: **b–d** GFP-FCHO1, green; DAPI, blue, **b** EPS15, **c** adaptin, **d** clathrin-red. **e** Quantification of data shown in **b** to **d**. Pearson correlation or co-localisation coefficients of FCHO1 wild-type and all tested mutants with EPS15, adaptin and clathrin. Pooled data of two to three independent experiments are depicted. Each symbol represents one region of 25 μ m². Up to three regions per cells were quantified. Horizontal lines indicate the median, whiskers indicate the range (min to max). Statistical analysis of significance was performed using one-way ANOVA test followed by Tukey's multiple comparison test to assess differences between groups. Source data are provided as a Source Data file.

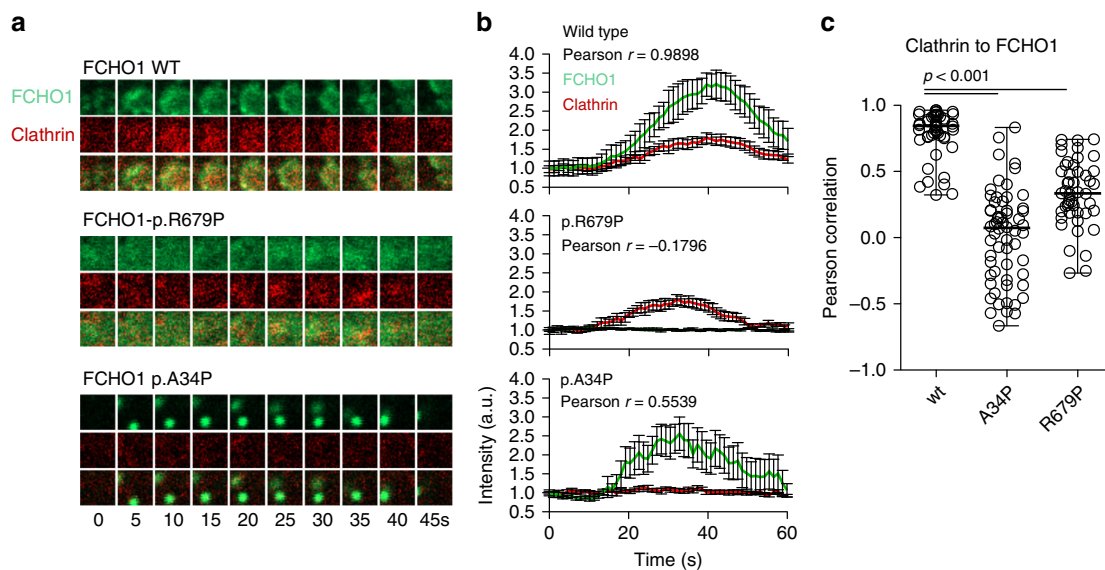


Fig. 3 Mutations in both μ HD and F-BAR domains of FCHO1 prevent nucleation of clathrin-coated pits (CCP). **a** The dynamics of FCHO1-mediated nucleation of CCP in FCHO1-deficient SK-MEL-2 cells expressing RFP-tagged clathrin light chain from endogenous locus ($CLTA^{RFP/wt}$) transduced with either wild-type (upper panel), μ HD-mutated (p.R679P—middle panel) or F-BAR-mutated (p.A34P—bottom panel) GFP-FCHO1 fusion protein. Two micrometre-wide sections of representative movies are shown. Full movies are available in supplemental materials. In the middle panel, contrast was reduced and brightness was increased as to show a diffused signal of GFP at the plasma membrane. **b** Time dependence of the fluorescent intensity of FCHO1 (green) and endogenous clathrin (red) averaged from nine independent movies. Only the fluorescence of wild-type but not mutant FCHO1 correlates with clathrin. Each channel was normalised to the background and the initial fluorescence was set to 1. Error bars represent SEM of mean fluorescence intensity, $n = 9$ biologically independent cells from minimum three independent experiments. **c** Pearson correlation of FCHO1 and clathrin from individual movies. Pooled data from three independent experiments. Each symbol represents one square region of 25 μ m². Up to three regions per cells were quantified. Horizontal lines indicate the median. Statistical analysis of significance was performed using one-way ANOVA test followed by Tukey's multiple comparison test to assess differences between groups. Source data are provided as a Source Data file.

cargo through its μ HD domain^{25,26}. It has been proposed that Syp1, the yeast FCHO1 homologue, recognises DxY motifs on its cargo²⁶. We hypothesised that human FCHO1 may also recognise its cargo via DxY motifs, in particular since CD3 ϵ and CD3 γ have DxY motifs in their cytoplasmic domain (Supplementary Fig. 9a). While we could confirm interaction of FCHO1 and EPS15 in Jurkat cells stably transduced with N¹- or C¹-flag FCHO1 fusion proteins, we could not observe any direct interaction with either of the CD3 molecules (Supplementary Fig. 9c–f). Thus, although CD3 molecules possess the putative sorting motifs recognised by FCHO1, we could not provide experimental evidence for direct FCHO1-CD3 interaction.

In sum, we provide evidence that FCHO1 plays a role in TCR-dependent T-cell activation. It affects TCR clustering upon

receptor triggering and modulates its internalisation. Finally, FCHO1 deficiency results in impaired mobilisation of Ca²⁺, directly linking the FCHO1 to TCR-associated signalling.

FCHO1 deficiency does not affect entry of VSV-G pseudotyped HIV-1. Infection of cells with vesicular stomatitis virus (VSV) is strongly dependent on CME. CME of VSV particles is initiated after interaction of the viral glycoprotein (VSV-G) with the cellular LDL (low-density lipoprotein) receptor²⁷. Entry of VSV or VSV-G pseudotyped lentiviruses into the cytoplasm occurs after endosomal acidification, which induces a conformational change of VSV-G followed by fusion of viral and cellular membranes²⁸.

To evaluate whether the absence of FCHO1 in Jurkat T cells has an impact on CME-dependent virus infection, Jurkat wt and

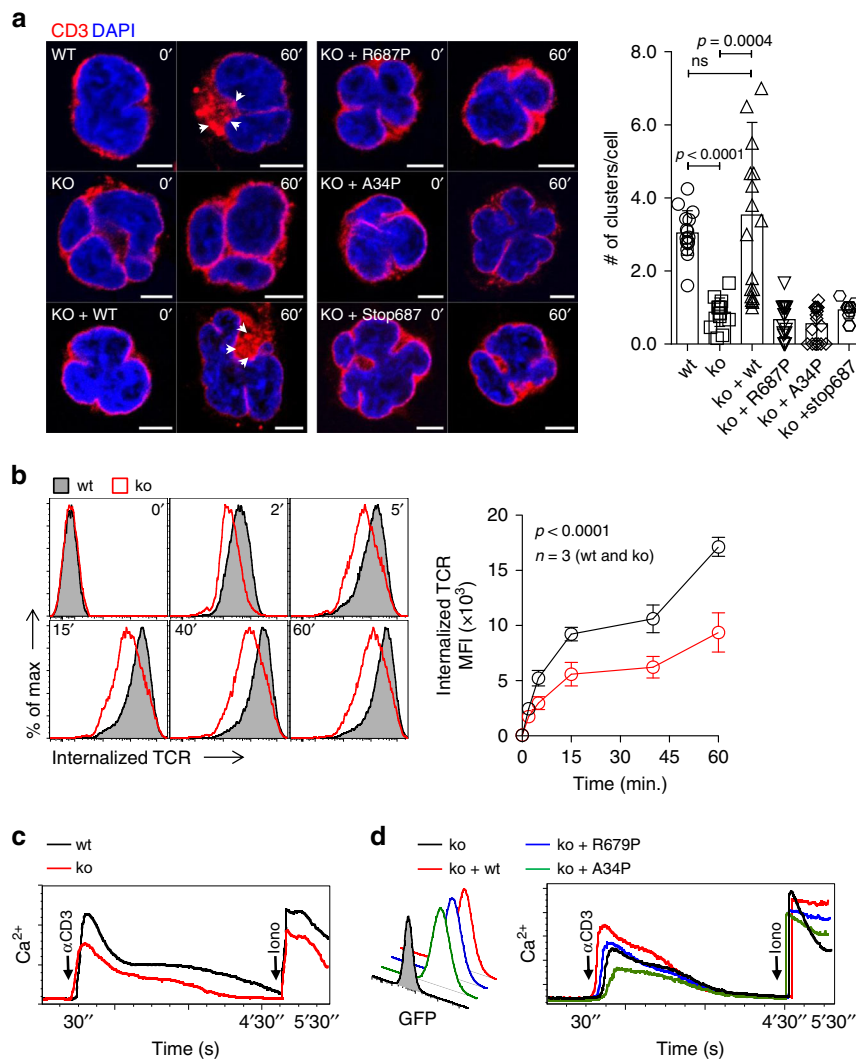


Fig. 4 FCHO1 deficiency impairs TCR internalisation. **a** FCHO1-sufficient and -deficient clones of Jurkat cells were used in the heterologous system, in which ko clones were left either non-transduced or stably transduced with wt or FCHO1 construct carrying one of the patient-associated mutations, as indicated. Cells were mock-treated (0') or stimulated with anti-CD3 Ab (60') at 37 °C, fixed and stained for CD3 and DAPI. Representative confocal microscopy pictures show that only wt FCHO1 facilitates the formation of CD3 puncta upon stimulation. Scale bar 5 μ m. White arrowheads indicate CD3 puncta. The chart summarises data of three independent experiments in which an average number of CD3 puncta per cell is shown. Each point indicates an average number of puncta per cell that could be found in one field of view. Statistical analysis of significance was performed using ANOVA test followed by Sidak's multiple comparison test to assess differences between groups, whiskers indicate the range (5–95 percentile). **b** FACS analysis of TCR internalisation in wt or FCHO1 ko Jurkat clones. Jurkat cells were stained with anti-CD3 Ab in cold and then TCR internalisation was assessed over time at 37 °C in the presence of anti-mouse F(ab')₂ fragments labelled with Ax647. At indicated time points remaining surface TCRs were stripped, thus fluorescent signal corresponds to the internalised TCR only. The chart summarises data of one representative experiment out of three, $n = 3$ clones per genotype. **c** Intracellular Ca^{2+} flux upon TCR stimulation. Wt or FCHO1 ko Jurkat clones were loaded with Ca^{2+} -sensitive FuraRed and Fluo-4 dyes and stimulated with anti-CD3 Ab and then Ca^{2+} flux was recorded flow cytometrically over time. α -CD3 and Iono indicate time points of respective stimulations. Data are representative of three independent experiments in which minimum three different clones of each genotype were analysed. **d** Ca^{2+} flux of FCHO1-deficient clones upon reconstitution with either wt or indicated mutants of FCHO1. GFP histogram indicates transduction efficiency. Intracellular Ca^{2+} flux was assessed as in **c**, representative data of two independent experiments are shown. Two FCHO1-deficient clones were analysed. **e** Statistical analysis was performed using two-way ANOVA (p -values for the effect of the genotype). Source data are provided as a Source Data file.

FCHO1 ko clones were challenged with HIV-1 particles, that are devoid of their own envelope glycoprotein but had been pseudotyped with VSV-G. The interaction of T cells with VSV-G HIV-1 was monitored using two established readouts, i.e., virion fusion and productive HIV-1 infection. The quantitative assessment of fusion of virions is based on the incorporation of a BlaM-Vpr chimeric fusion protein into VSV-G HIV-1 particles and their subsequent delivery into the cytoplasm of T cells as a result of virion fusion. Cleavage of the fluorescent CCF2 dye,

which is loaded into target cells, allows for detection of fusion events by flow cytometry^{29–31}. The successful infection of VSV-G HIV-1 pseudotyped can be quantified by intracellular staining for HIV-1 p24 antigen³².

Jurkat wt and FCHO1 ko clones were challenged with different multiplicities of infection of either VSV-G HIV-1 Δ Env (BlaM-Vpr) (Fig. 5a and Supplementary Fig. 10a) or VSV-G HIV-1 Δ Env (Fig. 5b and Supplementary Fig. 10b). FCHO1-deficient Jurkat T clones displayed a susceptibility to VSV-G pseudotyped HIV-1,

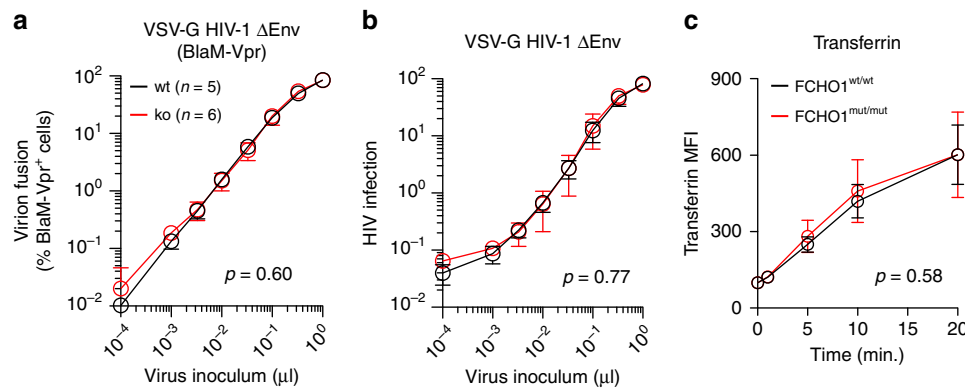


Fig. 5 FCHO1 deficiency does not alter global clathrin-mediated endocytosis. **a, b** Fusion of VSV-G HIV-1 Δ Env (BlaM-Vpr) virions (**a**) or infection by VSV-G HIV-1 Δ Env (**b**) of Jurkat cells. Wt or FCHO1-deficient clones were challenged with increasing volumes of the indicated VSV-G HIV-1 Δ Env. Virion fusion was monitored by flow cytometry as previously reported^{29–31} and the percentage of cleaved CCF2⁺/BlaM-Vpr⁺ cells is plotted relative to the virus inoculum. Infection of VSV-G HIV-1 Δ Env was monitored by intracellular HIV-1 p24 staining two days post challenge and the relative percentage of p24-positive cells is plotted relative to the virus inoculum³². Arithmetic means and standard errors are shown of results obtained for the indicated number of clones from either virion fusion (**e**) or infection (**f**). **c** Patient fibroblast or healthy donor fibroblast were subjected to the transferrin uptake assay. Cells were exposed to fluorescently labelled transferrin for the indicated time at 37 °C and subsequently analysed by FACS. Data are pooled of four independent assays; error bars represent standard deviation. **a–c** Statistical analysis was performed using two-way ANOVA (p -values for the effect of the genotype). Source data are provided as a Source Data file.

monitored by both virion fusion and productive infection, that was indistinguishable from that of wt clones. As controls of specificity, fusion of HIV-1 wt, but not of VSV-G HIV-1 Δ Env, was inhibited by the peptidic HIV-1 fusion inhibitor T20 (Supplementary Fig. 11a) and, importantly, infection by VSV-G HIV-1 Δ Env was blocked by the V-ATPase inhibitor bafilomycin A1, which prevents endosome acidification (Supplementary Fig. 11b).

Taken together, FCHO1 deficiency in Jurkat T cells does not functionally impair CME in the context of VSV-G-mediated entry and infection of a lentivirus pseudotype.

FCHO1 deficiency does not alter global endocytosis. To further assess whether FCHO1 deficiency has a global impact on CME, we tested transferrin receptor internalisation, a well-recognised model of a clathrin-dependent process³³. To this end, we incubated patient and healthy donor fibroblasts with fluorescently labelled transferrin in the cold and, following a temperature shift, its internalisation was monitored over time. Both wild-type and FCHO1-deficient primary cells were able to internalise transferrin through the TfR comparably (Fig. 5c), suggesting that FCHO1 deficiency does not affect general CME endocytosis, but selectively CME endocytosis of certain molecules.

FCHO1 modulates function of primary human T cells. The paucity of T cells in peripheral blood of most FCHO1-deficient patients precluded an in-depth investigation of primary lymphocytes. However, we were able to test functional consequences of FCHO1 deficiency on T cells isolated from the patient of kindred C. We assessed proliferation of T cells and their capacity to produce cytokines in response to TCR stimulation. First, we determined the frequency of T cells in peripheral blood of patient C1 (Fig. 6a). Although largely reduced in number when compared to her heterozygous siblings, peripheral blood T cells were abundant enough to perform a functional assay. To this end, PBMCs were labelled with CFSE and stimulated with α -CD3 and α -CD28 Abs. Cell proliferation and cytokine production were assessed after 3 and 5 days. At both time points, CD4 and CD8 T cells of healthy siblings responded vigorously to the stimulation whereas patient T cells failed to proliferate (Fig. 6b). Similarly,

FCHO1-deficient T cells produced considerably lower levels of IL-2 and IFN- γ . In contrast, secretion of TNF- α was comparable to healthy control cells, and IL-4 secretion was only marginally dependent of FCHO1 function (Fig. 6c). Of note, T cells from the heterozygous mother (and to a lesser extent the father) produced less cytokines when compared to FCHO1^{wt/wt} control T cells. The reason for this observation remains unclear. While a mild dominant-negative effect cannot be excluded, there is no *in vivo* evidence of T-cell dysfunction in healthy parents. (Fig. 6c).

In summary, FCHO1 deficiency impairs T-cell development and responsiveness to TCR stimulation.

Inhibition of CME arrests development of murine T cells *in vitro*. Our data highlighted a mechanistic link between impaired CME and ensuing T-cell deficiency. To further validate this notion, we employed OP9-DL1 and OP9 co-culture systems allowing us to study *in vitro* T-cell differentiation, as well as differentiation of B cells and myeloid cells³⁴. Purified thymus-derived, T-cell-committed double-negative (DN) three progenitors were co-cultured with OP9 DL1 cells for 10 days until ~50% of them co-expressed CD4 and CD8 co-receptors (double-positive, DP). At day 5 of culture, we exposed the cells to chlorpromazine, a known inhibitor of CME³⁵ (Fig. 7a). In a concentration-dependent manner, we observed inhibition of developmental transition between DN3 to DP stage. Whereas > 50% of cells reached the DP stage in the absence of CME inhibition, only 30–35% of chlorpromazine-treated showed progression to the DP stage. Even though minuscule surface expression levels of pre-TCR at this stage of thymocyte development prevented any direct measurements of TCR internalisation, it is known that thymocyte differentiation from DN3 to DP strongly depends on the quality of pre-TCR signal^{36,37}.

To exclude the general cytotoxic effect of chlorpromazine we co-cultured bone marrow-derived lineage-Sca-1⁺CD117⁺ (LSK) cells, the most versatile progenitors, which in similar conditions develop to nearly all hematopoietic lineages (albeit with different kinetics), and assessed how chlorpromazine affects development of various lymphoid and non-lymphoid cells. To this end, LSK co-cultured on OP9-DL1 cells gave rise to all pre-TCR independent thymocyte populations in an indistinguishable

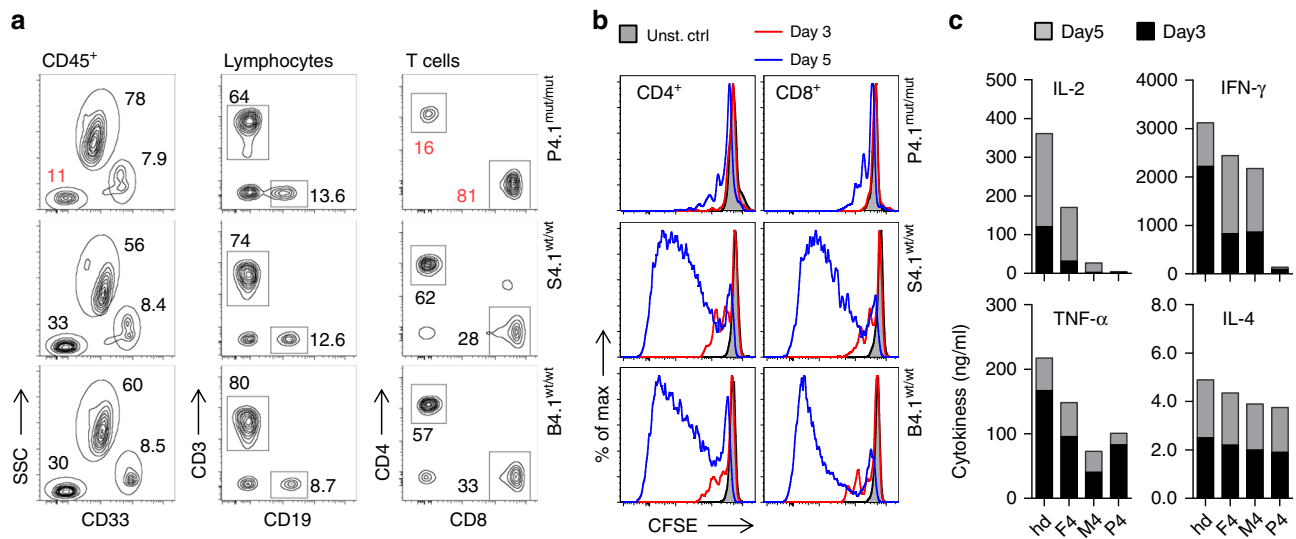


Fig. 6 Patient-associated mutation in *FCHO1* gene alters development and activation of T lymphocytes. **a** Density plots of blood leucocytes (CD45⁺) of the index case (upper row) homozygous for a mutation in the *FCHO1* locus and her siblings carrying the heterozygous mutation (middle and bottom rows). T helper cells were defined as CD45^{hi}CD33⁻SSC^{lo}CD3⁺CD4⁺ and cytotoxic T cells were CD45^{hi}CD33⁻SSC^{lo}CD3⁺CD8⁺. Numbers adjacent to the gates indicate percentages. **b** Histograms of CFSE-labelled T lymphocytes stimulated with anti-CD3 and anti-CD28 Ab for 3 (red line) or 5 (blue line) days. Unstimulated controls are depicted in grey. **c** Cytokine production by lymphocytes of patient and family members after anti-CD3 and anti-CD28 stimulation for the indicated periods of time. IL-2, IFN- γ , TNF- α and IL-4 were determined using cytometric bead assays. **a–c** Data are representative of two independent experiments, except data of day 3 shown in **c**, which was assessed once. Source data are provided as a Source Data file.

manner irrespective of presence or absence of chlorpromazine (Fig. 7b). Similarly, presence or absence of chlorpromazine in LSK and OP9 co-culture did not interfere with development of neither B220⁺CD19⁺ B-cell committed progenitors nor CD11b⁺Gr-1⁺ neutrophilic granulocytes (Fig. 7c, d).

Thus, chlorpromazine, a chemical inhibitor of CME, shows rather selective effects on the DN3-DP transition of thymocyte differentiation, known to be particularly vulnerable to disturbances of pre-TCR-signalling strength^{36,37}. Taken together, these data indirectly support our concept that T-cell differentiation in *FCHO1* deficiency is at least partially dependent on perturbed TCR internalisation/signalling.

Discussion

Here, we identify autosomal recessive *FCHO1* deficiency as a human genetic defect associated with combined immunodeficiency (CID). We show that six different mutations in the *FCHO1* gene, either point mutations resulting in amino acid substitutions, premature stop codons or affecting pre-mRNA splicing are deleterious for *FCHO1* function. T-cell deficiency predisposes affected patients to severe and persistent viral and fungal infections. Hypogammaglobulinemia is seen in all patients, except G1. It remains currently unclear whether B-cell defects are intrinsic or strictly dependent on defective T cells.

FCHO1 deficiency predisposes not only to infections but also to lymphoma¹³. Several patients died secondary to malignancies before definitive therapy in form of an allogeneic hematopoietic stem cell transplant could be done. Thus, *FCHO1* deficiency warrants rapid genetic diagnosis and provision of access to definitive cure.

Our studies have provided insights into the structural and functional biology of *FCHO1*. In a structure-guided prediction, Ma and colleagues¹⁴ concluded that a minimum of two aa substitutions in *FCHO1* (at positions K877E + R879A), located directly in the peptide-binding groove, are required to abolish interaction of the domain with its main interacting partner EPS15. Here, we show that a single substitution at R679P,

spatially distant from the groove, is sufficient to severely alter this interaction. Although localised opposite of the groove, replacement of the charged side chain of Arg with a nonpolar and rigid ring of Pro is sufficient to alter the domain function. Three mutations resulting in a premature stop codon at the beginning of μ HD domain further strengthen their significance for *FCHO1* function. Alterations in the F-BAR domain also prove to be deleterious, yet in a different mode. Substitution of Ala at position 34 with Pro, a known α -helix breaker, leads to dissociation of the *FCHO1* homodimers from the plasma membrane and hence abolishes the function. Although not directly tested, it is plausible that alternative splicing resulting in loss of 51 aa located within the F-BAR domain disrupts the protein structure. From a clinical point of view, the severity of the immunodeficiency, however, cannot directly be correlated to the type of the *FCHO1* mutation.

Given the central role of *FCHO1* for the formation of clathrin-coated pits and endocytosis it is surprising that *FCHO1* deficiency results in T-cell immunodeficiency rather than more global defects of development. In contrast, *Caenorhabditis elegans* deficient for *FCHO* show body malformation and uncoordinated locomotion³⁸. *FCHO* interacts with AP-2 and induces a conformational change, leading to AP-2 activation. Mutations in either *FCHO* or AP-2 result in a strikingly similar phenotype, indicating that the severe defects seen in *FCHO*-deficient worms are caused by aberrant activation of AP-2. In vertebrates, however, the interplay between AP-2 and *FCHO* is more complex. Morpholino-mediated knock-down of *Fcho1* in *Danio rerio* causes dorsoventral patterning defects and severe malformation at an early developmental stage, whereas transcriptional silencing of *Fcho2* is associated with notochord and somite malformations³⁸. In zebrafish, AP-2 deficiency results in a more severe, broader and earlier developmental phenotype than combined *Fcho1/2* deficiency, suggesting that AP-2 function is, at least in part, *Fcho1/2*-independent³⁹. The idea that the functional relevance of *FCHO* has changed during evolution is supported by the observation that a) two *FCHO* paralogs have emerged⁴⁰ and b) *FCHO* may act as receptor-specific adaptors (e.g., BMP-mediated signalling in zebrafish) rather than universally

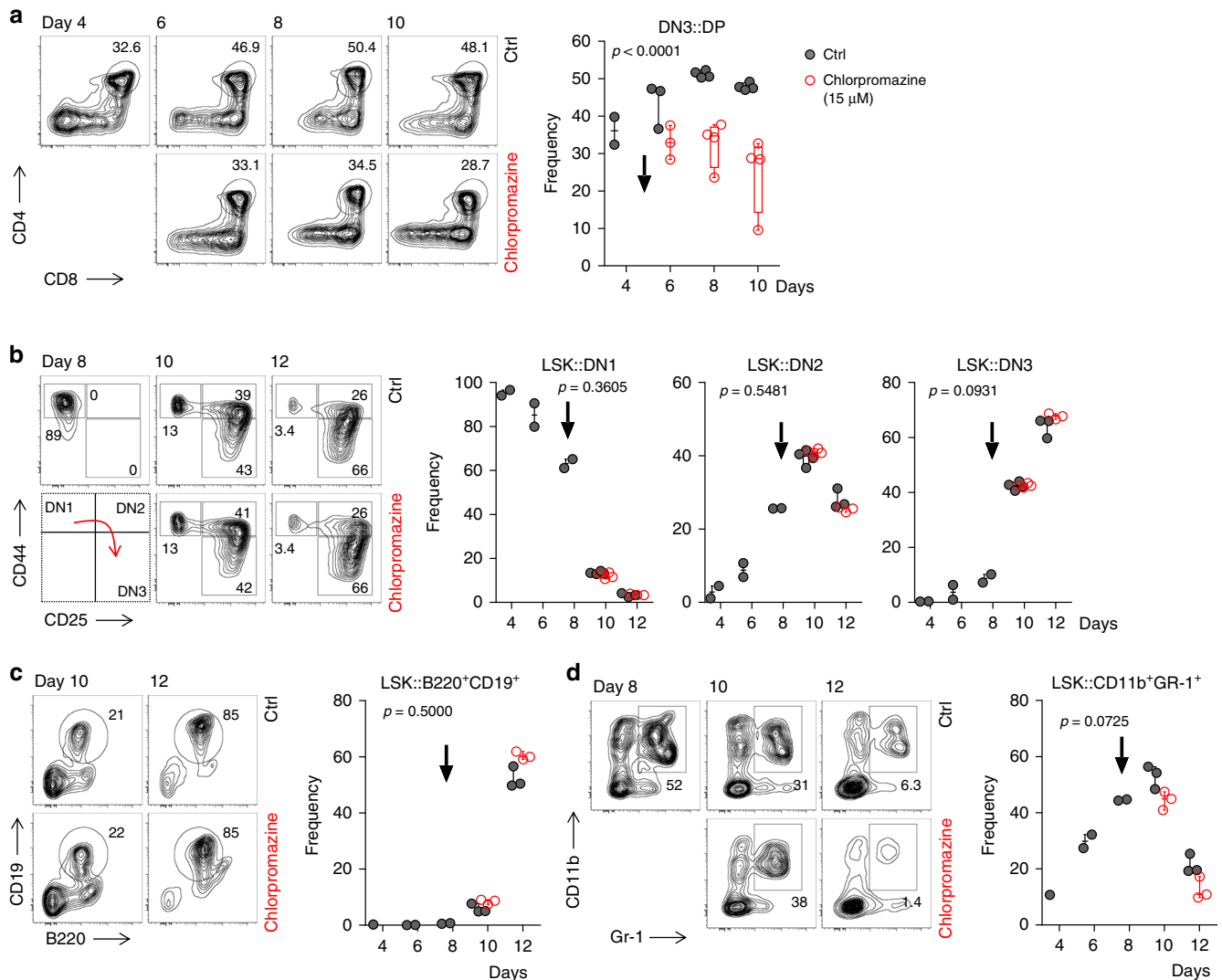


Fig. 7 Chlorpromazine-induced inhibition of CME arrests development of thymocytes. a Thymi-derived double-negative three progenitors (DN3: CD4⁻CD8⁻CD44⁺CD25⁻) were sorted and cultured on OP9-DL1 stroma cells in the presence of Flt-3L, SCF and IL-7. At day 5 of co-culture cells were left untreated (ctrl) or treated with chlorpromazine (15 μ M) to partially inhibit CME (chlorpromazine IC₅₀ for CME was established at 17.4 μ M³⁵). Subsequently, development of double-positive (DP: CD4⁺CD8⁺) progenitors was assessed by FACS (left) and quantified (right). **b** Bone marrow-derived LSK progenitors (lineage⁻Sca-1⁺CD117⁺) were sorted and cultured on OP9-DL1 stroma cells in the presence of Flt-3L, SCF and IL-7. Analogous to **a**, at day 8 of culture cells were left untreated (ctrl) or treated with 15 μ M chlorpromazine. Effect of partial CME inhibition on early-thymocyte progenitor development was assessed by FACS. Double-negative (DN) cells were defined as follows: DN1-CD44⁺CD25⁻; DN2-CD44⁺CD25⁺ and DN3-CD44⁻CD25⁺. **c, d** Bone marrow-derived LSK progenitors (lineage⁻Sca-1⁺CD117⁺) were sorted and cultured on OP9 stroma cells in the presence of Flt-3L, SCF and IL-7. At day 8 of culture cells were left untreated (ctrl) or treated with chlorpromazine (15 μ M) to partially inhibit CME. Subsequently, development of **c** B-cell committed progenitors defined as B220⁺CD19⁺ and **d** granulocytes (CD11b^{int-hi}Gr-1⁺) was assessed by FACS (left) and quantified (right). **a-d** Density FACS plots and charts are representative of two independent experiments where one to four wells were measured at each indicated time point. Number adjacent or within the gates indicate frequency. Each dot on the chart represents one well. Whiskers indicate the range (min to max). Arrows indicate time points when chlorpromazine was added. Statistical analysis was performed using two-way ANOVA (p -values for effect of chlorpromazine). Source data are provided as a Source Data file.

important initiators of clathrin-mediated endocytosis³⁹. This notion is also supported by the lack of functional consequences of FCHO1 deficiency observed on both VSV-G-mediated virus entry and TIR endocytosis in T cells. Both processes strictly rely on CME^{27,33}, but are apparently not affected in FCHO1-deficient cells. We conclude that FCHO1 deficiency does not generally affect cellular processes that require CME, underscoring a selective role of FCHO1.

This concept is further corroborated by a series of other studies focusing on central elements orchestrating clathrin-mediated endocytosis. Defects in prime molecules such as clathrin, epsin, AP-2 and dynamin, result in embryonic lethality in model organisms (reviewed in ref. 5). Mutations in proteins that are deemed to

be less pivotal for the clathrin-mediated endocytosis have been linked to a variety of diseases such as cancer, neuro-psychiatric disorders, metabolic syndromes, but not to inherited defects of the immune system⁸. Of note, a large number of FCHO1 and FCHO2 interacting partners have been identified, yet none of them have been linked to the adaptive immune system^{5,25,38,39,41,42}.

The quality of signal transmitted by pre-T-cell receptor (pre-TCR) and TCR is essential for T-cell development and homeostasis. During T-cell ontogeny, there are three stages in which such signal is critically required for selection, differentiation and commitment of developing thymocytes, respectively (reviewed in refs. 43,44).

The precise localisation of the TCR that is continuously internalised and recycled back to the plasma membrane is of critical importance for the quality of signal transduction. The TCR can be internalised via clathrin-dependent^{19–21,45} or clathrin-independent mechanisms⁴⁶. This process may be ligand-dependent or ligand-independent^{19,20,22,44,47,48}. Even though previous studies have linked TCR internalisation to a di-leucine sorting motif present in the CD3 γ subunit of the TCR:CD3 complex^{49,50}, we could not provide definitive evidence that FCHO1 directly binds to the CD3 γ sorting motifs. Nevertheless, we have shown that FCHO1 deficiency results in impaired TCR internalisation. Our data thus suggest that (a) we were not in the position to prove FCHO1/CD3 interaction using crude biochemical methods or (b) that FCHO1 interacts with other membrane-bound molecules to indirectly induce TCR internalisation.

In theory, FCHO1-dependent TCR internalisation can serve several purposes: (1) activation signals could be amplified via the scaffolding on early endosomes, (2) activation signals could be attenuated via lysosomal degradation of the TCR or (3) recirculation of the TCR to immune synapses via recycling endosomes may modulate TCR-dependent activation signals upon encountering antigen presenting cells. Integrating signal strengths relies on spatiotemporal organisation of the TCR and associated signalling molecules. Although the quality of the signal provided by TCR is essential for the outcome of thymopoiesis, our studies in FCHO1 deficiency do not provide definitive answers on detailed mechanisms of FCHO1 in T-cell differentiation. Indirectly, the link between CME and TCR-signalling is highlighted by our in vitro T-cell differentiation studies. In the presence of chlorpromazine, a chemical inhibitor of CME, we observed a rather specific effect of differentiation blockade at the DN3-DP transition. This step is known to be highly dependent on TCR-signalling strength^{36,37}.

Very recently, Calzoni et al.⁵¹ published a short letter and reported biallelic mutations in FCHO1 in four families. The phenotypes of these patients resembled the phenotype of our patients, but no functional experiments or proof-of-causality was provided. Based on experiments in activated T-cell blasts, the authors concluded that in the absence of FCHO1, CME is globally affected. In contrast, our data support the concept that FCHO1 does not globally affect CME.

In sum, our studies unravel a previously unrecognised role of FCHO1 in orchestrating the T-cell development and function. Our discovery also exemplifies how systematic studies of patients with inherited disorders help to uncover genes and pathways that were previously not associated with the function of the immune system. FCHO1 deficiency thus highlights a critical role of clathrin-mediated endocytosis for the development and function of human T cells.

Methods

Patients. Patients were referred to the clinical and scientific team of Professor Christoph Klein for further investigations. Informed consent/assent for the genetic and immunological studies, as well as their publication was obtained from all legal representatives and patients. Genetic and functional studies on biosamples from patients and their relatives were performed under the framework of a scientific project entitled “Genetic characterisation of congenital bone marrow failure and immunodeficiency syndromes”. This study was approved in 2011 by the ethics committee at LMU (438-11) and includes permission to publish the results.

Whole-exome sequencing and variant filtering. For family A we performed whole-exome sequencing (WES) for patient and father using Agilent V4 + UTR library preparation and a SOLiD sequencing platform. WES for the patient from the family B, the patient from family C, as well as for patient, mother and siblings (from family D) was performed after Agilent library preparation (V5 + UTR or V6 + UTR (SY265)) using an IlluminaNextSeq 500 platform. BWA (version 0.7.15) was used to align short reads to the human reference genome Grch37.p13. Variants were called and recalibrated according to the best practice pipeline by GATK (version 3.6). The final variants were then annotated with VEP release 85. A custom in-house database was used to filter variants to be rare (not reported in gnomAD or ExAC), as well as severe effects according to the Ensembl guidelines.

Effects of filtered variants on protein were predicted with SIFT⁵² and PolyPhen-2⁵³. The remaining variants were compiled and filtered for rare homozygous and compound heterozygous mutations following a pattern of autosomal recessive inheritance. Whole-exome sequencing of genomic DNA of kindred F patients was conducted using Illumina sequencing platforms. Bioinformatics analysis for detection of rare sequence variants following Mendelian inheritance patterns were performed as described previously⁵⁴.

Sanger sequencing. FCHO1 Sanger sequencing was performed to confirm WES-detected variants and their segregation with the clinical phenotype across the family members. Genomic DNA was PCR-amplified using OneTaq Polymerase (NEB), specific primers are provided in Supplementary Table 3. Amplicons were sequenced either in-house or by using the commercial service of Eurofins Genomics.

Structural analysis of FCHO1 mutants. Crystal structures of FCHO1 domain were modelled using PyMol software with the mutalyzer wizard⁵⁵. Mu homology domain of *Danio rerio* with bound Eps15 peptide (5JP2; <https://doi.org/10.2210/pdb5JP2/pdb>) and human FCHO2 F-Bar domain (2v00; <https://doi.org/10.2210/pdb2V00/pdb>) were chosen as template for structure modelling. To calculate effect of point mutations on the structures, rotamer configurations of the highest probability were chosen.

Cell lines. The SK-MEL-2 cell line, engineered using zinc finger nucleases (ZNF) genome editing to stably express RFP under the endogenous human clathrin light chain A locus (CLTA-RFP), was kindly provided by David G. Drubin, University of Berkeley¹⁵. The cell line with only one RFP-tagged CLTA locus was used to minimise putative side effects. Cells were maintained in Dulbecco's modified Eagle medium (DMEM)/F12 medium (ThermoFisher Scientific) supplemented with 10% fetal calf serum (FCS) (ThermoFisher Scientific), 100 U/ml of both penicillin and streptomycin (Gibco). Jurkat cells were purchased from ATCC, USA. They were maintained in RPMI1640 medium (ThermoFisher Scientific) supplemented with 10% FCS (ThermoFisher Scientific), 100 U/ml of both penicillin and streptomycin (Gibco) and 2 mM glutamine (Gibco). In all, 100 U/ml of penicillin and streptomycin (Gibco) HEK293T cells and NIH-3T3 cells (both from DSMZ—German Collection of Microorganisms and Cell Cultures) were maintained in DMEM (ThermoFisher Scientific) supplemented with 10% FCS (ThermoFisher Scientific), 100 U/ml each of penicillin and streptomycin (Gibco). Patient fibroblasts were grown in Iscove's Modified Dulbecco's Medium supplemented with 10% FCS. EBV-LCL were maintained in RPMI with 10% FCS. All cell lines were routinely tested for mycoplasma and were mycoplasma-negative throughout the study.

Plasmid DNA cloning. Full-length cDNA of the human FCHO1 isoform b (IMAGE 5757146), cloned into the pEGFP-C3 vector with modified MCS (EcoRI/SalI) was kindly provided by Emmanuel Boucrot (UCL London) and Harvey McMahon (MRC-LMB, Cambridge, UK)⁵. Patient mutations were introduced by site-directed PCR mutagenesis using Q5 site-directed mutagenesis kit (NEB) according to manufacturer's instruction with specific primers designed with NEBase Changer (NEB). Wt and mutated FCHO1 cDNAs were cloned as either GFP fusion proteins or as IRES-containing bicistronic lentiviral pRRL vectors with or without GFP as a reporter gene, respectively. Full-length cDNA of human clathrin light chain tagged with mRFP was kindly provided by Klemens Rottner from Technical University in Braunschweig⁵⁶. It was cloned to lentiviral pRRL vector for production of virus particles. The correctness of the sequences was routinely monitored by Sanger sequencing.

CRISPR/Cas9 genome editing. The genomic locus of FCHO1 (transcript ENST00000594202.1) was designated for gene disruption by inducing double-strand breaks in exon 7 (T1: 5'-GGACGTTCTCCGCTACGGCG AGG-3') and intron 7 (T2: 5'-GTGTCGTGGCGCCGCCAG CCG-3'). Genome editing of SK-MEL-2 and Jurkat cells was done cells using the Alt-R CRISPR-Cas9 technology (IDT technology, Belgium). Upon coinubation of crRNA and ATTO-TM 550 (ATTO-TEC, Germany) fluorescent dye-labelled tracrNA, the RNA duplexes were electroporated into target cells along with Cas9 nuclease (SG Cell Line 4D-Nucleofector X Kit and 4D-Nucleofector™ System Lonza, Switzerland). Red fluorescent protein (RFP)-positive cells were single-sorted using a BD FACSAria flow sorter (BD Bioscience, USA).

As endogenous expression of FCHO1 is too low for faithful assessment by western blot, deletion of FCHO1 was confirmed by PCR. The following primer pair was used for validation: (F: 5'-GTGACCGCTGATGAACCTGGGTGTG-3', R: 5'-TGATGTGGGTGACAGAGTGAGAC-3'). Cells carrying homozygous mutations are expected to have a long deletion, spanning between exon 7 and intron 7. A minimum of five clones carrying homozygous mutations resulting in frameshift were used for subsequent experiments (Supplementary Fig. 12). Unmodified clones were used as a FCHO1-positive control. To ensure deletion specificity, the ten most probable off-target sites were tested using direct Sanger sequencing, showing no signs of unspecific cuts.

Transient transfection. FCHO1 ko SK-MEL-2 cells and FCHO1 ko Jurkat cells were transfected using calcium phosphate transfection kit (Sigma, USA) and 0.1–1 µg of the various lentiviral plasmids carrying either wt or mutant FCHO1 cDNAs. Cells were typically incubated 24 h to express the constructs before imaging.

Lentiviral vector particles production and cell transduction. For production of vesicular stomatitis virus G glycoprotein (VSV-g)-pseudotyped lentiviral particles HEK293T cells were transfected using calcium phosphate transfection kit (Sigma, USA) and 5 µg respective lentiviral vector, 12 µg pcDNA3.GP.4xCTE (which expresses HIV-1 gag-pol), 5 µg pRSV-Rev and 1.5 µg pMD.G (which encodes VSV-g) in the presence of 25 µM chloroquine (Sigma, USA). Eight hours after transfection, medium was exchanged and supernatant containing lentiviral particles was collected after 24, 48 and 72 h post transfection. Viral titre were determined on 3T3 cells.

FCHO1 ko SK-MEL-2 cells and FCHO1 ko Jurkat cells were transduced with lentiviral particles through centrifugation at 900 × g for 4 h at 32 °C in the presence of polybrene (8 µg/ml) (Sigma, USA).

Production of HIV-1 stocks. The HIV-1_{NL4-3}wt plasmid was obtained from Nathaniel Landau (Alexandria Centre for Life Science, NYU, USA), the HIV-1_{NL4-3}ΔEnv plasmid was a kind gift of Oliver T. Fackler (Universitätsklinikum Heidelberg, Germany) and the BlaM-Vpr plasmid was a gift from Thomas J. Hope (Northwestern University, Chicago, USA). HIV-1_{NL4-3}ΔEnv and HIV-1_{NL4-3}ΔEnv (BlaM-Vpr), both VSV-G pseudotyped, or HIV-1_{NL4-3}wt (BlaM-Vpr) stocks were produced by PEI co-transfection of HEK293T cells. Forty-eight hours later, supernatants were collected and filtered through a 0.45 µm Stericup (Millipore). After sucrose cushion (25% in 1x phosphate-buffered saline (PBS₋)) purification at 24,000 rpm at 4 °C for 1.5 h (Sorvall WX + Ultra series; rotor: SW32, Beckmann Coulter), virus pellets were resuspended in PBS and stored at –80 °C until use.

Immunoprecipitation and western blot. To test for protein–protein interactions, FCHO1-deficient cell lines were used. SK-MEL-2 cells overexpressing different variants of GFP-FCHO1 fusion proteins were starved in serum-free medium for 1 h at 37 °C prior the assay. Jurkat lines were starved for 1 h and subsequently stimulated with an α-CD3 antibody (OKT3, 1 mg/ml, BD Biosciences) cross-linked by a goat α-mouse polyclonal antibody (0.5 mg/ml, Jackson ImmunoResearch) for 2 to 20 min at 37 °C. Stimulation was terminated by addition of ice-cold PBS. Cell pellets were lysed in RIPA buffer containing phenylmethylsulfonyl fluoride protease inhibitors for 30 min in cold. Next, the supernatants were collected for further analysis. GFP-tagged FCHO1 proteins were pulled-down by GFP-Trap magnetic beads (ChromoTek GmbH) and N^o or C^o Flag-tagged FCHO1 by anti-Flag M2 Affinity Gel (Sigma). After incubation, beads were collected and washed two times in RIPA buffer and the pellet was boiled in sample buffer containing SDS for 10 min at 95 °C. Equal amounts of protein were separated by SDS polyacrylamide gel electrophoresis and blotted onto polyvinylidene difluoride (PVDF) membranes using the Trans-Blot Turbo Transfer System (Bio-Rad). Membranes were blocked for 1 h at room temperature in 5% non-fat milk before staining. Following primary antibodies were used: FCHO1–rabbit, polyclonal, PA5-31603, lot Q12081994A, Thermo Scientific or rabbit, polyclonal, 84740, lot GR214150–4, Abcam; EPS15–rabbit, clone D3K8R, Cell Signalling; EPS15R–rabbit, clone EP1146Y, Abcam; adaptin–mouse, clone AP6, Abcam; CD3epsilon–rat, clone OKT3, ThermoFisher Scientific; CD3delta–rabbit, polyclonal, ThermoFisher Scientific; CD3 gamma–rabbit, polyclonal, ThermoFisher Scientific; GAPDH–mouse, clone 6C5, Santa Cruz. All antibodies used are summarised in Supplementary Table 4.

After washing in PBS-T, the PVDF membranes were exposed to horseradish peroxidase-conjugated secondary anti-mouse (BD), anti-rat (CS), or anti-rabbit (CST) Ig antibodies for 1 h at room temperature (RT). Western blots were detected using a chemiluminescent substrate (Pierce Technology) and images were captured on a Chemidoc XRS Imaging System (Bio-Rad Laboratories). Blots were stripped between exposures to different antibodies using a Restore Western Blot Stripping Buffer (Thermo Scientific). Data analysis was performed using Quantity One or Image Lab software (Bio-Rad Laboratories). Uncropped immunoblots are shown in Supplementary Figures.

Confocal microscopy analysis of fixed samples. To minimise dominant-negative effects on CCP dynamics resulting from prolonged overexpression of FCHO1 protein, only FCHO1-deficient SK-MEL-2 cell line transiently transduced with N-terminally tagged versions of GFP-FCHO1 were used for experiments. Cells with a low expression of FCHO1 were analysed typically 16 to 20 h post transfection. Cells were plated on glass coverslips (Karl Hecht, 0.13–0.16 mm thickness, diameter 20 mm) in 24-well tissue culture plates and cultured in complete DMEM/F12 medium for min 12 h to facilitate attachment. Coverslips were rinsed with PBS and fixed with 3% formaldehyde (Electron Microscopy Sciences) for 10 min at RT. Next, cells were washed in PBS and autofluorescence was quenched for 15 min using 50 mM NH₄Cl at RT. Coverslips were washed once in PBS and incubated for 30 min at RT in PBS containing 0.1% (w/v) bovine serum albumin (BSA; Sigma Aldrich), 0.05% (w/v) saponin (Sigma Aldrich). Further blocking solution was removed and cells were stained with the following primary antibodies: rabbit-α-Eps15 (clone D3K8R, Cell Signalling) or mouse-α-Adaptin (AP6, Abcam) at 4 °C, overnight.

Subsequently, cells were washed in PBS containing 0.05% (w/v) saponin (Sigma Aldrich), three times for 5 min each. The following secondary antibodies coupled to fluorochromes were used: goat-α-rabbit IgG, AlexaFluor 405 (Invitrogen) and goat-α-mouse IgG, AlexaFluor 633 (Invitrogen).

WGA (wheat germ agglutinin) staining was performed on transfected cells fixed with 3% formaldehyde (Electron Microscopy Sciences) for 10 min at RT. After extensive washing with phenol red free 1xHBSS, WGA conjugated to AlexaFluor 633 (Invitrogen) was added to the cells at concentration 1.25 µg/ml (in phenol red free 1xHBSS) and incubated for 5 min.

Some samples were co-stained with 300 nM DAPI (Invitrogen) for 2 min at RT. Cells were mounted on glass slides using Fluoromount-G (SouthernBiotech) and dried at RT in darkness for minimum 12 h before imaging. Samples were analysed by confocal fluorescent microscopy using the Zeiss LSM880 and Zeiss LSM800 inverted microscopes. Images were collected using 63×/1.4 NA or 40×/1.4 NA oil objectives (Zeiss). Four solid-state 5 and 10 mW laser (405, 488, 561, 640 nm) were used as light source; scanner frequency was 400 Hz; line-averaging 2. All images were obtained with GaAsP high-sensitivity detectors. Pearson correlation or co-localisation coefficient was assessed on 16-bits raw digital files on Zen Blue software (Zeiss). Representative cells from two to three independent experiments were chosen for analysis. Two to four 25 µm² square regions were selected and minimum ten cells per condition were analysed. To avoid bias during analysis, only one fluorescent channel was active while selecting regions.

Live-cell imaging. For live-cell imaging experiments stably transduced SK-MEL-2 cell lines were used. Cells were seeded on µ-dish 35 mm, high Glass Bottom (IBIDI, glass coverslip no.1.5 H, selected quality, 170 µm ± 5 µm) in complete DMEM/F1224h before imaging. Medium was exchanged directly before start of the experiment. During the experiment dishes were placed into a temperature-controlled chamber on the microscope stage with 95% air, 5% CO₂ and 100% humidity. Live-cell imaging data were acquired using a fully motorised inverted confocal microscope (Zeiss LSM800) using either 40×/1.4 NA or 63×/1.4 NA oil objectives (Zeiss) under control of Definite Focus for Axio Observer Z1 (Zeiss). Sixteen-bits digital images were obtained with GaAsP high-sensitivity detectors, confocal module and 488 and 561 nm laser lines and a dual (525/50; 605/70) BP filters. Cell regions were selected to allow for 500–950 ms-lasting intervals. Time dependence of the fluorescent intensity of FCHO1 and endogenous clathrin were assessed on movies from three independent experiments, using Zen Blue software (Zeiss). Up to three 25 µm² regions per cells were quantified. Both GFP and RFP channels were normalised to the background and initial fluorescence was set to 1.

Fusion of VSV-G pseudotyped HIV-1 ΔEnv to Jurkat T cells. The virion fusion assay was performed in principle as reported²⁹ employing HIV-1 particles carrying the HIV-1 Vpr protein fused to β-lactamase (BlaM-Vpr). In brief, after fusion of virus particles to target cells, the incorporated BlaM-Vpr protein is released into the cytoplasm and is able to cleave the CCF2 dye. This leads to a shift of the dye's emission maximum from 520 to 447 nm, which can be detected and quantified by flow cytometry. Jurkat T cells were plated at a density of 2 × 10⁵ cells per well (96-well conical plate, Corning, New York, USA). Where indicated, the HIV-1 fusion inhibitor T20 (50 µM, enfuvirtide, Roche, Rotkreuz, Switzerland) was added 1 h prior to virus challenge. Serial dilutions of VSV-G HIV-1_{NL4-3}ΔEnv (BlaM-Vpr) were performed in PBS. 4 h following challenge with either VSV-G HIV-1_{NL4-3}ΔEnv (BlaM-Vpr) or HIV-1_{NL4-3} (BlaM-Vpr), Jurkat T cells were washed and incubated with the CCF2 dye as previously reported^{30,31}. The following day, cells were fixed for 90 min with 4% PFA/PBS and analysed by flow cytometry.

Infection of Jurkat T cells with VSV-G HIV-1 ΔEnv. Jurkat T cells were plated at a density of 2 × 10⁵ cells per well. T20 (50 µM), the V-ATPase inhibitor bafilomycin A1 (100 nM, Sigma Aldrich, St. Louis, USA) or PBS were added 1 h prior to virus challenge. Cells were challenged with VSV-G HIV-1_{NL4-3}ΔEnv and 4 h later, 200 µl of fresh culture medium were added. 48 h later, cells were fixed for 90 min in 4% PFA/PBS and HIV infection was monitored using an intracellular p24 staining (anti-p24 antibody, clone KC57-FITC, Beckmann Coulter, Brea, USA) in principle as reported³².

Transferrin uptake. Fibroblasts from healthy donor (HD) and patient (kindred E) were detached using PBS containing 10 mM EDTA and serum-starved for 30 min in DMEM at 37 °C. Cells and transferrin conjugated to AlexaFluor 633 (ThermoFisher Scientific) were washed in glucose buffer (PBS supplemented with 20 mM Glucose and 1% BSA) and cooled down on ice. 25 µg/ml AlexaFluor 633-conjugated transferrin were added to cells and incubated on ice for 10 min. Cells were then transferred to 37 °C for indicated periods of time. Upon indicated time, surface-bound transferrin was stripped by acid wash (PBS supplemented with 0.1 M glycine and 150 mM NaCl at pH 3) and uptake of fluorescent transferrin was determined by flow cytometry. Data are pooled from four independent experiments. Error bars indicate mean ± SD. Statistical analysis using two-way ANOVA followed by Sidak's multiple comparisons test revealed no significant difference in transferrin uptake between HD and patient fibroblasts.

Flow cytometry. Blood samples were washed with PBS and stained with the following antibodies for 20 min at RT: α -CD45 BV711 or APC (HI30), α -CD33 PE-Cy7 (P67.6), α -CD3 PE (HIT3a), α -CD19 FITC (HIB19), α -CD8 α APC (RPA-T8), α -CD4 PE-Cy7 (A161A1) all from Biolegend. All antibodies used are summarised in Supplementary Table 4. Red blood cells were lysed using 1 \times BD FACS Lysing Solution (BD Biosciences) according to the manufacturer's instructions. The samples were acquired using a LSRFortessa (BD Bioscience) cytometer. Data were analysed using FlowJo Software (TreeStar), v9 and v10. Gating strategy to assess frequency of blood leucocytes is shown in Supplementary Fig. 13. Virion fusion and HIV infection of Jurkat T cells were recorded on a BD FACSLyric (BD Biosciences, Franklin Lakes, USA).

In vitro stimulation of PBMCs. PBMC were isolated from blood samples by Ficoll-Hypaque (Pharmacia) density gradient centrifugation. Cells were labeled with 1 μ M CFSE (eBioscience) according to the manufacturer's protocol. They were resuspended in complete RPMI1640, plated on 96-well flat bottom plates and stimulated with α -CD3-coupled beads (bio- α -CD3, clone OKT3 (eBioscience) coupled with α -biotin MACSiBeads (MiltenyiBiotec)) at a ratio 10:1, in the presence of 1 mg/ml of soluble α -CD28, clone CD28.2 (eBioscience). Proliferative response was measured after 3 and 5 days. Gating strategy to assess T-cell proliferation is shown in Supplementary Fig. 14. Supernatants (four technical replicates) were tested for the presence of IL-2, IL-4, IFN- γ and TNF- α using human FlowCytomix beads (eBioscience) according to the manufacturer's instructions.

Assessment of intracellular calcium flux. Up to five different FCHO1-sufficient or -deficient Jurkat clones were incubated for 1 h in Ca²⁺- and Mg²⁺-free Dulbecco's serum-free medium (Invitrogen) at room temperature at a density of 10⁷ cells/ml. Cells were then loaded with Ca²⁺-sensitive dyes, either Indo-1 or Fluo-4 (3 μ M) and FuraRed (6 μ M) for 45 min at 37 °C. Further, cells were rested for 30–45 min at 37 °C. After establishing of a baseline for 30 s, cells were stimulated with α -CD3 antibody (OKT3, 1 mg/ml, BD Biosciences) and goat- α -mouse polyclonal antibody (0.5 mg/ml, Jackson ImmunoResearch) to allow cross-linking and data acquisition was continued for four additional minutes. To ensure cell viability, 1 min before the end of acquisition, 2 μ g/ml ionomycin (Sigma) was added as positive Ca²⁺-flux control. Gating strategy to assess Ca²⁺ release is shown in Supplementary Fig. 15.

TCR internalisation assays on Jurkat cell lines. Confocal microscopy: FCHO1-sufficient or -deficient, or stably transduced (with wt or mutant FCHO1 viruses) Jurkat FCHO1^{-/-} cell lines were used to visualise TCR internalisation. Cells were plated on poly-D-lysine (0.1 mg/ml, Sigma Aldrich) and α -CD3 (clone OKT3, 0.5 mg/ml, eBioscience) coated glass coverslips (Karl Hecht, 0.13–0.16 mm thickness, diameter 20 mm) in 24-well tissue culture plates and incubated for indicated time points. Coverslips were rinsed with PBS and cells were fixed in 3% formaldehyde (Electron Microscopy Sciences) for 10 min at RT. Next, cells were washed in PBS and autofluorescence was quenched for 15 min at RT using 50 mM NH₄Cl. Coverslips were washed once in PBS and incubated for 30 min at RT in PBS containing 0.1% (w/v) BSA (Sigma Aldrich), 0.05% (w/v) saponin (Sigma Aldrich). Further, blocking solution was removed and cells were stained with mouse- α -CD3 (OKT3, eBioscience) and goat- α -mouse IgG, AlexaFluor 633 (Invitrogen). Samples were co-stained with 300 nM DAPI (Invitrogen) for 2 min at RT. Cells were mounted on glass slides using Fluoromount-G (SouthernBiotech) and dried at RT in darkness for at least 12 h before imaging. Samples were analysed by confocal fluorescent microscopy using the ZEISS LSM800 inverted microscopes (ZEISS) as described above. We used Fiji software⁵⁷ to quantify the number of CD3 puncta/cell. The number of puncta/cell was averaged on several random fields of view.

Flow cytometry: FCHO1-sufficient or -deficient Jurkat cells were stained with α -CD3 Ab (OKT3) in cold and TCR internalisation was assessed over time at 37 °C in the presence of anti-mouse F(ab')₂ fragments labelled with Ax647. After 2, 5, 15, 45 and 60 min of stimulation the remaining surface TCRs were stripped, thus fluorescent signal corresponds only to the internalised TCR. Gating strategy to assess TCR internalisation is shown in Supplementary Fig. 16.

Statistics. Statistical analysis was performed using GraphPadPrism software v.6. Pearson correlation and colocalization coefficient on selected cell fragments were assessed on raw files using Zen Blue software (Zeiss). Cell regions or entire cells are referred to as *n* unless indicated otherwise. No method of randomisation was used, and no samples were excluded from analysis. To avoid bias during analysis, cell regions were selected based on the signal from only one fluorescent channel. No statistical method was used to predetermine sample size for analyses. Two-way analysis of variance (ANOVA) or ANOVA analysis followed by Sidak's multiple comparison test were used to assess differences between groups. *p*-values < 0.05 were considered to be statistically significant.

Reporting summary. Further information on research design is available in the Nature Research Reporting Summary linked to this article.

Data availability

The source data underlying Figs. 2e, 3b, 3c, 4b, 5a–c, 6, 7a–d, Supplementary Figs. 1, 5, 10, 11 are provided as a Source Data file. All other data are available from the corresponding authors upon reasonable request. The identified FCHO1 mutations have been submitted to the ClinVar database with accession numbers SCV001146883, SCV001146884, SCV001146885, SCV001146886, SCV001146887 and SCV001146888. According to current regulatory frameworks, exome sequencing data cannot be made publicly available. For any further questions, the corresponding authors will share additional data in accordance with regulatory guidelines.

Received: 14 January 2019; Accepted: 23 January 2020;

Published online: 25 February 2020

References

- Roth, T. F. & Porter, K. R. Yolk protein uptake in the oocyte of the mosquito *Aedes Aegypti*. *L. J. Cell Biol.* **20**, 313–332 (1964).
- Pearse, B. Clathrin: a unique protein associated with intracellular transfer of membrane by coated vesicles. *Proc. Natl Acad. Sci. USA* **73**, 1255–1259 (1976).
- Robinson, M. S. Forty years of clathrin-coated vesicles. *Traffic* **16**, 1210–1238 (2015).
- Cocucci, E., Aguet, F., Boulant, S. & Kirchhausen, T. The first five seconds in the life of a clathrin-coated pit. *Cell* **150**, 495–507 (2012).
- Henne, W. M. et al. FCHO proteins are nucleators of clathrin-mediated endocytosis. *Science* **328**, 1281–1284 (2010).
- Pechstein, A. et al. Regulation of synaptic vesicle recycling by complex formation between intersectin 1 and the clathrin adaptor complex AP2. *Proc. Natl Acad. Sci. USA* **107**, 4206–4211 (2010).
- Di Paolo, G. & De Camilli, P. Phosphoinositides in cell regulation and membrane dynamics. *Nature* **443**, 651–657 (2006).
- McMahon, H. T. & Boucrot, E. Molecular mechanism and physiological functions of clathrin-mediated endocytosis. *Nat. Rev. Mol. Cell Biol.* **12**, 517–533 (2011).
- Dannhauser, P. N. & Ungewickell, E. J. Reconstitution of clathrin-coated bud and vesicle formation with minimal components. *Nat. Cell Biol.* **14**, 634–639 (2012).
- Koh, T. W. et al. Eps15 and Dap160 control synaptic vesicle membrane retrieval and synapse development. *J. Cell Biol.* **178**, 309–322 (2007).
- Kostmann, R. Hereditär reticulosos–en ny systemsjukdom. *Sven. Läkartidningen* **47**, 2861 (1950).
- Bruton, O. C. Agammaglobulinemia. *Pediatrics* **9**, 722–728 (1952).
- Picard, C. et al. International union of immunological societies: 2017 primary immunodeficiency diseases committee report on inborn errors of immunity. *J. Clin. Immunol.* **38**, 96–128 (2018).
- Ma, L. et al. Transient Fcho1/2Eps15/RAP-2 nanoclusters prime the AP-2 clathrin adaptor for cargo binding. *Dev. Cell* **37**, 428–443 (2016).
- Doyon, J. B. et al. Rapid and efficient clathrin-mediated endocytosis revealed in genome-edited mammalian cells. *Nat. Cell Biol.* **13**, 331–337 (2011).
- Lyszkiewicz, M. et al. miR-181a/b-1 controls thymic selection of Treg cells and tunes their suppressive capacity. *PLoS Biol.* **17**, e2006716 (2019).
- Zietara, N. et al. Critical role for miR-181a/b-1 in agonist selection of invariant natural killer T cells. *Proc. Natl Acad. Sci. USA* **110**, 7407–7412 (2013).
- Gaud, G., Lesourne, R. & Love, P. E. Regulatory mechanisms in T cell receptor signalling. *Nat. Rev. Immunol.* **18**, 485–497 (2018).
- Telerman, A. et al. Internalization of human T lymphocyte receptors. *Eur. J. Immunol.* **17**, 991–997 (1987).
- Dietrich, J., Hou, X., Wegener, A. M. & Geisler, C. CD3 gamma contains a phosphoserine-dependent di-leucine motif involved in down-regulation of the T cell receptor. *EMBO J.* **13**, 2156–2166 (1994).
- Boyer, C. et al. T cell receptor/CD3 complex internalization following activation of a cytolytic T cell clone: evidence for a protein kinase C-independent staurosporine-sensitive step. *Eur. J. Immunol.* **21**, 1623–1634 (1991).
- Crotzer, V. L., Mabardy, A. S., Weiss, A. & Brodsky, F. M. T cell receptor engagement leads to phosphorylation of clathrin heavy chain during receptor internalization. *J. Exp. Med.* **199**, 981–991 (2004).
- Dietrich, J., Kastrup, J., Nielsen, B. L., Odum, N. & Geisler, C. Regulation and function of the CD3gamma DxxxLL motif: a binding site for adaptor protein-1 and adaptor protein-2 in vitro. *J. Cell Biol.* **138**, 271–281 (1997).
- Balagopal, L., Barr, V. A. & Samelson, L. E. Endocytic events in TCR signaling: focus on adaptors in microclusters. *Immunol. Rev.* **232**, 84–98 (2009).
- Reider, A. et al. Syp1 is a conserved endocytic adaptor that contains domains involved in cargo selection and membrane tubulation. *EMBO J.* **28**, 3103–3116 (2009).
- Apel, A. R. et al. Syp1 regulates the clathrin-mediated and clathrin-independent endocytosis of multiple cargo proteins through a novel sorting motif. *Mol. Biol. Cell* **28**, 2434–2448 (2017).

27. Finkelshtein, D., Werman, A., Novick, D., Barak, S. & Rubinstein, M. LDL receptor and its family members serve as the cellular receptors for vesicular stomatitis virus. *Proc. Natl Acad. Sci. USA* **110**, 7306–7311 (2013).
28. Kim, I. S. et al. Mechanism of membrane fusion induced by vesicular stomatitis virus G protein. *Proc. Natl Acad. Sci. USA* **114**, E28–E36 (2017).
29. Cavrois, M., De Noronha, C. & Greene, W. C. A sensitive and specific enzyme-based assay detecting HIV-1 virion fusion in primary T lymphocytes. *Nat. Biotechnol.* **20**, 1151–1154 (2002).
30. Michel, N., Allespach, I., Venzke, S., Fackler, O. T. & Keppler, O. T. The Nef protein of human immunodeficiency virus establishes superinfection immunity by a dual strategy to downregulate cell-surface CCR5 and CD4. *Curr. Biol.* **15**, 714–723 (2005).
31. Venzke, S., Michel, N., Allespach, I., Fackler, O. T. & Keppler, O. T. Expression of Nef downregulates CXCR4, the major coreceptor of human immunodeficiency virus, from the surfaces of target cells and thereby enhances resistance to superinfection. *J. Virol.* **80**, 11141–11152 (2006).
32. Homann, S. et al. Determinants in HIV-1 Nef for enhancement of virus replication and depletion of CD4+ T lymphocytes in human lymphoid tissue *ex vivo*. *Retrovirology* **6**, 6 (2009).
33. Mayle, K. M., Le, A. M. & Kamei, D. T. The intracellular trafficking pathway of transferrin. *Biochim Biophys. Acta* **1820**, 264–281 (2012).
34. Schmitt, T. M. & Zuniga-Pflucker, J. C. Induction of T cell development from hematopoietic progenitor cells by delta-like-1 *in vitro*. *Immunity* **17**, 749–756 (2002).
35. Daniel, J. A. et al. Phenothiazine-derived antipsychotic drugs inhibit dynamin and clathrin-mediated endocytosis. *Traffic* **16**, 635–654 (2015).
36. von Boehmer, H. Unique features of the pre-T-cell receptor alpha-chain: not just a surrogate. *Nat. Rev. Immunol.* **5**, 571–577 (2005).
37. Gascoigne, N. R., Rybakin, V., Acuto, O. & Brzostek, J. TCR signal strength and T cell development. *Annu Rev. Cell Dev. Biol.* **32**, 327–348 (2016).
38. Hollopeter, G. et al. The membrane-associated proteins FCHO and SGIP are allosteric activators of the AP2 clathrin adaptor complex. *Elife* **3**, 1–23 (2014).
39. Umasankar, P. K. et al. Distinct and separable activities of the endocytic clathrin-coat components Fcho1/2 and AP-2 in developmental patterning. *Nat. Cell Biol.* **14**, 488–501 (2012).
40. Dergai, M., Iershov, A., Novokhatska, O., Pankivskiy, S. & Rynditch, A. Evolutionary changes on the way to clathrin-mediated endocytosis in animals. *Genome Biol. Evol.* **8**, 588–606 (2016).
41. Mulkearns, E. E. & Cooper, J. A. FCH domain only-2 organizes clathrin-coated structures and interacts with Disabled-2 for low-density lipoprotein receptor endocytosis. *Mol. Biol. Cell* **23**, 1330–1342 (2012).
42. Henne, W. M. et al. Structure and analysis of FCHO2 F-BAR domain: a dimerizing and membrane recruitment module that effects membrane curvature. *Structure* **15**, 839–852 (2007).
43. Brownlie, R. J. & Zamoyska, R. T cell receptor signalling networks: branched, diversified and bounded. *Nat. Rev. Immunol.* **13**, 257–269 (2013).
44. Miosge, L. & Zamoyska, R. Signalling in T-cell development: is it all location, location, location? *Curr. Opin. Immunol.* **19**, 194–199 (2007).
45. Ohno, H. et al. Interaction of tyrosine-based sorting signals with clathrin-associated proteins. *Science* **269**, 1872–1875 (1995).
46. Compeer, E. B. et al. A mobile endocytic network connects clathrin-independent receptor endocytosis to recycling and promotes T cell activation. *Nat. Commun.* **9**, 1597 (2018).
47. Monjas, A., Alcover, A. & Alarcon, B. Engaged and bystander T cell receptors are down-modulated by different endocytotic pathways. *J. Biol. Chem.* **279**, 55376–55384 (2004).
48. Finetti, F., Onnis, A. & Baldari, C. T. Regulation of vesicular traffic at the T cell immune synapse: lessons from the primary cilium. *Traffic* **16**, 241–249 (2015).
49. Krangel, M. S. Endocytosis and recycling of the T3-T cell receptor complex. The role of T3 phosphorylation. *J. Exp. Med.* **165**, 1141–1159 (1987).
50. Dietrich, J. et al. Ligand-induced TCR down-regulation is not dependent on constitutive TCR cycling. *J. Immunol.* **168**, 5434–5440 (2002).
51. Calzoni, E. et al. F-BAR domain only protein 1 (FCHO1) deficiency is a novel cause of combined immune deficiency in human subjects. *J. Allergy Clin. Immunol.* **143**, 2317–2321 e12 (2019).
52. Kumar, P., Henikoff, S. & Ng, P. C. Predicting the effects of coding non-synonymous variants on protein function using the SIFT algorithm. *Nat. Protoc.* **4**, 1073–1081 (2009).
53. Adzhubei, I., Jordan, D. M. & Sunyaev, S. R. Predicting functional effect of human missense mutations using PolyPhen-2. *Curr. Protoc. Hum. Genet.* **Chapter 7**, Unit7.20 (2013).
54. Field, M. A., Cho, V., Andrews, T. D. & Goodnow, C. C. Reliably detecting clinically important variants requires both combined variant calls and optimized filtering strategies. *PLoS ONE* **10**, e0143199 (2015).
55. DeLano, W. L. Pymol: an open-source molecular graphics tool. *CCP4 NewsL. Protein Crystallogr.* **40**, 82–92 (2002).

56. Benesch, S. et al. N-WASP deficiency impairs EGF internalization and actin assembly at clathrin-coated pits. *J. Cell Sci.* **118**, 3103–3115 (2005).
57. Schindelin, J. et al. Fiji: an open-source platform for biological-image analysis. *Nat. Methods* **9**, 676–682 (2012).

Acknowledgements

We thank the patients and their families for participating in this research. We would like to thank Alper Özcan, Murat Cansever, Fulya Bektas, Ebru Yilmaz, (Erciyes University, Kayseri, Turkey), Can Acıpayam (Kahramanmaraş Sütçü imam University, Kahramanmaraş) and all medical personnel for excellent patient care. We thank Andreas Krueger and Ludger Klein for critical review of this manuscript; Emmanuel Boucrot (University College London, UK) and Harvey McMahon (MRC-LMB, Cambridge, UK) for sharing various constructs of wt FCHO proteins. The SK-MEL-2 cell line with RFP-tagged clathrin light chain was kindly provided by David G. Drubin (UC Berkeley, USA). We are grateful to Jan E. Heil, Monica Stich and Alexander Liebsch from ZEISS laboratories for access to their facilities and technical help on microscopy experiments. The studies were supported by the Bundesministerium für Bildung und Forschung (BMBF) (German PID-NET, grants to K.S., M.H., J.R., and C.K.), the DAAD (Rare disorders of the immune system), the Else-Kröner-Fresenius Stiftung, DFG (Gottfried Wilhelm Leibniz programme and SFB914 (to C.K.), German Research Foundation (DFG LY150/1-1) (to M.L.), grants KE742/5-1 and KE742/7-1 (to O.T.K.)) and the Care-for-Rare Foundation.

Author contributions

M.L. and N.Z. initiated the project, designed the studies, performed experiments and analysed the data (pedigrees A–D); L.F. performed IP and microscopy experiments, analysed the data (pedigrees A–D); U.P. designed and performed experiments, analysed the data (pedigree F); M.S. performed HIV infection experiments and analysed the data; Y.L. designed and performed CRISPR/Cas9 knockout experiments; Y.F. performed IP experiments (pedigrees A–D); J.P. and S.H. performed bioinformatical analysis of WES data (pedigrees A–D); I.S. performed genotyping and WB experiments, analysed the data (pedigree E); M.R. performed Sanger sequencing and *in silico* prediction analyses of mutations (pedigrees A–D); K.-W.S. provided clinical data (pedigree A); O.T.K. designed and analysed HIV infection experiments; E.Ü. provided patient material, clinical data (pedigree C); M.K., T.P. provided patient material, clinical data (pedigree B, D); A.L., A.S. and R.S. provided patient material, clinical data and genetic analysis (pedigree E); M.H., J.R. and K.S. designed the studies, provided patient material, clinical data and genetic analysis (pedigree F and G); C.K. and E.K. performed family analyses, RNA and protein detection (Pedigree F). C.K. initiated the project, designed the studies and provided clinical and laboratory resources; (pedigrees A–E); M.L., N.Z. and C.K. wrote the manuscript.

Competing interests

The authors declare no competing interests.

Additional information

Supplementary information is available for this paper at <https://doi.org/10.1038/s41467-020-14809-9>.

Correspondence and requests for materials should be addressed to M.L. or C.K.

Peer review information *Nature Communications* thanks the anonymous reviewer(s) for their contribution to the peer review of this work. Peer reviewer reports are available.

Reprints and permission information is available at <http://www.nature.com/reprints>

Publisher's note Springer Nature remains neutral with regard to jurisdictional claims in published maps and institutional affiliations.



Open Access This article is licensed under a Creative Commons Attribution 4.0 International License, which permits use, sharing, adaptation, distribution and reproduction in any medium or format, as long as you give appropriate credit to the original author(s) and the source, provide a link to the Creative Commons license, and indicate if changes were made. The images or other third party material in this article are included in the article's Creative Commons license, unless indicated otherwise in a credit line to the material. If material is not included in the article's Creative Commons license and your intended use is not permitted by statutory regulation or exceeds the permitted use, you will need to obtain permission directly from the copyright holder. To view a copy of this license, visit <http://creativecommons.org/licenses/by/4.0/>.

© The Author(s) 2020